
Wayne State University Dissertations


January 2018

Drug Delivery Strategies For The Treatment Of Advanced Lung Cancer And Various Lung Metastases

Elizabeth Bielski

Wayne State University, dt8690@wayne.edu

Follow this and additional works at: https://digitalcommons.wayne.edu/oa_dissertations

 Part of the [Chemical Engineering Commons](#), [Medicinal Chemistry and Pharmaceutics Commons](#), and the [Polymer Chemistry Commons](#)

Recommended Citation

Bielski, Elizabeth, "Drug Delivery Strategies For The Treatment Of Advanced Lung Cancer And Various Lung Metastases" (2018). *Wayne State University Dissertations*. 2012.

https://digitalcommons.wayne.edu/oa_dissertations/2012

This Open Access Dissertation is brought to you for free and open access by DigitalCommons@WayneState. It has been accepted for inclusion in Wayne State University Dissertations by an authorized administrator of DigitalCommons@WayneState.

**DRUG DELIVERY STRATEGIES FOR THE TREATMENT OF ADVANCED LUNG
CANCER AND VARIOUS LUNG METASTASES**

by

ELIZABETH BIELSKI

DISSERTATION

Submitted to the Graduate School

of Wayne State University,

Detroit, Michigan

in partial fulfillment of requirements

for the degree of

DOCTOR OF PHILOSOPHY

2018

MAJOR: CHEMICAL ENGINEERING

Approved By:

Advisor

Date

© COPYRIGHT BY

ELIZABETH BIELSKI

2018

All Rights Reserved

ACKNOWLEDGEMENTS

It has been an amazing journey these past 6 years. It has been full of fun and wonderful surprises, which would not have been possible with all the wonderful family, friends, and colleagues I have been very honored to have met and shared these amazing years. I am so happy to have made such delightful personal and professional connections through this process, and I would like to take a moment to thank them all personally.

First and foremost, I would like to thank my family who have supported me unceasingly throughout my PhD. My mom Miriam and my dad Christopher, have been have supported me and my decisions and have always believed in my capabilities even in my moments of doubt. Their compassion, support, understanding, and unconditional love has been a keystone to my success, for which I am truly grateful. To my brother Christian, for his wonderful enthusiasm, love, and humor, that kept me motivated and strong, especially on those long days and nights. Also, a wonderful thanks to my grandmothers Regina and Ewa, who have been remarkable role models in my life and have passed on their wisdom and kindness and taught me to always believe in myself.

I would like to personally thank my advisor Dr. Sandro R. P. da Rocha for his guidance, compassion, and friendship though my time at Wayne State University. A special thanks to my committee members Dr. Matthew, Dr. Liu, and Dr. Merkel for participating and providing critical feedback on my research throughout my PhD. I would like to thank the Department of Chemical Engineering for this opportunity, all the professors in the department who were my instructors for their invaluable education. I would also like to put a special thanks to Dr. Manke, who has been a wonderful guide and advisor for all my questions and concerns. I would like to give another special thanks to

Angela Childrey, who has been invaluable in my transition in the late states of my PhD. I would also like to thank Dr. Manke, Dr. Salley, and Dr. Matthew for a wonderful experience of working with them as a teaching assistant. I would also like to thank Dr. Back and Dr. Rishi for their professional input into my research.

My special thanks for all the friends and colleagues that I was able to make during my time in Brazil. A special thanks to Dr. Bazito for accepting me and advising me as an exchange student during my stay. I would like to thank Ligia Maia and the rest of her wonderful family for hosting me and providing invaluable memories in my time in São Paulo. I would also like to thank all the wonderful friends I was able to make there and for all the wonderful memories including: Ingrid and Ricardo, Juliana and Gustavo, Bruno, Tatiana, Hans, and Denise and Hilderado.

For all those I have met during my time at Virginia Commonwealth University in the Department of Pharmaceutics, thank you for making the department a wonderful new home for me! A special thanks to Dr. Sweet and Dr. Byron for being very understanding, kind, and fun during my time at VCU. Another special thanks to Dr. Sakagami, Dr. Koblinski, Dr. Bos, and Dr. Hu for all their help and advice. A special thanks to all those who have helped me in the core facilities and have made my research life go smoothly. A special thanks to all the friends I made in the department by making my time at VCU a very memorable one – Serena, Varsha, Ray, Chris, Palak, Fay, Susan, Zaneera and Sneha. Without all your help and support, none of this would be possible.

To all my friends and lab mates that I have had throughout my time at WSU and VCU, a special thanks to you all for the support, friendship, joy, laughter, and hard work. You have made all this possible by your friendship and support throughout the years! A

special thanks to my former lab mates Denise, Lin, Qian, Daniel, Radovan, Jordan, Matthew, and Hamad for making the lab a wonderful place to work, for all work and input in associated with my research, and for the wonderful friendships. A special thanks to Qian, Matthew, and Hamad for being essential in the work that is presented in this dissertation. A special thanks to all my current lab mates who have also brought the same enthusiasm, friendship and hard work into the lab now – Ali, Rashed, Sulaiman, Hanming, Rodrigo, Fatemah, Younan and Justin. They have made the lab a wonderful place to work and have provided invaluable friendships inside and outside the lab that I cherish most deeply. A special thanks to Sulaiman, Hanming, and Rodrigo, Wei and Bin for all the hard work and dedication that was essential in the work presented in this dissertation.

I would like to thank Dr. da Rocha, the Department of Chemical Engineering and Materials Science and Graduate School at Wayne State University, the Department of Pharmaceutics and Virginia Commonwealth University, and NSF for all the financial support I have received over my many years as a graduate student.

And a last thanks to all my family and friends for making this possible. I give you all my gratitude for the many years of love and support. Your friendship, laughter, and understanding have made all my success imaginable. I couldn't have done any of this without you all!

TABLE OF CONTENTS

ACKNOWLEDGEMENTS	ii
LIST OF TABLES	xi
LIST OF FIGURES	xiii
LIST OF ABBREVIATIONS	xxii
LIST OF ORIGINAL PUBLICATIONS	xxvii
CHAPTER 1 – INTRODUCTION	1
1.1 Overview and Objectives	1
1.2 Relevance and Innovation	17
CHAPTER 2 – LITERATURE REVIEW	19
2.1 Lung Cancer and Other Common Cancers that Metastasize to the Lung	19
2.2 Current Therapies and Therapeutic Challenges in Addressing Drug Resistance and Metastasis to the Lung	21
2.3 Dendrimers and Dendrons as Polymeric Nanocarriers and Their Roles for Treatment of Primary and Secondary Lung Tumors and MDR	29
2.4 Mitochondrial Targeting of Chemotherapeutics as an Effective Strategy to Treat Primary and Secondary Lung Tumors and Address MDR	33
2.5 siRNA Delivery Strategy to Address Drug Resistance for Primary and Secondary Cancer Treatment	40
2.6. Direct Pulmonary Drug Delivery for the Treatment of Primary and Secondary Lung Tumors	44
2.7 Immunotherapy Strategies by Macrophage Modulation in the Tumor Microenvironment as Treatment Strategy for Primary and Secondary Lung Tumors	48
CHAPTER 3 – EFFECT OF THE CONJUGATION DENSITY OF TRIPHENYLPHOSPHONIUM CATION ON THE MITOCHONDRIAL TARGETING OF POLY(AMIDOAMINE) DENDRIMERS	54
3.1 Introduction	54

3.2 Materials and Methods.....	56
3.2.1 Materials.....	56
3.2.2 Conjugation of FITC to G4NH₂ Dendrimer	58
3.2.3 Conjugation of TPP to G4NH₂-FITC	58
3.2.4 Conjugation of Bifunctional PEG1000 to TPP.....	59
3.2.5 Conjugation of PEGTPP to G4NH₂-FITC.....	59
3.2.6 Cell Culture	60
3.2.7 Cytotoxicity of Dendrimer Conjugates	60
3.2.8 Cellular Internalization of the Dendrimer Conjugates Analyzed by Fluorescence Activated Cell Sorting (FACS).....	60
3.2.9 Colocalization of Dendrimer Conjugates by Confocal Microscopy	61
3.2.10 Statistical Analysis.....	62
3.3 Results	62
3.3.1 TPP and PEGTPP Conjugation.....	62
3.3.2 Cytotoxicity of the Dendrimer Conjugates.....	66
3.3.3 Cellular Internalization of Dendrimer Conjugates Analyzed by FACS.....	68
3.3.4 Colocalization of Dendrimer Conjugates	71
3.4 Discussion	74
3.5 Conclusions.....	81
3.6 Acknowledgements.....	82
CHAPTER 4 - TPP-DENDRIMER NANOCARRIERS FOR SIRNA DELIVERY TO THE PULMONARY EPITHELIUM AND THEIR DRY POWDER AND METERED-DOSE INHALER FORMULATIONS	83
4.1 Introduction	83
4.2 Materials and Methods.....	86

4.2.1 Materials.....	86
4.2.2 Conjugation of TPP to G4NH ₂ Dendrimer to Form G4NH ₂ -TPP Conjugates .	87
4.2.3 Preparation and Characterization of TPP-Dendriplexes	88
4.2.4 RNA Gel Complexation Assay.....	89
4.2.5 siRNA Release via Polyanion Competition Assay.....	89
4.2.6 <i>In Vitro</i> Gene Knockdown.....	90
4.2.7 <i>In Vitro</i> Cytotoxicity	91
4.2.8 Preparation and Characterization of 12TPP-Dendriplex/Mannitol Microparticles	92
4.2.9 Preparation and <i>in vitro</i> Aerosolization of the pMDI Formulation of 12TPP-Dendriplex/Mannitol Microparticles.....	93
4.2.10 Preparation and <i>in vitro</i> Aerosolization of the DPI Formulation of 12TPP-Dendriplex/Mannitol Microparticles.....	95
4.2.11 Statistical Analysis.....	95
4.3 Results	96
4.3.1 Conjugation of TPP to G4NH ₂ Dendrimer.....	96
4.3.2 Preparation and Characterization of TPP-Dendriplexes	97
4.3.3 RNA Gel Complexation Assay.....	99
4.3.4 siRNA Release via Polyanion Competition	100
4.3.5 <i>In Vitro</i> Gene Knockdown.....	102
4.3.6 <i>In Vitro</i> Cytotoxicity	104
4.3.7 Preparation and Characterization of 12TPP-Dendriplex/Mannitol Microparticles	106
4.3.8 The <i>in vitro</i> Aerosolization of 12TPP-Dendriplex/mannitol Microparticles Formulated as Dispersions in HFA-based pMDIs.....	107
4.3.9 The <i>in vitro</i> Aerosolization of DPI Formulation of 12TPP-Dendriplex/Mannitol Microparticles	109

4.4 Discussion	110
4.5 Conclusion.....	117
4.6 Acknowledgements.....	118
CHAPTER 5 – SYNTHESIS OF ASYMMETRIC DENDRIMERS CONTAINING DOX AND VARIOUS SURFACE MODIFICATIONS BY CLICK CHEMISTRY	119
5.1 Introduction	119
5.2 Materials and Methods.....	123
5.2.1 Materials.....	123
5.2.2 Conjugation of lauryl alcohol (LA) with succinic anhydride (SA) form lauryl-succinic acid (LA-SA)	124
5.2.3 Conjugation of LA-SA to Azido-G5-OH (N ₃ -G5-OH) dendron to form Azido-G5-LA	124
5.2.4 Conjugation of polyethylene glycol (PEG) with succinic anhydride to form PEG-SA	125
5.2.5 Conjugation of succinic anhydride (SA) to N ₃ -G5-OH to form N ₃ -G5-SA	125
5.2.6 Conjugation of Boc-6-Ahx-OH to N ₃ -G5-OH dendron followed by Boc deprotection to form N ₃ -G5-NH ₂ dendron	126
5.3 Results	126
5.3.1 Conjugation of lauryl alcohol (LA) with succinic anhydride (SA) form lauryl-succinic acid (LA-SA)	126
5.3.2 Conjugation of LA-SA to Azido-G5-OH (N ₃ -G5-OH) dendron to form Azido-G5-LA	127
5.3.3 Conjugation of polyethyleneglycol (PEG) with succinic anhydride to form PEG-SA.	128
5.3.4 Conjugation of PEG-SA to N ₃ -G5-OH to form N ₃ -G5-PEG dendron	129
5.3.5 Conjugation of succinic anhydride (SA) to N ₃ -G5-OH to form N ₃ -G5-SA	130
5.3.6 Conjugation of Boc-6-Ahx-OH to N ₃ -G5-OH dendron followed by Boc deprotection to form N ₃ -G5-NH ₂ dendron	131

5.4 Discussion	133
5.5 Conclusions.....	138
5.6 Acknowledgements.....	138
CHAPTER 6 – LOCALLY ADMINISTERED IMMUNOMODULATORS FOR MACROPHAGE REPOLARIZATION AND COMBINATION CHEMOTHERAPY FOR THE TREATMENT OF LUNG CANCERS	139
6.1 Introduction	139
6.2 Materials and Methods.....	142
6.2.1 Materials.....	142
6.2.2 Synthesis and Characterization of G4SA-hyd-DOX (DDOX).....	143
6.2.3 Cell Culture	144
6.2.4 Animals for <i>In Vivo</i> Experiments	144
6.2.5 Transformation of 4T1 Cells to Express tdTomato Fluorescence and Luciferase Bioluminescence.....	145
6.2.6 <i>In Vitro</i> Bioluminescence Kinetics Assay of 4T1-luc-tdTomato cells.....	146
6.2.7 Evaluation of 4T1-luc-tdTom Metastatic Growth to the Lungs in Female BALB/C mice	147
6.2.8 <i>In vivo</i> efficacy of PLX3397 for the treatment of Lung Metastases.....	148
6.2.9 Measurement of Macrophage Polarization by Flow Cytometry.....	149
6.2.10 Statistical Analysis.....	150
6.3 Results	150
6.3.1 Synthesis and Characterization of G4SA-hyd-DOX (DDOX).....	150
6.3.2 Transformation of 4T1 Cells to Express tdTomato Fluorescence and Luciferase Bioluminescence.....	151
6.3.3 <i>In Vitro</i> Bioluminescence Kinetics Assay of 4T1-luc-tdTomato cells.....	153
6.3.4 Evaluation of 4T1-luc-tdTom Metastatic Growth to the Lungs in Female BALB/C mice	154

6.3.5 <i>In vivo</i> efficacy of PLX3397 (PLX) for the treatment of Lung Metastases ...	157
6.3.6 Measurement of Macrophage Polarization by Flow Cytometry.....	161
6.4 Discussion	162
6.5 Conclusion.....	169
6.6 Acknowledgements.....	170
CHAPTER 7 – CONCLUSIONS AND FUTURE DIRECTIONS	172
APPENDIX A – SUPPORTING INFORMATION FOR CHAPTER 3.....	181
APPENDIX B – SUPPORTING INFORMATION FOR CHAPTER 4.....	183
APPENDIX C – SUPPORTING INFORMATION FOR CHAPTER 5.....	185
APPENDIX D – SUPPORTING INFORMATION FOR CHAPTER 6.....	194
APPENDIX E – PUBLICATION 1	201
APPENDIX F – PUBLICATION 2	202
APPENDIX G – PUBLICATION 3.....	203
REFERENCES.....	204
ABSTRACT	246
AUTOBIOGRAPHICAL STATEMENT.....	248

LIST OF TABLES

Table 3.1	The hydrodynamic diameter (HD) and surface charge (zeta potential, ζ) of the dendrimer conjugates measured by light scattering (LS). Measurements were performed in water. Data expressed as mean \pm standard deviation ($n \geq 3$). All carriers have an average of 2 FITC per G4NH ₂	64
Table 4.1	Characterization of G4NH ₂ -siRNA complexes by Light Scattering. Hydrodynamic diameters (HD), Polydispersity Index (PDI), and zeta potential (ζ) are summarized as a function of number density of TPP per G4NH ₂ (0-12) and also as a function of N/P ratio (5-30). HD was based on intensity measurements. HD = mean \pm s.d., PDI = mean \pm s.d., ζ = mean \pm s.d.....	98
Table 4.2	Hydrodynamic diameters (HD), Polydispersity Index (PDI), and zeta potential (ζ) of 12TPP-dendriplex (N/P 30) before formulation in mannitol-based microparticles and after reconstitution in DI H ₂ O. Light Scattering performed in DI water.....	107
Table 5.1	Characterization of modified Azido-G5-OH dendrons *MW based on MALD-TOF results.....	134
Table B1	Deposition of dendriplex mannitol micron particles (weight) and siRNA (densitometry) on different stages of the Andersen Cascade Impactor (ACI) from a pMDI formulation at a flow rate of 28.3 L/min. pMDI formulations at 2 mg microparticles/1 mL HFA227 propellant at 25 °C and saturation pressure of propellant. The payload of siRNA in microparticle is 0.025% wt/wt. The results were based on 20 actuations and represented with mean \pm s.d. ($n=3$). AC: actuator, IP: induction port, 0-7: plate 0-7, and F: filter. RF, FPF, MMAD and GSD refer to respirable fraction, fine particle fraction, mass median aerodynamic diameter and geometric standard deviation, respectively.....	183
Table B2	siRNA Deposition on the different stages of Andersen Cascade Impactor (ACI), as determined by densitometry. The 10-20 mg micron particles loaded into capsule were released into ACI from Rotahaler® (DPI formulation) at 25°C, 75% relative humidity, and a flow rate of 28.3 L/min for 4 s inspiration. The results are represented with mean \pm s.d. ($n=3$). IH: inhaler, IP: induction port, 0-7: plate 0-7, and F: filter. ED, RF, FPF, MMAD and GSD refer to emitted dose, respirable fraction, fine particle fraction, mass median aerodynamic diameter and geometric standard deviation, respectively.....	184

Table D1	p-values calculated after One-Way ANOVA by Tukey's Multiple Comparison (n≥6) for % tumor growth seen on Day 15 post tumor inoculation.....	199
Table D2	IC50 values of drugs when tested against 4T1-WT cells line. This was conducted after 48 h incubation and measured by MTT. DOX= doxorubicin, DDOX= PAMAM G4COOH-DOX conjugate, DOXTPP = Triphenylphosphonium-modified doxorubicin, DDOXTPP = PAMAM G4COOH-DOXTPP conjugate.....	200

LIST OF FIGURES

- Figure 2.1** **A) Metastasis.** Metastasis in cancer is when primary tumor cells break away from initial tumor, travel through the blood or lymph system to form new tumors (metastatic tumors) in other tissues or organs within the body;¹¹² **B) Steps of Metastasis.** Several steps are required for metastasis. First, the cell breaks free from primary tumor and through the stroma to reach the vasculature - intravasation. Once in the bloodstream (or lymph), the cancer cells express certain markers, circulate, and distribute to distant sites depending on the interaction of cancer cells and secondary organs in which they colonize. After reaching a secondary target organ site, they cancer cells can exit the bloodstream, and begin to proliferate by releasing pro-inflammatory compounds, inducing angiogenesis, and releasing other growth factors.⁸.....20
- Figure 2.2** **Various Mechanisms of multidrug resistance.** This includes efflux pumps, enhanced DNA repair, inactivation of drugs by metabolic pathways or mutation or altered drug targets, drug compartmentalization, and inactivation to apoptosis.²³.....25
- Figure 2.3** Representation of dendrimers demonstrating their structure. They comprise of a central core, repeating branches, and increase in number of surface groups with each generation.³⁵.....30
- Figure 2.4** Mitochondrial changes seen in cancer cells including transformed metabolism and alterations that make them resistant to apoptosis.⁶⁷.....34
- Figure 2.5** Promising direct and indirect targets for cancer therapies to induce apoptosis. ROS: reactive oxygen species, ER: endoplasmic reticulum, Nox: NADPH oxidase, OXPHOS: oxidative phosphorylation, TP50: translocator protein, cypD: cyclophilin D, HKII: hexokinase II, VDAC: voltage-dependent anion channel, MMP: mitochondrial membrane permeabilization.⁶⁷.....35
- Figure 2.6** The RNAi mechanism. The double-stranded RNA is cleaved by Dicer protein into siRNAs in ATP-dependent process. The siRNAs are incorporated in RISC complex, which unwinds the double stranded siRNA, which also requires ATP. Once unwound, the guide siRNA strand guides RISC to mRNA that has a complementary sequence, which leads to cleavage of the target mRNA.¹⁸⁸.....41
- Figure 2.7** General scheme of how Bcl-2 regulates intrinsic (mitochondrial) apoptosis. Bcl-2 is found on the outer mitochondrial membrane and interacts with Bak/Bax proteins, which prevents apoptosis from occurring. Stress induces BH3-only proteins to interact with Bcl-2, which allows Bcl-2 to disassociate

from Bak/Bax proteins. The Bak/Bax proteins can oligomerize and initiate mitochondrial outer membrane permeabilization, release of cytochrome c and other pro-apoptotic factors that initiate caspases and lead to programmed cell death.²⁰⁵.....43

Figure 2.8 Comparison of different lung epithelium at different lung regions. Aerosol particles can penetrate deeper in the lungs as the epithelium becomes thinner.²¹⁶.....45

Figure 2.9 Stimulation or suppression of the immune system by TAMs. Depending on the TME, the cytokines emitted by tumor cells, fibroblasts or other stromal cells, immune cells, and macrophages themselves that can polarize TAMs to M1-like or M2-like. M2 TAMs promote tumor growth (not illustrated here) as well as suppress various immune effector cells directly or through other immune cells that lead to tumor cell elimination. M1 TAMs can either directly kill tumor cells or stimulate/inhibit other immune cells to kill tumor cells by releasing of various cytokines/chemokines. M2 TAMs are known to express colony-stimulating factor 1 receptor (CSF1R) and is essential to their function, making CSF1R a desirable therapeutic target to eliminate/repolarize these cells.²⁰.....50

Figure 2.10 CSF1R activation. CSF1/IL-34 bind to ligand causing homodimerization. Subsequent phosphorylation (P) and ubiquitination (Ub) lead to receptor to be fully activated. Phosphorylation of 550 residue and ubiquitination are critical in further tyrosine phosphorylation and activation.²²⁴.....51

Figure 2.11 Examples of various CSF1R signaling blocking agents. PLX3397 is a tyrosine kinase inhibitor.²²².....52

Scheme 3.1 Synthesis of **A**) FTIC-labeled, generation 4, amine-terminated poly(amidoamine) dendrimer (*G4NH₂-FITC*); **B**) TPP-conjugated, FITC-labeled *G4NH₂* (*G4NH₂-TPP*); and **C**) **(i)** TPP-conjugated poly(ethylene glycol) 1000 MW (PEGTPP), and **(ii)** PEGTPP-conjugated, FITC-labeled *G4NH₂* (*G4NH₂-PEGTPP*).....63

Figure 3.1 Cell viability of **A**) *G4NH₂-TPP* conjugates and **B**) *G4NH₂-PEGTPP* conjugates measured by MTT assay at 24h incubation and increasing nanocarrier concentration. *, **, *** represents the statistical analysis between the control group indicated at 0 μM representing 100% viability. ●, ●●, and ●●● represents the statistical analysis between *G4NH₂-0TPP* group and other indicated dendrimer conjugates (* / ● p < 0.05, ** / ●● p < 0.01, *** / ●●● p < 0.001).....66

- Figure 3.2** Cellular uptake of **A)** G4NH₂-TPP conjugates and **B)** G4NH₂-PEGTPP conjugates analyzed by FACS. The median fluorescence intensity (MFI) provided by FITC labeling of the various conjugates was compared to bare FITC-labeled dendrimer (0 TPP) at various time points (* p < 0.05, ** p < 0.01 *** p < 0.001).....69
- Figure 3.3** A comparison of the cellular uptake of G4NH₂-10PEG and G4NH₂-10PEGTPP conjugates analyzed by flow cytometry. The MFI provided by FITC labeling of the various conjugates was compared between the two groups using two-tailed t test (* p < 0.05, ** p < 0.01 *** p < 0.001).....71
- Figure 3.4** Colocalization between dendrimer (green) and mitochondria (red) to assess the targeting ability of the various G4NH₂-TPP and G4NH₂-PEGTPP conjugates. The blue represents the nucleus (Hoeschst 3342-Nuc Blue stain), the red represents mitochondria (Mitotracker Deep Red FM) and green represents the dendrimer (FITC). The yellow color represents the overlap between the dendrimer and mitochondria signals. The dendrimer conjugates are seen in the following order: A) G4NH₂-0TPP, B) G4NH₂-5TPP, C) G4NH₂-10TPP, D) G4NH₂-5PEGTPP, E) G4NH₂-10PEGTPP, and F) G4NH₂-21PEGTPP.....72
- Figure 3.5** Pearson's Correlation Coefficient (PCC) of various dendrimer conjugates comparing the overlap of FITC (dendrimer) with Mitotracker Deep Red FM (mitochondria) based on confocal microscopy. *** compares each dendrimer conjugate with G4NH₂-0TPP dendrimer. ●●● represents the comparison between indicated groups. Data represents a mean ± standard deviation (***/●●● p < 0.001, n.s.d. = not statistically different).....73
- Scheme 4.1** Schematic of the TPP conjugation to the amine-terminated, generation 4 poly(amido)amine (PAMAM) dendrimer (G4NH₂). A) TPP is activated using EDC/NHS coupling to form TPP-NHS in DMSO. B) G4NH₂ was then later added to the activated TPP (TPP-NHS) in DMSO and allowed to react to form G4NH₂-TPP dendrimer conjugate. The amount of TPP-NHS added to the reaction mixture determined the conjugation density with the final density of TPP per dendrimer of ~ 0, 4, 8, 12 TPP.....96
- Figure 4.1** ¹H NMR characterization of G4NH₂-TPP conjugates in D₂O. The chemical structure is shown above with the corresponding peak shifts labeled within the spectrum.....97
- Figure 4.2** Scanning electron microscopy (SEM) of 12TPP-dendriplex at N/P 30. The geometric diameter represents ~ 340 particles.....99

- Figure 4.3** The siRNA complexation efficiency as a function of N/P ratio as visualized by gel electrophoresis. The dendriplexes were prepared with various ratios of TPP (as indicated to the left). The first lane contains untreated non-complexed siRNA as control and subsequent lanes with increasing N/P ratios as shown.....100
- Figure 4.4** Polyanion competition assay visualized by gel electrophoresis. The stability of the dendriplexes was tested for 0TPP-dendriplex (N/P 30) and 12TPP-dendriplex (N/P 30) by exposing each to increasing amounts of heparin. C = siRNA only, used as a control.....101
- Figure 4.5** *In vitro* gene knockdown of eGFP expression in stably expressing eGFP A549 cells. The dendriplexes (Dplex) were prepared at N/P ratio of 30 with eGFP siRNA and G4NH₂-TPP conjugates. The specificity of the knockdown was performed by comparing dendriplexes with a scramble eGFP sequence (-siRNA) to the correct corresponding eGFP sequence (+siRNA). Non-complexed siRNA (siRNA) was used as a negative control and the commercial reagent Lipofectamine 2000 (L) was used as a positive control. 20 pmol of siRNA (80 nM) was used for each sample while the amount of dendrimer-TPP ranged from 1.2-11.5 µg (0.3-2.4 µM) depending on the desired N/P ratio and TPP density of TPP-dendrimer sample. * represents a statistical difference ($p < 0.05$) between the non-complexed +siRNA and various +siRNA groups, while ρ represents a statistical difference of +siRNA between indicated groups as analyzed by One-Way ANOVA followed by Tukey's Multiple Comparison Test ($n \geq 3$) ($p < 0.05$), n.s.d. = not statistically different.....102
- Figure 4.6** Viability of eGFP A549 cells contacted with G4NH₂-TPP-siRNA dendriplexes (12TPP-dendriplexes) formed at N/P 30, as measured with an MTS assay after a 48-hour incubation with the dendriplex. The concentration of the dendriplex used was the same as the *in vitro* knockdown experiments. Statistical analysis was run between the control group (no dendriplex) representing 100 % cell viability, and the dendriplex formed with G4NH₂ with varying TPP density. One-Way ANOVA followed by Tukey's Multiple Comparison Test ($n \leq 3$). n.s.d. = not statistically different.....104
- Figure 4.7** The cell viability of eGFP A549 cells contacted with G4NH₂-12TPP dendriplex (12TPP-dendriplex) formed at N/P 30 as measured by the MTS assay after 48 h incubation and increasing dendriplex concentration. * represents the statistical analysis between the control group indicated at 0 µM representing 100 % cell viability and those of increasing concentrations,

as analyzed by One-Way ANOVA followed by Tukey's Multiple Comparison Test ($n \leq 3$). n.s.d. = not statistically different.....105

Figure 4.8 Scanning electron microscopy (SEM) of dendriplex/mannitol microparticles prepared by spray drying. The geometric diameter of dendriplex/mannitol particle (inset) represents the average of over 300 particles. Higher magnification image is shown as inset.....106

Figure 4.9 Deposition of 12TPP-dendriplex/mannitol microparticles on different stages of the Andersen Cascade Impactor (ACI) from a pMDI formulation at a flow rate of 28.3 L/min, as determined by siRNA densitometry method and particle mass method. pMDI formulations at 2 mg microparticles/1 mL HFA227 propellant at 25°C and saturation pressure of propellant. The payload of siRNA in microparticle is 0.025% wt/wt. The results were based on 20 actuations and represented with mean \pm s.d. ($n=3$). Statistical analysis was performed with Student t-test ($*p<0.05$). AC: actuator, IP: induction port, 0-7: plate 0-7, and F: filter.....108

Figure 4.10 Deposition of 12TPP-dendriplex/mannitol microparticles on the different stages of Andersen Cascade Impactor (ACI), as determined by siRNA densitometry method. The 10-20 mg micron particles loaded into capsule were released into ACI from Rotahaler® (DPI formulation) at 25°C, 75% relative humidity, and a flow rate of 28.3 L/min for 4 s inspiration. The results are represented with mean \pm s.d. ($n=3$). IH: inhaler, IP: induction port, 0-7: plate 0-7, and F: filter.....109

Scheme 5.1 The modification of LA to contain -COOH group by addition of succinic anhydride (SA) to form LA-SA.....126

Figure 5.1 **A)** Chemical structure of LA and LA-SA and the corresponding **B)** ^1H NMR and **C)** MALDI-TOF spectra.....127

Scheme 5.2 The modification of $\text{N}_3\text{-G5-OH}$ dendron to contain lauryl surface by addition of LA-SA to form $\text{N}_3\text{-G5-LA}$; Azido = N_3128

Figure 5.2 **A)** Chemical structure of $\text{N}_3\text{-G5-OH}$ and $\text{N}_3\text{-G5-LA}$, and the corresponding **B)** ^1H NMR and **C)** MALDI-TOF spectra.....128

Scheme 5.3 The modification of PEG to contain -COOH group by addition of SA to form PEG-SA.....129

Figure 5.3 **A)** Chemical structure of PEG and PEG-SA, and the corresponding **B)** ^1H NMR and **C)** MALDI-TOF spectra.....129

- Scheme 5.4** The modification of N₃-G5-OH with PEG by addition of PEG-SA to form N₃-G5-PEG.....130
- Figure 5.4** **A)** Chemical structure of N₃-G5-OH and N₃-G5-PEG, and the corresponding **B)** ¹H NMR and **C)** MALDI-TOF spectra.....130
- Scheme 5.5** The modification of N₃-G5-OH to contain -COOH surface by addition of SA to form N₃-G5-SA.....131
- Figure 5.5** **A)** Chemical structure of N₃-G5-OH and N₃-G5-SA, and the corresponding **B)** ¹H NMR and **C)** MALDI-TOF spectra.....131
- Scheme 5.6** The modification of N₃-G5-OH to contain -NH₂ surface by addition of **A)** AHA-Boc followed by **B)** Boc deprotection to form N₃-G5-NH₂.....132
- Figure 5.6** **A)** Chemical structure of N₃-G5-OH and N₃-G5-Boc, and N₃-G5-NH₂, and the corresponding **B)** ¹H NMR and **C)** MALDI-TOF spectra.....133
- Figure 6.1** Flow cytometry results of 4T1-luc-tdTomato cells after puromycin selection and sorting twice from cell sorter. **A)** Dot plots and **B)** histogram plots of wild-type 4T1 (green) and 4T1-luc-tdTomato cells (blue) distinguish a distinct cell population based on tdTomato fluorescence.....153
- Figure 6.2** *In vitro* kinetics assay of 4T1-luc-tdTomato cells. **A)** IVIS images of cells seeded in 96-well plate (cell numbers listed – max of 250,000 cells/well) and exposed to d-luciferin, each repeated in triplicate; **B)** plot of kinetics of bioluminescent signal (total flux) over time at different cell densities.....154
- Figure 6.3** Preliminary tumor growth experiment. **A)** IVIS images of mice from day 5 go day 18 after TV injection of 100k 4T1-luc-tdTomato cells. **B)** Measurement of total flux from IVIS images by combined signal from the dorsal and ventral side of each mouse focused in the lung region area...155
- Figure 6.4** Preliminary tumor growth experiment from TV injection of 250k 4T1-luc-tdTomato cells. **A)** *in vivo* IVIS images of dorsal and ventral side of mouse over 12 days post TV injection of tumor cells. **B)** IVIS images of lungs taken on specific days after TV injection. The number below lung refers to mouse number. **C)** Total flux (flux of ventral and dorsal images combined focused on lung region) from *in vivo* IVIS images of mice over various days post TV injection. **D)** Total flux taken from lungs on each day.....156

- Figure 6.5** The *in vivo* treatment strategy plan in treatment of lung metastases induced by 4T1-luc-tdTomato cells. 250k cells were injected TV in female BALB/C mice. Monitoring of tumor growth began by *in vivo* IVIS imaging of mice on Day 5 post tumor inoculation and continued for every other day till day 15. Treatment was given three times on days 7, 9, and 11 post-tumor implantation. Mice were sacrificed on Day 15.....157
- Figure 6.6** Evaluation of lung tumor burden by *ex vivo* imaging of lungs using IVIS. **A) & D)** *Ex vivo* lung images of treatment groups. **B & E)** corresponding total flux of lungs by combining flux of lungs imaged on two sides for each group as evaluated from IVIS images. **C & F:** Corresponding p-values comparing total flux of groups after running One-Way ANOVA analysis followed by Tukey's Multiple Comparison Test. All drugs were given via pulmonary route except PLX[#] group seen in D) in which PLX was delivered IV route.....158
- Figure 6.7** Average lung weight for corresponding group with **A)** representing first experimental group in which all drugs were given via pulmonary route and **B)** the second experimental group in which DDOX and DDOX+PLX were given pulmonary route and PLX[#] was given IV route, (*p<0.05, **** p<0.0001, n.s.d. = not statistically different).....160
- Figure 6.8** Macrophage tracking by flow cytometry. **A)** % total of macrophages compared to all cells in lung sample. **B)** % of Cells considered M1 TAM phenotype. **C)** % of cells considered that of M2 TAM phenotype.....161
- Figure A1** ¹H NMR spectra of the A) G4NH₂-FITC-TPP and B) G4NH₂-FITC-PEGTPP dendrimer conjugates in D₂O at 400 MHz on Agilent Mercury Spectrometer. The chemical structures are shown above with the corresponding peak shifts.....182
- Figure B1** The cell viability of A549 cells contacted with Lipofectamine® 2000 reagent at increasing concentrations as measured by the MTS assay after 48 h incubation. Statistical analysis between the control group indicated at 0 μM representing 100 % cell viability and those of increasing concentrations was analyzed by One-Way ANOVA followed by Tukey's Multiple Comparison Test (n < 7). **p ≤ 0.01, *** p < 0.001, n.s.d. = not statistically different.....185
- Scheme C1** Deprotection of GLFG-Fmoc from the resin. AcOH: acetic acid, TFE: Trifluoroethanol, DCM: dichloromethane. G-L-F-G: Peptide of glycine-leucine-phenylalanine – glycine.....187

- Scheme C2** **A)** Conjugation of DOX to GLFG-Fmoc to form DOX-GLFG-Fmoc, **B)** Deprotection of Fmoc from DOX-GLFG-Fmoc to form DOX-GLFG. EDC: (1-(3-Dimethylaminopropyl)-3-ethylcarbodiimide hydrochloride DIPEA: N,N-Diisopropylethylamine, DMF: dimethylformamide.....188
- Scheme C3** The modification of Acet-G5-OH dendron to contain -COOH group by addition of GA to form Acet-G5-GA. Acet-G5-OH: Acetylene Generation 5 Bis-MPA polyester dendron, DIPEA: N,N-Diisopropylethylamine, DMF: dimethylformamide.....189
- Figure C1** **A)** Chemical structure of Acet-G5-OH and Acet-G5-GA and the corresponding **B)** ¹H NMR and **C)** MALDI-TOF spectra.....191
- Scheme C4** Conjugation of DOX-GLFG to Acet-G5-GA dendron to form Acet-G5-GA-GFLG-DOX dendron. EDC: (1-(3-Dimethylaminopropyl)-3-ethylcarbodiimide hydrochloride NHS: N-Hydroxysuccinimide, DMF: dimethylformamide.....191
- Scheme C5** Conjugation of HO-G5-OH dendrimer from to Acet-G5-OH and N₃-G5-OH dendrons utilizing copper click chemistry. DIPEA: N,N-Diisopropylethylamine, DMF: dimethylformamide, ACN: Acetonitrile.....192
- Figure C2** MALDI-TOF of purified HO-G5-OH dendrimer after size exclusion chromatography. The expected MW (7393.9) as determined found for dendrimer while only very insignificant amount of dendrons remained in the product (Acet-G5-OH – 3634.7, N₃-G5-OH – 3770.8).....193
- Scheme D1.** **A)** Synthesis of hydrazine bond to the G4SA PAMAM dendrimer. TBC is added to G4SA by addition of NMM and IBCF in DMSO/DMF (10/90, v/v) followed by Boc deprotection by exposure to TFA/DCM (80/20, v/v). **B)** DOX addition by hydrazone bond was completed with TFA as acid catalyst and MeOH as solvent. G4SA: Generation 4 PAMAM succinamic acid surface dendrimer DMSO: dimethylsulfoxide DMF: dimethylformamide TBC: tert-butyl carbazate NMM: N-Methylmorpholine IBCF: isobutyl chloroformate TFA: trifluoroacetic acid DCM: dichloromethane MeOH: methanol DOX: doxorubicin.....194
- Figure D1** **A)** The chemical structure and corresponding ¹H NMR and **B)** the MALDI-TOF of G4SA, G4SA-TBC, G4SA-hyd, G4SA-hyd-DOX.....195
- Figure D2** Puromycin kill curve. 4T1 cells were exposed to various concentrations of puromycin (0-10 µg/ml) for 48 hours to determine the minimum amount of puromycin to kill all 4T1 cells.....196

- Figure D3** % Average body weight of mice for **A)** first experimental group in which all drugs administered were given pulmonary route and **B)** second experimental group in which DDOX and DDOX+PLX groups were given pulmonary route and PLX[#] was given IV route.....197
- Figure D4** Evaluation of lung tumor burden by *in vivo* imaging of mice near lung region using IVIS. **A) & C)** % Tumor growth rate over time. Day 7 total flux from *in vivo* IVIS images was normalized to 100% for each mouse. **B & D)** The corresponding % Tumor growth *in vivo* on Day 15 – final day of experiment imaged on two sides for each group as evaluated from IVIS images, *p<0.05. All drugs were given via pulmonary route except PLX[#] group seen in D) in which PLX was delivered IV route.....198
- Figure D5** % Cell viability (measured by MTT) of doxorubicin and modified doxorubicin formulations against 4T1-WT cells after 48-hour incubation. DOX= doxorubicin, DDOX= PAMAM G4COOH-DOX conjugate, DOXTPP = Triphenylphosphonium-modified doxorubicin, DDOXTPP = PAMAM G4COOH-DOXTPP conjugate.....200

LIST OF ABBREVIATIONS

¹H NMR	proton nuclear magnetic resonance
1xHBSS	1x Hank's Buffered Saline Solution
5-FU	5-Fluorouracil
ABC	ATP-Binding cassette
ACI	Anderson Cascade Impactor
AHA-Boc	6-(Boc-amino)hexanoic acid
BCRP	breast cancer resistance protein
Bis-MPA	2,2-bis(hydroxymethyl)propionic acid
CSCs	cancer stem cells
CSF1	colony-stimulating factor 1
CSF1R	colony-stimulating factor 1 receptor
CSF1Ri	colony-stimulating factor 1 receptor inhibitors
CTLA-4	cytotoxic T-lymphocyte-associated protein 4
DCM	dichloromethane
DDOX	G4SA-hyd-DOX (G4 PAMAM dendrimer-DOX conjugate)
DHB	2,5-dihydroxybenzoic acid
DI water	deionized water
DIPEA	N,N-Diisopropylethylamine
DLS	dynamic light scattering
DMAP	4-(Dimethylamino)pyridine
DMEM	Dulbecco's Modified Eagle Medium 1x high glucose
DMF	N,N-Dimethylformamide

DMSO	Methylsulfoxide
DNCs	dendrimer nanocarriers
DOX	doxorubicin
DOXTPP	triphenylphosphonium-modified doxorubicin
DPI	dry powder inhaler
ED	emitted dose
EDC	N-(3-dimethylaminopropyl)-N'-ethylcarbodiimide
eGFP	enhanced Green Fluorescent Protein
ER	estrogen receptor
Et₂O	ethyl ether
ETC	electron transport chain
FACS	flow associated cell sorting (flow cytometry)
FITC	fluorescein isothiocyanate
FPF	fine particle fraction
G4NH₂	Generation 4 amine-terminated PAMAM dendrimer
G4NH₂-PEGTPP	PAMAM dendrimer modified with PEGTPP
G4NH₂-TPP	PAMAM dendrimer modified with TPP
GA	glutaric anhydride
GFLG	glycine-phenylalanine-leucine-glycine peptide
GSD	geometric standard deviation
HER2	human epidermal growth factor receptor 2
HFAs	hydrofluoroalkanes
IAPs	inhibitor of apoptosis proteins

IBCF	isobutyl chloroformate
IL	interleukin
IV	intravenous
IVIS	in vivo imaging system
LA	lauryl alcohol
LS	light scattering
MALDI-TOF	Matrix-Assisted Laser Desorption Ionization Time-of-Flight
MDR	multidrug resistance
MDR1	multidrug resistance protein 1
MeOH	methanol
MFI	Median Fluorescence Intensity
MMAD	mean mass aerodynamic diameter
mRNA	messenger RNA
MRP1	MDR-associated protein 1
MTX	methotrexate
MWCO	Molecular Weight Cut Off
N₃-G5-OH	azido-terminated generation 5 Bis-MPA polyester dendron
NHS	N-Hydroxysuccinimide
NMM	N-Methylmorpholine
NSCLC	non-small cell lung cancer
OI	oral inhalation
PA	pulmonary administration
PAMAM	poly(amidoamine)

PCC	Pearson's correlation coefficient
PD1	programmed death 1
PDL1	programmed death ligand 1
PEG	polyethylene glycol
PEGTPP	polyethylene glycol modified with triphenylphosphonium ion (TPP)
PEI	poly(ethylene imine)
P-gp	p-glycoprotein
PLL	poly-L-lysine
PLX	PLX3397, Pexidartinib
pMDIs	pressurized metered dose inhalers
PNCs	polymeric nanocarriers
PPI	polypropyleneimine
PR	progesterone receptor
RF	respirable fraction
RISC	RNA induced silencing complex
RNAi	RNA interference
ROS	reactive oxygen species
SA	succinic anhydride
SEM	scanning electron microscopy
siRNA	short interfering RNA
TAMs	tumor associated macrophages
TBC	tert-butyl carbazate
TEA	triethylamine

TEER	transepithelial electrical resistance
TFA	trifluoroacetic acid
TME	tumor microenvironment
TPP	triphenylphosphonium
TPP-dendriplexes	siRNA complexed with G4NH ₂ -TPP PAMAM dendrimers
TV	tail vein

LIST OF ORIGINAL PUBLICATIONS

This dissertation is based on the following publications:

1. **Elizabeth R. Bielski**,^{1,2} Qian Zhong,^{1,3} Matthew Brown,¹ and Sandro R. P. da Rocha.^{1,2} Effect of the Conjugation Density of Triphenylphosphonium Cation on the Mitochondrial Targeting of Poly(amidoamine) Dendrimers. *Molecular Pharmaceutics* 2015, 12(8): 3043-3053.
2. Qian Zhong,^{1,3} **Elizabeth R. Bielski**,^{1,2} Leonan S. Rodrigues,¹ Matthew R. Brown,¹ Joshua J. Reineke,⁴ and Sandro R. P. da Rocha.^{1,2} Conjugation to Poly(amidoamine) Dendrimers and Pulmonary Delivery Reduce Cardiac Accumulation and Enhance Antitumor Activity of Doxorubicin in Lung Metastasis. *Molecular Pharmaceutics* 2016 13 (7): 2363-2375.
3. **Elizabeth Bielski**,^{1,2} Qian Zhong,^{1,3} Hamad Mirza,¹ Matthew Brown,¹ Ashura Molla,¹ Teresa Carvajal,⁵ Sandro R. P. da Rocha.^{1,2} Dendrimer-TPP Conjugates as Carriers for siRNA Delivery and their Dry Powder and Metered-dose Inhaler Formulations. *International Journal of Pharmaceutics* 2017, 527 (1-2): 171-183.

¹Department of Chemical Engineering and Materials Science, Wayne State University, Detroit, MI USA

²Department of Pharmaceutics, Virginia Commonwealth University, Richmond, VA, USA

³Radiology Department, Stanford University, Stanford, CA, USA

⁴Department of Pharmaceutical Sciences, South Dakota State University, Brookings, SD, USA

⁵Department of Agricultural & Biological Engineering, Purdue University, West Lafayette, IN, USA

CHAPTER 1 – INTRODUCTION

1.1 Overview and Objectives

Despite the many clinical advances in cancer treatment, *lung cancer* still remains one of the most prevalent cancers worldwide with 1.8 million new cases and 1.6 million deaths occurring in 2012.¹ It remains as the second leading cancer in estimated new cases and the leading cause of cancer related deaths in the United States for both men and women.² Most cases (57%) are diagnosed at the advanced stage of the disease (metastasized to other sites) which has kept the overall 5-year survival rate at diagnosis to 18.6% with half of those initially diagnosed expected to die within the year.³⁻⁵ Those at the metastatic stage (57% of cases) have only a five-year survival rate of 4.7%. Only a small decrease in lung cancer incidence and deaths (2.1% and 2.7%) has been seen in the past decade, which negatively compares with other forms of cancer such as prostate cancer which as seen a 10% annual decrease in incidence from 2010-2014 with colorectal cancer incidence rates declining 2-3% annually from 2005-2014.^{2, 3} Therefore, new therapeutic strategies to manage lung cancer are greatly needed.

Not only does primary lung cancer pose a serious challenge, secondary lung tumors that metastasize to the lungs from other primary tumors can be found in 30-55% of all cancer patients.⁶ This is an indicator of advanced stages of cancer, in which treatment for such cases proves to be more challenging. Of these cancers, breast cancer (the second- leading cause of cancer-related deaths for women and 1st in estimated new cases)² commonly metastasizes to the lung;^{7, 8} it is this metastatic stage – the metastases themselves – and not the primary tumor that is the true leading cause of death in such patients.^{9, 10} Metastatic relapses to the lungs (primary or secondary) is observed in

majority of patients, and chemoresistance that develops in most cases after clinical treatment including chemotherapy is what ultimately becomes the leading cause of death for these patients.^{6, 9, 11} Most metastasis cannot be cured.¹² Therefore, current clinical intervention most often fails in these cases leading a significant need to propose alternative pathways for treatment.

Current therapies often are used to slow tumor growth of alleviate symptoms.¹² The type of treatment strategy is highly dependent on tumor type and how advanced the stage of the cancer. For non-small cell lung cancer (comprises 85% of lung cancer cases)¹³ the most common treatment is surgery, radiation therapy, or chemotherapy, which can be given alone or in combination.¹⁴ In the advanced stages, radiation therapy chemotherapy, targeted therapy, or immunotherapy are used alone or in combination.¹⁴ Usually a combination of two drugs is used to increase therapeutic effectiveness for chemotherapy intervention.¹¹ Current therapies for breast cancer, as with lung cancer, also include surgery, radiation therapy, targeted therapy, and chemotherapy alone or in combination.¹⁵ In stage IV metastatic breast cancer, where secondary lung tumors can form, chemotherapy is the main treatment given.¹⁵ This includes triple-negative breast cancer, in which there are currently no effective targeted therapies that have yet been developed.^{15, 16} Also due to the unpredictability of metastasis development, chemotherapy is normally given as an adjuvant therapy in 80% of breast cancer cases.¹⁰ Chemotherapy is the main modality for treatment of metastatic cancers as well.

In recent years, significant advances in immunotherapy, especially in the field of immune-checkpoint inhibitors, has brought new hopes in clinical treatment for patients who suffer from primary and secondary lung tumors with several immune-checkpoint

inhibitors approved by FDA.¹⁷ Non-small cell lung cancer (NSCLC), which was once considered untreatable with immunological approaches, such as cancer vaccines, have now seen huge clinical benefit when in the advanced states of the disease with the treatment of immune checkpoint inhibitors.^{18, 19} However, only a small portion of the patients show response to this treatment, which includes a range of 15-25% of patients responding to immune various immune checkpoint inhibitors to cytotoxic T-lymphocyte-associated protein 4 (CTLA-4) receptor, programmed death-1 (PD-1), or programmed death ligand-1 (PD-L1).^{20, 21} This may be due to the heterogenous nature of NSCLC tumors and various resistance mechanisms that are not yet clearly understood.^{19, 20} This type of treatment has also led to immune-related adverse events in which the pathophysiology remains unknown, but may be related to the role of immune checkpoints in immunologic homeostasis.¹⁷ However, new alternative understanding in the tumor microenvironment (TME), and the search for alternative targets to mediate the immunosuppressive nature within the TME have kept advances in immunotherapies introduced in clinical trials.^{19, 20}

While new targets are being identified and issues related to long term side effects are still being understood, chemotherapy remains a significant part of treatment for primary and secondary lung cancer patients alone or in combination with immunotherapy.¹⁴ Since chemotherapy is a commonly used treatment modality in most advanced forms of cancers, including the metastatic form, and chemoresistance develops in most cases, chemoresistance is truly a formidable problem to be addressed. Acquired chemoresistance from treatment of tumors with various chemotherapeutics leads to cancerous cells developing multidrug resistance (MDR).^{22, 23} MDR remains one of the

major issues still facing effective cancer treatment.²³ Multiple genetic and environmental factors with tumors and the surrounding tumor microenvironment (TME) lead to the development of MDR and can vary from tumor to tumor.²⁴ Many of the MDR mechanisms include increased drug efflux out of cancerous tumors, alterations to drug via cellular metabolic pathways inactivating the drug, alteration in drug targets making drug ineffective, reduced apoptosis, increased DNA repair, compartmentalization of drugs, changes within the cell (genetic or epigenetic) that can influence the surrounding TME, presence of cancer stem cells, and molecular and genetic heterogeneity of cancerous cells within the tumor.²²⁻²⁴ Most MDR tumors utilize more than one of these resistant mechanisms simultaneously.²⁴ Due to this complexity in various MDR mechanisms, new drug delivery strategies to overcome these challenges are currently being developed. This has led to the use of a variety of nanotechnologies in the hope to overcome limitations seen by common chemotherapeutic treatments.²⁴

Nanotechnologies, such as polymeric nanocarriers (PNCs), have great potential in enhancing clinical treatment of cancers by improving drug availability and reducing systemic side effects by specific targeting of therapeutics to tissues of interest, which has proven to enhance clinical efficacy.²⁵⁻²⁷ Improved quality of life and longevity of patients has been demonstrated when specific targeting is used to selectively deliver chemotherapeutics towards malignancies, which has pushed many nanomedicines into the clinical phases for treatment of a variety of cancers.^{27, 28} Many PNCs can also be multifunctional, allowing for enhancement in many aspects of drug delivery including specific targeting, enhanced drug bioavailability, sustained drug release, decreased drug clearance, delivery of multiple drugs, controlled release of drug, and increased cellular

uptake, thus, enhancing overall drug efficacy and overcoming many resistance mechanisms to help address MDR.²⁷⁻³¹

Dendrimer nanocarriers (DNCs) represent a promising technology for delivery of chemotherapeutics.³² DNCs are tree-like polymers that have a central core with repeating branches.³³⁻³⁵ They have unique properties such high monodispersity,³³ small nm-scale range,³⁵ high density of surface groups that can be modified to increase solubility of therapeutic conjugated to the dendrimer,³³ multifunctionality for attachment of other targeting moieties or solubilizing groups,³⁴ controlled drug release,³⁴ controlled and reproducible pharmacokinetics,³⁶ enhanced targeting, and reduced systemic side effects to increase overall therapeutic efficacy.³⁴ These unique properties make DNCs particularly attractive choices for the delivery of both small molecules and biologics in the treatment of advanced lung cancers and secondary lung tumors.

DNCs can be synthesized via convergent or divergent synthesis strategies, and depending on the monomer chosen for synthesis, various classes of dendrimers have been formed including polyamidoamine (PAMAM), polypropyleneimine (PPI), poly-L-lysine (PLL), poly(glycerol-co-succinic acid), melamine, poly(glycerol), 2,2-bis(hydroxymethyl)propionic acid (Bis-MPA), poly(ethylene glycol) (PEG), and others.³⁷ Of those DNCs that have been formed, recently, polyester dendrimers made from Bis-MPA have emerged as a promising dendrimer chemistry, particularly for their biodegradability and decreased toxicity compared to other chemistries such as PAMAM dendrimers.³⁸ A significant amount of work on the use of Bis-MPAs for biomedical purposes has been more recently published.³⁹⁻⁴¹ Dendrons (Greek term for trees), is a class of dendritic architectures representing a branch or dendritic wedge-shaped

fragment in the tree-like structure.^{42, 43} Malkkoch et al. has explored the synthesis of bis-MPA polyester dendrimers by the conjugation of dendrons.⁴⁴ The conjugation of surface modified dendrons can be used to achieve controlled, stereo-specific bifunctionality so as to further modulate their interaction with the physiological environment.⁴⁵ Surface functionality plays a key role in *in vitro* cellular internalization and intracellular trafficking. It is known that the endocytic internalization and intracellular trafficking within cells can affect drug release and overall therapeutic performance as well as the biodistribution and pharmacokinetics,⁴⁶ as seen in methotrexate conjugated to cationic vs anionic dendrimers.⁴⁷ Consequently, choosing a desired surface functionality as well as linker between drug and dendrimer for conjugation can affect overall *in vitro* and *in vivo* therapeutic performance. Asymmetric dendrimers have been utilized for DOX delivery via hydrazone bond between dendrimer and DOX and polyethylene oxide conjugated to other side, and demonstrated less toxicity than free drug *in vitro*, however, demonstrated efficacy *in vivo* similar to that of Doxil.⁴⁰ Nevertheless, little is known on how asymmetry, varying surface chemistries, and route of delivery can affect overall therapeutic performance against lung tumors, especially in context of MDR. While the synthesis remains complex, advantages in their unique bifunctionality makes them potentially attractive and unique options for treatment of such complex disease states such as MDR and metastatic tumors.

Other strategies can be combined with drug conjugation to DNCs to help address MDR. The ability to target specific intracellular organelles can be used to repurpose cytotoxic drugs in cancer treatment. Mitochondria are intracellular organelles that maintain cellular homeostasis.⁴⁸ Mitochondria in cancerous cells are functionally and

structurally different as compared to normal cells, and have been implicated in tumor initiation and progression.⁴⁹ Since mitochondria regulate energy metabolism in the cell, production of reactive oxygen species (ROS), and apoptosis,⁵⁰ therapies that can alter metabolic processes associated with cancer cell survival,⁵¹ increase ROS production,⁵² induce apoptosis, or disrupt mitochondria integrity⁵³ have the potential to be developed as alternative drug strategies for cancer treatment. Mitochondrial targeting has been shown as an effective strategy to overcome MDR via attachment of mitochondrial targeting agent triphenylphosphonium (TPP) to small molecule cytoreductive agents.⁵⁴⁻⁵⁷ Therefore, providing a platform for targeting DNC-drug conjugates toward mitochondria has the potential enhance chemotherapeutic outcome and potentially improve strategies to address MDR.

Since acquired MDR can also come from treatment of chemotherapeutics, the use of an entirely different strategy, including the delivery of alternative therapeutic molecules, like short-interfering RNA (siRNA) can be also utilized alone or in combination to help address MDR as it can be used to modulate overexpression and assist in the induction of apoptosis.⁵⁸ One of the main advantages of siRNA therapy is its specificity and versatility. It allows for specific targeting of gene of interest without impacting other genes/cellular functions. However, one major challenge in such therapies is the ability to deliver such biologics intact to the cell cytosol. Nanotechnology seems to be particularly poised as a strategy to be able to address that challenge.^{59-61 62-64} Therefore, if a specific delivery strategy of siRNA is found effective, the versatile use of such strategy can be explored for the treatment of variety of gene targets to treat cancers as well as other disease states. Several nanoformulations have been explored for the delivery of siRNA

for cancer treatment, with some being tested in clinical trials.⁶⁵ The co-delivery of siRNA with chemotherapy for the treatment of MDR has been a focus of many groups demonstrating a synergistic effect.^{58, 66} Of siRNA targets, Bcl-2 and Survivin, genes associated with cellular apoptosis pathways found to be upregulated in many tumor types, associated with poor prognosis, and found upregulated in MDR cells,^{60, 66-70} are, therefore, great therapeutic targets. For the treatment of lung cancer and secondary lung tumors, a viable strategy in which the siRNA (as well as other therapies) can be delivered locally to the lungs directly via the pulmonary route could lead to significant improvement in bioavailability of siRNA.

Oral inhalation (OI) formulations for the treatment of lung metastasis and lung cancer remains a viable strategy to enhance overall efficacy of treatment. Since most chemotherapeutics used in lung cancer treatment are delivered intravenously (IV),⁷¹ multiple unwanted side effects are associated with such cytoreductive therapies. This problem is compounded by the fact that only a small fraction of dose actually makes to the lungs, with typical doses being very high, which may force patients to discontinue treatment. The use of OI can improve in overall success in treatment by increasing dose to target site while reducing systemic exposure, thus lowering side effects.^{72, 73} Higher bioavailability of therapeutic can be found as well by lower enzymatic activity in the lungs compared to the first-pass hepatic metabolism when delivered IV.^{73, 74} Higher amount and bioavailability of drug also allows to lower required dose for administration.⁷⁵ OI can also be utilized as strategy to deliver into systemic circulation non-invasively due to the large alveolar surface area and thin air-blood epithelial barrier^{73, 76}. When combined with DNCs, high doses of therapeutic molecules have been found in the lymph nodes upon pulmonary

administration, which is a primary site for metastases from lung cancer, and very hard to target when drug is administered systemically.^{77, 78} Therefore, the use of OI strategy for delivery of therapeutics for the treatment of lung cancer and lung metastasis remains highly relevant. The use of such a strategy can also be used for the delivery of immunotherapies. Recent advances in immunotherapy for lung cancer treatment highlight the potential of the pulmonary route. For example immune checkpoint inhibitors alone or in combination with colony-stimulating factor 1 receptor inhibitors (CSF1Ri) have been shown very effective in the treatment of non-small cell NSCLC.⁷⁹ However, both treatment strategies may induce liver toxicity,²⁰ and the ability to reduce dose and target disease tissue may prove essential to broaden the applicability of such combination treatments.

Immunotherapy with CSF1R inhibitors has recently been investigated in pre-clinical studies and clinical trials for treatment of a variety of tumors demonstrating great promise and providing an alternative strategy of treatment from current chemotherapy. CSF1Ri work to inhibit CSF1R, a critical receptor found particularly on macrophages.^{20, 80} Tumor associated macrophages (TAMs) are one of the main immune cells found within the TME. TAMs can be described having two main polarizing phenotypes: M1 and M2.⁸¹ M1 macrophages are immunostimulatory while M2 are immunosuppressive.⁸¹ M2 TAMs are known to promote tumor initiation, proliferation, metastasis, angiogenesis, modulate T cell responses, and correlated with resistance to conventional therapies.^{20, 80} CSF1R signaling initiates myeloid cells to differentiate into M2 phenotype. M2 CSF1R+ cells are correlated with poor survival in a variety of tumor types including lung cancer.^{20, 82} CSF1Ri can modulate the expression of M2 phenotype by selectively reducing the number of M2 and/or repolarization from M2 into M1 phenotype, therefore, increasing M1/M2 ratio.⁸³ A

high M1/M2 ratio has been shown to correlate with increased survival for patients as a monotherapy or combination therapy.^{20, 80} Therefore, the direct delivery of CSF1Ri to the tumor site – lung cancer tumors or secondary lung tumors – by pulmonary delivery could enhance overall treatment efficacy by all advantages discussed previously, as a monotherapy or in combination with other treatments.

Within this context, the **objectives** of this dissertation are as follows:

Objective # 01: Develop mitochondrial-targeting dendrimer nanocarriers (DNCs) as a platform for the repurposing of chemotherapeutics with potential applicability in the treatment of MDR in primary and secondary lung cancer.

Mitochondria play a crucial role in cellular homeostasis, including production of cellular energy, production of reactive oxygen species (ROS), and intrinsic apoptosis.^{48, 50, 84, 85} Alterations in mitochondria occur in cancerous cells in which lead mitochondria to become dysfunctional or “resistant.”^{48, 67} Changes in cellular metabolism from aerobic respiration to aerobic glycolysis – an effect known as the Warburg effect – and alterations in intrinsic apoptotic pathways – impaired apoptosis – occur in these mitochondria.⁴⁸ Since mitochondria play crucial roles in cell survival and proliferation in cancerous tumors, therapeutic agents that can be directed toward the mitochondria have great potential in elimination of such tumors^{49, 86} by altering metabolic processes essential in cancer cell survival,⁵¹ leading to mitochondrial destabilization to induce apoptosis.⁵³ This direct targeting of therapies toward the mitochondria can also help overcome MDR, a major obstacle in current chemotherapy treatment by redirecting therapeutics, for example, whose nuclear target may have been compromised due to MDR, allowing the repurposing of that same molecule.⁶⁷ We, therefore, designed a DNC platform to target the

mitochondria. We selected a known mitochondriotropic agent, the delocalized lipophilic cation triphenylphosphonium (TPP) ion, that was conjugated directly to amine-terminated, generation 4, poly(amidoamine) (PAMAM) dendrimer (G4NH₂-TPP) nanocarriers or to G4NH₂ through a polyethylene glycol (PEG) linker (G4NH₂-PEGTPP). The synthesis, *in vitro* cellular uptake, cytotoxicity, and mitochondrial colocalization of conjugates was investigated. The conjugation of TPP to various nanocarriers for chemotherapeutic delivery⁸⁷⁻⁹¹ or to the drug/therapeutic themselves^{52, 54-57, 92} has demonstrated increased cytotoxicity and enhanced efficacy *in vitro*^{87, 88, 90, 91}, anti-tumor activity *in vivo*,^{87, 88, 93} and the ability to overcome drug resistance.^{54, 56, 57, 94} The details on the studies of the G4NH₂-TPP modified and G4NH₂-PEGTPP modified dendrimers will be further discussed in the following chapters.

Objective # 02: Develop siRNA/TPP-DNCs as a platform for pulmonary delivery of siRNAs with potential applicability in the treatment of MDR in primary and secondary lung cancer. The inactivation of apoptosis through the increase in anti-apoptotic genes expression including is one of the known mechanisms employed in MDR cells.²²⁻²⁴ Bcl-2 and Survivin overexpression have both been implicated with poor survival and drug resistance in many cancer types including lung and breast cancer.^{22, 66, 67, 69} Therefore, the downregulation of these genes can induce a synergistic interaction with other therapies^{66, 95} and potential in overcoming MDR. However, the delivery of siRNA to the lungs has remained a challenge including finding efficient and safe vectors for siRNA delivery to lungs, extracellular and intracellular barriers that prevent efficient siRNA transport to target lung tissues,⁹⁶⁻⁹⁹ and challenges for their formulations into portable oral inhalation devices – including pressurized metered dose inhalers (pMDIs) and dry

powdered inhalers (DPIs). Therefore, we designed an efficient platform for the delivery of siRNA to the lungs. Firstly, an TPP-modified G4-NH₂ PAMAM dendrimer was synthesized and complexed with siRNA (TPP-dendriplexes) to enhance the transfection efficiency of siRNA in an *in vitro* model of pulmonary epithelium. Secondly, particle engineering strategies for the efficient formulations of such complexes for pMDIs and DPIs were developed. The details of synthesis, characterization, *in vitro* gene knockdown and inhalation formulations will be further described in the following chapters.

Objective # 03: Develop novel asymmetric polyester dendrimers for increasing efficacy of chemotherapeutics with potential applicability in the treatment of MDR in primary and secondary lung cancer. Despite the many advantages that PAMAM dendrimers possess, they have some limitations in terms of toxicity well-documented in various cell lines.¹⁰⁰⁻¹⁰³ PAMAM dendrimers are also not degraded under physiological conditions.¹⁰⁴ Therefore, a push for a less toxic and more biodegradable option of dendrimers have led to the design of dendrimers made from 2,2-bis(hydroxymethyl)propionic acid (Bis-MPA) – a polyester based material with demonstrated decreased toxicity and biodegradability.³⁸ Also the requirement of dendrimers to become multifunctional has led to the design of heterobifunctional (asymmetric) dendrimers for biomedical applications.⁴⁵ However, the synthesis of such asymmetric remains a challenge.⁴⁵ There are no studies that have shown the effect of asymmetry in the role of cellular internalization and intracellular trafficking and how that may play a role in drug internalization, release, overall efficacy, and intracellular targeting. Because drug conjugation may alter the interaction of the DNC with the physiological environment, the ability to create highly controllable structures through dendrons may

provide for a pathway for enhanced cellular targeting and yet ability to co-locate with desired organelle, and thus yet another strategy in the repertoire to target MDR.¹⁰⁵ In order to realize such potential, we designed a facile way for modification of surface of polyester Bis-MPA dendrons with various surface groups containing different surface properties (cationic, anionic, neutral hydrophilic, hydrophobic). We combined this dendron side with another dendron side where a power cytoreductive agent broadly used in chemotherapy treatment of a variety of tumors (doxorubicin = DOX) is conjugated through a degradable peptide bond. The final product is an asymmetric dendrimer containing DOX on one side and varying surface chemistries on the other. The details on the synthesis and characterization of dendrons and dendrimers will be discussed in the following chapters.

Objective # 04: Develop pulmonary delivery strategy for TAM-targeting immunotherapy with potential applicability in the treatment of MDR in primary and secondary lung cancer. Chemotherapy remains the main modality to treat metastatic cancers. However, MDR is typically developed along cytoreductive treatment.²² IV delivery of small molecule chemotherapeutics and other therapeutics used in the treatment primary and secondary lung tumors also leads to unwanted side effects, limitations in drug dose and bioavailability, and small portion of drug making to the lung tumor site.^{73-75, 106} Therefore, alternative types of therapies and routes of delivery to treat these tumors may be critically needed to bring about innovations that may help address MDR and to improve overall treatment efficacy. We have thus tested a combination chemo- and immuno- therapy strategy for the treatment of lung cancers that combines a small molecule CSF1Ri and a cytoreductive agent. We established an *in vivo* mouse

model of metastatic breast cancer to the lungs and tested the efficacy of such combination therapy upon local delivery to the lungs. This study will be described in detail in the following chapters.

The rest of this document is organized as described next. In Chapter 2 we present a literature review about the following topics: lung cancers and other common cancers that metastasize to the lung; current treatment strategies for primary and secondary lung tumors; challenges in MDR; dendrimers' role as effective polymeric nanocarriers for therapeutic delivery, mitochondrial targeting of chemotherapeutics as an effective strategy for primary and secondary lung tumors and MDR; siRNA delivery to lungs and potential use in overcoming MDR; advantages in direct pulmonary delivery of for treatment of lung tumors; and immunotherapy to modulate tumor associated TAMs as a treatment strategy.

In Chapter 3 we discuss the mitochondrial targeting ability of TPP-modified G4-NH₂ PAMAM dendrimers. The goal of this work was to establish a platform for mitochondrial targeting that may open up possibilities for drug repurposing in MDR. Conjugation of TPP was either directly conjugated to the surface of G4-NH₂ PAMAM dendrimer (G4NH₂-TPP) or via a PEG linker (G4NH₂-PEGTPP). The synthesis and characterization are fully described. Their biological activity was tested at various surface densities of TPP or PEGTPP in an *in vitro* model of human alveolar carcinoma cell line (A549). This included the testing of cellular uptake by flow cytometry, cytotoxicity by MTT assay, and mitochondrial colocalization by confocal microscopy *in vitro*. The main effects on the type of TPP conjugation (direct or through a PEG linker) were assessed for each dendrimer conjugate. This chapter is based on the published manuscript: **Bielski, E. R.**,

Zhong, Q., Brown, M., & da Rocha, S. R. Effect of the conjugation density of triphenylphosphonium cation on the mitochondrial targeting of poly (amidoamine) dendrimers. *Molecular Pharmaceutics*, **2015**,12, (8), 3043-3053.

In Chapter 4 we discuss the formation and oral inhalation formulations of TPP-dendriplexes as a siRNA delivery strategy to the lungs. siRNA delivery to the lungs remains a huge challenge due to the poor bioavailability of siRNA when administered IV and difficulty in maintaining siRNA integrity and activity when formulating for use in portable inhalation devices.¹⁰⁷ G4NH₂ PAMAM dendrimers were modified at various TPP densities (G4NH₂-TPP) to enhance *in vitro* transfection ability when delivery siRNA to an *in vitro* model of the pulmonary epithelium. G4NH₂-TPP dendrimers were complexed with siRNA to form TPP-dendriplexes and were characterized by light scattering and SEM. Varying TPP densities and N/P ratios were analyzed. The complexation efficiency of various TPP-dendriplexes were assessed by gel electrophoresis and polyanion competition assay. The *in vitro* toxicity and gene knockdown efficiency were evaluated against eGFP-expressing A549 cells. TPP-dendriplexes were engineered into micron particles utilizing spray drying. These particles were characterized by Light Scattering and SEM, their *in vitro* gene knockdown ability was assessed, and their aerosol characteristics for both pMDIs and DPIs was determined by Anderson Cascade Impactor. This chapter is based on the published manuscript: **Bielski, E.**, Zhong, Q., Mirza, H., Brown, M., Molla, A., Carvajal, T., & da Rocha, S. R. TPP-dendrimer nanocarriers for siRNA delivery to the pulmonary epithelium and their dry powder and metered-dose inhaler formulations. *International Journal of Pharmaceutics*, **2017**, 527, (1-2), 171-183.

In Chapter 5 we discuss the synthesis and characterization of surface modifications for polyester Bis-MPA dendrons. Surface modifications of dendrimers have been demonstrated to affect cellular internalization and intracellular trafficking in various cell lines. Cationic and neutral PAMAM dendrimers were found to be internalized via non-clathrin, non-caveolae-mediated mechanisms endocytosis., anionic dendrimers were seen to be internalized in A549 cells by a caveolae-dependent mechanism¹⁰⁸ Hydrophilic PEG modification of dendrimers has shown to decrease the rate of cellular uptake of dendrimers but does not reach saturation in cellular internalization at short times.⁷⁸ Hydrophobic lauryl modifications have been demonstrated to increase internalization of G3-PAMAM dendrimers by caveolae-dependent endocytosis and micropinocytosis in HT-29 cell line,¹⁰⁹ and increase transport across Caco-2 cells via transcellular and paracellular routes.¹¹⁰ However, little is known about the cellular internalization and intracellular trafficking of asymmetric dendrimers, in which critical understanding of these pathways has the potential to increase drug efficacy *in vitro* and *in vivo*. For example, one dendron can be used to carry drug or drug-intracellular targeting agent, while the other dendron may lead to enhanced uptake. Also, synthesis of asymmetric dendrimers still remains highly complex as well and new protocols may support their development.⁴⁵ Therefore, a facile way to modify polyester dendrons is described. The azido-G5-OH (N₃-G5-OH) polyester Bis-MPA dendrons were synthesized and characterized with unmodified hydroxyl (-OH), anionic carboxyl (-COOH), cationic (-NH₂), hydrophilic PEG (-PEG) and hydrophobic lauryl (-LA) functionalities. The synthesis and characterization by ¹H NMR, MALDI-TOF, and Light Scattering of modified dendrons is described. The attachment of DOX via peptide (-GFLG-) and linked to Acet-G5-SA modified dendron is

also discussed. The use of click chemistry to conjugate the Acet-G5-OH and N₃-G5-OH dendrons to form dendrimers as potential strategy for formation of asymmetric dendrimers is described.

In Chapter 6 we describe the pulmonary delivery of a CSF1Ri (PLX3397) for the treatment of lung tumors, in this case using an *in vivo* model of secondary lung tumors developed from a murine model of stage IV metastatic breast cancer. The efficacy of PLX3397 (PLX) delivered via pulmonary route, also its combination with chemotherapeutics (DOX) had not been previously explored. In this study we transduced a mouse (Balb/c) breast cancer (4T1) cell line to contain fluorescence and bioluminescence vectors (luc-tdtomato-4T1). Cell sorting following by fluorescence expression determination by flow cytometry and bioluminescence expression determined by IVIS imaging were utilized to establish the cell line. An *in vivo*, syngeneic (4T1/Balb/c) immunocompetent tumor model of lung metastasis was established with the transformed cells. The effectiveness of PLX and DOX treatment delivered via pulmonary route was assessed *in vivo* by measurement of tumor burden via IVIS imaging. Macrophage polarization induced by PLX was assessed by flow cytometry.

In Chapter 7 we conclude the work as we try to unify all the treatment strategies discussed above as potential means to address MDR in lung cancers and propose next steps that can be taken in each project based on the knowledge acquired during the execution of these multifaceted projects.

1.2 Relevance and Innovation

The relevance of this work stems from the fact that the development of MDR remains the greatest challenge in the management of primary and secondary lung

cancer.^{6, 7} Therefore, new therapeutic strategies that can increase efficacy of overall treatment are needed. Here we present several different platforms that have the potential to treat highly metastatic tumors and overcome MDR. Firstly, mitochondrial intracellular targeting of therapeutics has been demonstrated by others to overcome MDR in some MDR-cell lines *in vitro* and enhanced efficacy *in vivo* - for small molecules only.⁵⁴⁻⁵⁷ We are the first group to assess the effect of TPP and PEGTPP density on dendrimers in general, and the impact of such modification on their cellular internalization and mitochondrial targeting, thus demonstrating their potential as a platform for delivery of therapeutics to overcome MDR. We are also the only group to demonstrate the ability of dendrimer-TPP conjugates to enhance *in vitro* transfection ability of siRNA in lung alveolar cells and the successful aerosol formulations of such complexes in both pMDIs and DPIs. This provides for a strategy for local targeting of siRNA to lungs that can also potentially be used alone or in combination to address MDR. We are also the first group to synthesize and characterize various surface modifications to N₃-G5-OH polyester dendrons for the formation of asymmetric dendrimers containing DOX and varying surface chemistries. The study of cellular internalization and cellular trafficking on effect of drug release and efficacy *in vitro* and *in vivo* biodistribution and pharmacokinetics has many implications in improving overall polymer-drug design and enhanced treatment efficacy in metastatic and MDR tumors. Lastly, we are the first group to test the delivery of PLX via pulmonary route as potential treatment of metastatic tumors in the lungs, demonstrating potential immunotherapy route by direct pulmonary administration to the lungs that can enhance efficacy of treatment in metastatic tumors in the lung as well the potential to address MDR.

CHAPTER 2 – LITERATURE REVIEW

2.1 Lung Cancer and Other Common Cancers that Metastasize to the Lung

Lung cancer is the second most diagnosed cancer with estimated new cases comprising of 13.5% (with 14% for men and 13% for women) with 6.2 percent of the population will be diagnosed at some point in their lifetime.^{2, 3} It still remains the leading cause of cancer-related death in the United States regardless of gender or ethnicity comprising of 25.3% (~155,000 Americans) - 26% for men and 25% for women.^{2, 3} Lung cancer has been the leading cause of death for women since 1987, killing almost twice as many woman than breast cancer.¹¹¹ More lives are lost to lung cancer than colorectal, breast, and prostate cancer combined.¹¹¹ The five-year survival rate after initial prognosis is 18.6%.³ There are few to no symptoms in most reported cases of lung cancer, therefore, leading most patients being diagnosed at the advanced stage of the disease; about 57% of cases diagnosed when lung cancer is in the distant stage (metastasized to distant sites) in which the 5-year survival rate drops down to 4.7%.^{3, 4} Although a slow progression in decrease of lung cancer incidence (2.1%) and deaths (2.7%) in the past decade, it still remains the top in cancer-related deaths, which can be reflected from only 6% of government money funded for cancer research is dedicated to lung cancer.^{2, 3}

Not only lung cancer that remains a critical in terms of cancer-related incidences and deaths, metastasis to the lung by other cancer types also remains a major challenge. Metastasis is most commonly the final and fatal progressive step in solid tumor progression.^{6, 7} Metastasis is the spread of cancer from the primary (original) tumor site that travels through the body and forms a new tumor in another organ or tissue type (Figure 2.1A).¹¹² This tumor is known as the metastatic tumor and is the same type of

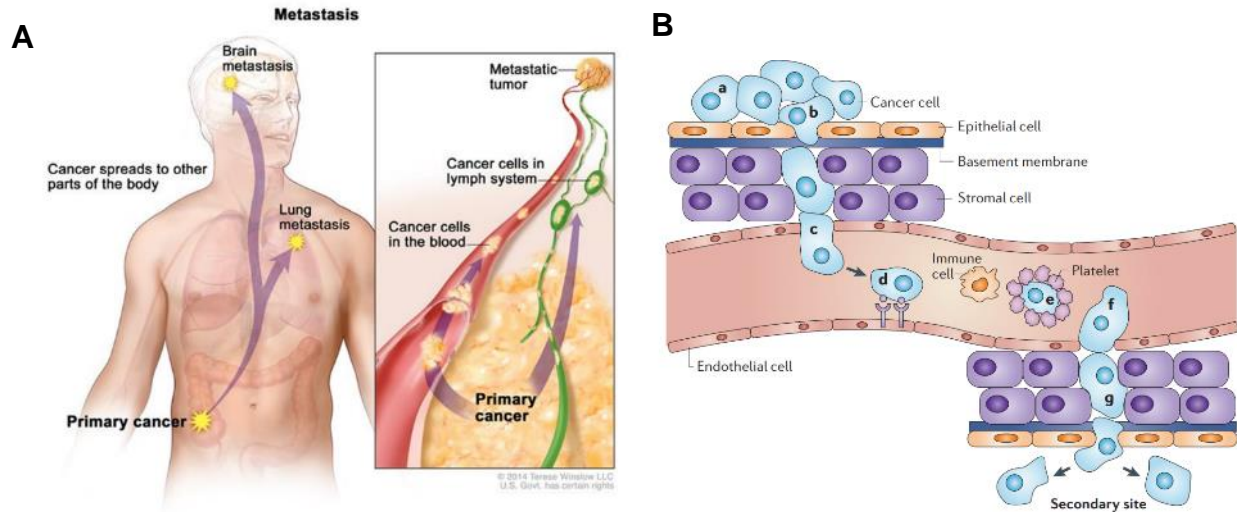


Figure 2.1. A) Metastasis. Metastasis in cancer is when primary tumor cells break away from initial tumor, travels through the blood or lymph system to form new tumors (metastatic tumors) in other tissues or organs within the body;¹¹² **B) Steps of Metastasis.** Several steps are required for metastasis. First, the cell breaks free from primary tumor and through the stroma to reach the vasculature - intravasation. Once in the bloodstream (or lymph), the cancer cells express certain markers, circulate, and distribute to distant sites depending on the interaction of cancer cells and secondary organs in which they colonize. After reaching a secondary target organ site, they cancer cells can exit the bloodstream, and begin to proliferate by releasing pro-inflammatory compounds, inducing angiogenesis, and releasing other growth factors.⁸

cancer as the primary tumor. The metastatic process includes several steps including: cell intravasation, survival in circulation, extravasation to distant organ/tissue site, angiogenesis, and uninhibited growth (Figure 2B).^{6, 8} The molecular mechanisms of the primary tumor to metastasize to other organ sites is tissue-specific, and the tendency of primary tumors to metastasize to specific organs has been observed for more than a century.^{6, 7}

Secondary lung tumors and are metastatic tumors found in the lung. These secondary lung tumors can be found in 30-55% of all cancer patients, though the frequency of these tumors depends on the cancer type of the primary tumor.⁶ Cancer spread to the lungs is often a marker of the disease being advanced. Almost any cancer can has the ability to spread to the lungs, however, some more commonly do so and

include the following: bladder cancer, melanoma, breast cancer, colon cancer, prostate cancer, head and neck cancer, thyroid cancer, renal cell cancer, choriocarcinoma, testicular cancer, osteosarcoma, Ewing sarcoma, Wilms tumor, Rhabdomyosarcoma, and neuroblastoma.⁶ Of these primary cancers, breast cancer is the leading new estimated cases for women in the US in 2018 at 30% (266,120) and 2nd in estimated deaths for women – 14% (40,920).² It metastasizes most commonly to the lymph, bone, liver, and lung, in which bone and lung are the most common targets of breast cancer metastasis in humans.^{7, 8} Not the primary tumor of breast cancer, but the metastatic form is the leading cause of death in these patients and where current clinical intervention has failed.^{9, 10}

Secondary lung tumors can be from the initial spread of primary tumors before clinical intervention, however, it can also be as a consequence from treatments itself (chemotherapy or radiotherapy).⁶ Once metastasis is found, few patients can be cured by surgical intervention or other treatment modalities.⁸ Chemoresistant malignancies is the leading cause of death for patients, in which adjuvant chemotherapy, often accompanied by surgery has failed and led the development of resistance.^{9, 11} Across any cancer type, the five-year survival rate for patients exhibiting metastatic form of cancer is 20%.⁸ Therefore, new interventions for these patients are much desired.

2.2 Current Therapies and Therapeutic Challenges in Addressing Drug Resistance and Metastasis to the Lung

The aim of current treatment strategies is to stop or slow the growth of tumor or to relieve symptoms.¹² Current therapies for cancers is highly dependent on the tumor type

(primary tumor) and how progressive the disease state is. When it comes to metastasis, some types can be cured by current treatment, however, most cannot be cured.¹²

The treatments offered for lung cancer (more specifically non-small cell lung cancer - NSCLC) is normally a regimen of surgery, chemotherapy, and/or radiation therapy or a combination of these.¹¹ For advanced stage-lung cancer, radiation therapy, chemotherapy, or a combination is the main treatment.¹⁴ The standard chemotherapeutics given in this case include platinum-based drugs Cisplatin and Carboplatin.^{11, 14} Other common drugs include Paclitaxel, Albumin-bound paclitaxel, Docetaxel, Gemcitabine, Vinorelbine, Irinotecan, Etoposide, Vinblastine, and Premetrexed.¹⁴ Normal chemotherapy regimen usually comprises of a combination of two drugs, usually with cisplatin or carboplatin plus a secondary drug or gemcitabine with vinorelbine or paclitaxel.¹⁴ The combination of two drugs is to mitigate unwanted side effects of any one particular drug by reducing total amount and increasing overall therapeutic effectiveness.¹¹ However, combination of three drugs has not shown much clinical benefit, which has kept standard treatment to a combination of two drugs.¹⁴ Treatments are given intravenously in cycles – 1 to 3 days with rest lasting for 3 to 4 weeks. If the lung cancer is in the advanced stage, the combination of chemotherapy is given up to 4 to 6 cycles.¹⁴ If the initial treatment fails to garner a response, a second-line chemotherapeutic such docetaxel or pemetrexed, a targeted therapy, or immunotherapy treatment is given.¹⁴

Current therapies for breast cancer also include surgery, radiation therapy, chemotherapy, or a combination of these as for lung. If the breast cancer is found in Stage I-III, surgery and radiation therapy followed by chemotherapy is normally given either

before or after surgery.¹⁵ If found in stage IV (metastatic breast cancer), chemotherapy is the main treatment modality.¹⁵ All chemotherapies are typically given intravenously (IV).⁷¹ However, unlike lung cancer, treatments are dependent on the genetic status of the tumor including the expression of estrogen receptor (ER), progesterone receptor (PR) and HER2.¹⁵ If positive for ER or PR (tumor highly expresses ER or PR), then they are more likely to grow in the presence of the hormones estrogen and progesterone and more likely to respond to hormone therapy, and hormone therapy will be included after first-line treatment of surgery, chemotherapy, and/or radiation therapy.¹⁶ If the breast tumor has more expression of HER2 (human epidermal growth factor 2) protein, a receptor protein that promotes growth (seen in ~20% of cases), trastuzumab, along with chemotherapy is commonly given after surgery.¹⁶ However, 10-20% cases where these proteins are not overexpressed is known as triple-negative breast cancer. This type of breast cancer is more aggressive, and chemotherapy is the standard treatment given.^{15, 16} Currently, there are not targeted therapies yet developed for this type.¹⁶

Chemotherapy for breast cancer is given as a neoadjuvant, adjuvant therapy, and for the advanced form of the disease.⁷¹ It is difficult to predict the risk of metastasis development, therefore, more than 80% of patients are given chemotherapy as an adjuvant therapy.¹⁰ In most cases, chemotherapy is effective when chemotherapeutics are given in combination. However, there is no set clear combination that has proven to be generally effective in all patients.⁷¹ The most common drugs given for adjuvant and neoadjuvant therapy are anthracyclines – doxorubicin and epirubicin, taxanes – paclitaxel and docetaxel, 5-fluorouacil, Cyclophosphamide, and Carboplatin. A combination of these drugs (2 or 3) are usually given.⁷¹ When breast cancer is in the

advanced stages, the drugs that are given include taxanes – paclitaxel, docetaxel, albumin-bound paclitaxel, anthracyclines – doxorubicin, pegylated liposomal doxorubicin, epirubicin, platinum agents – cisplatin, carboplatin, and others such as vinorelbine, capecitabine, gemcitabine, ixabepilone, and eribulin.⁷¹ Unlike early stages of breast cancer, the advanced stage is usually treated with a single chemotherapeutic.⁷¹ In all cases when chemotherapy is added to the treatment regimen, the chemotherapy cycles will depend on the drug administered. These usually occur by giving dose of drug once – few times a week followed by a rest period. The cycles usually last 2 to 3 weeks.⁷¹ Neoadjuvant and adjuvant therapy is normally given for a total of 3 to 6 months.⁷¹ If in the advanced state, the length you are in treatment depends on health status of patient and how well it is working.⁷¹

As one can denote, chemotherapy is one major modality of treatment for cancer, especially metastatic cancer. One of the major problems in effectiveness of chemotherapy treatment is the ability of chemoresistance to develop. Chemoresistance can be broadly divided into two major categories: intrinsic or acquired.²² Intrinsic resistance refers to resistance that already exists within the tumor prior to chemotherapeutic treatment, thus the tumor containing resistance factors that make the therapy ineffective.²² Secondly, acquired resistance in which a tumor develops various mechanisms of resistance in response to chemotherapeutic treatment. Exposure to chemotherapeutic agents can lead to drug resistance in multiple cytotoxic drugs – known as multidrug resistance (MDR) – which continues to be a dominant obstacle in cancer therapy.²³ The reason for numerous failures in patients with metastatic cancer is due to this spectrum of mechanisms that lead to MDR, whether intrinsic or acquired.²³

MDR and chemoresistance develop from a multiple and various molecular mechanisms and is governed by both genetic and environmental factors within tumors and the tumor microenvironment (TME).²⁴ Figure 2.2 summaries some of these mechanisms and include increased rates of drug efflux, alterations in drug metabolism and drug targets, alterations in signaling pathways to reduce apoptosis, enhanced DNA repair, drug compartmentalization, genetic and epigenetic changes that influence the

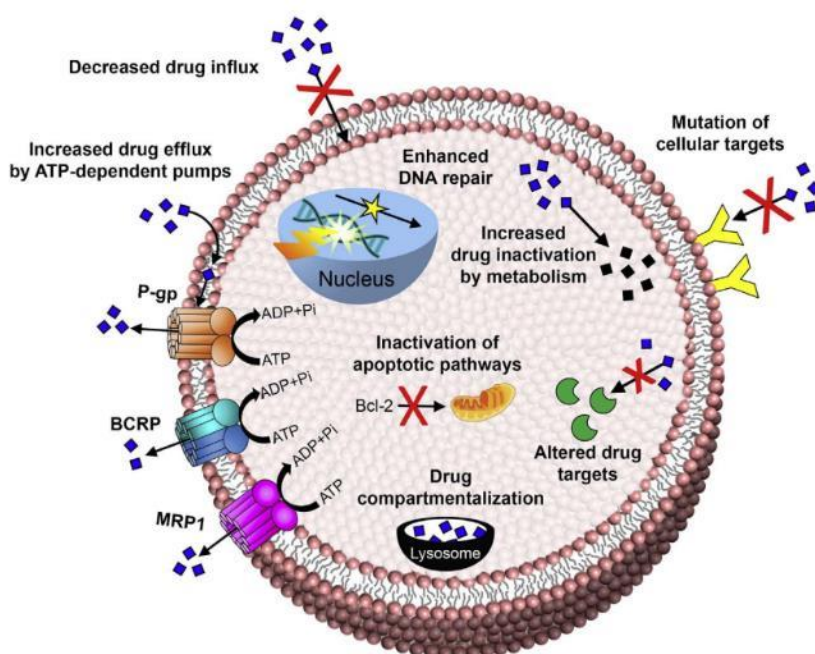


Figure 2.2. Various Mechanisms of multidrug resistance. This includes efflux pumps, enhanced DNA repair, inactivation of drugs by metabolic pathways or mutation or altered drug targets, drug compartmentalization, and inactivation to apoptosis.²³

local TME, molecular and genetic heterogeneity within the tumor as well as presence of cancer stem cells.²²⁻²⁴ Generally, cancerous tumors utilize several of these resistance mechanisms either sequentially or concurrently.²⁴

One well-known mechanism of MDR is drug efflux by cell membrane transporter proteins. The most-well known group of transporters is the ATP-binding cassette (ABC) transporter family that can transport a variety of diverse substrates out of cells.²²⁻²⁴ 49

ABC transporters have been identified in humans, with 15 known to export chemotherapeutics out of cells.²³ The most notable ones include the multidrug resistance protein 1 MDR1 (ABCB1, p-glycoprotein- P-gp), MDR-associated protein 1 (MRP1, ABCC1), and breast cancer resistance protein (BCRP, ABCG2).²²⁻²⁴ These three have broad and overlapping substrate specificity and can eliminate many hydrophobic chemotherapeutics including taxanes (paclitaxel, docetaxel), topoisomerase inhibitors (doxorubicin), and anitmetabolites.²² Rapid upregulation and overexpression of the ABC transporters has been seen in a variety of tumors and demonstrated resistance to a variety of chemotherapeutics.²²⁻²⁴ Overexpression in MDR1 and its correlation to chemoresistance has been seen in kidney, colon, liver cancers, lymphomas, and leukemias.²² MRP1 overexpression is seen in prostate, lung, and breast cancer leading to MDR.²² BCRP overexpression has led to chemoresistance in both leukemia and breast cancer.²²

An alternative resistance mechanism besides efflux pumps normally assist in resistance to chemotherapy treatment including alteration in drug targets. Such alterations in drug targets can include mutations to the drug target itself or changes in expression level.^{22, 24} Downregulation of target gene is one common mechanism of resistance. For example, this can be seen for the effect of doxorubicin and downregulation of topoisomerase II α , its target protein.²⁴ Other common resistance mechanism includes mutation in target protein including mutations in topoisomerase II α , and it is commonly seen in receptor tyrosine kinases when targeted therapies are utilized.^{22, 24}

Another important resistance mechanism employed by MDR cells included the downregulation or inactivation of apoptosis.²²⁻²⁴ The pathways that regulate apoptosis are

known to become dysfunctional in cancer, and can also lead to MDR. A key feature to resistance is signaling that allows for cell survival and prevents cell death.²⁴ This can occur usually by the upregulation of anti-apoptotic proteins – such as overexpression of Bcl-2 gene,^{22, 23} inhibitor of apoptosis proteins (IAPs),²² and FLIP (a caspase 8 inhibitor).²² The role of Bcl-2 gene and its family members in response to chemotherapy has been the most extensively studied, and has shown to play a role in chemoresistance.²²

There are many other important factors that can lead to MDR, and many can be implemented sequentially or concurrently.²⁴ This includes (but not limited to) drug inactivation by cancer cellular metabolism, enhanced DNA repair, and compartmentalization of drugs.²²⁻²⁴ Altered metabolism can lead to drug resistance by inactivation of drug itself. These metabolic pathways are more specific each drug and its mechanism of action. One example includes platinum-based drugs (Cisplatin, carboplatin, oxaliplatin) can be inactivated by presence of glutathione in which glutathione can bind to platinum decreasing its ability to bind to site of action – cisplatin binding to DNA.^{22, 113} DNA damage can be caused by a variety of chemotherapeutic drugs either directly (platinum-based drugs) or indirectly (topoisomerase inhibitors), and as cancer progresses, an increased repair to DNA damage occurs and can lead to resistance.^{22, 24} Compartmentalization of chemotherapeutics away from target site can also occur. Drugs can be sequestered into organelles like lysosomes keeping the drug away from site of action, in which lysosomes release drug outside the cell via exocytosis.²³

Tumor heterogeneity and the TME also influence drug effectiveness and resistance.¹¹⁴ Genetic instability of within cancer cells themselves and epigenetic alterations can lead to genomic and phenotypic heterogeneity in the tumor.²³ This can

occur due to the positive selection of resistant phenotypes due to treatment and the adaptation garnered based on signaling from the tumor microenvironment (TME).^{22, 23} The TME contains a variety of cells including tumor cells, cancer stem cells, extracellular matrix, cancer-associated fibroblasts, immune cells, inflammatory cells, and blood vessels.²² The presence of cancer stem cells (CSCs) or tumor-initiating cells within the tumor are known to evade chemotherapy and allow for resistance to build.²⁴ The tumor stroma with increased expression of extracellular matrix has been shown to play a crucial role in invasiveness and metastasis as well as sensitivity of tumor to drug treatments.¹¹⁴ TME can lead to hypoxic regions, which increases expression in genes related to angiogenesis and cell survival, which have been shown to play a role in drug resistance.^{23, 114} Signaling and interaction of various cell types with the tumor cells can lead to signaling (cytokines and growth factors) to activate a variety of cell survival pathways, enhance invasiveness and metastasis potential, and evade immune system.^{22, 115} Therefore, the acknowledgement of the complexity of the TME as well as an understanding the roles and mechanisms at play that lead to drug resistance is vitally important in order to enhance current chemotherapy treatment.

Due to the complexity of cancer as a disease and multiple mechanisms for drug resistance, new drug delivery strategies to overcome these challenges have emerged including the use of nanotechnology. Nanomedicines have been able to overcome some limitations of current chemotherapy including unwanted side effects, low bioavailability due to the hydrophobic nature of most chemotherapeutic agents, invasiveness of chemotherapy treatment, and non-specific in delivery killing normal and cancerous tissue.^{11, 23} Nanomedicines have been able to enhance delivery of chemotherapeutics to

tumor site and address drug resistance by passively and actively targeting tumor tissues, increase solubility of hydrophobic drugs, delivery of combination of drugs/biologics, and control drug release at target tumor site.²³

2.3 Dendrimers and Dendrons as Polymeric Nanocarriers and Their Roles for Treatment of Primary and Secondary Lung Tumors and MDR

Nanotechnology, or more specifically, polymeric nanocarriers (PNCs), can be utilized to improve drug availability and efficacy, reduce toxicity and systemic side effects by enhancing specific targeting of the drugs to the diseased tissue of interest,^{25, 30} and have shown improved clinical efficacy,²⁶ therefore, they hold great potential in the chemotherapy treatment.^{25, 27} The specific targeting and selectivity of chemotherapeutics towards malignant tissues is directly correlated to improved quality of life and survival of patients,²⁸ allowing for many nanotechnological carriers entering clinical practice and numerous studies conducted on optimizing the application of nanomedicines for the treatment of cancer.²⁷ PNCs remain a relevant strategy due to the majority of cancer chemotherapeutics, including 40% of active substances being identified through combinatorial screening programs,²⁵ are poorly water soluble limiting their dose, administration, and bioavailability;¹¹ Polymeric nanocarriers have the potential to increase the solubility and bioavailability of such newly discovered agents. PNCs also offer an opportunity to improve drug efficiency by mediating the interaction with the various extracellular barriers until their target tissues and intracellular targets can be reached.³¹ Desirable PNCs are preferably multifunctional, allowing for targeting a specific diseased tissue with increasing local concentration at that site, avoidance of biological barriers, increase cellular uptake, and enhancement in drug efficacy^{27, 28, 30, 31}.

Among the different PNCs, dendrimer nanocarriers (DNCs) are a promising carriers for the delivery of chemotherapeutics.³² DNCs are polymeric hyper-branched tree-like structures of nanometer sizes comprising of a central core, repeated branches increasing with each generation, with a large number of functional groups on the surface as seen in Figure 2.3.³³⁻³⁵ Safety and drug loading capacity are major factors in determining if a PNC can be used as an efficient drug delivery vehicle.¹¹⁶ While some PNCs may be limited in their drug loading efficiency,³⁰ DNCs hold unique promise due to the presence of multiple attachment sites, where both therapeutics and other relevant ligands including solubilization enhancers such as polyethylene glycol (PEG), and ligands

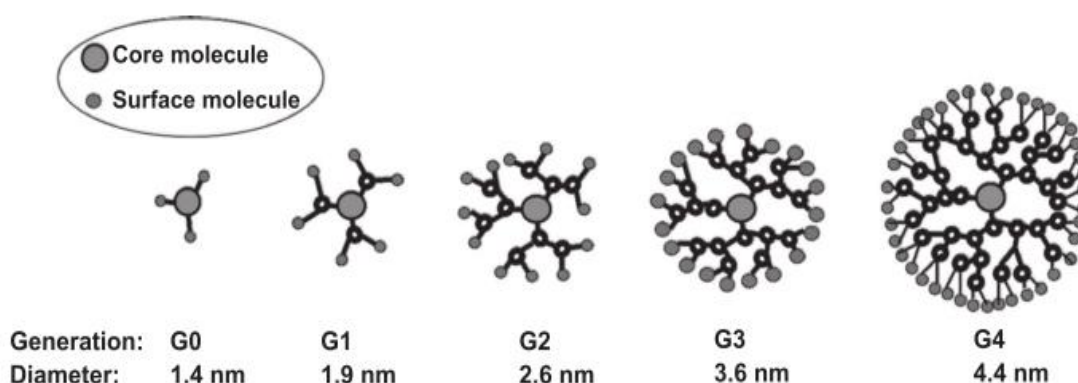


Figure 2.3. Representation of dendrimers demonstrating their structure. They comprise of a central core, repeating branches, and increase in number of surface groups with each generation.³⁵

for targeting specific cell types or tissues, making them a desired multifunctional nanocarrier for targeted drug delivery^{33, 34, 36, 117-122}.

Other unique properties that make DNCs desirable drug delivery candidates include increased solubility and bioavailability of the therapeutic attached,^{36, 116, 123} they preserve their physical and structural integrity within biological systems,^{33, 121} they are monodisperse,^{33, 36, 42, 108, 121, 122, 124-126} biocompatible,^{33, 42, 121, 125} have a tunable size,^{33, 36} reproductive pharmacokinetics,^{36, 42, 121, 125} increased cellular uptake,^{36, 124} non-

immunogenic,^{36, 118, 125} can control or program drug release,^{34, 36, 37, 116, 124} and have potential for targeted delivery to reduce systemic side effects and increase efficacy of drug at targeted tissue site.³⁴ These numerous characteristics and properties make DNCs a desirable choice for the targeted treatment of lung cancer and lung metastasis.

DNCs are synthesized by divergent or convergent synthesis strategies, which allows for precise control on dendritic architecture and monodispersity, allowing for its predictable properties. Depending on the monomer used for synthesis, various classes of dendrimers have been made including polyamidoamine (PAMAM), polypropyleneimine (PPI), poly-L-lysine (PLL), poly(glycerol-co-succinic acid), melamine, poly(glycerol), poly[2,2-bis(hydroxymethyl)propionic acid] (Bis-MPA), poly(ethylene glycol) (PEG), and others.³⁷ Of these PAMAM and PPI have been the most extensively investigated.³⁷ Specifically, PAMAM dendrimers have remained the most studied dendrimer for anticancer drug delivery strategies.³⁷ PAMAM dendrimers have been utilized to conjugate/encapsulate doxorubicin (DOX),^{77, 117, 127-135} docetaxel,¹³⁶ 5-Fluorouracil (5-FU),¹³⁷⁻¹³⁹ Cisplatin,¹⁴⁰⁻¹⁴² methotrexate,¹⁴³⁻¹⁴⁷ paclitaxel,¹⁴⁸⁻¹⁵⁰ chlorambucil,^{151, 152} gemcitabine,¹⁵³⁻¹⁵⁵ Trastuzumab,^{156, 157} and others.

Although PAMAM dendrimers have been the most widely utilized in anticancer drug delivery, PAMAM dendrimers have some limitations. Known cytotoxicity of PAMAM dendrimers across various mammalian cell lines has been well-documented.¹⁰⁰⁻¹⁰³ PAMAM dendrimers demonstrated higher toxicity in various cell lines with increasing generation.¹⁰⁰⁻¹⁰² The toxicity is also highly dependent on surface charge, in which cationic demonstrating the most toxicity,^{100, 101} including *in vivo* situations.^{103, 158} Neurotoxicity was also noted for G5 cationic PAMAM dendrimers causing irreversible

membrane effects on neuronal cells not demonstrated with G4.5 anionic PAMAM dendrimers.¹⁵⁹ Surface modifications of cationic PAMAM dendrimer, such as acetylation,¹⁶⁰ pegylation,¹⁰⁰ and addition of lauryl,¹⁰⁰ can overcome some of these issues. However, due to their nature, they are not biodegradable and must be cleared intact by body through renal excretion (for low generation PAMAM dendrimers) or cleared by liver if surface contains charge or has a hydrophobic nature.¹⁰⁴ Therefore, a push for alternative dendrimers that are less toxic and more biodegradable have led to the synthesis of polyester dendrimers based on bis-MPA.

Bis-MPA polyester dendrimers hold great promise including all same unique features of other dendrimers in addition to their unique properties including biodegradability and biocompatibility. Bis-MPA polyester dendrimers were first characterized by Ihre et al.¹⁶¹ For the utilization of such dendrimers for biomedical applications, an assessment its biocompatibility, immunotoxicity, and biodegradability of and its potential fragments, Bis-MPA monomer, and trimethylpropane core were evaluated *in vitro* and compared to G4 PAMAM dendrimers.³⁸ Feliu et al. were able to demonstrate biodegradability a physiological pHs and body temperature (37°C) allowing the macromolecule to degrade within a few days, unlike PAMAM dendrimers that are resistant to hydrolysis.³⁸ They were also able to demonstrate that polyester Bis-MPA dendrimers and its components were not toxic to a few human cell lines including macrophages, which cationic G4 PAMAM dendrimers did acquire a time and dose-dependent toxicity demonstrating its great potential as a nanomaterial for biomedical applications.³⁸ Various biomedical applications utilizing this polyester Bis-MPA dendrimer has been investigated including its investigations *in vivo*,^{39, 162} its use for positron emitting

probes for *in vivo* imaging,¹⁶³ for use in pressurized metered-dose inhalers (pMDIs),¹⁶⁴ and delivery of chemotherapeutic drugs.^{40, 165, 166}

Dendrons, a class of dendritic architectures, has been utilized to form a variety of dendrimers. The use of bis-MPA polyester dendrons for form dendrimers have been explored by Malkkoch.⁴⁴ Due to the increased interest in dendrimers to contain multifunctionality, the heterobifunctional or asymmetric dendrimers have now been explored.⁴⁵ Fréchet et al. was the first to describe Bis-MPA heterobifunctional dendrimers made from two connecting dendrons called “bow-tie” or Janus-type dendrimers in which the convergent and divergent synthesis were used.¹⁶⁷ Further refinement in synthesis techniques and use of CuAAC Copper-click chemistry and strain promoted azide-alkyne cycloaddition (SPAAC) has been utilized to synthesize a variety of heterobifunctional dendrimers.¹⁶⁸⁻¹⁷¹ A few studies utilizing these bifunctional dendrimers in biomedical applications and drug and gene delivery has recently been explored.³⁹⁻⁴¹ However, its major drawback remains in the complexity of the synthesis of such dendrimers.⁴⁵ Much potential remains in exploring the use of such asymmetric dendrimers as multifunctionality in dendrimers remains a high priority in successful drug delivery strategies, especially in treatment of complex disease states such as metastatic cancers.

2.4 Mitochondrial Targeting of Chemotherapeutics as an Effective Strategy to Treat Primary and Secondary Lung Tumors and Address MDR

Mitochondria are cellular organelles that maintain cellular homeostasis and are critical players in cellular life and death.^{48, 49} It has been implicated in multiple aspects of tumorigenesis and its progression,⁴⁹ since mitochondria are structurally and functionally different in cancer cells compared to normal cells.⁴⁸ This includes the Warburg effect in

which there is a metabolic reprogramming of cancer cells from aerobic respiration to aerobic glycolysis.⁵¹ Limitless proliferative potential, enhanced anabolism, decreased autophagy, and impaired apoptosis have also been linked to mitochondrial dysfunction.⁴⁸ Mitochondria are essential in regulation of energy metabolism, production of reaction oxygen species (ROS), and apoptosis.⁵⁰ Many of the changes seen associated with mitochondria in cancer are summarized in Figure 2.4.⁶⁷ Since mitochondria are essential in these key aspects, agents and therapies that can directly target the mitochondria have tremendous potential in the elimination of cancerous tumors^{49, 86} by altering metabolic processes required for cancer cell survival,⁵¹ increasing ROS production and oxidative stress,⁵² and through mitochondrial destabilization,⁵³ ultimately leading to the induction of apoptosis.

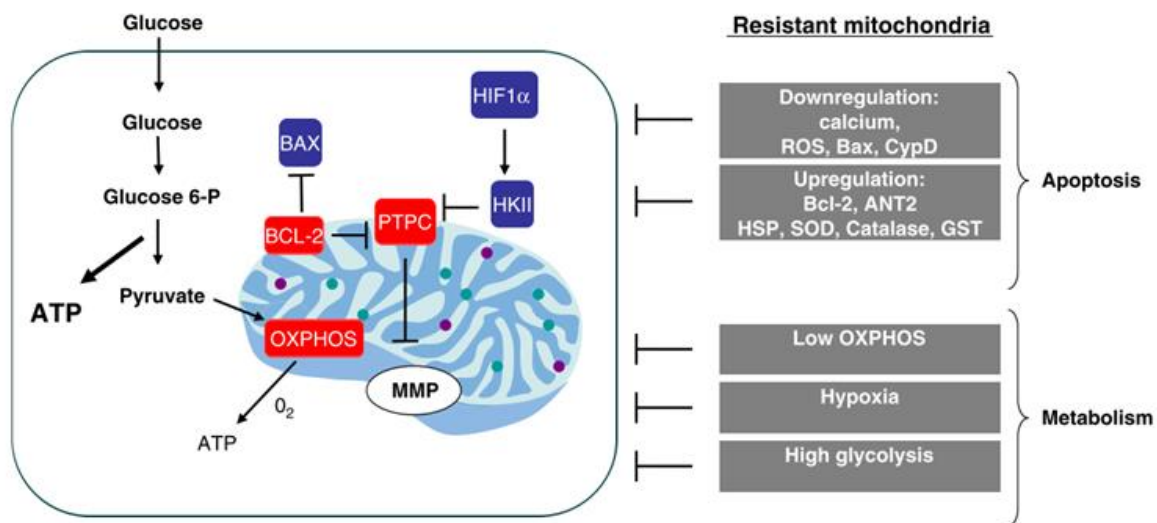


Figure 2.4. Mitochondrial changes seen in cancer cells including transformed metabolism and alterations that make them resistant to apoptosis.⁶⁷

Direct and indirect targeting of the mitochondria to induce apoptosis in cancerous cells is a promising area in cancer-based therapy and may help to overcome drug resistance.⁶⁷ Figure 2.5 demonstrates promising targets for cancer therapy, which include

direct and indirect routes of modulating mitochondrial function.⁶⁷ Both direct and indirect targeting of the mitochondria can help overcome resistance of cancer cells to apoptosis by directly inducing apoptosis through direct targeting of mitochondria or by gene modulations in which a down-regulation of certain pro-survival genes that are overexpressed in cancer by utilizing systems like RNAi mechanism. Therefore, by directly and indirectly altering mitochondrial function within cancer cells may be able to overcome resistance of cancerous tumors that evade cell apoptosis.

Many studies have begun to explore targeting specific agents by direct conjugation of the targeting moiety and therapeutic agent toward the mitochondria to enhance their efficacy in treating various cancers. One of the most common targeting moieties used are delocalized lipophilic cations such as the triphenylphosphonium (TPP) ion,^{50, 84} which

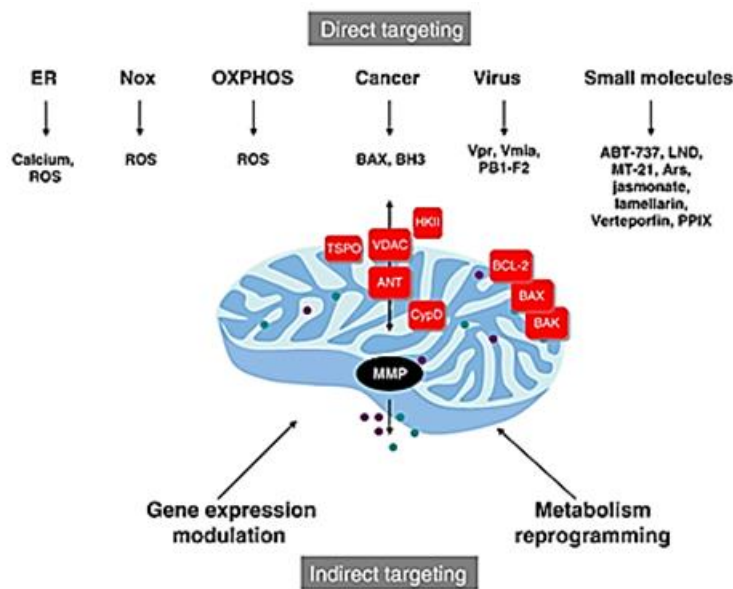


Figure 2.5. Promising direct and indirect targets for cancer therapies to induce apoptosis. ROS: reactive oxygen species, ER: endoplasmic reticulum, Nox: NADPH oxidase, OXPPOS: oxidative phosphorylation, TPSO: translocator protein, cypD: cyclophilin D, HKII: hexokinase II, VDAC: voltage-dependent anion channel, MMP: mitochondrial membrane permeabilization.⁶⁷

have been shown to accumulate specifically in the inner mitochondrial membrane into the

mitochondrial matrix⁵⁰ due to their lipophilic delocalized positive charge allowing them to permeate through membrane bilayers and electrostatic attraction to the mitochondrial membrane due to the large negative membrane potential across it.¹⁷² They have also been shown to accumulate more specifically to cancerous cells because mitochondria within these cells have an increased mitochondrial membrane potential ~ 60 mV, showing a tenfold increase in accumulation.⁸⁴

The utilization of TPP targeting by direct conjugation to specific therapeutic molecule has been investigated. Dual targeting using folic acid (FA) and triphenylphosphonium (TPP) cation via direct conjugation of pro-apoptotic peptide has been demonstrated, and it was shown able to be internalized into mitochondria, causing induction of apoptosis within these cells, demonstrating great potential in targeting specific peptides to mitochondria for cancer treatment.⁹² TPP conjugated to a Vitamin E succinate (α -tocopheryl succinate) was shown to have increased efficacy for this compound compared to untargeted compound by increasing ROS production, modulating Bcl-family of proteins (proteins involved in cell death), and triggering of mitochondria-dependent apoptosis.⁵² Direct conjugation of TPP to DOX to form DOXTPP, was shown to increase cytotoxicity in a DOX-resistant cell line with increase in apoptosis induction in both the DOX-resistant and wild-type cell lines.⁵⁴ Recently, DOXTPP loaded into hyaluronic acid nanoparticles also demonstrated improved anticancer effects, enhanced tumor apoptosis, and better safety profile when compared to free DOX *in vivo* in mice bearing MCF-7/ADR (DOX-resistant) tumors.⁵⁵ Also the combination of DOX delivery with DOXTPP has also been utilized as strategy for dual intracellular targeting of nucleus (DOX) and mitochondria (DOXTPP) to overcome drug resistance.^{56, 57} Direct conjugation

of targeting moieties like TPP have shown increased efficacy of various anticancer therapeutics.

An alternative strategy has included the use of targeted nanocarriers encapsulating a variety of anticancer therapeutics for their delivery to the mitochondria. This has included modified liposomes or with TPP⁸⁷⁻⁸⁹ or rhodamine-123¹⁷³ and loaded with common chemotherapeutics such as paclitaxel,^{87, 88} or doxorubicin,⁸⁹ demonstrating increased cytotoxicity in cancer cells compared to free drug and non-targeted liposomes^{87, 88, 173} and anti-tumor efficacy in mouse experiments.^{87, 88} Another mitochondrial-targeted liposome system delivered resveratrol to the mitochondria of lung cancer cells and apoptosis resistant lung cancer cells and in a xenograft mouse model demonstrating enhanced anticancer efficacy.¹⁷⁴ Targeted carbon nanotubes have superior efficacy in delivering an encapsulated platinum(IV) pro-drug of cisplatin and a chemo-potentiator, 3-bromopyruvate compared to free drug.¹⁷⁵ The use of PLGA-b-PEG-TPP nanoparticles with encapsulated lonidamine and α -tocopheryl succinate has been shown to improve therapeutic index for cancer treatment.¹⁷⁶ A polymer-based nanocarrier system where TPP was conjugated to hyper-branched poly(ethylene imine) (PEI) and encapsulated chemotherapeutic doxorubicin or a combination of doxorubicin with a chemosensitizer chloroquine was shown to possess rapid and severe cytotoxicity in prostate carcinoma cells.^{90, 91} Self-assembled nanoparticles with Tryphenylphosphonium conjugated-cyanostilbene demonstrated enhanced mitochondrial targeting of DOX, increased ROS generation, and decreased mitochondrial membrane potential in cancerous tissues, also suppressing tumor growth *in vivo* in a xenograft model.⁹³ Micelles targeting DOX have also been investigated. DOX was shown to^{94, 177} accumulate more

rapidly towards the mitochondria in resistant cells *in vitro* and resistant tumors *in vivo*, thus indicating that targeting DOX to the mitochondria could help overcome some resistant cancer types.⁹⁴ The accumulation of DOX toward the mitochondria was shown to increase mitochondrial-mediated cell apoptosis in drug resistant cells using nanoparticles.¹⁷⁷ These various studies have demonstrated that targeting specific anticancer agents towards mitochondria can lead to higher efficacy of the agent including overcoming multidrug resistance and may avoid unwanted side effects as seen with free chemotherapeutics.

Doxorubicin (DOX) is a widely used chemotherapeutic to treat a variety of cancers. It is an antitumor anthracycline antibiotic that was first isolated from *Streptomyces peucetius* in 1967.¹⁷⁸ DOX has shown to interact with the nucleus, mitochondria, and biological membranes affecting all cells.¹⁷⁸ The main mechanisms of action include: 1) intercalation into the DNA, which inhibits protein synthesis and DNA replication; 2) ROS production leading to DNA, protein, lipid damage; 3) DNA binding, cross-linking, and alkylation; 4) interference in helicase activity and DNA unwinding and separation; 5) disruption of bilayer structure of the membrane, and 6) inhibition of topoisomerase II leading to DNA damage.¹⁷⁸ The major side effect of DOX is cardiotoxicity with decline in cardiac function, and chronic or delayed cardiomyopathy, which can ultimately lead to congestive heart failure.¹⁷⁸⁻¹⁸⁰ This has limited its therapeutic efficacy.¹⁸⁰ Therefore, as discussed above, several drug delivery systems, such as polymeric nanoparticles,^{90, 91, 93, 177, 181} liposomes,⁸⁹ and micelles,⁹⁴ have been used to reduce these side effects and increase therapeutic efficacy of DOX.

It has also been shown that when DOX has been targeted towards the mitochondria, it can overcome drug resistant cancer cells and tumors.^{54-57, 94, 177, 182} However, the entire mechanism of how DOX interacts with various processes in the mitochondria is not yet known. It has been proposed that mitochondrial Complex I transforms DOX into a more reactive semiquinone radical resulting in increased ROS production and higher oxidative stress.^{178, 179} Also, the inhibition of the electron transport chain (required for the synthesis of ATP- energy source of cells) by DOX via inhibition of complexes I and II may also lead to increased ROS production.¹⁷⁹ The increase of ROS production by DOX can lead to redox modifications to proteins, lipids, and DNA within the mitochondria affecting its structural integrity and function, and can ultimately lead to mitochondrial-induced apoptosis.¹⁷⁹ Short term incubation of DOX to cancerous cells also brought about rapid changes in mitochondrial function including changes in mitochondrial redox potentials towards an increased oxidative state, depolarization of the inner mitochondrial membrane, increased matrix calcium levels, and increased mitochondrial ROS production.¹⁸³ Long term effects included an inhibition of respiration, ATP depletion, and increased production of proteins associated with cell cycle arrest and cell death.¹⁸³ Also, DOX's ability to intercalate with DNA may affect the integrity of mtDNA, which could also contribute to a decrease in electron transport chain complexes and overall electron transport chain (ETC) function. A synergistic effect of prodrug nitrooxy-doxorubicin demonstrated a targeting ability of prodrug to localize to the mitochondria and induce oxidative and nitrosative stress and activation of apoptotic factors.¹⁸⁴ The DOXTPP drug also demonstrated an increase in apoptosis induction indicated by an increase in apoptotic proteins PARP and caspase 3 as well as showing an increase in efficacy against

DOX-resistant cell lines.^{54, 56} The fact that it has been demonstrated by previous studies to be effective in resistance cancer cells makes DOX a highly relevant choice to target towards the mitochondria.

2.5 siRNA Delivery Strategy to Address Drug Resistance for Primary and Secondary Cancer Treatment

The delivery of short interfering RNAs (siRNAs) utilizes the RNAi mechanism and can be used to indirectly target the mitochondria to help induce intrinsic apoptosis. The RNAi mechanism, a unique form of post-transcriptional gene silencing provides a way to downregulate specific target proteins or oncogenes, many of which are overexpressed in cancers, and thus may be used to help induce apoptosis.^{58, 185-187} The RNAi mechanism, as seen in Figure 2.6,¹⁸⁸ can be exploited to induce gene silencing by the delivery of siRNAs, which are double-stranded RNA molecules that are 19-25 nucleotides long.^{58, 186} The siRNA is incorporated into a RNA induced silencing complex (RISC), which unwinds the two strands with the passenger strand being discarded and the guide strand is used for messenger RNA (mRNA) recognition. The binding of guide strand of the siRNA with mRNA recognition in RISC allows for site-specific cleavage of the mRNA, degradation of mRNA, and the silencing of the gene expression. The siRNA loaded RISC is then allowed to find another mRNA within the cytoplasm leading to a reduction in amount of overall protein being made within the cell without modifying the cell's DNA.¹⁸⁶ By using the RNAi mechanism, specific pro-survival proteins associated with mitochondrial-controlled

apoptosis such as Bcl-2 can be downregulated in order to help induce cell death within cancerous tissues.

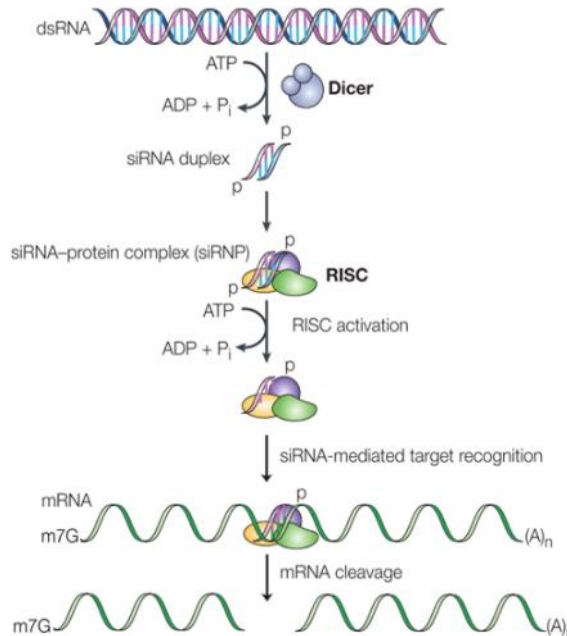


Figure 2.6. the RNAi mechanism. The double-stranded RNA is cleaved by Dicer protein into siRNAs in ATP-dependent process. The siRNAs are incorporated in RISC complex, which unwinds the double stranded siRNA (also requiring ATP). Once unwound, the guide siRNA strand guides RISC to mRNA that has a complementary sequence, which leads to cleavage of the target mRNA.¹⁸⁸

For efficient delivery of siRNA to the cell, however, the siRNA must be able to cross the lipid bilayer of the cell membrane. Free siRNA has low transport across the lipid membrane as it is a negatively charged macromolecule.⁵⁸ Therefore, a carrier is often required to help siRNA cross the plasma membrane and protect the siRNA from degradation by nucleases. The most likely mechanism of internalization into the cell will be non-receptor mediated endocytosis, where the siRNA and nanocarrier must avoid endosomal/lysosomal degradation and escape to the endolysosomal compartments in order to be released in the cytoplasm.⁵⁸ Therefore, many researchers have been looking at utilizing nanotechnology to efficiently deliver siRNA to the cytoplasm.

Several groups have explored the use RNAi mechanism for cancer treatment by delivering siRNA incorporated into nanoformulations to the cell cytoplasm. Some groups have focused on delivering one type of siRNA to inhibit EGFR, c-myc, survivin, Bcl-2 expression using liposome-polycation nanoparticles, gold nanoparticles, and dendrimers complexes as nanocarriers.^{66, 189-191} This has led some of these nanosystems incorporating siRNA into Phase I or Phase II clinical trials.⁶⁵ However, because of the complexity of cancer, crosstalk in multiple signaling pathways, the co-delivery of multiple siRNAs or siRNAs with chemotherapeutic agents has been more recently the focus, especially in cancer cells that exhibit multidrug resistance (MDR).^{58, 192} The various nanocarriers include liposome-polycation nanoparticles, polymeric nanoparticles, liposomes, mesoporous silica nanoparticles, lipid-nanocarriers, micelles, chitosan nanoparticles, and PEI-Graphine oxide to deliver various siRNAs targeting P-gp, MRP1, Bcl-2, VEGF, mTERT, c-myc, survivin, and Mcl-1 in conjunction with chemotherapeutics such as Doxorubicin, Paclitaxel, and Cisplatin.^{60, 185, 187, 192-203} These formulations have seen higher effectiveness in treatment of cancer due to the synergistic effect siRNA and chemotherapeutic agents can bring by targeting multiple cell-signaling pathways and help overcome MDR. Therefore, a combination of treatments to directly target a chemotherapeutic to the mitochondria and indirectly modulate signaling proteins associated with the mitochondria by delivering siRNAs may contribute to a synergistic effect for cancer treatment.

The siRNAs of interest that are involved in intrinsic apoptosis include Bcl-2 and Survivin. Bcl-2 is a protein that belongs to Bcl-2 family of proteins that regulate cell survival and cell death.²⁰⁴ Bcl-2 prevents intrinsic (mitochondrial-dependent) apoptosis

by interacting with other members of Bcl-2 family of proteins on the outer mitochondrial

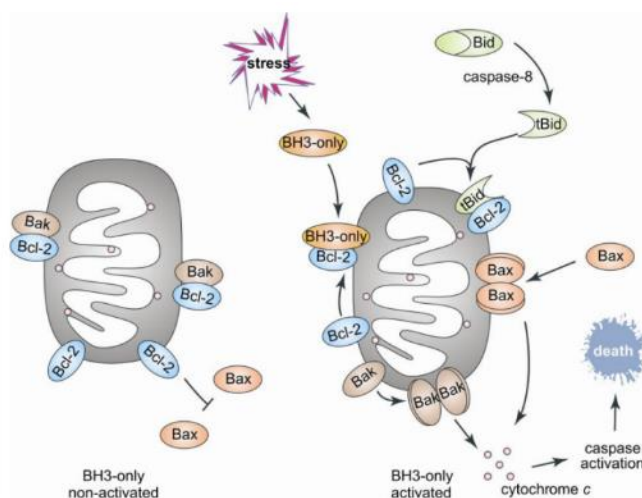


Figure 2.7. General scheme of how Bcl-2 regulates intrinsic (mitochondrial) apoptosis. Bcl-2 is found on the outer mitochondrial membrane and interacts with Bak/Bax proteins, which prevents apoptosis from occurring. Stress induces BH3-only proteins to interact with Bcl-2, which allows Bcl-2 to disassociate from Bak/Bax proteins. The Bak/Bax proteins can oligomerize and initiate mitochondrial outer membrane permeabilization, release of cytochrome c and other pro-apoptotic factors that initiate caspases and lead to programmed cell death.²⁰⁵

membrane as seen in Figure 2.7²⁰⁵. Bcl-2 upregulation has been associated with poor cancer prognosis and drug resistance and has also been implicated in preventing cell death by its ability to modulate cellular redox status and mitochondrial metabolism.^{22, 67} Survivin is a 16.5 kDa intracellular protein that belongs to the Inhibitor of Apoptosis Protein (IAP) family.^{68, 206} It is another protein that promotes cell survival and inhibits cell death by inhibiting caspases, the protein executioners of programmed cell death.^{95, 206, 207} It also has roles in regulation of cell division and has also been implicated to play a role in angiogenesis as well as cell motility increasing the ability of tumor growth and metastasis to occur.^{68, 206, 208} Survivin is also usually not found in normal adult tissues, but commonly expressed in high levels in cancerous tumors including lung cancer (more specifically NSCLC) and breast cancers as well as a variety of others.^{66, 95, 206-211} Overexpression of survivin has been linked to unfavorable outcome of the disease, increased rates of

recurrences, resistance to treatments, and poor survival in patients with NSCLC.^{66, 206, 209} It has also been implicated that increased survivin expression was associated with increase overexpression of MDR1 resulting in multidrug resistance MCF-7 breast cancer cells,⁶⁹ as well as elevated erbB3 expression in paclitaxel-resistance in breast cancer cells.⁷⁰ Decreased expression of survivin using siRNA results in apoptosis within these cells and sensitized these cells to anti-cancer therapeutics.^{66, 95} Bcl-2 and survivin are known to be overexpressed in a wide variety of cancerous tumors, associated with poor prognosis, and have been correlated with multidrug resistance, making them both great therapeutic targets^{60, 66-68}. Therefore, the indirect mitochondrial targeting of Bcl-2 and survivin by downregulation using siRNA holds promise as a treatment strategy, including its co-delivery with mitochondrial-targeted anticancer agents and regional delivery to the lungs.

2.6. Direct Pulmonary Drug Delivery for the Treatment of Primary and Secondary Lung Tumors

Oral inhalation (OI) is a promising route of administration to directly target therapeutics to (regionally) and through (systemically) the lungs. The use of OI is a non-invasive way to directly target the lungs,⁷² increased selectivity, and lower systemic exposure,⁷³ thus resulting in fewer side effects compared to other commonly used routes, including intravenous (IV) injection— i.e., IV administration of nanocarriers has been shown to significantly accumulate into the liver, thus significantly reducing the amount that reaches the tumor site.^{74, 75, 106} The low enzymatic activity in the lungs also allows for higher bioavailability of drug and can bypass the first-pass hepatic metabolism as compared to IV, therefore, the required dose can be reduced as well as lowering costs.⁷³⁻

^{75, 212, 213} A higher absorption rate and rapid onset of action also make the pulmonary route a desired route of delivery.²¹²⁻²¹⁴ Some other advantages to pulmonary delivery include large surface area-to-mass of the lungs (> 100 m²), epithelial permeability (epithelium layer – 0.2-1 μm thick), and small aqueous volume at the absorptive surface ^{74, 213, 215-217}. OI also represents a non-invasive alternative for systemic delivery of therapeutics due to the lungs providing a large alveolar surface area and thin epithelial air-blood barrier providing a rapid absorption of molecules from the alveolar space to the blood stream,⁷³ which can be attractive to treat lung cancer metastasis that accounts for majority of the cases diagnosed.^{8, 76} Due to these advantages, OI for treatment of lung cancer and lung metastases is the most appropriate route for administration of drugs.⁷⁵

Despite all the advantage OI brings, there are also challenges when delivering drugs directly to the lungs. The lung physiology itself provides extracellular barriers when it comes to the delivery of therapeutics to the lungs. This includes the fact that the lungs have a branched architecture and the type of lung epithelium found in each region (Figure 2.8)²¹⁶. The lungs bifurcate 16 times in the conducting airways followed by 6 bifurcations of the respiratory bronchioles⁷³. The particles will be deposited into the airways depends

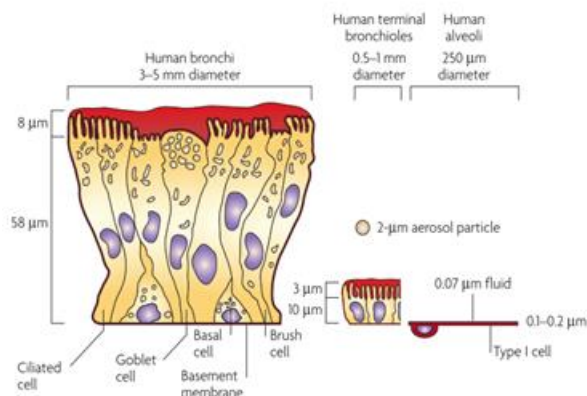


Figure 2.8. Comparison of different lung epithelium at different lung regions. Aerosol particles can penetrate deeper in the lungs as the epithelium becomes thinner.²¹⁶

on the force that dominates the particles, in which aerodynamic size of the particles plays a huge importance²¹⁶. The branched architecture and type epithelium affect clearance mechanism (mucocilliary and cough) encountered when the particles are deposited, the lung surfactant encountered (alveolar region), as well as the immune response and clearance mediated by macrophages.^{73, 216} Therapeutic drugs can be rapidly cleared by mucocilliary escalator, metabolized locally, diffuse across lung epithelia to penetrate bloodstream, or taken up by resident alveolar macrophages.²¹⁴ Therefore, the nanocarriers must possess desired characteristics that enable them to be deposited in specific region of lungs and overcome these challenges to be effective. They must be designed to bypass the above-mentioned clearance mechanisms of the lungs, provide prolonged residence times of the therapeutic within correct targeted lung tissue.⁷³ They must possess the correct aerodynamic size, contain a neutral surface charge and be hydrophilic in nature to allow for passive diffusion and prevent strong interactions with negatively-charged molecules within the mucus, and be nonimmunogenic to avoid macrophage clearance, target specific cell lung populations, protect the therapeutic from degradation, enhance therapeutic solubility of hydrophobic therapeutics, and control therapeutic release.^{73, 216, 218} If these challenges can be overcome, one must be able to design nanocarrier in suitable aerosol formulations for portable inhalers.

The two most widely used portable inhalers include pressurized metered dose inhalers (pMDIs) and dry powder inhalers (DPIs). pMDIs contain a formulation in which the therapeutic is dissolved or suspended in a propellant – commonly hydrofluoroalkanes (HFAs).²¹³ The device, when actuated, a metered volume of propellant and therapeutic are pushed through a valve system, in which the propellant

aerosolizes the therapeutic.²¹³ Dosing with this device is very uniform and is more reproducible compared to DPIs.^{74, 213} However, pMDIs are limited in some respects including high breath coordination of patient, limited dose per actuation, and high oral deposition.⁷⁴ DPIs are devices are breath-actuated devices that aerosolize dry powder through shear-induced force.²¹³ DPIs do not depend on coordination of patient breaths, however, the amount of dose delivered is highly dependent on the inspiratory flow rate making dose replication difficult.^{74, 213} Also, dry powder formulations tend to have electrostatic interactions between the particles and/or hygroscopic phenomena, which can inhibit aerosolization.^{74, 213} Despite these limitations, DPIs are typically easier to use not requiring coordination of actuation and inhalation (like pMDIs) and do not require propellant.²¹³ Therefore, both pMDIs provide various advantage and disadvantages that need to be optimized with formulation development.

Nanotechnology has made significant enhancements in the *in vitro* and *in vivo* performances of aerosol formulations for pMDIs and DPIs. In pMDIs, nanoparticle formulations have been able to provide better dose uniformity and lowering dose requirements.²¹⁹ Nanoparticle suspension formulations have minimized potential *in vivo* toxicity by lowering solvent presence in formulation.²¹⁹ For DPIs, nanoparticle formulations provide a lower density compared to dense particles of same size, which results in a lower mass median aerodynamic diameter (MMAD) allowing for deeper lung deposition, and improves powder flowability.²²⁰ In both cases, nanoparticle formulation have shown to increase residence time of drug into lungs and reduced mucociliary clearance.⁷⁴ Nanoparticles do provide these advantages listed here, but still require to have micron sized 1-5 μm to be considered optimal for deep lung deposition.²¹⁴ Therefore,

in some situations, nanoparticles can be up formulated into suitable aerosol sizes using such techniques as spray-drying in which nanoparticles are spray-dried in sugar excipients to achieve optimal aerosol sizes of micron size. Our group has demonstrated the use of PAMAM dendrimers and polyester Bis-MPA dendrimers can be formulated for aerosol delivery in pMDIs or DPIs with or without use of spray drying technique including delivery of chemotherapeutic doxorubicin and siRNA.^{96, 127, 134, 164, 221} Therefore, use of dendrimers in aerosol formulations provides a relevant strategy for the noninvasive delivery of therapeutics for the treatment of lung cancer and lung metastases.

2.7 Immunotherapy Strategies by Macrophage Modulation in the Tumor Microenvironment as Treatment Strategy for Primary and Secondary Lung Tumors

While the tumor microenvironment (TME) includes cancerous cells, leukocytes, fibroblasts, vascular endothelial cells, immune cells comprise of a major component of cell type found.⁸¹ These immune cells interact with tumor cells to influence various processes including tumor initiation, growth, and metastasis.⁸⁰ Of these immune cells, there is the present of highly plastic cell type present: macrophages. Macrophages present within the TME are known as tumor-associated macrophages (TAMs) and influence a variety of activities within the TME.⁸⁰ TAMs are derived from circulating monocytes and are one of the most abundant normal cells within the TME.⁸¹ Recently, tumor-associated macrophages (TAMs) have been considered an attractive target for therapy against many types of cancers. It has been demonstrated by preclinical and clinical studies that TAM number and density is associated with poor prognosis.^{81, 222} Many preclinical studies have demonstrated that therapy response can be enhanced when macrophage entry to TME is blocked or phenotype of these TAMs is manipulated.⁸¹

Macrophages have spectrum of phenotypes, however, for simplicity, are characterized into two polarized types: M1 or M2. M1 macrophages, or classically activated macrophages, are known to be proinflammatory, immunostimulatory, or antitumor.⁸¹ They are activated by cytokines interferon- γ and produce proinflammatory and immunostimulatory cytokines such as interleukin-12 (IL-12) and IL-23.⁸⁰ TAMs are believed to resemble more M2-polarized macrophages, in which they are anti-inflammatory, proangiogenic, immunosuppressive, and protumor.^{80, 81} The presence of TAMs – or M2-like macrophages – are seen in early stages of cancer as well as the metastatic type, and especially when tumors have been treated with chemotherapeutics.^{20, 81} M2 macrophages (TAMs) are stimulated by Th2 cytokines (I-L4, IL-10, and IL-13) within the TME and are known to promote tumor proliferation, invasion, metastasis, angiogenesis, inhibit tumor response mediated by T cells, allow for tumor progression, and demonstrate resistance to therapy.^{20, 80} The regulation and pathways between of the two TAM phenotypes and interaction with tumor cells is summarized in Figure 2.9.²⁰

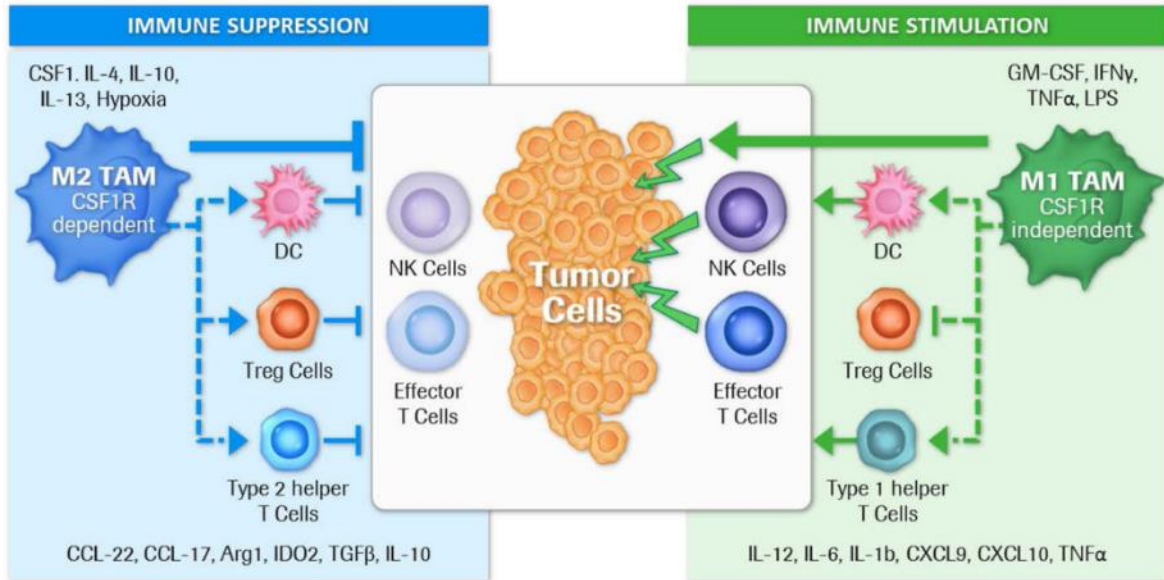


Figure 2.9. Stimulation or suppression of the immune system by TAMs. Depending on the TME, the cytokines emitted by tumor cells, fibroblasts or other stromal cells, immune cells, and macrophages themselves can polarize TAMs to M1-like or M2-like. M2 TAMs promote tumor growth (not illustrated here) as well as suppress various immune effector cells directly or through other immune cells that lead to tumor cell elimination. M1 TAMs can either directly kill tumor cells or stimulate/inhibit other immune cells to kill tumor cells by releasing of various cytokines/chemokines. M2 TAMs are known to express colony-stimulating factor 1 receptor (CSF1R) and is essential to their function, making CSF1R a desirable therapeutic target to eliminate/repolarize these cells.²⁰

The colony-stimulating factor 1 receptor (CSF1R) is a critical receptor for mononuclear phagocyte system, and in particular macrophages and macrophage polarization.^{20, 80} CSF1R belongs to a type III tyrosine kinase receptor family, in which CSF1 or IL-34 can bind to receptor causing homodimerization and subsequent activation and rapid endocytosis.^{20, 223} The details of activation can be seen in Figure 2.10.²²⁴

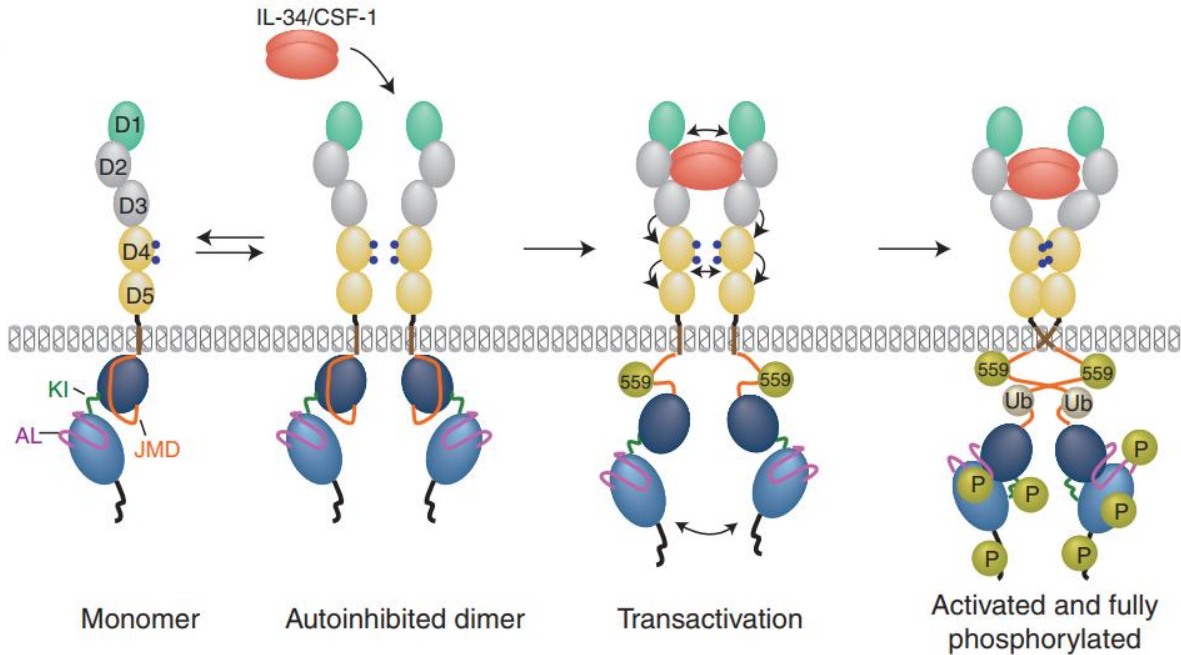


Figure 2.10. CSF1R activation. CSF1/IL-34 bind to ligand causing homodimerization. Subsequent phosphorylation (P) and ubiquitination (Ub) lead to receptor to be fully activated. Phosphorylation of 550 residue and ubiquitination are critical in further tyrosine phosphorylation and activation.²²⁴

CSF1/CSF1R signaling promotes proliferation and differentiation of myeloid cells into M2 TAMs and recruitment into tumors, and CSF1R+ macrophages have been correlated with poor survival in several types of tumors.^{20, 82} Therefore, inhibition of CSF1R by the use of various inhibitors (seen in Figure 2.11)²²² have recently been testing preclinically and clinically.⁸⁰ The inhibition of CSF1R can lead to the elimination of M2 TAMs or their repolarization to M1 phenotype. Therefore, the change in M1/M2 ratio by increasing M1 phenotype and decreasing M2 phenotype is thought to increase efficacy of treatment.

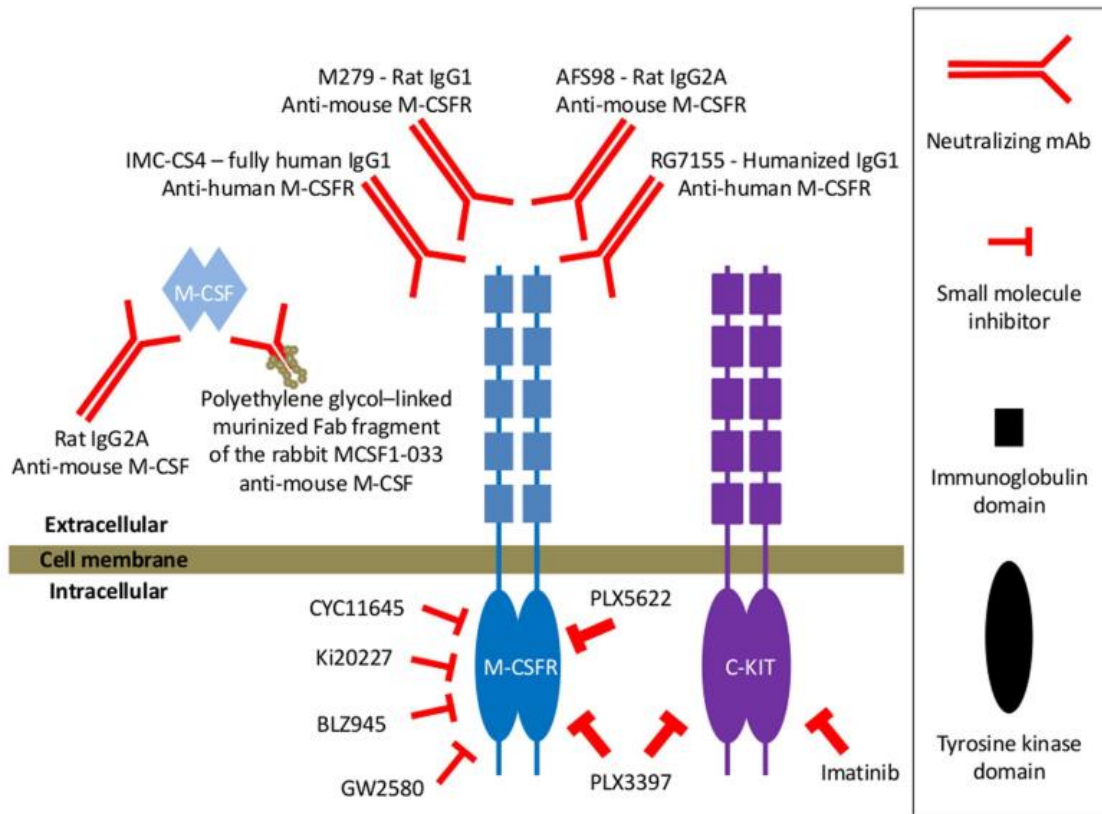


Figure 2.11. Examples of various CSF1R signaling blocking agents. PLX3397 is a tyrosine kinase inhibitor.²²²

Of these CSF1R inhibitors, the small molecule PLX3397 an oral tyrosine kinase inhibitor has shown great promise in increasing efficacy preclinically with current clinical trials taking place. Its target is intracellular (Figure 2.11) by inhibiting the phosphorylation of the kinase domains, therefore, preventing the CSF1R activation.^{222, 225} It has been shown to repolarize M2 TAMs to M1 TAMs or eliminating M2 TAMs to alter the overall M1/M2 ratio.⁸³ It has been demonstrated efficacy *in vivo* and is currently in clinical trials for use as a monotherapy and combination therapy.^{20, 80} As a monotherapy, it is currently in ongoing or complete clinical trials for c-kit-mutated melanoma, glioblastoma, prostate cancer, sarcoma, neurofibroma, classical Hodgkin lymphoma, and leukemias.²⁰ Combination therapies include PLX3397 in combination with chemotherapeutics,

irradiation, anti-angiogenic molecules, as well as other cancer immunotherapies for treatment of variety of cancers including prostate cancer, breast cancer, glioblastomas, and melanomas, and various other solid tumors.^{20, 82} Of the clinical trials, CSF1R inhibitors in combination with various immunotherapies (immune-checkpoint inhibitors, which has shown great promise in over conventional therapy including for NSCLC) is the dominant combination group being tested.²⁰ For PLX3397, it is being combined with anti-PD1 monoclonal antibody Pembrolizumab for the treatment of various tumors including NSCLC, solid tumors, malignant melanoma, and others.²⁰ The efficacy and various combinations of most effective treatment has not been concluded and may depend on tumor type. Currently, research on effectiveness in various situations and desired synergistic combinations is yet to be discovered.

CHAPTER 3 – EFFECT OF THE CONJUGATION DENSITY OF TRIPHENYLPHOSPHONIUM CATION ON THE MITOCHONDRIAL TARGETING OF POLY(AMIDOAMINE) DENDRIMERS

3.1 Introduction

Mitochondria are responsible for maintaining cellular homeostasis and producing cellular energy (adenosine triphosphate - ATP) via oxidative phosphorylation.^{84, 85} They are also key players in the production of reactive oxygen species as well as regulating calcium homeostasis and the intrinsic apoptotic pathway.^{48, 50, 84} Mitochondria are organelles of great relevance in a variety of important highly energy-dependent tissues, including brain, heart, and muscle.^{84, 226} As a consequence, mitochondrial dysfunction has been linked to a range of diseases in these tissues (and others) including neurodegenerative and neuromuscular disorders, cancer, ischemia-reperfusion injury, metabolic diseases such as diabetes and obesity, chronic autoimmune inflammatory diseases, kidney and liver diseases, and aging.^{50, 53, 84, 227-230} In spite of the clinical relevance of these mitochondrial-related diseases many still lack effective therapeutic options.^{84, 231} The ability to design mitochondrial-targeting systems may therefore provide valuable alternative strategies to enhance therapeutic outcomes of mitochondrial-related diseases while at the same time minimizing side effects associated with the therapeutic molecules.²³²

One major class of mitochondrial-targeting molecules is delocalized lipophilic cations (DLCs). Triphenylphosphonium cation (TPP),^{50, 84} one of the most common DLCs, has been shown to accumulate preferentially at the inner mitochondrial membrane,⁵⁰ at concentrations approximately 5-10 fold greater in the cytoplasm compared to the extracellular environment, with a further accumulation of hundreds of

times within the mitochondria when compared to the cytoplasm.²²⁶ The colocalization efficiency of TPP with the mitochondria is related to its lipophilic nature and delocalized positive charge, which allows TPP to permeate through membrane bilayers (hydrophobic) that have large negative potentials such as that of the mitochondria - 150-180 mV.^{172, 233} The unique properties of TPP has been explored to help target a number of therapeutic agents to mitochondria including antioxidants,^{176, 226, 229, 234} anticancer agents,^{54, 87, 90, 176, 235, 236} peptides,⁹² nucleic acids,²³⁷ and photosensitizers for photodynamic therapy²³⁸⁻²⁴⁰ through direct conjugation to the drug or via a versatile nanocarrier. The ability to combine the targeting properties of DLCs with nanocarrier systems may thus result in the development of new drug delivery technologies with the potential to address mitochondrial-related disorders as higher payloads, spatially and temporally controlled drug release, and improved pharmacokinetics can be potentially achieved by controlling the chemistry of the nanocarrier.²³¹

Within this context, poly(amidoamine) (PAMAM) dendrimers are very relevant nanocarrier candidates as they possess a large density of surface functional groups,^{34, 35, 231} which can be used to conjugate therapeutic molecules of interest. Drug conjugation to the dendrimers may also help increase the solubility and bioavailability of the conjugated therapeutic^{36, 116, 123} and the preservation of their physical and structural integrity within biological systems.^{121, 231} Dendrimers also display highly reproducible pharmacokinetic profiles due to their uniform structure.^{36, 42, 121, 125} They are also a very relevant option for the delivery of combination therapies, which is highly significant for the treatment of multidrug resistant (MDR) cancers.¹⁹² . Their surface groups can also be modified with ligands that may help further enhance the solubility of the drug-dendrimer

conjugates,^{36, 116, 123} increase circulation time,^{116, 241} reduce toxicity,^{42, 241} and also act as flexible linkers to targeting moieties such as TPP.^{242, 243}

Considering the challenges and opportunities stated previously, the goal of this study was to systematically investigate the effect of the number density of TPP conjugated to PAMAM dendrimer nanocarriers (DNCs) on the mitochondrial-targeting ability of such nanocarriers. More specifically, we report here the synthesis, cellular uptake, cytotoxicity, and mitochondrial colocalization of TPP-modified, amine-terminated, generation 4 PAMAM (G4NH₂) dendrimer nanocarriers on an *in vitro* model of the human alveolar epithelium (A549 cells). We study the effect of the type of conjugation between TPP and dendrimer: direct (G4NH₂-TPP) vs. that through a flexible poly(ethylene) glycol (PEG) linker (G4NH₂-PEGTPP). We also determine the impact of the number density of conjugated TPP (TPP or PEGTPP) on the interaction of the DNCs with A549 cells and their mitochondrial colocalization. Three levels were investigated for G4NH₂-TPP: no (0 TPP); low (5 TPP); and medium (10 TPP); and three for G4NH₂-PEGTPP: low (5 PEGTPP); medium (10 PEGTPP) and high (21 PEGTPP).

3.2 Materials and Methods

3.2.1 Materials

Generation four, amine-terminated, poly(amidoamine) (PAMAM) dendrimer (G4NH₂) provided in methanol at 9.8% w/w was purchased from Dendritech Inc. (Midland, MI). G4NH₂ dendrimer was heated at 70°C for 30-40 minutes and dried under vacuum to remove methanol solvent prior to further reaction. Methylsulfoxide (DMSO) anhydrous (Acros), Fluorescein isothiocyanate (FITC) (Pierce), N-Hydroxysuccinimide (NHS) (Acros), sodium chloride (NaCl), phosphate buffered saline (PBS, 10x), and (4-(2-

hydroxyethyl)-1-piperazineethanesulfonic acid) (HEPES) were purchased from Thermo Fischer Scientific (Rockford, IL). (3-Carboxypropyl)triphenylphosphonium bromide (TPP), P-toluenesulfonic acid (p-TSA) and triethylamine (TEA) were purchased from Sigma Aldrich (St. Louis, MO). N-(3-dimethylaminopropyl)-N'-ethylcarbodiimide (EDC) was purchased from Advanced ChemTech Inc. (Louisville, KY). NH₂-PEG1000Da-COOH (PEG) was purchased from Jenkem Technology (Plano, TX). All chemicals were used as received unless otherwise specified. Spectra/Por cellulose ester membrane dialysis tubing was purchased from Spectrum Laboratories, Inc. (Rancho Dominguez, CA). Deuterated DMSO (d-DMSO) and Deuterium Oxide (D₂O) were purchased from Cambridge Isotope Laboratories (Tewksbury, MA). Hank's Balanced Salt Solution (1xHBSS) supplemented with 0.01 M HEPES was prepared according to recipe provided by Irvine Scientific (Santa Anna, CA). Deionized (DI) water (resistivity of 18.2 MΩ.cm) was obtained from NANOpure[®] Diamond UV ultrapure water system (Barnstead International - Lake Balboa, CA). Amicon Centrifugal Filters were purchased from EMD Millipore (Billerica, MA). Dulbecco's Modified Eagle Medium 1x high glucose (DMEM), Penicillin–Streptomycin, Mitotracker[®] Deep Red FM (Molecular Probes[®], Invitrogen), NucBlue™ Live Cell Stain (R37605) (Molecular Probes[®]), Trypan Blue (0.4 %), and 3-(4,5-dimethylthiazol-2-yl)-2,5-diphenyltetrazolium bromide (MTT) were purchased from Life Technologies (Grand Island, NY). Fetal Bovine Serum (FBS, non-heat inactivated) was purchased from Atlanta Biologicals (Flowery Branch, GA). Trypsin-EDTA (1x) (Corning[®]), and 24-well and 96-well cell culture plates (Corning[®]) were purchased from VWR International.

3.2.2 Conjugation of FITC to G4NH₂ Dendrimer

G4NH₂ (437 mg) was dissolved in dimethyl sulfoxide (DMSO, 44.24 mL) with the addition of p-TSA (118.05 mg) and FITC (20.06 mg) was stirred at room temperature for 24 hours to form the G4NH₂-FITC conjugate. The product was dialyzed against DI water for 24 hours using a Spectra/Por dialysis membrane (MWCO 1000 Da), and further purified using an Amicon Ultra 15 centrifugal filter (MWCO 3000 Da) against a 1xPBS, 1 M NaCl solution (pH 7.2) followed by DI water. The product was then frozen overnight and lyophilized to obtain solid product - G4NH₂-FITC conjugate. The G4NH₂-FITC conjugate was characterized by ¹H-NMR (Varian Mercury 400 MHz). Light Scattering (LS, Malvern Zetasizer) was used to obtain the hydrodynamic diameter (HD) and zeta potential (ζ) of the conjugates. ¹H-NMR analysis was conducted with 9.91 mg dissolved in d-DMSO. 1 mg/mL of G4NH₂-FITC dissolved in DI water and analyzed for LS. The G4NH₂-FITC conjugate was then used as reactant in the addition of TPP or PEGTPP, as described below, or kept as the G4NH₂-FITC-0TPP (also called G4NH₂-0TPP), a negative control group (no mitochondrial-targeting TPP). The G4NH₂-0TPP product was left in DMSO and frozen at -20°C until needed.

3.2.3 Conjugation of TPP to G4NH₂-FITC

TPP was activated using EDC/NHS coupling reaction adding 1.2:1 molar ratio of both EDC and NHS to TPP dissolved in anhydrous DMSO and allowed to stir at room temperature for 3 hours to obtain activated TPP. G4NH₂-0TPP conjugate was added to the activated TPP dissolved in DMSO and the reaction mixture was allowed to proceed at room temperature for 3 days. TPP was conjugated to G4NH₂-FITC at various TPP densities by increasing the molar feeding ratios of activated TPP to G4NH₂-FITC to form

G4NH₂-FITC-TPP – also called G4NH₂-TPP. The reaction mixture was then dialyzed against distilled water using a Spectra/Por dialysis membrane (MWCO 8000 Da). The product was further purified using an Amicon Ultra 15 centrifugal filter (MWCO 3000 Da) against a 1xPBS, 1 M NaCl solution (pH 7.2) and again against distilled water. The G4NH₂-TPP conjugates were characterized by ¹H-NMR and LS as discussed above.

3.2.4 Conjugation of Bifunctional PEG1000 to TPP

The conjugation of TPP to NH₂-PEG1000-COOH to form PEGTPP was achieved by activating TPP using EDC/NHS coupling reaction with 1:1 molar ratio of TPP:EDC and TPP:NHS in anhydrous DMSO and stirred at room temperature for 12 hours. NH₂-PEG1000-COOH (70 mg) was dissolved in anhydrous DMSO with TEA (34.2 μL) at a molar ratio of 2:1 of TEA:PEG and added to the reaction mixture of activated TPP and allowed to stir at room temperature for 24 hours. The DMSO was removed using vacuum pump for 24 hours.

3.2.5 Conjugation of PEGTPP to G4NH₂-FITC

Once the PEGTPP product was synthesized, PEGTPP was dissolved in anhydrous DMSO and activated using EDC/NHS coupling reaction with a 1:1 molar ratio of PEGTPP:EDC and PEGTPP:NHS. The mixture was let to stir at room temperature for 10 minutes. The activated PEGTPP was added to the G4NH₂-FITC conjugate at increasing molar feeding ratios to form G4NH₂-FITC-PEGTPP (also called G4NH₂-PEGTPP) at several PEGTPP densities, and then stirred at room temperature for 5 days. The reaction mixture was then dialyzed against 1xPBS for 24 h and DI water for an additional 48 h using a Spectra/Por dialysis membrane (MWCO 8000 Da). The G4NH₂-PEGTPP products were frozen overnight and lyophilized to form solid products.

The G4NH₂-PEGTPP conjugates were characterized by ¹H-NMR and LS as discussed above.

3.2.6 Cell Culture

A459 lung adenocarcinoma cells were grown in DMEM supplemented with 10% fetal bovine serum (FBS) and 1% Penicillin Streptomycin (100 U/mL Penicillin and 100 µg/mL Streptomycin) antibiotics (AB) and cultured at 37°C with 5% CO₂.

3.2.7 Cytotoxicity of Dendrimer Conjugates

A549 cells were seeded at a density of 5,000 cells/well in a 96-well plate in DMEM supplemented with 10% FBS and 1% AB and incubated for 24 hours under 5% CO₂ at 37°C. Dendrimer conjugates were added at concentrations varying from 0-20 µM in fresh culture medium (DMEM) and incubated for an additional 24 hours under 5% CO₂ at 37°C. DMEM with no dendrimer conjugates were placed in wells and used as the controls. Cell viability was analyzed using MTT Cell Proliferation Assay (Molecular Probes). Briefly, medium from each well was removed. Subsequently 110 µL of 1 mM MTT solution was added to each well and incubated for 4 hours at 5% CO₂ at 37°C. 85 µL was removed from each well and replaced with 75 µL of DMSO and let to incubate for 1 additional hour. The absorbance was measured at 540 nm using a microplate reader (Spectra MAX 250) and analyzed by SOFTmax PRO software. Cell viability was calculated as (absorbance of treated cells/absorbance of control cells) x 100%.

3.2.8 Cellular Internalization of the Dendrimer Conjugates Analyzed by Fluorescence Activated Cell Sorting (FACS)

A549 cells were seeded at 300,000 cells per well in a 24-well plate in DMEM medium supplemented with 10% FBS and 1% AB and cultured at 37°C with 5% CO₂. The

following day, the cells were pre-incubated in 1xHBSS (Hank's Balanced Salt Solution) for 30 minutes prior to incubation of various dendrimer conjugates at 1 μM in 1xHBSS adding 500 μL per well at various time points ranging from 0.25 hours to 5 hours. Cells were then washed with 1xHBSS (pH 7.2) and 0.2 mL of 0.1% w/v of Trypan Blue was added to each well to quench any fluorescence associated the conjugates that are retained on the surface of cells. The cells were then again washed with 1xHBSS and removed from each well. The cells were then centrifuged at room temperature at 1500 rpm for 5 min to form a pellet. The pellet was resuspended in 1xHBSS buffer to be analyzed via FACS using a HWCRC 615- BD LSR II Analyzer. The data was analyzed by FlowJo software. The median fluorescence intensity (MFI) of FITC was used as to analyze the rate of cellular internalization of dendrimer conjugates into the cells as a function of the dendrimer chemistry and time after incubation.

3.2.9 Colocalization of Dendrimer Conjugates by Confocal Microscopy

A549 cells were seeded at 300,000 cells per well in a 24-well plate containing a circular cover glass in each well 24 hours prior to treatment. 500 μL of a 2 μM dendrimer conjugate solution in 1xHBSS was added to each well and incubated for 5 hours at 5% CO_2 and 37 $^\circ\text{C}$. The cells were then stained with 100 nM of Mitotracker Deep Red FM (Life Technologies) for 30 minutes followed by Hoechst 3342-Nuc Blue stain for 15 minutes. The cells were washed twice with 1xHBSS between each staining. The cells were then fixed with 4% p-Formaldehyde for 15 minutes. The colocalization of the dendrimer conjugates to the mitochondria was analyzed using a Zeiss LSM 780 confocal microscope with a 40x oil objective lens. The Pearson's Correlation Coefficient (PCC) was determined by analyzing each image using Volocity Software to quantify the degree

of colocalization between the dendrimer conjugates (FITC) and the mitochondria (Mitotracker Deep Red FM).

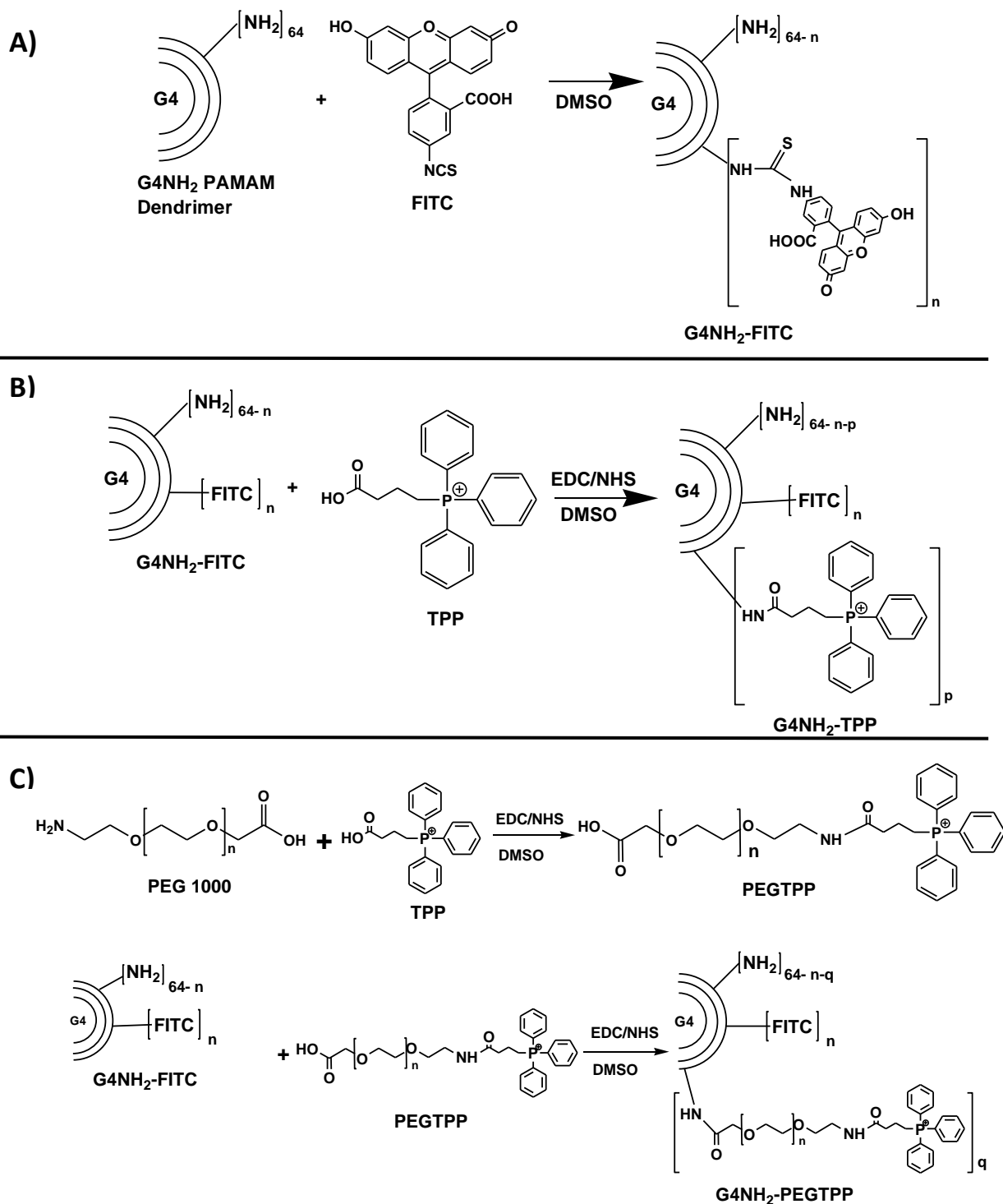
3.2.10 Statistical Analysis

All data is presented as a mean \pm standard deviation. The mean was calculated from a minimum of three independent trials for each measurement ($n \geq 3$). One-way analysis of variance (ANOVA) followed by Tukey's Multiple Comparison Test or an unpaired t-test was performed using GraphPad Prism 5 software. Means were considered statistically significant if $p < 0.05$.

3.3 Results

3.3.1 TPP and PEGTPP Conjugation

FITC was conjugated to the primary amines of G4NH₂ to prepare fluorescently-labeled dendrimers (G4NH₂-FITC), as shown in Scheme 3.1A.



Scheme 3.1. Synthesis of **A)** FITC-labeled, generation 4, amine-terminated poly(amidoamine) dendrimer ($G4NH_2-FITC$); **B)** TPP-conjugated, FITC-labeled $G4NH_2$ ($G4NH_2-TPP$); and **C)** (i) TPP-conjugated poly(ethylene glycol) 1000 MW (PEGTPP), and (ii) PEGTPP-conjugated, FITC-labeled $G4NH_2$ ($G4NH_2-PEGTPP$).

The conjugation of FITC was confirmed by ^1H NMR, as shown in Figure A1 in Appendix A. The results indicate 2 FITC molecules conjugated per dendrimer on average as calculated by peak area represented by protons on FITC in peak at 6.4 ppm (labeled FITC – Figure A1). Conjugation of FITC is done in order to follow the rate of cellular internalization and co-localization of the nanocarriers. The size (HD) and ζ of the FITC-conjugated G4NH₂ (also called G4NH₂-0TPP) is shown in Table 3.1.

Table 3.1. The hydrodynamic diameter (HD) and surface charge (zeta potential, ζ) of the dendrimer conjugates measured by light scattering (LS). Measurements were performed in water. Data expressed as mean \pm standard deviation ($n \geq 3$). All carriers have an average of 2 FITC per G4NH₂.

Compound	Light Scattering	
	HD \pm s.d [#] (nm)	$\zeta \pm$ s.d [#] (mV)
G4NH ₂ -0TPP	6 \pm 2	30 \pm 7
G4NH ₂ -5TPP	7 \pm 3	34 \pm 7
G4NH ₂ -10TPP	6 \pm 2	43 \pm 8
G4NH ₂ -5PEGTPP	8 \pm 2	53 \pm 8
G4NH ₂ -10PEGTPP	9 \pm 3	18 \pm 6
G4NH ₂ -21PEGTPP	12 \pm 4	14 \pm 5

TPP and PEGTPP were subsequently conjugated to G4NH₂-FITC, as shown in Scheme 1B and C, respectively. Two TPP densities were targeted. An average of 5 and 10 TPP molecules were attached to each G4NH₂-FITC dendrimer, as confirmed by ^1H NMR in deuterium Oxide (D₂O) solvent measured at 400 MHz on Aligent Mercury Spectrometer - shown in the ^1H NMR spectra Figure A1, Appendix A. The peak areas representing the protons found on the phenyl rings on TPP (two peaks found between 7.6-7.8 ppm, peak f – Figure A1) and peak found on alkyl chain of TPP (peak at 1.8-1.9 ppm, peak e – Figure A1) were used to calculate the average numbers of TPP per

dendrimer (Figure A1). These conjugates were termed as follows: G4NH₂-5TPP, and G4NH₂-10TPP. The HD and ζ of the TPP conjugates are also shown in Table 3.1.

The G4NH₂-TPP conjugates all had similar sizes, between 6-7 nm in diameter. The ζ for all the G4NH₂-TPP conjugates was positive. A slight increase in ζ from G4NH₂-0TPP to G4NH₂-5TPP to G4NH₂-10TPP was observed, but it was not statistically different between each of the conjugates (Table 3.1). Therefore, each of the G4NH₂-TPP conjugates was similar in size as well as containing similar positively-charged surfaces.

To evaluate the effect of PEG on the surface properties and mitochondrial targeting of G4NH₂ dendrimers, TPP was conjugated to PEG to form PEGTPP, which in turn was conjugated to G4NH₂-FITC dendrimers to form G4NH₂-FITC-PEGTPP – also called simply G4NH₂-PEGTPP. The successful conjugation PEGTPP to G4NH₂-FITC was also confirmed by ¹H NMR, as shown in Figure A1 in Appendix A. The peak areas representing the phenyl rings on TPP (7.6-7.8 ppm, peak f – Figure A1), the peak area representing PEG chain (3.6 ppm, peak g – Figure A1) and peak area of CH₂ group near the amide bond between the dendrimer and PEG (4.0 ppm, peak h – Figure A1) were used to estimate the average numbers of PEGTPP molecules added per dendrimer. An increase in PEGTPP to G4NH₂-FITC-0TPP feeding ratio resulted in an increase in density of PEGTPP. An average of 5, 10, and 21 PEGTPP molecules were attached to each G4NH₂ dendrimer, as confirmed by ¹H NMR spectra as seen in Figure A1 in Appendix A.

The HD and ζ of these conjugates were also determined and shown in Table 3.1. The HD of the conjugates increased slightly from 8 nm to 12 nm, as the density of PEGTPP conjugated to G4NH₂ increases from 5 PEGTPP to 21 PEGTPP. The ζ for G4NH₂-5PEGTPP increased to +53 ± 8 mV, being the highest ζ of all conjugates.

However, as the PEGTPP density increases from 10 (G4NH₂-10PEGTPP) to 21 (G4NH₂-21PEGTPP), the ζ of the conjugates decreased to $+18 \pm 6$ mV and $+14 \pm 5$ mV, respectively, remaining overall positively charged (Table 3.1).

3.3.2 Cytotoxicity of the Dendrimer Conjugates

The cytotoxicity of the various dendrimer conjugates was determined using the MTT assay. TPP- and PEGTPP-conjugates were incubated with A549 cells for 24h at increasing concentrations of the respective conjugates, and their cellular viability assessed. The results are summarized in Figure 3.1.

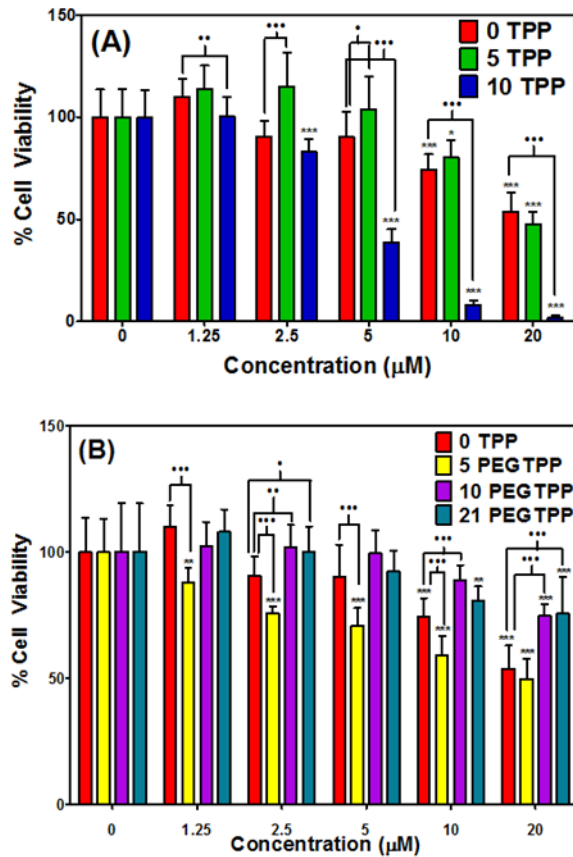


Figure 3.1. Cell viability of **A)** G4NH₂-TPP conjugates and **B)** G4NH₂-PEGTPP conjugates measured by MTT assay at 24h incubation and increasing nanocarrier concentration. *, **, *** represents the statistical analysis between the control group indicated at 0 μM representing 100% viability. ●, ●●, and ●●● represents the statistical analysis between G4NH₂-0TPP group and other indicated dendrimer conjugates (* / ● p < 0.05, ** / ●● p < 0.01 *** / ●●● p < 0.001).

The results demonstrate that the density of TPP as well as that of PEGTPP does have an effect on the toxicity of the dendrimer conjugate. As the TPP density increases to 10 TPP molecules per dendrimer, a greater cellular toxicity is observed when compared to G4NH₂-0TPP, at all concentrations investigated. Furthermore, a statistical difference between that and control is seen at a much lower concentration (2.5 μM), which is not observed for the other G4NH₂-TPP conjugates. On the other hand, G4NH₂-5TPP did not show a significant increase in cytotoxicity when compared to G4NH₂-0TPP. These two groups had similar differences to control (100% cell viability) with toxicity (statistical difference from control) only observed at 10 μM or greater concentration. The G4NH₂-5TPP conjugate demonstrated a decreased toxicity compared to G4NH₂-0TPP at 2.5 and 5 μM concentrations and no statistical difference at all the other concentrations tested. Therefore, a low enough TPP density (5 or below) has no significant effect on the toxicity of the dendrimer.

The attachment of PEG as a linker between the TPP targeting moiety and the G4NH₂ dendrimer also had an effect on toxicity. The G4NH₂-5PEGTPP is significantly more cytotoxic than G4NH₂-0TPP. Of all the groups, G4NH₂-5PEGTPP was the most toxic early on, showing a statistical difference from 100% cell viability as early as 1.25 μM and being statistically different from G4NH₂-0TPP at all concentrations but 20 μM, where there was no statistical difference in toxicity. However, the dendrimer conjugates containing a higher density of PEGTPP showed a decrease in cytotoxicity compared to G4NH₂-0TPP. G4NH₂-10PEGTPP only showed a statistical difference from 100% cell viability at 20 μM. The G4NH₂-10PEGTPP conjugate only demonstrated a significant difference in cytotoxicity at 2.5, 10, and 20 μM, being less cytotoxic than G4NH₂-0TPP.

G4NH₂-21PEGTPP did not show any significant difference in cytotoxicity when compared to G4NH₂-0TPP when both are compared to 100 % cell viability, with both groups showing a statistical difference at 10 μM. The only statistical difference between G4NH₂-0TPP and G4NH₂-21PEGTPP was seen at 20 μM. Therefore, the addition of PEGTPP at a density greater than 5 PEGTPP did (positively) affect the toxicity of the dendrimer conjugates; it decreased their toxicity, showing statistical differences compared to G4NH₂-0TPP at higher concentrations tested (those concentrations where G4NH₂-0TPP showed a statistical difference from 100% viability).

3.3.3 Cellular Internalization of Dendrimer Conjugates Analyzed by FACS

The extent and rate of internalization of the dendrimer conjugates was determined by FACS. The effect of TPP density as well as PEGTPP density was analyzed. The median fluorescence intensity (MFI) as a function of contact time between the various conjugates and A549 cells is summarized in Figures 3.2A and B.

As the density of TPP in G4NH₂-TPP increases, the rate and extent of internalization of the conjugate is observed to increase dramatically (Figure 2A). G4NH₂-5TPP showed a 3.5 ± 0.3 -fold increase in internalization over the various time points when compared to G4NH₂-0TPP, while the MFI of G4NH₂-10TPP increased 10.0 ± 2.0 -fold (except at 0.25 hour, which showed a ~20-fold increase) in internalization as compared to G4NH₂-0TPP at the various time intervals measured. G4NH₂-10TPP also showed a 3.4 ± 0.9 -fold increase in internalization compared to G4NH₂-5TPP at various time points. Similar trends are seen when the rates of internalization are compared. The internalization rates for G4NH₂-0TPP, G4NH₂-5TPP, and G4NH₂-10TPP are 214.01 a.u./hr, 681.4 a.u./hr, and 2050.5 a.u./hr, respectively. A clear increase in rate with the

increase in TPP density of the dendrimer is seen: ~ 3-fold increase for G4NH₂-5TPP when compared to G4NH₂-0TPP and a ~ 10-fold increase for G4NH₂-10TPP compared to G4NH₂-0TPP. Also, there was a ~ 3-fold increase in rate when comparing G4NH₂-10TPP group with G4NH₂-5TPP group.

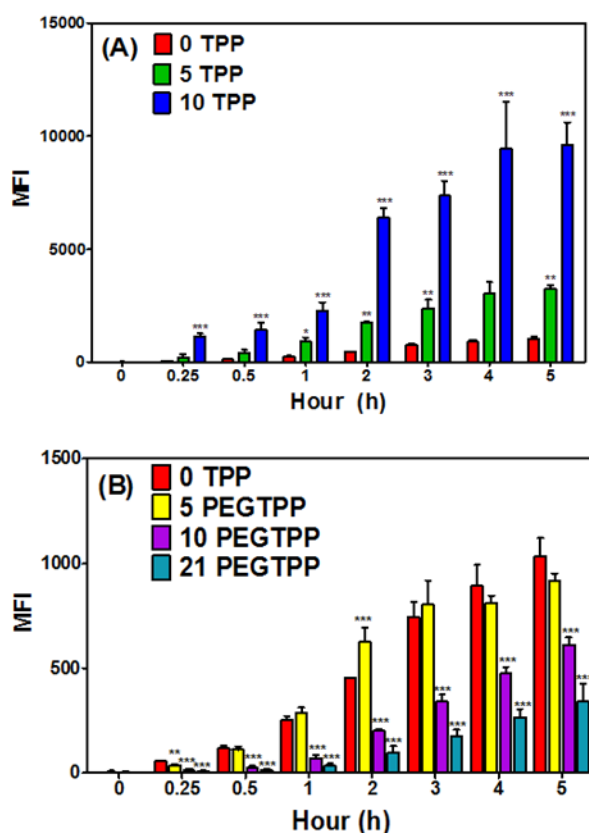


Figure 3.2. Cellular uptake of **A)** G4NH₂-TPP conjugates and **B)** G4NH₂-PEGTPP conjugates analyzed by FACS. The median fluorescence intensity (MFI) provided by FITC labeling of the various conjugates was compared to bare FITC-labeled dendrimer (0 TPP) at various time points (* p < 0.05, ** p < 0.01 *** p < 0.001).

Therefore, the conjugation of TPP to dendrimer is seen to lead to an increase in the rate and extent of internalization of the dendrimer.

The effect of PEGTPP on internalization of the dendrimers on A549 cells was also analyzed. The results are compared against those for G4NH₂-0PEGTPP (Figure 2B). As seen in Figure 2B, at the final time point (5 h), no statistical difference in the extent of

internalization is seen between G4NH₂-5PEGTPP and G4NH₂-0PEGTPP. However, the MFI is seen to decrease when compared to G4NH₂-0PEGTPP as the density of PEGTPP increased to 10PEGTPP, and further decrease at 21PEGTPP (Figure 2B). G4NH₂-10PEGTPP showed a 3.0 ± 1.3 -fold decrease in MFI and G4NH₂-21PEGTPP showed a 5.0 ± 2.0 -fold decrease in MFI at various time points when compared to G4NH₂-0PEGTPP. By 5 hours, the internalization decreased to 1.7-fold for G4NH₂-10PEGTPP and 3.0-fold for G4NH₂-21PEGTPP. There is also a 1.8 ± 0.2 -fold decrease in internalization at various time points when comparing G4NH₂-21PEGTPP to G4NH₂-10PEGTPP. The rates of internalization for G4NH₂-5PEGTPP, G4NH₂-10PEGTPP, and G4NH₂-21PEGTPP are as follows: 196.3 a.u./hr, 125.3 a.u./hr, and 69.5 a.u./hr, respectively. There is no significant change in the rate of internalization between G4NH₂-5PEGTPP and G4NH₂-0TPP, while a decrease in rate of ~2 between G4NH₂-10PEGTPP and G4NH₂-0TPP and decrease of ~3 between G4NH₂-21PEGTPP and G4NH₂-0TPP was observed. A ~2-fold decrease in rate of uptake is observed when comparing G4NH₂-21PEGTPP and G4NH₂-10PEGTPP.

The effect of TPP attached to the end of PEG on the internalization of the conjugates was also evaluated by comparing the internalization of G4NH₂-10PEGTPP to that of G4NH₂-10PEG (no TPP), as shown in Figure 3.3.

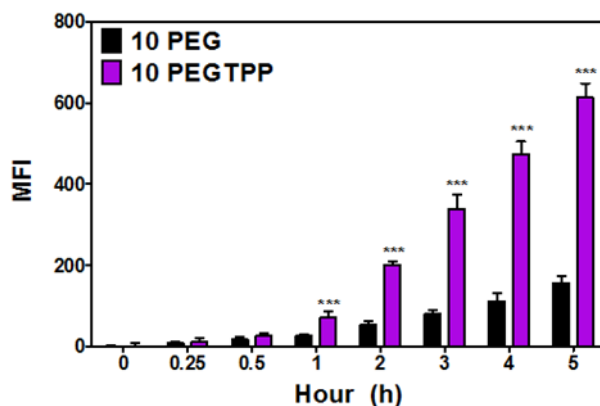


Figure 3.3. A comparison of the cellular uptake of G4NH₂-10PEG and G4NH₂-10PEGTPP conjugates analyzed by flow cytometry. The MFI provided by FITC labeling of the various conjugates was compared between the two groups using two-tailed t test (* p < 0.05, ** p < 0.01 *** p < 0.001).

After 1 h, a significant increase in the extent of internalization is seen for the conjugate containing TPP. At 1 hour, the internalization of G4NH₂-10PEGTPP is 2.8-fold greater than that for G4NH₂-10PEG. From 2 h to 5 h, the internalization G4NH₂-10PEGTPP is 4.0 ± 0.3 -fold that of G4NH₂-10PEG. When comparing the rates of internalization, G4NH₂-10PEGTPP (125.3 a.u./hr) is ~ 4-fold greater than that for the G4NH₂-10PEG conjugate (29.5 a.u./hr). Thus, the presence of TPP on PEG does affect the internalization of the dendrimer by increasing its rate and extent of cellular uptake.

3.3.4 Colocalization of Dendrimer Conjugates

The mitochondrial targeting ability of the dendrimer conjugates was evaluated by confocal microscopy. The dendrimer conjugates were labeled with FITC in order to quantify their colocalization with the mitochondria, which were stained with Mitotracker Deep Red FM. Figure 3.4 shows the results of the incubation of the FITC-labeled dendrimer conjugates with mitochondria in A549 cells.

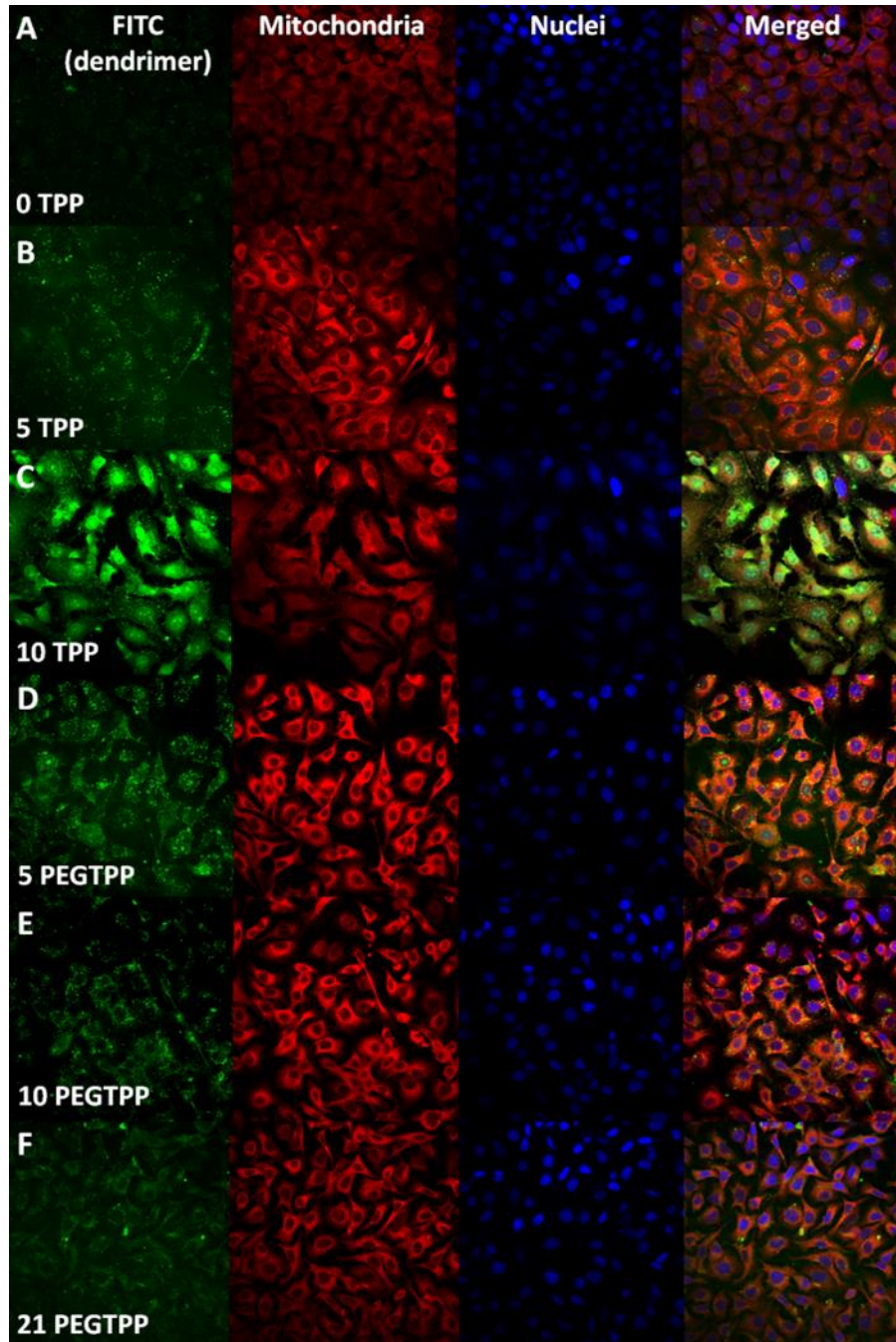


Figure 3.4. Colocalization between dendrimer (green) and mitochondria (red) to assess the targeting ability of the various G4NH₂-TPP and G4NH₂-PEGTPP conjugates. The blue represents the nucleus (Hoeschst 3342-Nuc Blue stain), the red represents mitochondria (Mitotracker Deep Red FM) and green represents the dendrimer (FITC). The yellow color represents the overlap between the dendrimer and mitochondria signals. The dendrimer conjugates are seen in the following order: A) G4NH₂-0TPP, B) G4NH₂-5TPP, C) G4NH₂-10TPP, D) G4NH₂-5PEGTPP, E) G4NH₂-10PEGTPP, and F) G4NH₂-21PEGTPP.

The last (fourth) panel indicates the merged areas of co-localization between the green signal from the FITC-labeled dendrimer conjugates (first panel) with the red signal from stained mitochondria (second panel). The co-localization produced a yellow color. The third panel shows the nuclei in blue. The degree of co-localization was quantified with the help of the Pearson's correlation coefficient (PCC) for the various conjugates. The results are summarized in Figure 3.5.

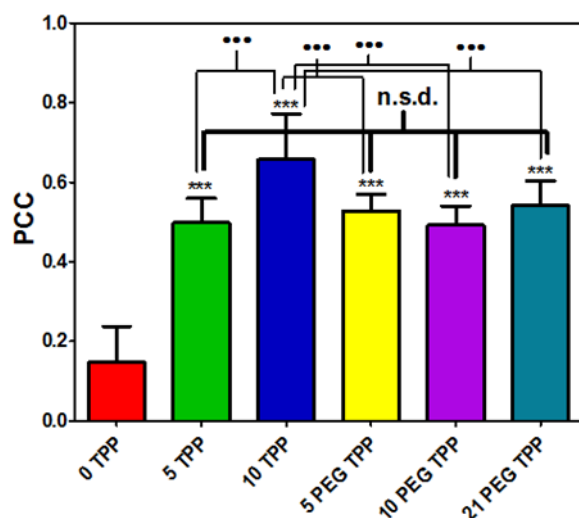


Figure 3.5. Pearson's Correlation Coefficient (PCC) of various dendrimer conjugates comparing the overlap of FITC (dendrimer) with Mitotracker Deep Red FM (mitochondria) based on confocal microscopy. *** compares each dendrimer conjugate with G4NH₂-0TPP dendrimer. ●●● represents the comparison between indicated groups. Data represents a mean \pm standard deviation (***/●●● $p < 0.001$, n.s.d. = not statistically different).

All dendrimer conjugates demonstrated an increased targeting toward the mitochondria compared to G4NH₂ bearing no TPP targeting moiety. The dendrimer conjugate that showed the highest targeting ability was G4NH₂-10TPP – statistically significant enhancement in targeting as compared with all other conjugates. All other dendrimer conjugates, excluding G4NH₂-10TPP, had the same ability to target mitochondria, which was significantly greater than the control. Therefore, the presence

of PEG as a flexible linker between the dendrimer and TPP did not affect the mitochondrial targeting ability of the conjugates.

3.4 Discussion

Cellular organelle drug targeting has many potential advantages including a decrease in the side effects as well as enhancement of the efficacy of the chosen therapeutic molecules.²³² Mitochondrial targeting continues to gain attention in the scientific community since the discovery that many diseases of great medical relevance are associated with mitochondrial dysfunction.^{50, 53, 84, 227-230} Mitochondrial dysfunction can occur due to mutations in mitochondrial DNA (mtDNA) or alterations in mitochondrial signal transduction pathways.²³¹ Due to a lack of therapeutic options for many mitochondrial diseases, there is a great need for the development of alternative therapeutic strategies that target mitochondria.^{84, 231}

TPP has been explored as a mitochondrial targeting agent due to its delocalized cationic and lipophilic nature. TPP is attracted to and tends to cross cellular and mitochondrial membranes to preferentially accumulate in the mitochondria.^{50, 84, 172, 233} TPP has been utilized to target a range of therapeutics, including antioxidants,^{176, 226, 229} anticancer agents,^{54, 87, 90, 176, 235} peptides,⁹² nucleic acids,²³⁷ and photosensitizers^{238, 239} towards the mitochondria. These have included TPP conjugated directly to therapeutic of choice^{54, 92, 226} as well as TPP conjugated to a nanocarrier^{87, 90, 176, 235, 237, 239} for targeted therapeutic delivery. Nanocarriers are of great interest in the delivery of a variety of drugs as they can be used to effectively alter the behavior of the drug *in vivo*,³⁵ improve efficacy of the drug,^{35, 36} minimize side effects,^{35, 36} target specific tissues,³⁵ control drug release,³⁵ and show great promise in the treatment of a variety of diseases.³⁶

In this work we seek to further recent work that has demonstrated that the direct attachment of TPP to G4NH₂ leads to an enhancement in targeting of the mitochondria²³¹ by systematically investigating the effect of the number density of TPP conjugated to G4NH₂ on the mitochondrial targeting ability of the DNCs. We propose two conjugation strategies: (i) the direct conjugation of TPP to dendrimer, and (ii) the conjugation of TPP to G4NH₂ through a PEG linker. PEG is relevant in many ways. PEG may act as a flexible linker thus potentially providing for a greater opportunity for the conjugated TPP to interact with the mitochondrial membrane – perhaps at lower number density. PEGylation also helps enhance aqueous solubility of the nanocarrier,^{116, 122} increase biocompatibility,^{116, 241} mediate the interaction of the dendrimer drug carrier with the physiological environment,^{116, 122} and enhance its pharmacokinetic profile.^{116, 241}

Three levels of direct TPP conjugation were investigated: no TPP (G4NH₂-0TPP); 5 TPP (G4NH₂-5TPP) and 10 TPP (G4NH₂-TPP). We observe from Table 3.1 that the direct conjugation of TPP to the dendrimer did not have a significant effect on the size (HD) or surface charge (ζ) of the nanocarriers. The HD remained around 6-7 nm for all G4NH₂-TPP. The ζ seems, on average, to increase as the density of TPP increases with a value of +43 mV for G4NH₂-10TPP and +34 mV for G4NH₂-5TPP, while in the absence of TPP, the surface charge was +30 mV. While under physiological conditions (where pH = 7.4) the primary (surface) amine groups of NH₂ are expected to be fully protonated to NH₃⁺,²⁴⁴⁻²⁴⁶ at the conditions where ζ was measured (water), the pH increases during protonation, and an equilibrium is reached before full protonation. The conjugation of TPP as a delocalized cation should thus result in an increase in the overall surface charge

of the system, as it will tend to substitute amine groups that would potentially otherwise not be protonated.

There is a direct correlation between the surface charge of the nanocarriers and their rate and extent of cellular internalization within A549 cells (Figure 3.2). The internalization of G4NH₂-5TPP is statistically significantly higher than that for G4NH₂-0TPP, and so is that for G4NH₂-10TPP, which was also higher than that for G4NH₂-5TPP. A similar trend was observed in terms of the rate of internalization. This increase in rate and extent of internalization with increase in TPP density can be attributed to the cationic and lipophilic nature of the TPP that allows it to interact with the cellular membrane given its negative potential and hydrophobic nature.^{50, 84, 172, 233} A similar correlation was observed in terms of co-localization with the mitochondria (Figures 3.4 and 3.5). While in the absence of TPP (G4NH₂-0TPP) the PCC was only 0.15 ± 0.09 , PCC for G4NH₂-5TPP was 0.50 ± 0.06 , and that for G4NH₂-10TPP 0.66 ± 0.12 , being both statistically significantly higher than control - and at 10 TPP higher than at 5 TPP. However, as the density of TPP increases so does the toxicity of the conjugate. A comparison of the half maximal inhibitory concentration (IC₅₀), the concentration of conjugate required to inhibit biological function (*in vitro* potency – A549 % cell viability) clearly demonstrates this. G4NH₂-10TPP has an IC₅₀ of 2.95 μ M, while G4NH₂-0TPP's IC₅₀ is found at significantly higher concentrations (greater than 20 μ M) (54 ± 9 % at 20 μ M) ~ 7 fold greater (Figure 3.1). At the same time, it is observed that the addition of 5 TPP does not affect the toxicity profile of the conjugate – no statistical difference compared to G4NH₂-0TPP.

In conclusion, the direct conjugation of TPP is seen to promote the rate and extent of cellular internalization as well as the mitochondrial targeting. However, the maximum

density of TPP is limited by toxicity effects. For the series of conjugates investigated in this work, it seems that 5 TPP represents the optimum number of TPP, where a significant enhancement in targeting is observed, while the toxicity profile of the conjugate is not altered relative to the bare dendrimer.

In order to address potential limitations of the direct TPP conjugation strategy discussed earlier, the conjugation of TPP through a PEG linker to G4NH₂ is also proposed. Three levels of PEGTPP density, plus the control were investigated: (i) no PEGTPP (control, G4NH₂-0TPP); (ii) 5PEGTPP (G4NH₂-5PEGTPP); (iii) 10PEGTPP (G4NH₂-10PEGTPP); and (iv) 21PEGTPP (G4NH₂-21PEGTPP).

The addition of PEGTPP is seen to lead to a significant change in the HD and ζ of the dendrimers – Table 3.1. The HD of the dendrimers is seen to increase with an increase in PEGTPP density with a dendrimer HD at 6 ± 2 nm for G4NH₂-0TPP and increasing to 8 ± 2 nm, 9 ± 3 nm, and 12 ± 4 nm for G4NH₂-5PEGTPP, G4NH₂-10PEGTPP, and G4NH₂-21PEGTPP, respectively. The addition of PEGTPP, as expected,^{122, 247} leads to an increase in the overall HD as the PEG forms an outer polymer layer. This PEG layer may have been shown to either interact with the protonated amines, extend outward, or a mix of both depending on the density and size of PEG.^{122, 247}

The surface charge for G4NH₂-10PEGTPP and G4NH₂-21PEGTPP decreased compared to the control - G4NH₂-0TPP. One could expect that the conjugation of PEG alone would lead to a decrease in the overall system charge, but since the delocalized cation TPP is conjugated to PEG, this effect should be somewhat muted. Nevertheless, the ether oxygen of PEG may also interact with the amine groups of G4NH₂, further reducing the system charge,^{122, 241} and this is the mechanism we expect to be operating

here. However, surprisingly, G4NH₂-5PEGTPP has a ζ that is larger than the ζ seen for all the dendrimer conjugates investigated in this work. The reasons for such a large ζ have not been fully elucidated yet, but one could hypothesize that at higher PEG densities of 10PEGTPP and 21PEGTPP (but not too high), the protonated amines can interact with a large number of ether oxygens²⁴⁷ without requiring the positively charged TPP ions conjugated at the end of PEG to get to close to the positively charged surface of the G4NH₂ dendrimer. There is also a greater chance of the ether groups of PEG to interact and bury TPP counterions. At lower PEGTPP densities, the interaction between protonated amines from the dendrimer and ether oxygen will more likely lead to the close approximation of the charged TPP to NH₃⁺ groups on the dendrimer surface, which is unfavorable. In that case, the presence of TPP would reduce the neutralization of the amine groups of dendrimers by PEG ethers, thus increasing the overall ζ . The synthesis and characterization of these conjugates were repeated several times and by different group members to confirm this behavior. The toxicity and internalization of these carriers also follow a trend based on ζ , further supporting the results discussed here. Therefore, the PEGTPP density plays a critical role in terms of characteristics of G4NH₂.

The use of the PEG as a linker to TPP is seen to produce the desirable characteristic of reduced cytotoxicity compared to the conjugates formed with the direct TPP conjugation, except for G4NH₂-5PEGTPP (Figure 3.1). G4NH₂-10PEGTPP and G4NH₂-21PEGTPP do not show any toxicity up to 5 μ M concentration. At high concentrations, they were also significantly less toxic than the non-conjugated G4NH₂-0TPP control (bare dendrimer). The toxicity profile of G4NH₂-5PEGTPP seems to correlate with its high surface charge, showing some toxicity at low concentrations, and

being significantly more toxic than the non-conjugated control (G4NH₂-0TPP) at all concentrations studied. While a reduction in toxicity is achieved for the TPP-conjugated dendrimers by using a PEG linker, the presence of PEG negatively affects the dendrimer internalization (Figure 3.2). As the density of PEGTPP increases, the rate and extent of internalization in A549 cells decreases, except for G4NH₂-5PEGTPP, which remains relatively unchanged compared to the non-conjugated control (G4NH₂-0TPP). It is interesting to note that when compared to the control of PEGylated dendrimer with no TPP (Figure 3 – G4NH₂-10PEG vs. G4NH₂-10PEGTPP), it is observed that the presence of TPP significantly enhances the rate and extent of internalization indicating the relevance of TPP as a potentially general strategy for the enhancement of cellular internalization of PEGylated dendrimers.

G4NH₂-FITC-5PEGTPP had similar characteristics to that of bare dendrimer (G4NH₂-FITC-0TPP) in terms of internalization and cytotoxicity. This can be attributed to a balance between the TPP increasing internalization while the PEG decreasing internalization. Therefore, both groups contain similar properties. However, the main difference between these groups is the localization of the dendrimer into the mitochondria which is seen in the G4NH₂-FITC-5PEGTPP group and not in the G4NH₂-FITC-0TPP group. Therefore, the G4NH₂-FITC-5PEGTPP group acts very similarly *in vitro* as bare dendrimer while localizing in the mitochondria. This can be a useful strategy if similar dendrimer properties (surface charge, rate of internalization, biodistribution, etc.) are required for a particular application. However, if the application requires a higher solubility of therapeutic, increased circulation time, reduced toxicity (as seen with PEGylated dendrimers) then a higher density of PEGTPP can be used, which would alter these

various parameters while maintaining the mitochondrial targeting ability of the nanocarrier.

While the presence of PEG as a linker to TPP in G4NH₂-PEGTPP decreases the rate and extent of cellular internalization at higher densities (10 PEGTPP and above), co-localization results (Figure 3.4 and 3.5) demonstrate that they are still actively targeting mitochondria with PCC similar to G4NH₂-5TPP and statistically significantly higher than G4NH₂-0TPP. The PCC of G4NH₂-PEGTPP is not affected by the density of PEGTPP and is only smaller to that of G4NH₂-10TPP, which had pronounced toxicity. The ability of the G4NH₂-PEGTPP to target mitochondria equally well, irrespectively of the density of TPP, may be hypothesized to be due to the fact that TPP is further expanded from the surface of the nanocarrier when conjugated to PEG and also due to the flexibility of the linker that may allow as many TPP as possible to better interact with its target – the mitochondria.

The use of TPP conjugated directly or through a PEG linker has shown to effectively target dendrimer nanocarriers toward the mitochondria, which present a useful strategy for delivery of therapeutics to the mitochondria. The direct conjugation of TPP to the dendrimer only requires a small density of TPP (~ 5 TPP) in order to be effective in targeting the dendrimer to the mitochondria as well as increasing internalization without producing toxic effects. The use of PEG can also modulate various properties of the dendrimer (solubility, biocompatibility, interaction of dendrimer with physiological environment, pharmacokinetic profile) and is thus a promising linker between the dendrimer nanocarrier and TPP. In this case we show that the presence of PEG helps

decrease toxicity of the nanocarriers while still maintaining their mitochondrial targeting ability.

3.5 Conclusions

The *in vitro* characteristics of mitochondrial targeting G4NH₂ conjugates were assessed in this work using a human alveolar carcinoma cell model (A549 cells). Two strategies of conjugation of the mitochondrial targeting moiety TPP were investigated: direct TPP conjugation (G4NH₂-TPP) or conjugation of TPP to G4NH₂ through a flexible PEG linker (G4NH₂-PEGTPP). Both strategies result in significant enhancement in mitochondrial targeting relative to the non-conjugated control. While direct TPP conjugation shows a direct correlation between targeting and TPP number density, the conjugation of TPP through a PEG linker results in high targeting for all TPP densities with targeting not being affected by the degree of PEGylation. Therefore, both direct and indirect conjugation, separately or in combination, are potential strategies for the delivery of therapeutics to address mitochondrial dysfunctions. The conjugation of PEGTPP may be used to enhance the cellular internalization of PEGylated dendrimers and target mitochondria, so as to reach high local concentration of drug-conjugated therapeutics near the mitochondria such as, for example, ROS scavengers.²²⁶ This is relevant as often times PEGylation is a required motif in the design of the nanocarriers so as to improve their function – e.g. aqueous solubility of the conjugate^{116, 122} or to modulate the interactions with the physiological environment.^{116, 122} Direct TPP conjugation may be used in those cases where small molecules need to reach not only high local concentration near the mitochondria, but also be internalized. For example, the conjugation of doxorubicin (DOX) to TPP (DOX-TPP) has been recently demonstrated as

a potential strategy to fight multi-drug resistant cancer, with DOX-TPP enhancing levels of apoptosis in both wild-type and DOX-resistant human breast carcinoma cell line as compared to DOX alone.⁵⁴ The direct conjugation of many DOX-TPP (or other small molecules) to dendrimers may thus result in enhanced therapeutic efficacy. As more evidence accumulates the involvement of mitochondrial signaling process, bioenergetics, and biosynthesis in tumorigenesis,²⁴⁸ the major challenges still remain to design therapeutic strategies that increase the presence of anticancer drugs that can directly target the mitochondria, which the TPP-targeted dendrimer has great potential in addressing.

3.6 Acknowledgements

The authors would like to give thanks for the financial support from Wayne State University (WSU) and NSF-CBET #0933144. The authors would also like to thank Microscopy, Imaging, and Cytometry Resources Core at Wayne State University, School of Medicine for Flow Cytometry and Confocal Microscopy for access to equipment and data analysis where the flow cytometry and confocal microscopy was performed and analyzed. A special thanks to Dr. Howard Matthew in Chemical Engineering at WSU for access to the plate reader.

CHAPTER 4 - TPP-DENDRIMER NANOCARRIERS FOR SIRNA DELIVERY TO THE PULMONARY EPITHELIUM AND THEIR DRY POWDER AND METERED-DOSE INHALER FORMULATIONS

4.1 Introduction

Synthetic small interfering RNA (siRNA) is a promising therapeutic for the treatment of a variety of lung diseases including asthma,²⁴⁹ chronic obstructive pulmonary disease (COPD),²⁵⁰ cystic fibrosis,²⁵¹ viral infections,²⁵²⁻²⁵⁴ pulmonary tuberculosis,²⁵⁵ lung cancer,^{190, 256} and also for the treatment of the so called “non-druggable” diseases.²⁵⁷ Despite recent developments and the many promising applications of siRNA therapeutics, there are still many challenges that hinder the efficient and safe use of siRNA to treat pulmonary disorders including the formulation of siRNA and their vectors for efficient local lung delivery,^{96, 97} and the extra and intracellular barriers that exist for the transport of bioactive siRNA to the cytoplasm of relevant cells in the lungs.^{98, 99}

Non-viral vectors such as cationic polymers represent one of the promising approaches for the efficient delivery of siRNA.⁵⁹ Amine-terminated, poly(amidoamine) (PAMAM) dendrimers have been widely investigated as gene delivery vectors including carriers of siRNA,⁶⁴ and their use in oral inhalation to the lungs.^{96, 127, 258} PAMAM dendrimers are hyperbranched polymers with uniform structure and size and with multifunctional modifiable surface groups.³⁴ Amine-terminated PAMAM dendrimers carry a positive surface charge due their protonatable surface primary amines and can thus serve to induce the formation of complexes with anionic siRNA via electrostatic interactions.^{64, 259} Such nanoscale structures, termed dendriplexes, have been shown to promote cellular internalization of siRNA. However, gene knockdown efficiency is

relatively low, and cytotoxicity profiles in models of the pulmonary epithelium are not very favorable.^{96, 99}

In order to increase the transfection efficiency and biocompatibility of PAMAM dendrimers, a variety of modifications to the dendrimer surface have been explored.²⁶⁰ Of these modifications, the use of a triphenylphosphonium (TPP) ion has been recently reported via direct conjugation to PAMAM dendrimers.^{33, 237, 261} TPP is a delocalized lipophilic cation and well-known mitochondrial-targeting agent.²³³ The conjugation of TPP to PAMAM dendrimers enhances mitochondrial targeting, as well as internalization and accumulation of dendrimers into cells while exhibiting relatively low cytotoxicity.^{33, 261} TPP conjugation has led to enhanced delivery of DNA/dendrimer complexes *in vitro* and their improved transfection ability.²³⁷ Therefore, the modification of TPP to amine-terminated PAMAM dendrimers holds great promise in enhancing the transfection ability and biocompatibility of dendrimers for siRNA delivery to the lung tissue.

Oral inhalation (OI) is promising route for local siRNA delivery to the lungs as it avoids systemic degradation²⁶² and poor lung targeting associated with i.v. administration.²⁶³ Pressurized metered dose inhalers (pMDIs) and dry powder inhalers (DPIs) are the two most widely used portable inhalation devices.^{97, 264} In a pMDI, the therapeutic particles are suspended in the propellant (hydrofluoroalkanes – HFAs).⁹⁷ The propellant aerosolizes the therapeutic for inhalation when the device is actuated.^{97, 264} DPIs allow for the inhalation of dry powders as an aerosol cloud upon breath actuation.⁹⁷ In order to achieve successful delivery of siRNA to the lungs using such portable inhalers, the nanoscale dendriplexes must be formulated into particles that form aerosols with optimum aerosol diameters within the range of 1-5 μm . This process must be done

without compromising the biological activity of siRNA.⁹⁹ We have previously reported successful use of spray drying technique with sugar excipients to formulate dendriplexes into suitable micron-sized particles that results in optimum aerosol sizes when formulated in pMDIs.⁹⁶ The use of spray drying can also be easily extended for preparation of DPI formulations as well, and has been shown to work successfully to formulate micron particles of PLGA-siRNA nanoparticles via spray drying with sugar excipients.²⁶⁵

Considering the challenges and opportunities stated above, the goal of this study was twofold: (i) to design a PAMAM-based dendrimer conjugate that led to improvements in gene knockdown efficiency in an *in vitro* model of the pulmonary epithelium when compared to the unmodified amine-terminated counterpart, (ii) and to develop efficient strategies for the formulation of such dendriplexes in portable oral inhalation devices. We conjugated generation 4, amine-terminated PAMAM dendrimers (G4NH₂) with increasing TPP densities (0, 4, 8, 12 TPP/dendrimer). Complexes of G4NH₂-TPP dendrimers with siRNA (G4NH₂-TPP-dendriplexes) at various N/P ratios were prepared and characterized. The gene knockdown efficiency and toxicity of these G4NH₂-TPP-dendriplexes (simply, TPP-dendriplexes) was tested in an *in vitro* model of the pulmonary, namely stably-transfected, green fluorescent protein (GFP) expressing A549 cells. The most effective TPP-dendriplex system was selected to be formulated in portable OI devices. Micron-sized particles of the TPP-dendriplex were prepared using mannitol as an excipient and spray dried. The aerosol characteristics of the mannitol-TPP-dendriplex particles formulated in pMDIs and DPIs were assessed using an Anderson Cascade Impactor (ACI). This study demonstrates the successful use of TPP-targeted PAMAM dendrimers as vectors for siRNA delivery for a model of the pulmonary epithelium, and

their formulations using pMDIs and DPIs for direct and noninvasive siRNA delivery to the lungs.

4.2 Materials and Methods

4.2.1 Materials

Generation four, amine-terminated, poly(amidoamine) (PAMAM) dendrimer (G4NH₂) in methanol at 9.8% w/w was purchased from Dendritech Inc. (Midland, MI). Double-stranded Dicer substrate siRNA targeting eGFP ((+) siRNA) and double stranded respective mismatch as a negative control ((-) siRNA) was obtained from Integrated DNA Technologies (Leuven, Belgium).⁹⁶ Dimethyl sulfoxide (DMSO) anhydrous (Acros), N-Hydroxysuccinimide (NHS) (Acros), agarose, sodium chloride (NaCl), potassium chloride (KCl), potassium phosphate, monobasic, anhydrous (KH₂PO₄), potassium hydroxide (KOH) agarose, and (4-(2-hydroxyethyl)-1-piperazineethanesulfonic acid) (HEPES) were purchased from Thermo Fischer Scientific (Rockford, IL). Sodium phosphate, dibasic, anhydrous (Na₂HPO₄) was purchased from EMD Chemicals, Inc. (Gibbstown, NJ). (3-Carboxypropyl) triphenylphosphonium bromide (TPP), P-toluenesulfonic acid (p-TSA), D-Mannitol (98%), and heparin sodium salt (194 U/mg) were purchased from Sigma Aldrich (St. Louis, MO). N-(3-dimethylaminopropyl)-N'-ethylcarbodiimide (EDC) was purchased from Advanced ChemTech Inc. (Louisville, KY). Diethylpyrocarbonate (DEPC) and ethylenediaminetetraacetic acid (EDTA) (pH 8, 0.5 M, sterile) were acquired from Amresco (Solon, OH, United States). Dymel 227 ea/P hydrofluoroalkane (HFA227) propellant was a gift from DuPoint (Fort Worth, Texas, United States). Spectra/Por cellulose ester membrane dialysis tubing was purchased from Spectrum Laboratories, Inc. (Rancho Dominguez, CA). Deuterium Oxide (D₂O) were purchased from Cambridge

Isotope Laboratories (Tewksbury, MA). Hank's Balanced Salt Solution (1xHBSS) supplemented with 0.01 M HEPES was prepared according to the recipe provided by Irvine Scientific (Santa Anna, CA). Deionized (DI) water was obtained from NANOpure® Diamond UV ultrapure water system (Barnstead International - Lake Balboa, CA). Amicon Centrifugal Filters were purchased from EMD Millipore (Billerica, MA). Trypsin-EDTA (1x) (Corning®), and 24-well and 96-well cell culture plates (Corning®) were purchased from VWR International. SeaKem LE Agarose was purchased from Lonza Group Ltd (Rockland, ME, United States). Ethidium bromide (98%, 10 mg/mL) was supplied by IBI Scientific (Peosta, IA, United States).

4.2.2 Conjugation of TPP to G4NH₂ Dendrimer to Form G4NH₂-TPP Conjugates

G4NH₂ PAMAM dendrimer (95.08 mg) was dissolved in 9.5 mL of DMSO with the addition of p-TSA (25.97 mg) and left to stir at room temperature for 24 h. TPP was activated using EDC/NHS coupling reaction adding 2:1 molar ratio of both EDC and NHS to TPP dissolved in anhydrous DMSO and allowed to stir at room temperature overnight to obtain activated TPP. G4NH₂/p-TSA mixture was added to the activated TPP dissolved in DMSO and the reaction mixture was allowed to proceed at room temperature for 3 days. The molar ratios of activated TPP to G4NH₂ were varied to conjugate different TPP densities to G4NH₂ to form G4NH₂-TPP conjugates in separate reactions. The reaction mixtures were then dialyzed against distilled water followed by Phosphate Buffered Saline (1xPBS – pH 7.2) solution using a Spectra/Por dialysis membrane. The products were further purified using an Amicon Ultra 15 centrifugal filter against a 10xPBS solution (pH 7.2) and again against distilled water. The G4NH₂-TPP conjugates were frozen and

lyophilized to remove water, then characterized by $^1\text{H-NMR}$ in D_2O (Varian Mercury, 400 MHz).

4.2.3 Preparation and Characterization of TPP-Dendriplexes

G4NH₂-TPP-dendriplexes (or simply TPP-dendriplexes) were formed by a dropwise addition of GNH₂-TPP conjugates (10-4,100 $\mu\text{g/mL}$, 20 nM Tris-HCl pH 7.4) to siRNA (17 pmol-80 pmol, RNase-free distilled water) and vortexed for 1 min. The TPP-dendriplexes were incubated for 30 minutes at room temperature to ensure complete complexation. The concentrations of G4NH₂-TPP conjugates were varied in order to obtain the desired N/P ratio – the molar ratio between the remaining unconjugated primary amine groups (N) of G4NH₂-TPP conjugates and phosphate groups (P) on the siRNA sugar backbone.

The size (hydrodynamic diameter, HD) and zeta potential (ζ) were evaluated for each TPP-dendriplex at various N/P ratios using Light Scattering (LS, Malvern ZetaSizer Nano ZS). HD was based on the intensity measurement provided by LS. Each sample contained 80 nM of siRNA and was performed at 25°C diluted in buffer for size, and in DI-water for ζ utilizing the refractive index, viscosity, and dielectric constant of DI water. A minimum of three independent measurements were taken for each sample to obtain an average size and ζ . A representative scanning electron microscopy (SEM) image was taken of the 12TPP-dendriplex, and geometric size based on ~340 particles was evaluated (Zeiss EVO 50 XVP SEM). TPP-dendriplexes were prepared as described earlier, with minor change that both the TPP-dendrimer and siRNA were dissolved in DI water. The final concentration of TPP-dendriplexes contained 80 nM of siRNA.

4.2.4 RNA Gel Complexation Assay

The complexation efficiency of G4NH₂-TPP conjugates to form TPP-dendriplexes was analyzed by gel electrophoresis. Various TPP-dendriplexes were formed as described previously using the equivalent of 300 ng of siRNA (RNase free DI-water) and G4NH₂-TPP conjugates containing an average of 0, 4, 8 and 12 TPP (20mM Tris-HCl buffer at pH of 7.4) at N/P ratios of 0, 0.2, 0.8, 1, 2, 3, 5, 10, 20, and 30. Each TPP-dendriplex sample was run in a 1.5% w/v agarose gel (1.5% w/v in tris base, acetic acid, and EDTA (TAE) 1X pH 8) at 90 V (E0160-VWR Mini Gel Electrophoresis) for 30 min. The migration of non-complexed siRNA was visualized under UV irradiation and images were obtained (Gel DocTM EZ, Bio-Rad).

4.2.5 siRNA Release via Polyanion Competition Assay

The release of siRNA from TPP-dendriplexes due to the addition of competing polyanionic heparin was determined as a measure of complex stability.²⁶⁶ Briefly, TPP-dendriplexes with an N/P ratio of 30 were formed (200 ng siRNA) and incubated at room temperature for 30 min. The dendriplexes were then incubated with increasing concentrations of heparin (0, 5, 10, 15, 20, 25, 30, 35 µg/µg, heparin/siRNA) under 5% CO₂ at 37°C for 1 hour. The samples were loaded onto a casted non-denaturing agarose gel and subjected to electrophoresis as stated previously. Non-complexed siRNA was loaded as a reference in each gel. The gels were subsequently imaged under UV irradiation and images were recorded using the Gel DocTM EZ (Bio-Rad). The binding for each G4NH₂-TPP conjugate was performed at least in 2 independent experiments.

4.2.6 *In Vitro* Gene Knockdown

The knockdown efficiency of the various TPP-dendriplexes were analyzed *in vitro* against A549 cells stably expressing GFP – eGFP-A59 cells. The development of eGFP A549 was described previously.⁹⁶ TPP-dendriplexes containing a scramble (-) siRNA sequence were used as a negative control to account for any off-target effects. These were also compared to non-complexed siRNA ((-) and (+) sequences) and to the commercial reagent Lipofectamine® 2000 (Life Technologies), the positive control. Briefly, eGFP-A549 cells were cultured in Dulbecco's Modified Eagle Medium 1 x high glucose (DMEM, Life Technologies) supplemented with 10% (v/v) fetal bovine serum (FBS, Atlanta Biologicals) and 2.5 µg/mL of puromycin selective antibiotic (Toku-E Biotechnology), and non-eGFP expressing A549 cells (AATC) were cultured in DMEM supplemented with 10% FBS and 1% Penicillin Streptomycin (100 U/mL Penicillin and 100 µg/mL Streptomycin) antibiotics (AB, Life Technologies). Both were cultured at 37°C with 5% CO₂ and used once culture reached 90% confluency. 50,000 cells per well (2 wells with A549, 22 wells with eGFP-A549 cells) were seeded in 24 well plate and incubated for 24 hours at 37°C and 5% CO₂. The cells were then washed with 1xPBS and 250 µL of transfection solution (dendriplexes of +siRNA (n=3) and –siRNA (n=3) dissolved in 250µl of DMEM + 10%FBS + 1%AB) was added to each well and allowed to incubate for 6 hours, followed by the replacement of 500 µL of fresh culture medium. The TPP-dendriplexes were made as discussed earlier. Each TPP-dendriplex contained 20 pmol of siRNA. An appropriate amount of TPP-dendrimer (1.2-11.5 µg) was added to culture medium to a final volume of 250 µL. The 12TPP-dendriplexes were encapsulated into mannitol to form microparticles were also tested with same amount of siRNA (20 pmol) –

to assess the impact of the particle formation strategy on the biological activity of the siRNA. Some transfection solutions contained no TPP-dendriplexes for controls. The cells were then allowed to incubate at 37°C and 5% CO₂ for 48 hours. The cells were then removed from the 24 well plate and resuspended in Attune® Focusing Fluid (1X). The median fluorescent intensity (MFI) from the GFP was measured using flow cytometry (Attune™ Flow Cytometer, Thermo Fisher Scientific). MFI of non-eGFP A549 cells used as a negative control to take away any artifacts of fluorescence not produced by GFP and the average MFI from the negative control was subtracted from MFI of all the other samples – MFI_{sample}. eGFP A549 cells alone were used as a positive control – MFI_{+control}. Data was analyzed using Attune® Cytometric Software v2.1. Percent (%) eGFP knockdown was calculated as follows in Equation (4.1):

$$\% \text{ eGFP Knockdown} = \left(\frac{\text{MFI}_{+control} - \text{MFI}_{sample}}{\text{MFI}_{+control}} \right) \times 100\% \quad (4.1)$$

4.2.7 *In Vitro* Cytotoxicity

A549 cells were seeded using a 96 well plate at a density of 5 x 10³ cells per well. The cells were allowed to grow in DMEM + 10% FBS + 1% AB (v/v) for 24 hours at 37°C and 5% CO₂. TPP-dendriplexes (0.2 mL) were formed as previously stated at N/P ratio of 30 and at the same concentrations utilized for *in vitro* gene knockdown experiment. Also, 12TPP-dendriplex at N/P 30 was further analyzed by increasing siRNA concentration (0-0.4 μM) and 12TPP-dendriplex concentration (0-12 μM) in DMEM + 10% FBS +1% AB. These TPP-dendriplexes were incubated with the cells for an additional 48 hours under 5% CO₂ at 37°C in DMEM + 10% FBS +1% AB. Wells with no TPP-dendriplexes were

used as the control. Cell viability was analyzed using CellTiter 96® Aqueous Non-Radioactive Cell Proliferation Assay (Promega). Briefly, the cells were rinsed twice with 1xHBSS and 120 µL of MTS/PMS solution made in DMEM medium was added to each well and incubated for an additional 4 hours at 37°C and 5% CO₂. The absorbance was read at 490 nm using ELISA plate reader (Multiskan™ GO Microplate Spectrophotometer, Thermo Fisher Scientific). Cell viability was calculated using Equation 4.2 (n=5).

$$\% \text{ Cell Viability} = \frac{\text{Absorbance of treated cells}}{\text{Absorbance of control cells}} \times 100\%, \text{ (4.2)}$$

4.2.8 Preparation and Characterization of 12TPP-Dendriplex/Mannitol Microparticles

The 12TPP-dendriplex (N/P=30) was prepared as described earlier. A known volume (600 µL) of the 12TPP-dendriplex solution (30 µg siRNA equiv.) was mixed up with 2.4 mL RNase-free DI H₂O with D-mannitol (90 mg equivalent). The mixture was immediately spray-dried using Mini Spray Dryer B-290 (BUCHI) with the following setup: inlet temperature = 45°C, outlet temperature = 31-36°C, atomizing nitrogen flow rate 40 mm (473 L/h), pump ratio 5% (1.5 mL/min), aspiration rate 70% (approximately 35 m³/L = 100%), and nozzle cleaning 0. The 12TPP-dendriplex/mannitol microparticles were collected at the end of the gas cyclone. The collected microparticles were lyophilized overnight to remove any residual H₂O and were then placed in desiccator for future use.

The yield of the spray drying was calculated by Equation 4.3:

$$\text{Yield} = \frac{\text{mass of collected microparticles (mg)}}{(90+0.03) \text{ (mg)}} \text{ (n=3) (4.3)}$$

The payload of siRNA in 12TPP-dendriplex/mannitol microparticle was determined by incubating a certain amount of microparticles with 0.1 mL heparin aqueous solution (450 U) for 0.5 h followed by analysis with agarose gel electrophoresis and densitometry (n=3). The geometric diameter of spray-dried 12TPP-dendriplex/mannitol particle was measured with scanning electron microscopy (SEM). The microparticles were sprayed onto copper tape and then were sputtered with gold for 30 s. The SEM was performed at 5 kV. To measure the solvated diameter (SD) of the 12TPP-dendriplex/mannitol microparticles, a dispersion of the microparticles was prepared in 2H,3H-perfluoropentane (HPFP) and measured by light scattering using Nano ZS Zetasizer (Malvern Instruments, United Kingdom), (n ≥ 3). To measure the hydrodynamic diameter (HD) and zeta potential (ζ) of “reconstituted 12TPP-dendriplex”, 12TPP-dendriplex/mannitol microparticles were redissolved in RNase-free DI H₂O (1 mg/mL) and then sonicated for 30 s at room temperature. HD and ζ were determined immediately with Nano ZS Zetasizer (Malvern Instruments, United Kingdom), (n ≥ 3).

4.2.9 Preparation and *in vitro* Aerosolization of the pMDI Formulation of 12TPP-Dendriplex/Mannitol Microparticles

The 12-TPPdendriplex/mannitol microparticles formulated as described earlier were weighed in pressure-proof glass vial (West Pharmaceutical Services) and manually crimped with 63 μ L metering valves (Bespak). HFA227 was filled with a glass vial using a manual syringe pump (HiP, 50-6-15) and home-built high-pressure filler to make a final particle concentration of 2 mg/mL. The glass vial was placed in VWR PC250 sonicator bath at 5-10°C (VWR International) for 20 min. The stability of the formulation was

performed by visually monitoring the dispersion of the microparticles in propellant as a function of time.

An Andersen Cascade Impactor (Copley Scientific) with a USP induction port (IP) and eight stages was used to test the *in vitro* aerosol characteristics of the prepared pMDI formulation. The *in vitro* aerosol performance was assayed at a flow rate of 28.3 L/min, 25°C and 75% relative humidity. First several shots were fired to waste and then 40 actuations were puffed into the ACI with 10 s intervals between every two shots. The ACI was disassembled soon after the last shot. The actuator, IP, and the plates on each of the 8 stages were rinsed carefully with 10 mL RNase-free DI H₂O and stored in separated centrifuge tubes. These 12TPP-dendriplex/mannitol microparticles were frozen and then lyophilized. The particles in each tube were carefully weighed for further analysis. The microparticles collected from each tube were redissolved in 100 µL heparin-containing TE buffer (heparin 455 U/mL, pH 8.0, 1X) and the incubation was performed for 30 min at 37°C. 10 µL of the above buffer solution was loaded into an agarose gel. The gel electrophoresis was performed at 60V for 40 min. The amount of siRNA was quantified with densitometry using ImageJ 1.42q (National Institutes of Health). Respirable fraction (RF, Equation 4), fine particle fraction (FPF, Equation 5), mass median aerodynamic diameter (MMAD), and geometric standard deviation (GSD) were calculated with two methods: mass method and densitometry method. In the mass method, the net weight of microparticles deposited on each stage was used to determine RF and FPF from Equations 4 and 5. In the densitometry method, the mass of siRNA was assessed from densitometry and used in Equations 4.4 and 4.5.

$$RF = \frac{\text{Mass from Stage 0 to Filter}}{\text{Total Mass Released to ACI}} \quad (4.4)$$

$$FPF = \frac{\text{Mass from Stage 3 to Filter}}{\text{Mass from Induction Port to Filter}} \quad (\text{Aerodynamic diameter} \leq 4.7 \mu\text{m}) \quad (4.5)$$

MMAD and GSD were calculated as described previously.²⁶⁷

4.2.10 Preparation and *in vitro* Aerosolization of the DPI Formulation of 12TPP-Dendriplex/Mannitol Microparticles

The aerosolization of the DPI formulations was also determined with an 8-stage Andersen Cascade Impactor (Copley Scientific Limited) to which a pre-separator (Copley Scientific Limited) was attached to prevent large particles or aggregates from reaching the stages. A dose of 12TPP-dendriplex/mannitol microparticles (10-20 mg) was loaded into a capsule and inserted into Rotahaler® device (Cipla Limited), and then dispersed at an inspiration rate of 28.3 L/min for 4 s. The plates from each stage were carefully rinsed with 20 mL RNase-free H₂O. The collected aqueous solution was frozen and then lyophilized for 72 hours. The lyophilized particles from the inhaler device, induction port, and 8 plates were individually dissolved in 100 µL heparin TE 1X solution (455 U/mL) for 0.5 h and the siRNA amount was quantified by agarose gel electrophoresis and densitometry. Emitted dose (ED) was considered as the difference between the initial mass and the mass of microparticles left in the inhaler or capsule after the inspiration process. The RF, FPF, MMAD and GSD were calculated as previously noted.

4.2.11 Statistical Analysis

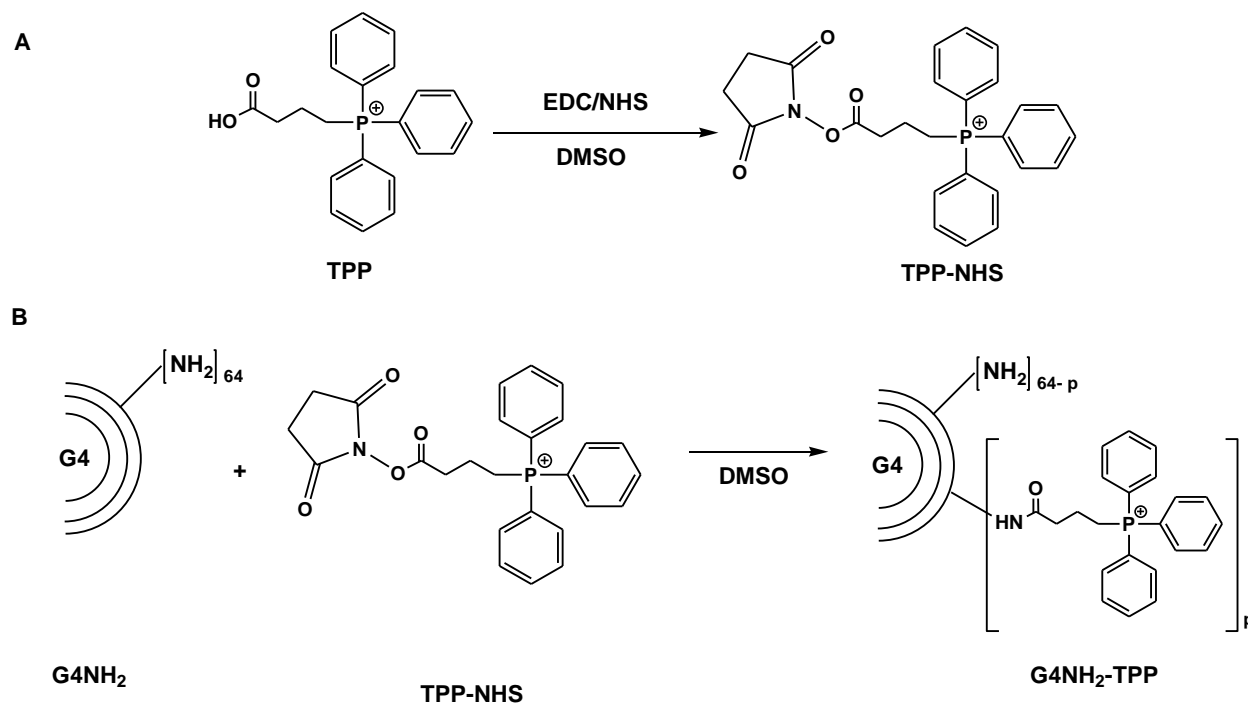
All data are presented as a mean ± standard deviation. The means were calculated from a minimum of three independent trials for each measurement (n ≥ 3). One-way

analysis of variance (ANOVA) followed by Tukey's Multiple Comparison Test or an unpaired t-test was performed using GraphPad Prism 5 software. Means were considered statistically significant if $p < 0.05$.

4.3 Results

4.3.1 Conjugation of TPP to G4NH₂ Dendrimer.

TPP was conjugated to the primary amines of G4NH₂ (Scheme 4.1).



Scheme 4.1. Schematic of the TPP conjugation to the amine-terminated, generation 4 poly(amido)amine (PAMAM) dendrimer (G4NH₂). A) TPP is activated using EDC/NHS coupling to form TPP-NHS in DMSO. B) G4NH₂ was then later added to the activated TPP (TPP-NHS) in DMSO and allowed to react to form G4NH₂-TPP dendrimer conjugate. The amount of TPP-NHS added to the reaction mixture determined the conjugation density with the final density of TPP per dendrimer of ~ 0, 4, 8, 12 TPP.

The conjugation of TPP to G4NH₂ to form G4NH₂-TPP was confirmed by ¹H NMR D₂O (Figure 4.1).

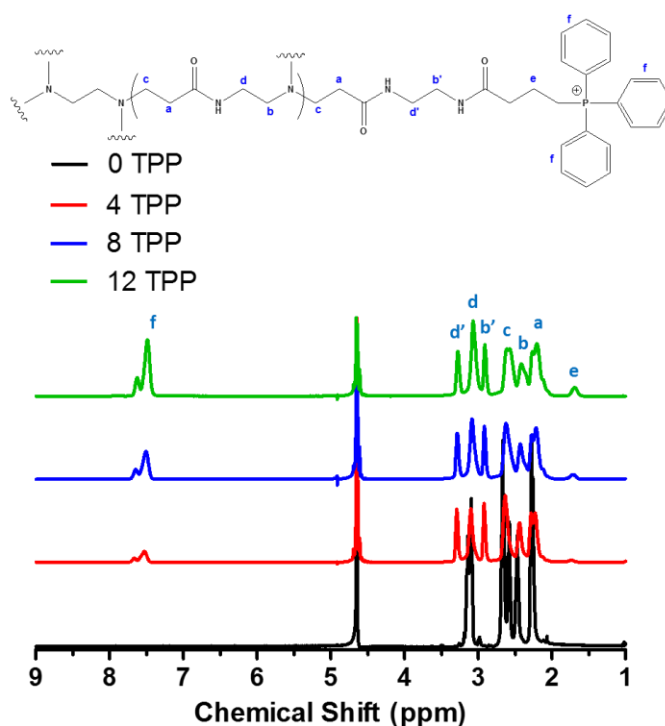


Figure 4.1. ¹H NMR characterization of G4NH₂-TPP conjugates in D₂O. The chemical structure is shown above with the corresponding peak shifts labeled within the spectrum.

G4NH₂ with increasing density of TPP were prepared to assess the effect of TPP on the gene knockdown efficiency of the dendriplexes. The results indicate that an average of 4, 8, and 12 TPP molecules were conjugated per dendrimer.

4.3.2 Preparation and Characterization of TPP-Dendriplexes

TPP-dendriplexes were prepared by combining positively-charged G4NH₂-TPP conjugates with negatively-charged siRNA. The TPP-dendriplexes were named based on the TPP conjugation density to G4NH₂: 0TPP-dendriplex, 4TPP-dendriplex, 8TPP-dendriplex, and 12TPP-dendriplex. They were characterized for their size (HD), and surface charge (ζ) via LS (Table 4.1).

Table 4.1. Characterization of G4NH₂-siRNA complexes by Light Scattering. Hydrodynamic diameters (HD), Polydispersity Index (PDI), and zeta potential (ζ) are summarized as a function of number density of TPP per G4NH₂ (0-12) and also as a function of N/P ratio (5-30). HD was based on intensity measurements. HD = mean \pm s.d., PDI = mean \pm s.d., ζ = mean \pm s.d.

	0 TPP			4 TPP			8 TPP			12 TPP		
N/P ratio	HD (nm)	PDI	ζ (mV)	HD (nm)	PDI	ζ (mV)	HD (nm)	PDI	ζ (mV)	HD (nm)	PDI	ζ (mV)
5	172 \pm 26	0.44 \pm 0.04	37 \pm 7	304 \pm 75	0.47 \pm 0.08	16 \pm 5	372 \pm 29	0.52 \pm 0.04	43 \pm 8	310 \pm 12	0.30 \pm 0.08	22 \pm 2
10	129 \pm 3	0.31 \pm 0.02	33 \pm 3	367 \pm 120	0.50 \pm 0.15	12 \pm 7	323 \pm 20	0.47 \pm 0.06	25 \pm 8	218 \pm 42	0.36 \pm 0.07	33 \pm 5
20	343 \pm 20	0.38 \pm 0.08	33 \pm 3	327 \pm 34	0.45 \pm 0.07	42 \pm 10	379 \pm 26	0.56 \pm 0.09	31 \pm 10	382 \pm 37	0.56 \pm 0.06	23 \pm 7
30	339 \pm 21	0.39 \pm 0.11	34 \pm 7	364 \pm 32	0.49 \pm 0.03	17 \pm 3	361 \pm 20	0.49 \pm 0.05	27 \pm 5	363 \pm 55	0.36 \pm 0.15	40 \pm 3

The average density of TPP (0, 4, 8, 12 TPP molecules per G4NH₂ dendrimer) and N/P ratio (5, 10, 20, 30) were varied for each TPP-dendriplex. All TPP-dendriplexes were able to form nanoparticles with sizes ranging from 120 nm – 400 nm in diameter, most being in the 300 nm range (Table 4.1). The PDI ranged from 0.2-0.5, therefore demonstrating that stable complexes of similar sized could be formed. These PDI values are less than 0.7, which indicates that the sizes have some spread in their distribution but are still producing relatively similar sizes. The N/P ratio and TPP density do not seem to greatly impact the HD of the TPP-dendriplex. The ζ of all TPP-dendriplexes were positively charged, ranging from +12-43 mV. No obvious trend in surface charge with TPP

density of the TPP-dendriplexes was seen either. SEM image (Figure 4.2) of 12TPP-dendriplexes (N/P 30) revealed spherical nanoparticles with an average geometric diameter of 160 ± 50 nm.

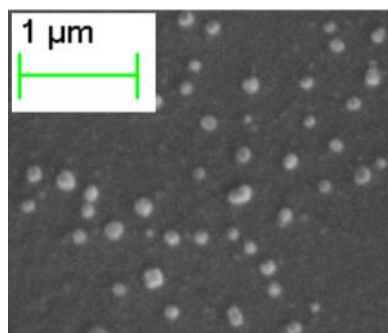


Figure 4.2. Scanning electron microscopy (SEM) of 12TPP-dendriplex at N/P 30. The geometric diameter represents ~ 340 particles.

4.3.3 RNA Gel Complexation Assay

The complexation ability of the TPP-dendriplexes was tested using a complexation assay. TPP-dendriplexes were added to a constant amount of siRNA (300 ng) and increasing the N/P ratio (amount of dendriplex compared to siRNA) for TPP-dendriplexes with different average densities of TPP (Figure 4.3).

The non-complexed siRNA band can be seen in the first lane at N/P = 0.0. As the N/P ratio increased, the amount of non-complexed siRNA decreased. The N/P ratios where no non-complexed siRNA band can be seen demonstrates full complexation with G4NH₂-TPP to form TPP-dendriplex with the amount of siRNA present. For TPP-dendriplex with 0 and 4 TPP groups on average, an N/P ratio of 1 was enough to ensure full complexation. The conjugation of TPP above the average of 4TPP on the dendrimer required an increase in N/P ratio from 1 to 2 to fully complex all the siRNA. For all groups, an N/P ratio of 2 was able to fully complex all siRNA present, which is seen as an absence of non-complexed siRNA band in the agarose gel (Figure 4.3).

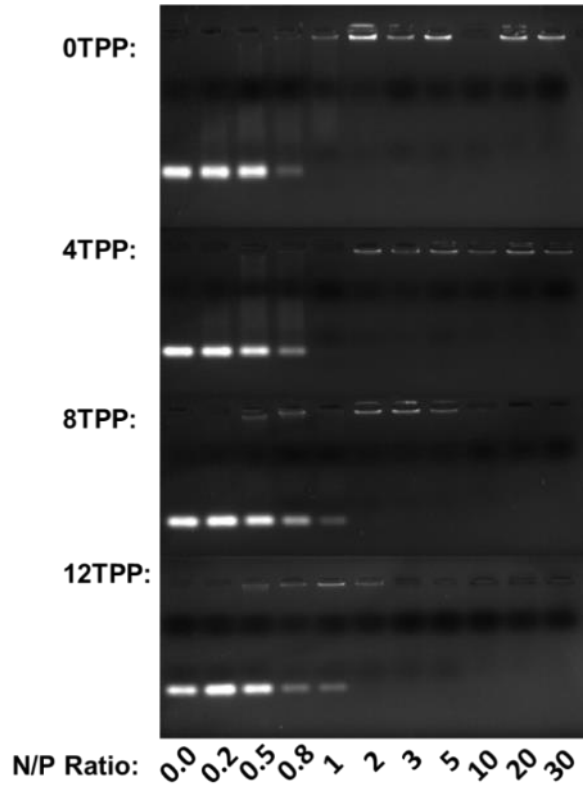


Figure 4.3. The siRNA complexation efficiency as a function of N/P ratio as visualized by gel electrophoresis. The dendriplexes were prepared with various ratios of TPP (as indicated to the left). The first lane contains untreated non-complexed siRNA as control and subsequent lanes with increasing N/P ratios as shown.

4.3.4 siRNA Release via Polyanion Competition

A measure of complex stability was assessed using heparin as a polyanion competitor (Figure 4.4).

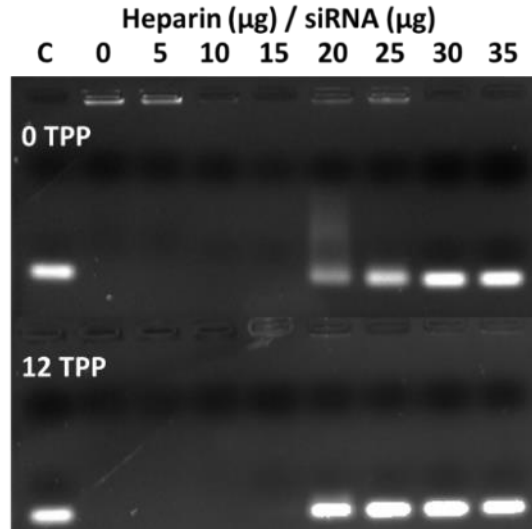


Figure 4.4. Polyanion competition assay visualized by gel electrophoresis. The stability of the dendriplexes was tested for 0TPP-dendriplex (N/P 30) and 12TPP-dendriplex (N/P 30) by exposing each to increasing amounts of heparin. C = siRNA only, used as a control.

Heparin, a highly negatively charged anion, can act as a competitor for complexation relative to nucleic acids and, therefore, be used as a way to measure complex stability. The comparison was made between the dendriplex group containing no TPP (0TPP-dendriplex, N/P 30) and that with most TPP (12-TTP dendriplex, N/P 30). The success of decomplexation was demonstrated by the non-complexed siRNA band in the agarose gel. The results demonstrated less heparin was needed to fully decomplex the siRNA from the TPP-dendrimer for the 12-TTP dendriplex (Figure 4.4). Almost full decomplexation at 20 heparin (μg)/siRNA (μg) is achieved for 12TPP-dendriplex. However, for the complex formed with the dendrimer without TPP, most of the siRNA is still complexed until 30 heparin (μg)/siRNA (μg). Therefore, a reduction in complex stability can be observed upon the conjugation of TPP to the surface of the dendrimer.

4.3.5 *In Vitro* Gene Knockdown

The gene knockdown ability of the TPP-dendriplexes was tested *in vitro* by the delivery of siRNA targeting eGFP gene in eGFP-expressing A549 cells. The results (Figure 4.5) are expressed as the percent of eGFP knockdown (% eGFP knockdown).

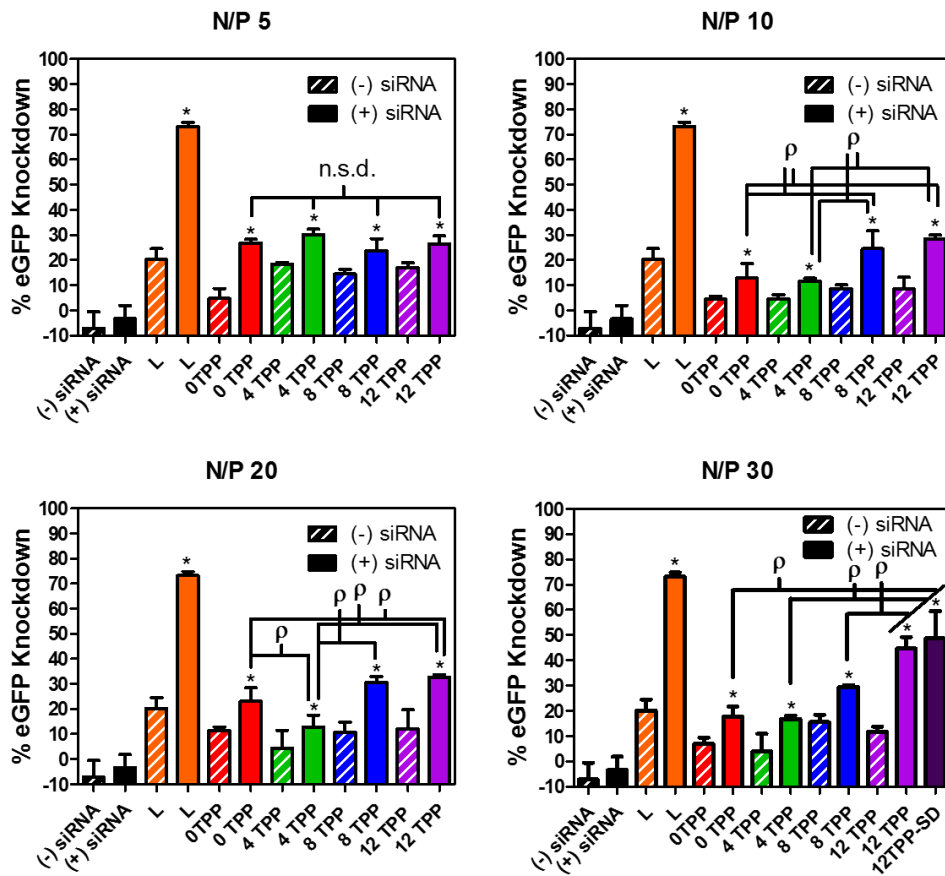


Figure 4.5. *In vitro* gene knockdown of eGFP expression in stably expressing eGFP A549 cells. The dendriplexes (Dplex) were prepared at N/P ratio of 30 with eGFP siRNA and G4NH₂-TPP conjugates. The specificity of the knockdown was performed by comparing dendriplexes with a scramble eGFP sequence (-siRNA) to the correct corresponding eGFP sequence (+siRNA). Non-complexed siRNA (siRNA) was used as a negative control and the commercial reagent Lipofectamine 2000 (L) was used as a positive control. 20 pmol of siRNA (80 nM) was used for each sample while the amount of dendrimer-TPP ranged from 1.2-11.5 μ g (0.3-2.4 μ M) depending on the desired N/P ratio and TPP density of TPP-dendrimer sample. * represents a statistical difference ($p < 0.05$) between the non-complexed +siRNA and various +siRNA groups, while ρ represents a statistical difference of +siRNA between indicated groups as analyzed by One-Way ANOVA followed by Tukey's Multiple Comparison Test ($n \geq 3$) ($p < 0.05$), n.s.d. = not statistically different.

A scramble sequence ((-) siRNA) was used as a negative control to account for off-target effects and compared with the eGFP sequence ((+) siRNA). Also, the effect of N/P ratios and varying TPP densities were compared to naked siRNA delivery and with the commercial siRNA delivery vehicle Lipofectamine® 2000. All N/P ratios were chosen above where full complexation is known to occur between the siRNA and the TPP-dendrimers, as demonstrated by the complexation assay.

There was no significant difference seen between the (-) siRNA and (+) siRNA sequences for 0TPP-dendriplex at N/P 10, and 4TPP-dendriplex at N/P of 20, and naked (-) siRNA and (+) siRNA sequences, which may indicate that any gene knockdown seen may only be due to off-target effects and not due to the successful siRNA delivery and gene knockdown. All other groups when comparing the (-) siRNA and (+) siRNA TPP-dendriplexes and various controls, a statistically significant difference was observed, which demonstrates that eGFP knockdown was above and beyond any off-target effects. All groups at all the N/P ratios demonstrated a significant increase in eGFP knockdown when compared to delivering (+) siRNA alone to the cells. At N/P 5, all TPP-dendriplexes were able to knockdown the eGFP gene but showed no statistical difference between any group and showed only moderate knockdown compared to Lipofectamine® 2000. As the N/P ratio increased (N/P 10, 20, & 30), changes in gene knockdown efficiency between the various TPP-dendriplexes was observed. In general, an increase in TPP density and increase in N/P ratio lead to an increase in gene knockdown efficiency.

The most effective TPP-dendriplex system was found to be 12TPP-dendriplex at N/P ratio of 30 with % eGFP knockdown at 45 ± 5 %. This group was used to formulate mannitol microparticles suitable for pulmonary delivery. After formulation in mannitol,

gene knockdown efficiency of the recovered dendriplexes was unchanged to $49 \pm 11\%$ - Figure 4.5 – N/P30 12TPP-SD. The results can be directly contrasted with the positive control, Lipofectamine® 2000, which showed a gene knockdown ability at $73 \pm 2\%$.

4.3.6 *In Vitro* Cytotoxicity

The toxicity of the TPP-dendriplex nanocarrier was also tested *in vitro* against A549 cells at the same incubation period (48 hours) and concentrations utilized in the *in vitro* gene knockdown experiments, using TPP-dendriplexes formulated at N/P 30 – the N/P ratio that resulted in highest gene knockdown efficiency. The results reveal no significant difference in toxicity between the TPP-dendriplexes and that of the control (no dendriplex), demonstrating no cell toxicity at the concentrations tested (Figure 4.6).

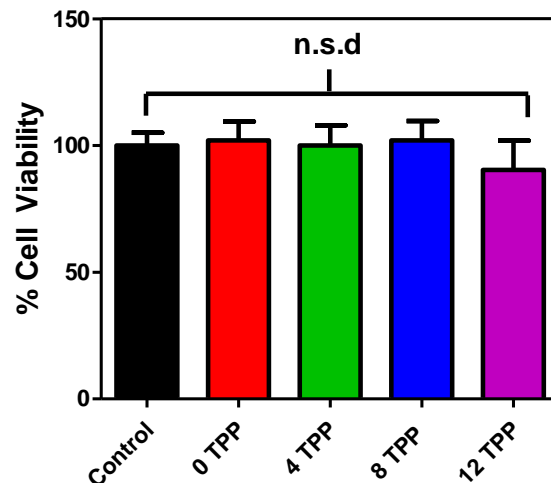


Figure 4.6. Viability of eGFP A549 cells contacted with G4NH₂-TPP-siRNA dendriplexes (12TPP-dendriplexes) formed at N/P 30, as measured with an MTS assay after a 48-hour incubation with the dendriplex. The concentration of the dendriplex used was the same as the *in vitro* knockdown experiments. Statistical analysis was run between the control group (no dendriplex) representing 100 % cell viability, and the dendriplex formed with G4NH₂ with varying TPP density. One-Way ANOVA followed by Tukey's Multiple Comparison Test ($n \leq 3$). n.s.d. = not statistically different.

The toxicity of 12TPP-dendriplex was also tested at the same incubation period of 48 hours and increasing concentrations of 12TPP dendriplex but maintaining the N/P 30 ratio - the system (N/P ratio and TPP density) with highest gene knockdown efficiency (Figure 4.7).

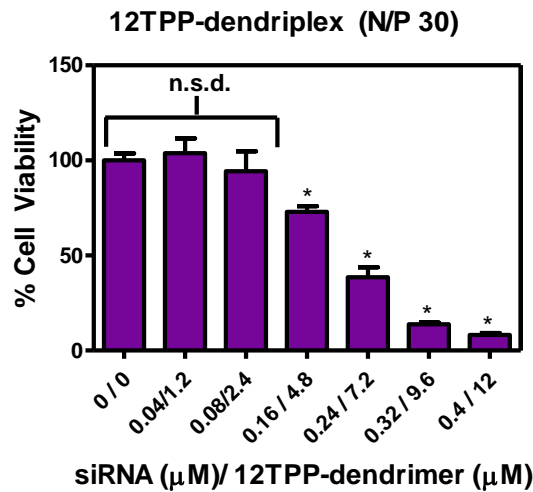


Figure 4.7. The cell viability of eGFP A549 cells contacted with G4NH₂-12TPP dendriplex (12TPP-dendriplex) formed at N/P 30 as measured by the MTS assay after 48 h incubation and increasing dendriplex concentration. * represents the statistical analysis between the control group indicated at 0 μM representing 100 % cell viability and those of increasing concentrations, as analyzed by One-Way ANOVA followed by Tukey's Multiple Comparison Test ($n \leq 3$). n.s.d. = not statistically different.

The highest concentration for which no cell toxicity was seen for 12TPP-dendriplex at N/P 30 was 0.08 μM siRNA / 2.4 μM 12TPP-dendrimer, while 0.16 μM siRNA / 4.8 μM 12TPP-dendrimer led to a statistically significant decrease in % cell viability ($73 \pm 3\%$). The concentration used for *in vitro* gene knockdown experiments was 0.1 μM siRNA / 3.0 μM 12TPP-dendrimer. This was also considered a concentration that did not affect cell viability (Figure 4.6) and correlates with these findings (Figure 4.7).

4.3.7 Preparation and Characterization of 12TPP-Dendriplex/Mannitol Microparticles

The system that displayed the highest *in vitro* gene knockdown ability (12TPP-dendriplex at N/P 30) was selected for formulation into inhalable microparticles using mannitol as the excipient. The 12TPP-dendriplex/mannitol microparticles were formed using the spray drying technique and characterized by LS, SEM, and gel electrophoresis. The percent yield of the powders prepared by spray drying was $76 \pm 5\%$. The nanocomplexes were loaded with high efficiency into the microparticles - $75.1 \pm 6.7\%$ relative to theoretical payload. The payload of siRNA within the TPP-dendriplex-mannitol microparticles was determined by densitometry - $0.025 \pm 0.004\%$ (wt/wt, n=3).

The microparticles were visualized using SEM (Figure 4.8) revealing a smooth and spherical shape.

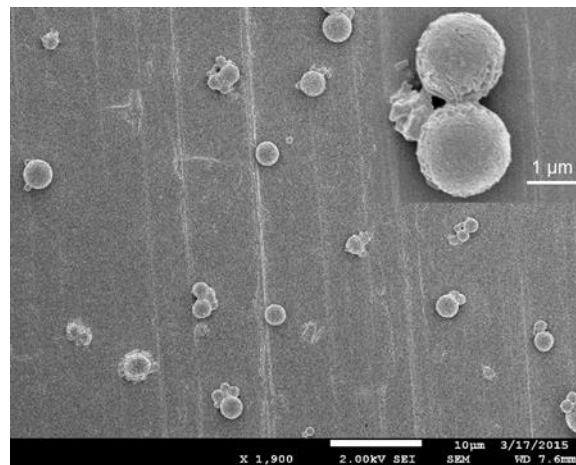


Figure 4.8. Scanning electron microscopy (SEM) of dendriplex/mannitol microparticles prepared by spray drying. The geometric diameter of dendriplex/mannitol particle (inset) represents the average of over 300 particles. Higher magnification image is shown as inset.

The geometric diameters of microparticles was also qualitatively assessed by SEM and compared to the solvated diameter (SD) utilizing LS where the 12TPP-dendriplex/mannitol microparticles were dispersed in HPFP, a model propellant. The results revealed a geometrical diameter of $2.4 \pm 0.9 \mu\text{m}$ and a SD of $4.2 \pm 0.5 \mu\text{m}$. The redispersability of the dendriplexes encapsulated within the microparticles upon breakdown in aqueous media is an important factor for lung deposition and intracellular internalization of siRNA. LS results (Table 4.2) revealed that the HD of the 12TPP-dendriplex reconstituted from the microparticles ($340 \pm 154.5 \text{ nm}$) was similar as that of freshly prepared dendriplex ($363 \pm 55 \text{ nm}$) indicating the 12TPP-dendriplex structure remained intact during the spray drying process.

Table 4.2. Hydrodynamic diameters (HD), Polydispersity Index (PDI), and zeta potential (ζ) of 12TPP-dendriplex (N/P 30) before formulation in mannitol-based microparticles and after reconstitution in DI H₂O. Light Scattering performed in DI water.

	HD (nm)	PDI	ζ (mV)
Dendriplex	363 ± 55	0.36 ± 0.15	$+40 \pm 3$
Reconstituted dendriplex	340 ± 150	0.20 ± 0.02	$+27 \pm 7$

The surface charge of the 12TPP-dendriplex remained positive in both cases, however, did decrease from +40 mV to +26.5 mV – note that the media in which they were measured is slightly different, as the reconstituted dendriplexes were measured in the presence of mannitol.

4.3.8 The *in vitro* Aerosolization of 12TPP-Dendriplex/mannitol Microparticles Formulated as Dispersions in HFA-based pMDIs

The 12TPP-dendriplex/mannitol microparticles were tested for their aerosol performance utilizing an *in vitro* lung model, the Anderson Cascade Impactor (ACI), for the pMDI formulations. The ACI comprises eight different stages representing different areas of lung deposition, and the amount of deposition was determined either by

quantifying the siRNA levels (densitometry) or the siRNA and the total mass of microparticles (siRNA + mannitol) in each plate (Figure 4.9). The aerosol characteristics of the pMDI formulations, including respirable fraction (RF), fine particle fraction (FPF), mean mass aerodynamic diameter (MMAD), and geometric standard deviation (GSD) were determined (Table B1). The % deposition of the siRNA/microparticles on the various stages of the ACI have indicated that besides the IP and AC, highest deposition of siRNA (on respirable stages) was on stages 3, 4 (Figure 4.9).

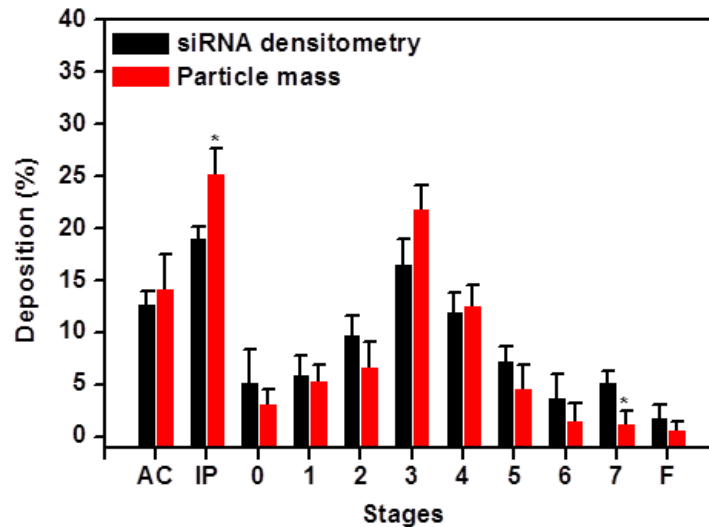


Figure 4.9. Deposition of 12TPP-dendriplex/mannitol microparticles on different stages of the Andersen Cascade Impactor (ACI) from a pMDI formulation at a flow rate of 28.3 L/min, as determined by siRNA densitometry method and particle mass method. pMDI formulations at 2 mg microparticles/1 mL HFA227 propellant at 25°C and saturation pressure of propellant. The payload of siRNA in microparticle is 0.025% wt/wt. The results were based on 20 actuations and represented with mean \pm s.d. (n=3). Statistical analysis was performed with Student t-test (*p<0.05). AC: actuator, IP: induction port, 0-7: plate 0-7, and F: filter.

The FPF calculated for the pMDI formulations by mass method was $50.3 \pm 2.6\%$ and by the siRNA densitometry was $53.7 \pm 3.0\%$, demonstrating good correlation between the two methods. MMAD was determined to be $3.8 \pm 0.2 \mu\text{m}$ (mass method) and

3.6 ± 0.1 (μm siRNA densitometry method), while the calculated GSD was 1.4 ± 0.1 (mass method) and 1.8 ± 0.2 (siRNA densitometry method).

4.3.9 The *in vitro* Aerosolization of DPI Formulation of 12TPP-Dendriplex/Mannitol Microparticles

The inhalable 12TPP-dendriplex/mannitol microparticles were also tested as a formulation for dry powder inhalers (DPIs). The *in vitro* deposition of the DPI formulation loaded in the Rotahaler™ was also assayed at 28.3 L/min and 75% relative humidity using 8-stage ACI equipped with a preseparator. The deposited particles on each stage were collected, and the siRNA was visualized with gel electrophoresis and quantified by densitometry (Figure 4.10).

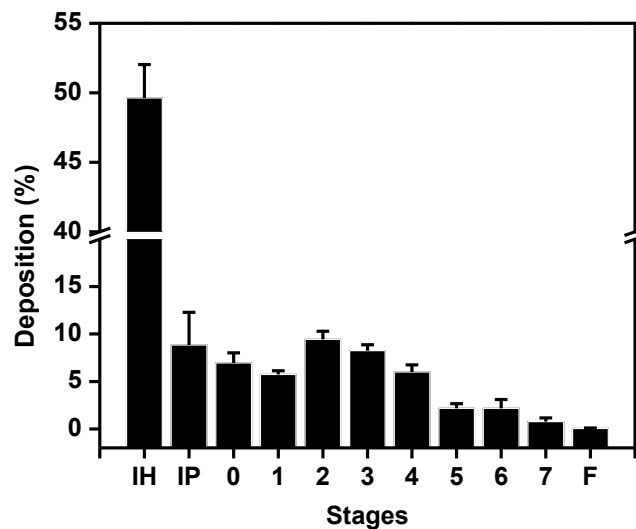


Figure 4.10. Deposition of 12TPP-dendriplex/mannitol microparticles on the different stages of Andersen Cascade Impactor (ACI), as determined by siRNA densitometry method. The 10-20 mg micron particles loaded into capsule were released into ACI from Rotahaler® (DPI formulation) at 25°C, 75% relative humidity, and a flow rate of 28.3 L/min for 4 s inspiration. The results are represented with mean \pm s.d. (n=3). IH: inhaler, IP: induction port, 0-7: plate 0-7, and F: filter.

The aerosolization parameters were further calculated based the deposition data (Table B2). A relatively large interparticulate cohesion was seen for the 12TPP-

dendriplex/mannitol microparticles, where $49.6 \pm 2.4\%$ was retained in the inhaler device and capsule. The particles with low micron size tend to be sticky due to the propensity to reduce surface energy upon aggregation.²⁶⁸ In addition, the residual water content in mannitol microparticles can exacerbate the stickiness via capillary force.²⁶⁹ ED, RF, and FPF were $50.4 \pm 2.4\%$, $41.5 \pm 2.6\%$, and $38.5 \pm 3.1\%$, respectively. MMAD and GSD based on deposition data were $4.8 \pm 0.3 \mu\text{m}$ and 1.4 ± 0.2 , respectively (Table B2).

4.4 Discussion

There are many potential advantages in developing effective carrier-based systems for siRNA intracellular delivery^{190, 270} and innovative strategies for local delivery of siRNA to the lungs^{270, 271} for the treatment of a variety of pulmonary disorders. The literature strongly suggests that synthetic polymers may be employed for enhanced siRNA delivery to various tissues.^{272, 273} PAMAM dendrimers are particularly attractive as their surface chemistry can be used not only to provide complexation sites with siRNA, and in the process reduce siRNA degradation and enhance cellular uptake,^{274, 275} but can also be modified to control important aspects of siRNA delivery upon cellular internalization and potentially be used to target intracellular organelles.²⁶¹ Motivated by recent literature work that demonstrates that linear polymers modified with phosphonium-containing groups can enhance the delivery of siRNA to the cell cytoplasm,²⁷⁶ and that TPP-modified dendrimers are effective carries for pDNA,²³⁷ in this work we investigate the effect of TPP conjugation on the surface of G4NH₂ on their efficacy in delivering siRNA to the cell cytosol and to silence genes in an *in vitro* model of the pulmonary alveolar epithelium. In this context, we were successfully able to formulate G4NH₂-TPP-dendriplexes (or simply TPP-dendriplexes) with various TPP densities and N/P ratios that

formed positively-charged nanoparticles (ca. 300 nm). Importantly, we also investigate particle engineering strategies that can address the formulation of such siRNA-dendrimer complexes in portable inhalers for pulmonary delivery of siRNA. In this case, we demonstrated successful micron-particle formulation of TPP-dendriplex systems (12TPP-dendriplex/mannitol microparticles) for pMDIs and DPIs.

Firstly, the effect of the TPP density and N/P ratio on the influence of TPP-dendriplexes ability to successfully deliver siRNA to lung alveolar cells *in vitro* was investigated. Certain characteristics such as complexation ability of TPP-dendrimer to siRNA was influenced by increasing presence of TPP on the dendrimer. The amount of TPP-dendrimer required to fully complex siRNA increased with the increase in TPP density (Figure 4.3) as well as requiring less heparin to separate the siRNA from the dendrimer (Figure 4.4) which demonstrates that a looser association between the TPP-dendrimer and siRNA. While complexes with dendrimer with both TPP and no TPP remain positively charged, the TPP-modified dendrimer contained a positive charge that is delocalized by the hydrophobic phenyl rings present, thus decreasing the binding ability of dendrimers to siRNA. Therefore, this difference in complex stability cannot be attributed due to differences in surface charge but are more likely related to the hydrophobic nature and steric effects of the phenyl rings present in TPP. Consequently, the loose complexation of siRNA with the TPP-dendrimer may provide for a strategy to modulate siRNA release, which is a critical step when the nanocarriers reach the cytosol,²⁷⁷ and thus overcome an existing challenge in the use of bare cationic PAMAM dendrimers.

Subsequently, the gene knockdown ability of the TPP-dendriplexes was also affected by TPP density and N/P ratio. An increase in gene knockdown efficiency was

observed with an increase in both TPP density and an increase in N/P ratio, as seen by the increase in % eGFP knockdown in eGFP-expressing A549 cells (Figure 4.5). However, the modification with only 4 TPP molecules per dendrimer did not show any increase in transfection ability. Therefore, a threshold of TPP density is required to be able enhance transfection ability of dendrimers: >1/16 surface functionalization (greater than 4 TPP molecules per 64 available surface groups on G4NH₂ PAMAM dendrimer). 12TPP-dendriplex at N/P of 30 resulted in the highest transfection efficiency (45 ± 5%), and was higher than our previous study of unmodified dendriplexes in the same cell line (22-37%)⁹⁶ and what is reported here as a function of N/P ratio (8-25%).

This increase in transfection ability may be due to several factors. This includes a weaker complexation of siRNA with 12TPP dendrimer allowing for facilitated decomplexation once the TPP-dendriplex has been internalized into the cell - based on evidence seen with the complexation and polyanion competition assays. A balance between complexation and decomplexation of the siRNA once internalized into the cell must be reached for high gene transfection.²⁷⁸ If the electrostatic interaction is too strong between the dendrimer and siRNA, this can lead to a failure in siRNA release and gene knockdown,²⁷⁸ which may be a reason for lower transfection ability of 0TPP-dendriplex. Other reports have shown that the addition of heparin and other anionic oligomers increase the transfection ability of PAMAM/DNA complexes, suggesting that not as strong association between the DNA and dendrimer in the presence of heparin could allow for higher transfection ability.^{279, 280} Therefore, the looser association between dendrimer and siRNA may account for some increase gene knockdown seen. However, it is also known that TPP-modified PAMAM dendrimers can lead to enhanced cellular internalization of

dendrimers compared to unmodified dendrimers,^{33, 261} and this effect depends on TPP density.²⁶¹ This could potentially lead to higher amounts of siRNA being delivered to cells over time. Other factors, including increased mitochondrial targeting and efficient endolysosomal escape of the dendrimer with TPP may also play important roles in the increased transfection ability.²³⁷ The transfection ability could also be potentially increased if an increase of TPP density on dendrimer were to occur, however, this would have to be balanced with potential toxic effect TPP modification can impart, as seen in our previous work.²⁶¹

The toxicity of TPP-dendriplexes was also monitored to make sure any off-target effects were not due to overt toxicity. Off-target effects can include toxicity of the gene vector itself^{281, 282} and similarities in (-) siRNA mRNA motifs not specifically targeted by siRNA.^{283, 284} These off-target effects are not uncommon, as seen in the use of the Lipofectamine® 2000 commercial reagent, and may be difficult to avoid since they are not well-understood.²⁸⁵ No significant toxicity of the TPP-dendriplexes (N/P 30) was seen for concentrations used in the eGFP knockdown experiment (Figure 4.6), which demonstrate the off-target effects seen by delivery of (-) siRNA cannot be attributed to toxicity of the TPP-dendrimer. Since the 12TPP-dendriplex at N/P 30 demonstrated the highest transfection efficiency, toxicity studies with increasing concentrations of the TPP-dendriplex was performed to determine the highest concentration of complex that could be used without any toxicity seen on the cell model (Figure 4.7). In this case, the maximum amount of siRNA that can be delivered to A549 cells *in vitro* with the TPP-dendrimer constructs without toxic effects fell between 20-32 pmol of siRNA (0.10-0.16 μ M siRNA/3.0-4.8 μ M 12TPP-dendrimer). This contrasts greatly with Lipofectamine®

2000 where toxic effects were seen against A549 cells at a concentration of 4 ug/mL, which corresponds to 20 pmol of siRNA delivery (Figure B1). This concentration of Lipofectamine® 2000 was the concentration utilized in the gene knockdown experiments, which may have contributed to some of the off-target effects seen for Lipofectamine® 2000 as well as demonstrating its limitations in terms of safe siRNA delivery. Therefore, the TPP-dendriplex system compared to Lipofectamine® 2000 has the potential to deliver more siRNA with less toxic effects.

From the *in vitro* knockdown and toxicity studies, the dendriplex with 12TPP and at 30 N/P ratios have emerged as the most promising system and was thus selected to be tested in the development of the portable oral inhalation formulations for pulmonary delivery. There are lots of potential benefits in providing patients with a range of devices that they can choose from when dealing with pulmonary drug administration, including compliance,²⁸⁶ which is why formulations for both pMDIs and DPIs were developed. PAMAM dendrimers have been utilized for pulmonary delivery *in vivo*^{77, 78, 116, 287} and formulated for use in nebulizers,²⁵⁸ pMDIs^{96, 127} and DPIs.²⁸⁸ A key aspect of the design of oral inhalation formulations is the particle aerodynamic diameter emitted from the device, which should fall within the range of 1-5 μm .^{99, 216}

A strategy to deliver such dendriplexes, whose geometric size are quite different from the aerosol requirements for deep lung deposition, is to engineer particles with non-active ingredients encapsulating the TPP-dendriplexes and having appropriate micron-sizes. Spray drying provides for an easy and scalable strategy to engineer particles with a well-defined size range and morphology.^{97, 289} Mannitol has been widely used as a promising excipient in portable inhalers as early studies demonstrated improvement in

respiratory symptom and quality of life of lung dysfunction-stricken patients.²⁹⁰ Spray drying has been also recently used to prepare microparticles of mannitol and siRNA-loaded PLGA nanoparticles for dry powder formulation.²⁶⁵ However, in that study, the performance (aerosol characteristics) of the powder formulation was not tested *in vitro*. We also recently investigated the use of spray drying to form microparticles for metered-dose inhaler formulations of siRNA-dendriplexes.⁹⁶ Based on the successes of these previous studies, we investigated the ability of engineering microparticles of TPP-dendriplexes and mannitol using spray drying, and the aerosol characteristics of the resulting formulations in both pMDI and DPI form. Spray drying 12TPP-dendriplex system in mannitol produced desired geometric sizes that are required for within desired size ranges.

We also investigated the characteristics of reconstituted TPP-dendriplexes (dendriplexes after spray drying with mannitol and dissolution of mannitol in water) compared with TPP-dendriplex before the generation of the microparticles as to maintain as close as possible the original characteristics of the dendriplex. The 12TPP-dendriplex and reconstructed 12TPP-dendriplex revealed similar nanoparticle sizes, and the surface charge remained positive but was lower after formulation in mannitol. This may be due to the presence of mannitol within the system. Also, the 12TPP-dendriplex/mannitol microparticles revealed a slight increase in % eGFP knockdown but not statistically different from 12TPP-dendriplexes strongly suggesting that biological activity of siRNA remains unaffected upon spray drying (Figure 4.5).

Consequently, 12TPP-dendriplex/mannitol microparticles were further tested for their aerosol performance in pMDI and DPI formulations *in vitro* using an Anderson

Cascade Impactor (ACI). An ACI, comprised with eight stages, has been widely recognized as an adequate *in vitro* lung model to assess the aerosol performance of the pMDI and DPI formulations in which various aerosol performance characteristics/values can be determined.²⁹¹ Median mass aerodynamic diameter (MMAD) is defined as median of airborne particle mass distribution with respect to aerodynamic diameter,⁹⁶ signifying the aerodynamic diameter which half of the aerosolized drug mass is below the diameter stated.²⁹² Geometric standard deviation (GSD) is always reported with MMAD, showing the variability of particle size distribution, the spread of the aerodynamic diameters from the median.^{96, 292} Both the MMAD and GSD values for the pMDI and DPI formulations demonstrated appropriate values suitable for deep lung deposition efficient deposition in deep lung (Table B1, Table B2).²⁹³

One key aerosol characteristic that was measured is the fine particle fraction (FPF). The FPF is an indicative of the efficiency of deep lung deposition of inhalation formulations, with aerodynamic diameters of less than 5 μm .²⁹⁴ The FPF is considered an important aerosol characteristic to determine the therapeutically beneficial proportion of the siRNA that can reach the lower lung airways (trachea to alveoli). The FPF of the pMDI formulation (Table S1) is comparable to commercial HFA-based pMDI formulations of small molecule therapeutics (range on average 30-55%),²⁹⁵ whose formulation and device are extensively optimized before reaching the market. These results are also consistent with our previous particle engineering strategies whereby biodegradable polymers were employed to encapsulate siRNA-G4NH₂ dendriplexes, where we reported an FPF of ca. 49 \pm 6 % for dendrimer-siRNA complexes (no TPP).⁹⁶ The DPI formulation revealed an FPF (Table B2) that falls in the reported range that varies from 12 to 40% of

emitted dose among different DPIs.²⁹⁶ Therefore, this formulation falls within what is generally seen with DPI formulations. In conclusion, the particle PMDI and DPI formulation strategies were successful in producing microparticles containing inhalable siRNA with suitable aerosol characteristics.

4.5 Conclusion

Synthetic siRNA can be an effective therapeutic in the treatment of a number of lung diseases. In this work, we evaluated the impact of TPP surface modification of G4NH₂ dendrimers on the modulation of their interaction with siRNA, and subsequently on the gene knockdown ability of the dendriplexes in an *in vitro* model of the pulmonary epithelium. The presence of TPP on the dendrimer surface resulted in enhanced eGFP gene knockdown in eGFP-A549 cells. Dendriplexes with the dendrimers containing the highest surface density of TPP (G4NH₂-12TPP) and at N/P 30 showed the best gene knockdown efficiency compared to all other systems, including G4NH₂-0TPP. The improvement in transfection efficiency was associated with looser complexation of siRNA with dendrimer and may also be associated with other factors including mitochondrial targeting, enhanced cellular internalization, and more efficient endolysosomal escape of the TPP-dendriplexes. The G4NH₂-12TPP-dendriplexes were also formulated in portable inhalers to assess their potential for the local delivery of siRNA to the pulmonary epithelium. G4NH₂-12TPP-dendriplexes were spray-dried with mannitol resulting in micron particles with high encapsulation efficiency. These particles were formulated in pMDIs and DPIs, with resulting aerosol characteristics that are conducive to deep lung deposition (FPF of ca. 50% and 39%, respectively), while the formulation and aerosolization had no impact on the transfection efficiency of the G4NH₂-12TPP-

dendriplexes. The proposed G4NH₂-12TPP-dendriplexes and their aerosol formulations hold promise in the local delivery of siRNA to the lung epithelium for the treatment of relevant pulmonary diseases.

4.6 Acknowledgements

The authors would like to thank financial support provided by NSF-DMR Grant no. 1508363. We would also like to thank the VCU Microscopy Facility, supported, in part, by funding from NIH-NCI Cancer Center Support Grant P30 CA016059 for the sample preparation and use of the Zeiss EVO 50 XVP SEM with the help of Judy Williamson.

CHAPTER 5 – SYNTHESIS OF ASYMMETRIC DENDRIMERS CONTAINING DOX AND VARIOUS SURFACE MODIFICATIONS BY CLICK CHEMISTRY

5.1 Introduction

Of all the polymeric nanocarriers, dendrimers have shown great promise in the delivery of various drugs, peptides, antibodies, and genetic materials (DNAs/siRNAs) into intracellular targets within cells, as well as altering the pharmacokinetics and biodistribution.^{36, 47} Dendrimers are hyperbranched tree-like polymers with nanometer sizes containing a central core, repeating branching units (known as dendrons) with a multitude of surface groups.³⁵ They are characterized by their unique properties including monodispersity, small tunable sizes, and multiple surface groups for modification, reproducible pharmacokinetics, and controlled therapeutic release.^{33, 36} This allows for the increase in the solubility and bioavailability of therapeutics attached covalently, encapsulated, or complexed with, and allow for multiple attachments for therapeutics as well as targeting ligands and surface modulators that can enhance pharmacokinetics and biodistribution while reducing unwanted side effects.^{34, 36} These characteristics make dendrimers an attractive choice for polymeric drug delivery.

It is known that the endocytic internalization and intracellular trafficking within cells can affect the therapeutic performance.⁴⁶ There are several mechanisms of cellular transport across cellular membranes including endocytosis, passive diffusion, and paracellular transport.⁴⁷ It has been demonstrated that major factors that influence cellular internalization and intracellular trafficking of dendrimers, as well as their *in vitro* and *in vivo* toxicity is the size (molecular weight and generation) and the surface chemistry.^{47, 297} Of dendrimers, PAMAM dendrimers were the most extensively studied. It was found that PAMAM dendrimers were more readily transported across epithelial

barriers compared with water-soluble linear polymers.⁴⁷ Charged dendrimers have shown increase permeability compared to neutral dendrimers. Cationic amine-terminated (-NH₂) were demonstrated the highest permeability compared to anionic carboxyl-terminated (-COOH) dendrimers, in which -NH₂ decreases with size as -COOH increases with size.⁴⁷

However, these parameters (molecular weight, generation, and surface charge) can also largely dependent on cell type taken up.⁴⁷ Studies on human lung alveolar epithelial adenocarcinoma cells (A549) revealed PAMAM G4-COOH anionic dendrimers were internalized by caveolae-mediated endocytosis whereas cationic G4-NH₂ and neutral G4-OH dendrimers were internalized by non-clathrin, non-caveolae-mediated mechanisms that involved electrostatic interactions or other non-specific fluid-phase endocytosis.¹⁰⁸ Also, it was demonstrated that cationic G4-NH₂ dendrimers, once internalized were found more in peripheral vesicles, whereas anionic G4-COOH and neutral G4-OH dendrimers were found in lysosomes.¹⁰⁸ When it comes to polarized epithelial cells such as Caco-2 or Calu-3, paracellular transport can also occur.^{287, 298} In this case Kitchens et al. demonstrated extensive studies on dendrimer size (generation and MW) and surface charge (neutral, anionic, cationic) on the ability to permeate Caco-2 cells, demonstrating similar trends as described above.²⁹⁸ However, a reduction in transepithelial electrical resistance (TEER) readings was seen for cationic PAMAM -NH₂ dendrimers and with anionic PAMAM -COOH dendrimers within a specific size range (G2.5-3.5), demonstrating enhanced permeability of dendrimers by opening of tight junctions suggesting PAMAM dendrimers are also transported through paracellular route. This was not seen for neutral PAMAM -OH dendrimers.²⁹⁸ Therefore, it is important not

only to understand dendrimer properties, but how those properties influence the cellular environment in which you intend to expose them to.

Modifications to the dendrimer surface including addition of linear water-soluble polymers like poly(ethylene)glycol (PEG) and lipophilic molecules like lauryl chains can also influence the cellular internalization pathways and intracellular trafficking. Addition of PEG to dendrimers been shown to modulate PAMAM dendrimer properties by decreasing toxicity, improving circulation time, protecting therapeutic payload, increasing aqueous compatibility, and modulating cellular internalization.²⁸⁷ The modification of G3-NH₂ PAMAM dendrimers with PEG on surface was able to demonstrate decrease internalization within polarized Calu-3 cells (human lung epithelial cells), however, increased transport across monolayer via transcellular and paracellular routes.²⁸⁷ This was further demonstrated *in vivo* when these dendrimers were delivered via pulmonary route, in which high peak plasma concentrations were seen when G3-NH₂ PAMAM dendrimers were PEGylated demonstrating dendrimers being transported across the lungs into systemic circulation.²⁸⁷ The addition of lauryl groups has also be added to dendrimers to modulate decrease toxicity (cationic dendrimers), increased internalization by interactions with the fluidity of the membrane and regulation of paracellular route.¹¹⁰ G3-NH₂ dendrimers modified with two lauroyl chains was found to be internalized by caveolae-dependent and clathrin-dependent endocytosis as well as micropinocytosis with trafficking to endosomes and lysosomes in an human colon adenocarcinoma cell line – HT-29.¹⁰⁹ It was also demonstrated that G2-G4 PAMAM -NH₂ dendrimers modified with lauroyl chloride was able to decrease toxicity of cationic dendrimers as well as increase transport across Caco-2 cells via transcellular and paracellular routes.¹¹⁰

Understanding internalization pathways and cellular trafficking can in the specific cell type of interest had important implications in choosing and designing correct type of nanocarrier and drug-nanocarrier conjugation. This has been demonstrated with the efficacy of methotrexate (MTX) conjugated to cationic vs anionic dendrimers. Anionic-MTX dendrimers were 25 times more efficacious than cationic-MTX dendrimers in which there higher localization and increased residence time in lysosomes was seen for anionic-MTX dendrimers.⁴⁷ Therefore, designing the correct dendrimer system, conjugation between therapeutic and dendrimer, and route of delivery must all be coordinated in order to achieve the highest efficacy.

Recent advances in dendrimers has also been established by formation of dendrimers formed from polyester-based materials. Bis-MPA polyester dendrimers, first described by Ihre, et al.,¹⁶¹ and have been shown to provide an alternative dendrimer compared to PAMAM as demonstrating decreased toxicity compared to G4 PAMAM dendrimers, as well as providing a more biodegradable and biocompatible option. We have previously demonstrated that the use of Bis-MPA polyester dendrimers and PEGlyated bis-MPA dendrimers demonstrating decreased internalization and increased transport of dendrimers across Calu-3 epithelium as seen with PAMAM dendrimers.^{164,}²⁸⁷ The increased interest in multifunctionality has expanded the pursuit of asymmetric or heterobifunctional dendrimers.⁴⁰ However, little is known on the internalization pathways and cellular trafficking of such heterobifunctional dendrimers and how this can influence drug release and overall efficacy *in vitro* and *in vivo*.

Considering these aspects, the goal of this study was to synthesize dendrons containing different surface chemistries that could potential alter cellular internalization

and cellular trafficking, which attached with drug could influence overall efficacy of drug-polymer conjugate. Here we modified Generation 5 Bis-MPA polyester dendrons with various modifications to change surface chemistry including cationic amine-terminated (-NH₂), anionic carboxy-terminated (-COOH), neutral hydroxy-terminated (-OH), hydrophilic PEGylated (-PEG), and hydrophobic lauryl-modified (-LA) functionalities. The chemical synthesis and characterization of all modified dendrons were established.

5.2 Materials and Methods

5.2.1 Materials

32 hydroxyl, 1 azide, generation 5, 95% (N₃-G5-OH), succinic anhydride (SA), glutaric anhydride (GA), 2,5-dihydroxybenzoic acid (DHB), were purchased from Sigma-Aldrich (St Louis, MO, USA). N,N-Diisopropylethylamine (DIPEA) was purchased from TCI Co., Ltd. (Tokyo, Japan). Dichloromethane (DCM), hexane, dimethylformamide (DMF), dimethyl sulfoxide (DMSO), ethyl ether (Et₂O), and methanol (MeOH) were purchased from VWR International (Radnor, PA, USA). 1-dodecanol (lauryl alcohol, LA), 1-(3-Dimethylaminopropyl)-3-ethylcarbodiimide hydrochloride (EDC), 4-(Dimethylamino)pyridine (DMAP), N,N-Dimethylformamide (DMF), anhydrous, 99/8+%, 6-(Boc-amino)hexanoic acid (AHA-Boc), and 4M Hydrogen chloride in 1,4-dioxane was purchased from Alfa Aesar (Haverhill, MA, USA). Dimethyl Sulfoxide-D6 (with TMS - 0.03 vol%), Methanol-D4, and magnesium sulfate anhydrous were purchased from EMD Millipore (Burlington, MA, USA). Deuterium Oxide (D₂O, 99.9%) was purchased from Cambridge Isotope Laboratories, Inc. (Tewksbury, MA, USA). Poly(ethylene)glycol 1000 monomethyl ether (PEG) was purchased from Fluka (Mexico City, Mexico).

5.2.2 Conjugation of lauryl alcohol (LA) with succinic anhydride (SA) form lauryl-succinic acid (LA-SA)

Lauryl alcohol (LA) was modified to contain carboxyl group by addition of succinic anhydride (SA) for form LA-SA product. 1.205 ml (5.37 mmol) of LA was reacted with 1.07727 g (10.77 mmol) of succinic anhydride (SA) with 3.651 ml (21.47 mmol) of N,N-Diisopropylethylamine (DIPEA) in a mixture of 11 ml DCM/DMF (6:5, v/v) at room temperature for 24 h. The solvents were removed, and product was redissolved in 50 ml ethyl ether followed by extraction with hexane. The hexane was removed by rotary evaporation (Buchi Rotavapor® R-3) (40°C) to obtain white/pink crystal product. The LA-SA product was characterized with MALDI-TOF (Voyager-DE PRO, JBI Scientific) and ¹H NMR (Bruker NanoBay Avance III 400 MHz NMR spectrometer).

5.2.3 Conjugation of LA-SA to Azido-G5-OH (N₃-G5-OH) dendron to form Azido-G5-LA

N₃-G5-LA was synthesized by addition of 16.82 mg (4.49 μmol) of polyester bis-MPA dendron – 32 hydroxyl, 1 azide, generation 5, (N₃-G5-OH) with 26.05 mg (90.95 μmol) of LA-SA, 27.12 mg (141.46 μmol) of EDC, and 16.79 mg (137.43 μmol) of DMAP in 3 ml of DMF and left to stir at room temperature for 3 days. The DMF solvent was removed by high vacuum. The product was redissolved in 1 ml of DMSO and put on dialysis against DI water for 24 h using Spectra/Por® 7 RC membrane dialysis tubing (MWCO = 1 kDa). The product was removed from dialysis tubing adding a small amount of DMSO. The DMSO solvent was removed by high vacuum to obtain sticky clear product. The N₃-G5-LA product was characterized using MALDI-TOF, ¹H NMR and Light Scattering (Malvern Zetasizer Nano ZS).

5.2.4 Conjugation of polyethylene glycol (PEG) with succinic anhydride to form PEG-SA

5.44 g (5.44 mmol) of Poly(ethylene)glycol 1000 monomethyl ether (PEG) was modified by addition of 1.08172 g (10.81 mmol) of SA with 3.671 ml (21.07 mmol) of DIPEA in 2.5 ml of DMF and stirred at room temperature for 24 h to form PEG-SA. PEG-SA product was then precipitated in 70 ml of cold ethyl ether followed by suction filtration. The precipitated product was then dissolved in 75 ml of acidic water (pH 3.0) and extracted with dichloromethane (DCM), 3 x 50 ml. The collected DCM with PEG-SA product was dried over anhydrous magnesium sulfate overnight, followed by filtration and removal of DCM solvent by rotary evaporation (40°C). The PEG-SA product was redissolved in DI water, frozen, and lyophilized to obtain white crystal. The PEG-SA was characterized by MALDI-TOF and ^1H NMR.

5.2.5 Conjugation of succinic anhydride (SA) to N₃-G5-OH to form N₃-G5-SA

10.08 mg (2.69 μmol) of Polyester bis-MPA dendron – 32 hydroxyl, 1 azide, generation 5, (N₃-G5-OH) was added with 295.27 mg (268.43 μmol) of PEG-SA catalyzed by 86.46 mg (450.99 μmol) of EDC and 50.82 mg (415.98 μmol) of DMAP in 3.8 ml of DMF and allowed to react at room temperature for 5 days. The DMF solvent was removed by high vacuum followed by dialysis against DMSO using Spectra/Por[®] 7 RC membrane dialysis tubing (MWCO = 8 kDa) for 24 hours. The excess DMSO was removed by high vacuum to leave sticky clear product. The N₃-G5-PEG product was characterized with MALDI-TOF, ^1H NMR, and Light Scattering.

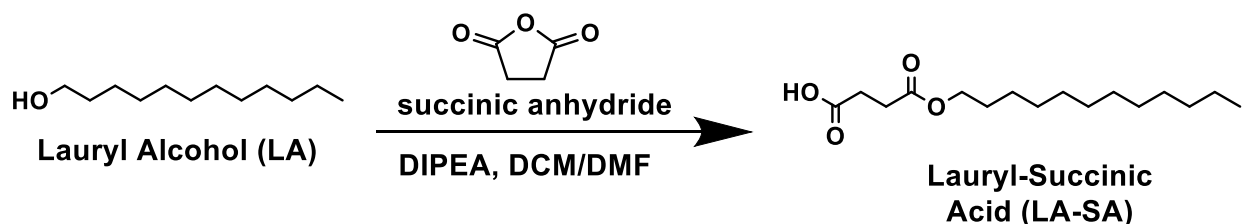
5.2.6 Conjugation of Boc-6-Ahx-OH to N₃-G5-OH dendron followed by Boc deprotection to form N₃-G5-NH₂ dendron

Amine modification of dendron was synthesized by addition of 10.56 mg (2.82 μmol) N₃-G5-OH dendron with 52.73 mg (227.98 μmol) 6-(Boc-amino)hexionic acid (AHA-Boc), 66.61 mg (347.45 μmol) of EDC, and 44.98 mg (368.18 μmol) of DMAP in 5.1 ml in DMF and allowed to react for 9 days at room temperature. The DMF solvent was subsequently removed by high vacuum without further purification. The Boc deprotection was performed by addition of 1 ml of 4 M HCl in 1,4-dioxane for 30 min at room temperature. The solvent was then removed by rotary evaporation followed by dialysis against DMSO using Spectra/Por[®] 7 RC membrane dialysis tubing (MWCO = 1 kDa) for 2 days. After dialysis, the DMSO solvent was removed by high vacuum to leave sticky clear product. The N₃-G5-NH₂ product was characterized by MALDI-TOF, ¹H NMR and Light Scattering.

5.3 Results

5.3.1 Conjugation of lauryl alcohol (LA) with succinic anhydride (SA) form lauryl-succinic acid (LA-SA)

Lauryl alcohol (LA) was modified with succinic anhydride (SA) to form LA-SA as seen in Scheme 5.1.



Scheme 5.1. The modification of LA to contain -COOH group by addition of succinic anhydride (SA) to form LA-SA.

The characterization of LA-SA with ^1H NMR and MALDI-TOF can be found in Figure 4.1.

LA-SA: $^1\text{H-NMR}$ (MeOD, 400MHz, ppm): δ 4.08 (t, 2H), 2.58 (s, 4H), 1.63 (m, 2H), 1.30 (s, 18H), 0.90 (t, 3H). **MALDI-TOF MS:** 309.7.

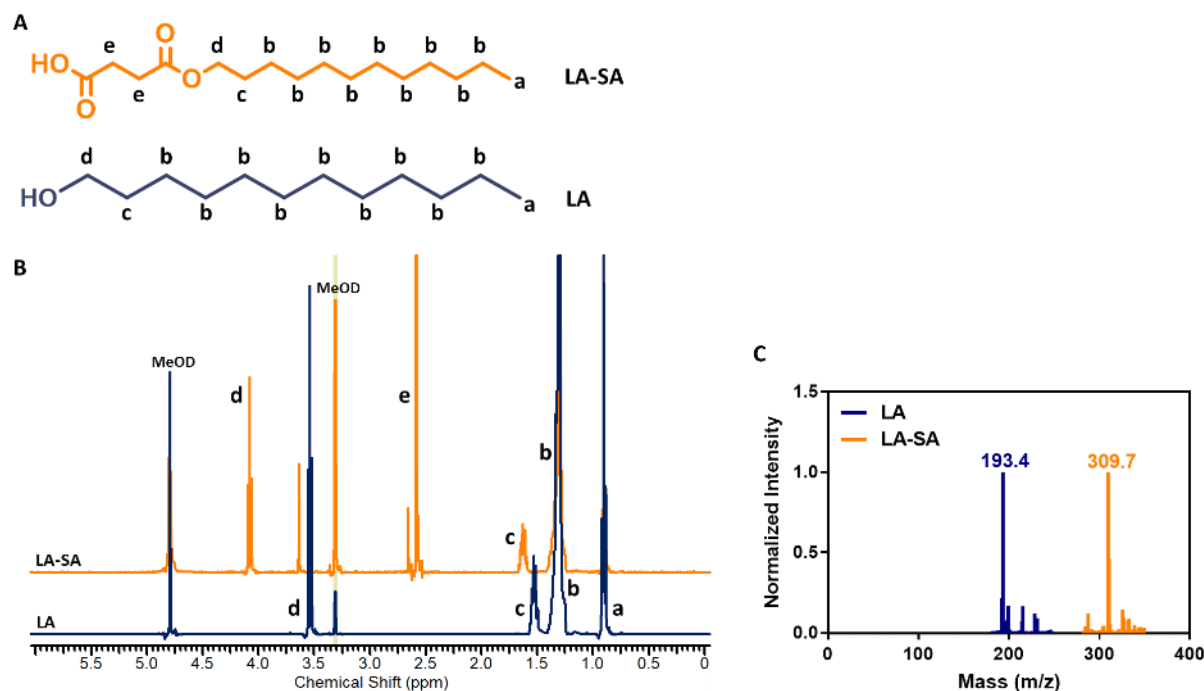
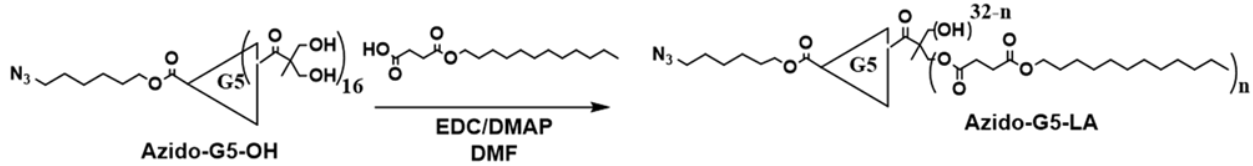


Figure 5.1. A) Chemical structure of LA and LA-SA and the corresponding **B)** ^1H NMR and **C)** MALDI-TOF spectra.

5.3.2 Conjugation of LA-SA to Azido-G5-OH ($\text{N}_3\text{-G5-OH}$) dendron to form Azido-G5-

LA

LA-SA was added to the surface of $\text{N}_3\text{-G5-OH}$ dendron to form $\text{N}_3\text{-G5-LA}$ as seen in Scheme 5.2.



Scheme 5.2. The modification of N₃-G5-OH dendron to contain lauryl surface by addition of LA-SA to form N₃-G5-LA; Azido = N₃.

The characterization of N₃-G5-LA with ¹H NMR and MALDI-TOF can be found in Figure 5.2. **N₃-G5-LA: ¹H-NMR (DMSO-*d*₆, 400MHz, ppm):** δ 4.10-3.43 (m, 170H), 2.37-2.22 (m, 48H), 1.68-1.53 (m, 32H), 1.24 (s, 216H), 1.19-1.04 (m, 92H) 0.85 (t, 36H). **MALDI-TOF MS: 6965.5. LS ζ-potential: +27 ± 6 mV**

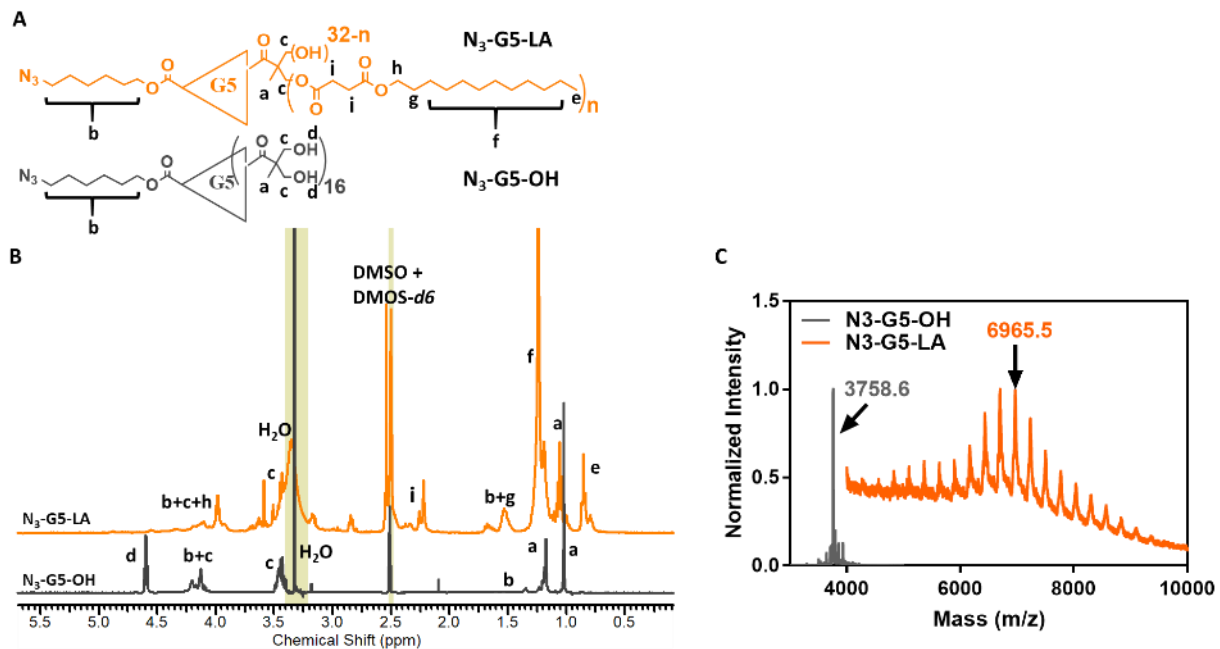
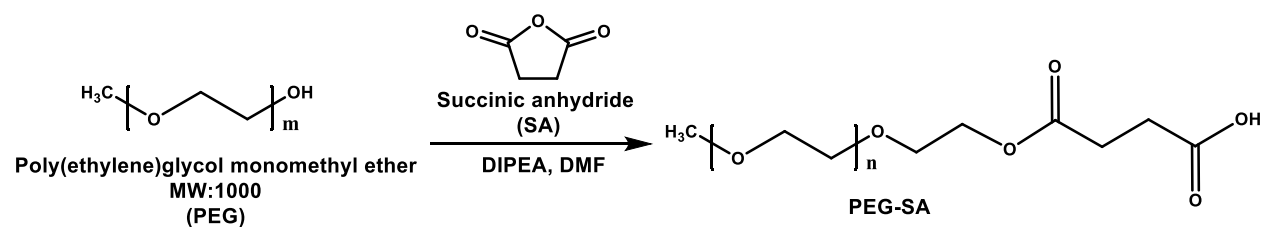


Figure 5.2. A) Chemical structure of N₃-G5-OH and N₃-G5-LA, and the corresponding **B)** ¹H NMR and **C)** MALDI-TOF spectra.

5.3.3 Conjugation of polyethyleneglycol (PEG) with succinic anhydride to form PEG-SA.

Poly(ethylene) glycol monomethyl ether (PEG, MW:1000) modified with succinic anhydride (SA) to form PEG-SA as seen in Scheme 5.3.



Scheme 5.3. The modification of PEG to contain -COOH group by addition of SA to form PEG-SA.

The characterization of PEG-SA with ^1H NMR and MALDI-TOF can be found in Figure 5.3. **PEG-SA: ^1H -NMR (D_2O , 400MHz, ppm):** δ 4.28 (m, 2H), 3.69 (s, 172H), 3.37 (s, 32H), 2.69 (s, 4H). **MALDI-TOF MS:** 1123.6.

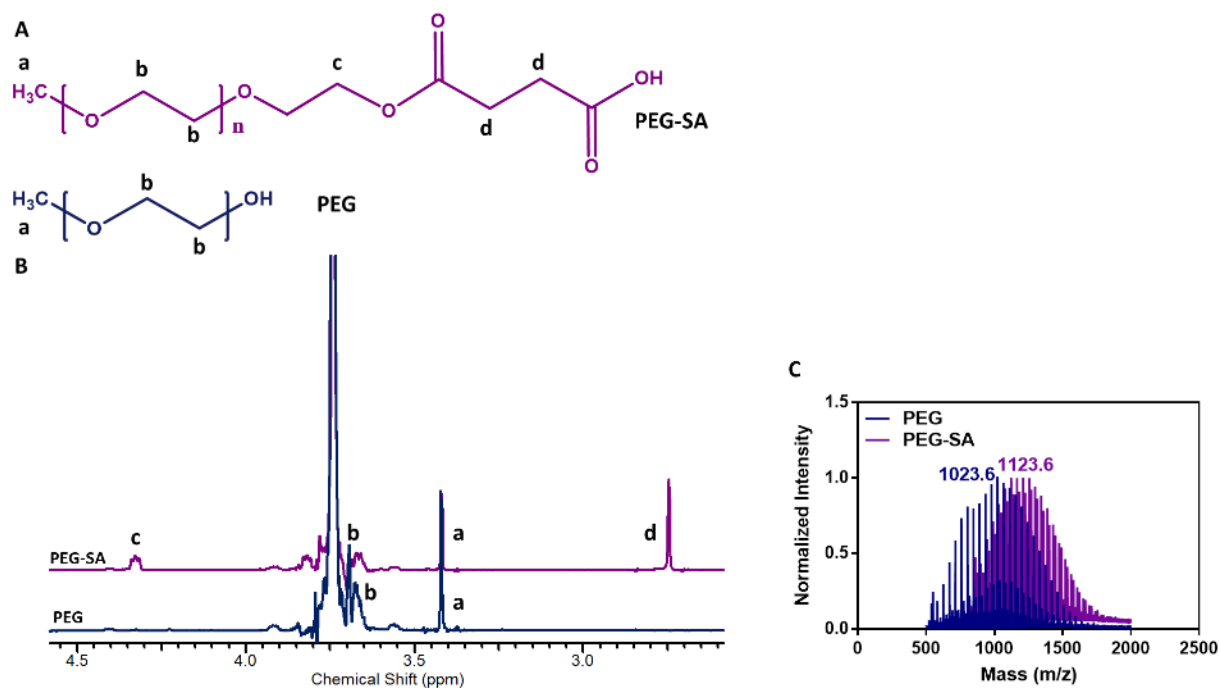
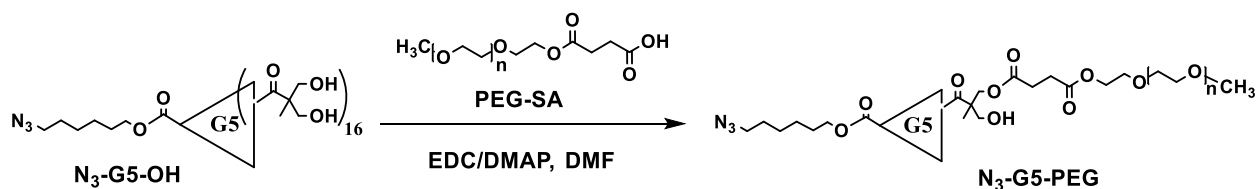


Figure 5.3. A) Chemical structure of PEG and PEG-SA, and the corresponding B) ^1H NMR and C) MALDI-TOF spectra.

5.3.4 Conjugation of PEG-SA to $\text{N}_3\text{-G5-OH}$ to form $\text{N}_3\text{-G5-PEG}$ dendron

PEG-SA was added to the surface of $\text{N}_3\text{-G5-OH}$ dendron to form $\text{N}_3\text{-G5-PEG}$ as seen in Scheme 5.4.



Scheme 5.4. The modification of $\text{N}_3\text{-G5-OH}$ with PEG by addition of PEG-SA to form $\text{N}_3\text{-G5-PEG}$.

The characterization of $\text{N}_3\text{-G5-PEG}$ with ^1H NMR and MALDI-TOF can be found in Figure 5.4. **$\text{N}_3\text{-G5-PEG}$: $^1\text{H-NMR}$ (DMSO- d_6 , 400MHz, ppm):** δ 4.31-4.11 (m, 133H), 3.51 (s, 2580H), 3.24 (s, 245H), 2.51 (m, 60H), 1.24 (s, 216H), 1.16-1.00 (m, 92H). **MALDI-TOF MS:** 20277.1. **LS ζ -potential:** -13 ± 4 mV.

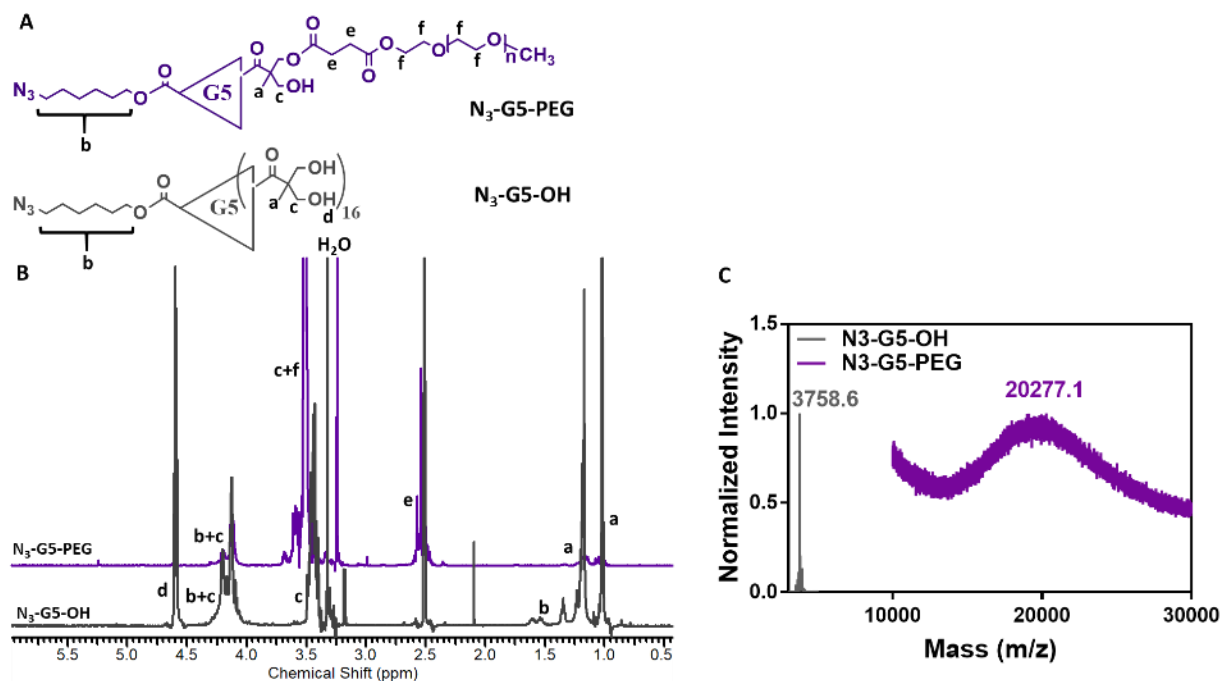
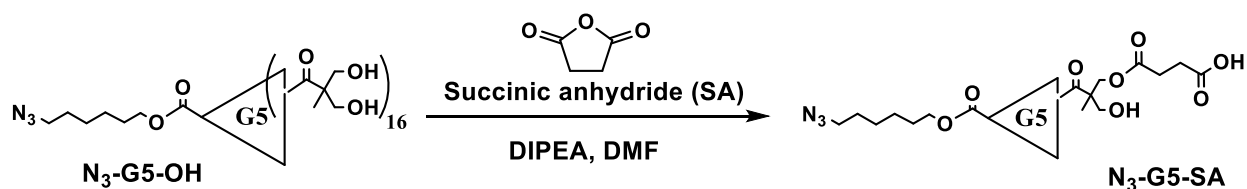


Figure 5.4. A) Chemical structure of $\text{N}_3\text{-G5-OH}$ and $\text{N}_3\text{-G5-PEG}$, and the corresponding B) ^1H NMR and C) MALDI-TOF spectra.

5.3.5 Conjugation of succinic anhydride (SA) to $\text{N}_3\text{-G5-OH}$ to form $\text{N}_3\text{-G5-SA}$

Succinic anhydride (SA) was added to the surface of $\text{N}_3\text{-G5-OH}$ dendron to form $\text{N}_3\text{-G5-SA}$ as seen in Scheme 5.5.



Scheme 5.5. The modification of $\text{N}_3\text{-G5-OH}$ to contain $-\text{COOH}$ surface by addition of SA to form $\text{N}_3\text{-G5-SA}$.

The characterization of $\text{N}_3\text{-G5-SA}$ with $^1\text{H-NMR}$ and MALDI-TOF can be found in Figure 5.5. **$\text{N}_3\text{-G5-SA}$: $^1\text{H-NMR}$ (DMSO- d_6 , 400MHz, ppm):** δ 4.19-4.12 (m, 129H), 2.52-2.41 (m, 128H), 1.59-1.33 (m, 8H), 1.20-1.14 (m, 92H). **MALDI-TOF MS:** 6960.6. **LS ζ -potential:** -30 ± 8 mV.

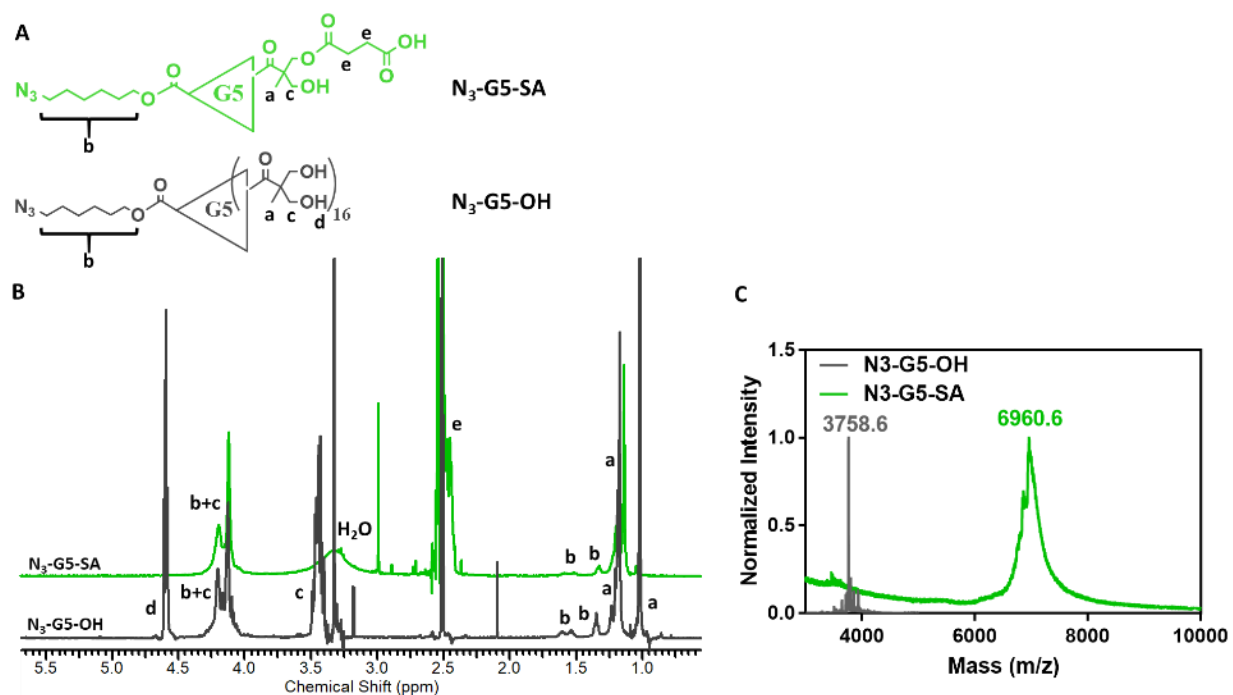
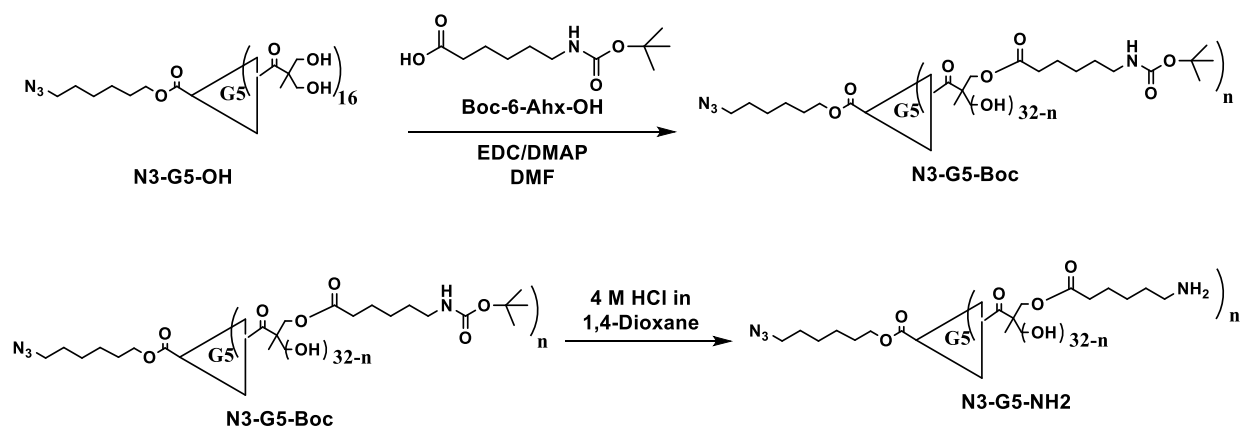


Figure 5.5. A) Chemical structure of $\text{N}_3\text{-G5-OH}$ and $\text{N}_3\text{-G5-SA}$, and the corresponding **B)** $^1\text{H-NMR}$ and **C)** MALDI-TOF spectra.

5.3.6 Conjugation of Boc-6-Ahx-OH to $\text{N}_3\text{-G5-OH}$ dendron followed by Boc deprotection to form $\text{N}_3\text{-G5-NH}_2$ dendron

Boc-6-Ahx-OH was added to the surface of N₃-G5-OH dendron to form N₃-G5-Boc followed by subsequent Boc deprotection to form N₃-G5-NH₂ as seen in Scheme 5.6.



Scheme 5.6. The modification of N₃-G5-OH to contain -NH₂ surface by addition of **A**) AHA-Boc followed by **B**) Boc deprotection to form N₃-G5-NH₂.

The characterization of N₃-G5-NH₂ with ¹H NMR and MALDI-TOF can be found in Figure 5.6. **N₃-G5-NH₂: ¹H-NMR (DMSO-*d*₆, 400MHz, ppm):** δ 4.18.-4.04 (m, 108H), 3.51-3.41 (m, 14H), 2.74-2.73 (m, 52H), 2.37-2.27 (m, 52H), 1.59-1.47 (m, 108H) 1.32-1.31 (m, 56H), 1.19-0.96 (m, 92H). **MALDI-TOF MS:** 6685.9. **LS ζ-potential:** +48 ± 7 mV.

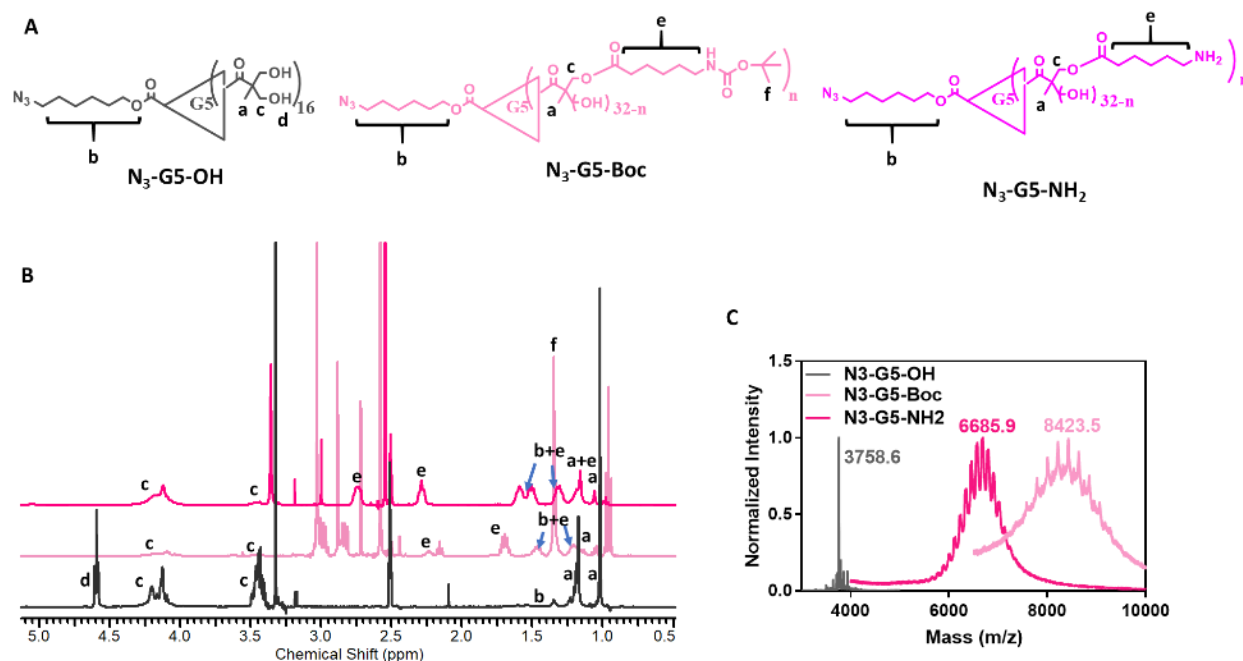


Figure 5.6. A) Chemical structure of N₃-G5-OH and N₃-G5-Boc, and N₃-G5-NH₂, and the corresponding B) ¹H NMR and C) MALDI-TOF spectra.

5.4 Discussion

Recently, the versatility and complexity of dendrimer synthesis has been explored for various biological and drug delivery applications.³⁹⁻⁴¹ Bis-MPA polyester dendrimers have emerged as an alternative improvement on other dendrimers such as PAMAM dendrimers by being biodegradable via hydrolysis (not seen with PAMAM) and more biocompatible (less toxic and less immunogenic).³⁸ Heterobifunctional (AKA bow-tie, Janus-type) asymmetric Bis-MPA polyester dendrimers have gained interest due to their multifunctionality.^{45, 167} However, the major drawback remains the complexity of synthesis in such type of systems.¹⁶⁷ In this study, we present here a facile way of modifying the surface of Azido-G5-OH polyester Bis-MPA dendrons with various surface modifications: -COOH (anionic), -NH₂ (cationic), hydrophilic (-PEG), hydrophobic (-Lauryl), and unmodified neutral (-OH).

Here, successful synthesis and characterization of the surface modifications N₃-G5-OH polyester Bis-MPA dendrons are described and characterized. A summary of overall modifications is described in Table 5.1.

Table 5.1. Characterization of modified Azido-G5-OH dendrons *MW based on MALD-TOF results.

Dendron	Group	# Modified	MW (g/mol)*	ζ potential (mV)
N₃-G5-OH	-OH (hydroxyl)	32	3742.8	+31 ± 6
N₃-G5-SA	-COOH (carboxyl)	32	6959.4	-30 ± 8
N₃-G5-NH₂	-NH ₂ (amine)	26	6685.9	+48 ± 7
N₃-G5-PEG	-PEG	15	20277.1	-13 ± 4
N₃-G5-LA	-lauryl	12	6966.6	+27 ± 6

The neutral N₃-G5-OH remained unmodified from the company it was purchased with 32 -OH surface groups available for attachment. Surface charge measured by LS was found to be positively charged, mainly due to the presence of the azido group (-N₃). Once conjugated to other dendron to form dendrimer, without presence of azido, a decrease in surface charge more towards neutral is expected, which was seen when two dendrons were conjugated to form -OH dendrimer when overall dendrimer became negatively charged (Appendix 5 -Section C5). All bonds within the polyester dendron as well as surface modifications are linked by ester groups. This maintains the biodegradability of the dendrons via hydrolysis. However, the hydrolysis of dendrons may be affected by the presence of various surface groups, as was seen in PEGylation of TMPG4OH polyester dendrimers, in which the degradation was delayed from starting after 5 hours for TMPG4OH and delayed to 5 days at physiological conditions (pH = 7.4, 37°C),¹⁶⁴ and can have large implications in terms of stability *in vivo*. However, to this date, no polyester dendrimer degradation profile has been measured *in vivo* demonstrating a need for

further investigation. Of the modifications an anionic carboxyl group (-COOH) was modified to the surface to all available 32 surface groups. The surface charge measured by LS demonstrates an overall negative charge, a reversal seen from unmodified dendron, and can represent an anionic surface modification. An amine (-NH₂) modified dendrimer was also successfully attached to the N₃-G5-OH dendron to form N₃-G5-NH₂. Of the 32 groups available, 26 groups were modified to amine. A positive surface charge was measured by LS and proved to be larger than that of unmodified N₃-G5-OH dendron, demonstrating an overall positive surface charge providing a cationic surface, which is believed to be maintained after the conjugation of dendron to form an asymmetric dendrimer. To provide hydrophilic and hydrophobic surfaces, the N₃-G5-OH dendron was modified with PEG and lauryl groups, respectively. N₃-G5-PEG had a modification of 15 of the surface groups while lauryl had a surface modification of around 12 of the surface groups. The surface charge for N₃-G5-PEG became overall negatively-charged (Table 4.1). It was expected to provide a more neutral charge to dendron as PEG has proven to do so previously.¹⁶⁴ The presence of some negative charge may be due to the fact of a small presence of PEG-SA, in which SA itself containing carboxyl group may be attributing to the negative charge measured from LS. The surface charge for the N₃-G5-LA was positively charged, however, slightly less than N₃-G5-OH dendron and not overall statistically different. Therefore, the presence of LA did not affect the overall surface charge of the dendron. Overall, the various surface modifications represent different surface properties, which has been shown to affect cellular internalization and cellular trafficking of various dendrimers before.⁴⁷

These surface modifications have implications on drug delivery by altering the cellular internalization and cellular trafficking into cells.⁴⁷ Depending on the cell type and surface modification on dendron, varied cellular internalization pathways as well as cellular trafficking can occur. This can influence efficacy of drug conjugated to polymer systems in which the type of linker containing a liable bond between drug and polymer can be effectively broken. Such linkers include peptide bonds and pH-sensitive bonds (cis-aconityl, hydrazine, acetal).¹⁸⁶ These linkers need to be internalized and trafficked to correct location in order to have optimal linker breakage and controlled release of the drug. Also, implications on cell type and route of administration can play a huge role in drug efficacy and need to be tailored for specific drug delivery applications.^{36, 47}

With the success in surface modifications on N₃-G5-OH have been established, a drug conjugation to another dendron using a linker will have to take place. In this case, the use of doxorubicin (DOX) as our model drug will be linked to the Acet-G5-OH Bis-MPA polyester dendrons using a small peptide linker between the dendron and DOX for enzymatically controlled release. A chemical scheme strategy for modifications has been proposed (Schemes C1-C4). A peptide linker Gly-Phe-Leu-Gly (GLFG) was chosen to be at cleavable linker between DOX and Acet-G5-OH. This GFLG linker strategy has been utilized for DOX conjugation to polymer previously.^{299, 300} GLFG linker is enzymatically degraded by protease cathepsin B,¹⁸⁶ which and upregulated in many cancerous tumors.³⁰¹ They are expressed constitutively, and the protein and mRNA levels has been found localized in perinuclear vesicles (lysosomes) and vesicles in the cytoplasm and cell periphery where its main function is to assist in cell degradation processes associated with tumor proliferation, invasion, and metastasis.³⁰¹ Therefore, once internalized into

cells, the bond between the DOX can be released by enzymatic degradation of GFLG peptide, allowing for controlled release of the DOX. We currently have formulated GFLG-DOX in which synthesis and characterization can be found in Appendix C – Sections C2 and C3. Modification of Acet-G5-OH dendron was also required for formation of -COOH surface functionality. This -COOH allows for amide formation between the dendron and GFLG-DOX, which has also been synthesized and characterized (Appendix C – Section C4, Scheme C3). Therefore, the conjugation between the acet-G5-GA and GFLG-DOX has been proposed (Scheme C4). The potential of this conjugation scheme has been tested on a G4 carboxyl-terminated PAMAM dendrimer with success. A matter of upscaling GFLG-DOX product remains the limiting factor.

Another question to consider is the formation of the asymmetric dendrimers from GFLG-DOX containing dendron and the dendrons modified with various surface modalities. Each dendron contains an acetylene and azide group, which can be conjugated through Azide/Alkyne cycloaddition click chemistry.¹⁶⁸ A modification of the chemistry proposed by Ackermann, et al.³⁰² was tested between Acet-G5-OH and N3-G5-OH dendrons. Due to the steric hindrance of these two molecules, modifications in the protocol were required to increase yield of dendrimer formation from dendrons and size exclusion chromatography allowed for successful purification of dendrimer formed from dendrons (Appendix C – Section C5, Scheme C5, Figure C2). This strategy can be applied to connect GFLG-DOX containing dendron and the dendrons modified with various surface modalities. The limitations may occur based on difficulty in chemistry involved in these reactions to form asymmetric dendrons, which remains the main challenge for this type of dendrimer formation for drug delivery. However, the potential

benefits may be elucidated once these asymmetric dendrimers can be tested *in vitro* and *in vivo*.

5.5 Conclusions

The potential benefits from formation of asymmetric dendrimers for drug delivery needs to be further explored, especially in terms of cellular internalization and cellular trafficking, pharmacokinetics and pharmacodynamics of such systems and how it can influence drug efficacy. The largest challenge in formation of asymmetric dendrimers is the synthesis of such complex polymers.⁴⁵ Here, we proven a facile way to modify the surface of N3-G5-OH Bis-MPA polyester dendrons with varying surface groups with different surface characteristics. The addition of DOX conjugated through GFLG linker to acet-G5-OH dendron has been proposed and use of click chemistry and size exclusion chromatography to form asymmetric dendrimers has been tested. The potential in such asymmetric dendrimers remains to be elucidated in order to optimize drug efficacy.

5.6 Acknowledgements

The authors would like to give thanks for the financial support given NSF-DMR Grant: # 1508363. The authors would also like to thank Dr. Matthew Hartmann in Chemistry Department at Virginia Commonwealth University for the use of the MALDI-TOF instrument, the Nuclear Magnetic Resonance Center in the Department of Chemistry at Virginia Commonwealth University for use of NMR spectrometer, the Department of Medicinal Chemistry at Virginia Commonwealth University for the use of the NMR spectrometer and Liberty Blue Automated Microwave Peptide Synthesizer.

CHAPTER 6 – LOCALLY ADMINISTERED IMMUNOMODULATORS FOR MACROPHAGE REPOLARIZATION AND COMBINATION CHEMOTHERAPY FOR THE TREATMENT OF LUNG CANCERS

6.1 Introduction

Tumor associated macrophages (TAMs) are the most abundant cell-type besides cancerous cells found within the tumor microenvironment (TME), and are known to influence tumor initiation, growth, and metastasis.^{80, 81} TAMs are derived from circulating monocytes and preclinical studies have demonstrated enhanced therapeutic performance when TAMs entry to TME is blocked or when TAM phenotype is manipulated.⁸¹ TAM phenotypes are seen as a continuous spectrum, however, can be classified into two opposing types: M1 and M2. M1 TAMs are known as classically activated macrophages and are known to be antitumor, proinflammatory, and immunostimulatory.⁸¹ M2 TAMs are known to be protumor, anti-inflammatory, immunosuppressive, and proangiogenic.^{80, 81} The presence of M2 TAMs are found in early stages of tumors as well as the metastatic stages, and especially in cases when tumors have been treated with chemotherapeutics.^{20, 81} Many preclinical and clinical studies have demonstrated that TAM density, and more specifically small M1/M2 ratios (high density of M2), is correlated with poor prognosis, which has lead TAMs to be an attractive therapeutic target in many cancer types.^{81, 222} Resistance to therapy can be correlated with M2 TAM presence, and is known to inhibit tumor response mediated by T cells, promotes tumor proliferation, progression, invasion, metastasis, and angiogenesis.^{20, 80}

Macrophage polarization is critically controlled by the colony-stimulating factor 1/ colony-stimulating factor 1 receptor (CSF1R/CSF1R) signaling process.^{20, 80}

CSF1/CSF1R signaling promotes proliferation and recruitment to tumors of myeloid cells and differentiation of these myeloid cells into M2 TAMs.⁸² The CSF1R+ macrophages have been correlated with poor survival in several tumor types.²⁰ The inhibition of CSF1R by has been recently tested preclinically and clinically demonstrating selective reduction of M2 TAMs or polarization of M2 TAMs to M1 phenotype.^{80, 222} An increase in M1/M2 ratio by increasing M1 phenotype and/or decreasing M2 phenotype has shown improved efficacy in cancer treatment, alone or in combination with other therapies, extending survival in many types of cancer.²²²

There are a range of antibodies and small molecules known to target and inhibit CSF1R. These include monoclonal antibodies (RG7155, IMC-CS4) that inhibit the extracellular domain and small molecule inhibitors (CY11645, GB2580, BLX945, PLX5622, PLX3397) that inhibit the intracellular kinase domains of CSF1R.²²² Despite the success of antibody treatments, they remain highly costly, which limit potential benefit and usage.³⁰³ Therefore, the use of small molecules has become an attractive choice for CSF1Ri. Of these, the one currently commercially available and is currently undergoing numerous clinical trials is PLX3397.²⁰

PLX3397 (PLX) is an example of a small molecule inhibitor of CSF1R (CSF1Ri). PLX is a tyrosine kinase inhibitor, when given orally, and demonstrated increased efficacy in treatment preclinically^{82, 225} and is currently undergoing clinical trials.^{20, 80} PLX prevents intracellular phosphorylation of CSF1R on kinase domains, thus inhibiting CSF1R activation.^{222, 225} The inhibition of CSF1R thus repolarize M2 TAMs to M1 and/or selectively reduce M2 TAMs, thus increasing overall M1/M2 ratio.⁸³ PLX has been used a monotherapy as well as in combination with chemotherapeutics, irradiation, anti-

angiogenic therapies, and other immunotherapies for treatment of variety of tumors including breast and lung tumors.^{20, 82} The prevalence of PLX in clinical trials as a monotherapy and in combination with other treatments demonstrates its potential as a immunomodulator influencing TAMs within the TME.

Of these, the combination of PLX with doxorubicin (DOX) remains of interest. DOX is a common chemotherapeutic that is administered patients who have metastatic form of breast cancer and delivered intravenously (IV).⁷¹ However, DOX has limitations in terms of clinical benefit including limited aqueous solubility, rapid elimination from blood circulation, and severe cardiomyopathy.³⁰⁴⁻³⁰⁶ Despite these issues with DOX, conjugation to polymeric nanocarriers such as polyamidoamine dendrimers (PAMAM) can overcome some of these limitations by enhancing drug solubility, enhance pharmacokinetics and pharmacodynamics, and reduce unwanted side effects.^{34, 36} Recently, our group has investigated the potential of conjugation of DOX to PAMAM dendrimer (DDOX) and its pulmonary delivery, demonstrating controlled drug release, increased efficacy to treat secondary lung tumors from B16F10 murine metastatic melanoma, increased drug dose to target site, and reduced cardiotoxicity.⁷⁷ Therefore, the testing of DDOX and PLX in combination was by pulmonary administration (PA) may provide a synergetic effect and increase overall treatment efficacy.

Consequently, the efficacy of PLX alone or in combination remains to be explored. The combination of PLX with DOX and DDOX has not been tested for synergistic interactions. The use of PLX given via other routes besides oral has also not been evaluated. Therefore, this study was conducted to investigate the potential synergistic effect of PLX with DOX/DDOX for treatment of lung tumors metastasized from metastatic

breast cancer to the lungs (secondary lung tumors) upon pulmonary administration. Efficacy of PLX alone or in combination when administered intravenously (IV) was also evaluated as control. The treatments (PLX, DOX, and DDOX) were tested *in vivo* on 4T1-induced lung metastases established in female BALB/C mice. This, thus represents an immune competent syngeneic model. Preliminary results investigating the effectiveness of treatment strategies was evaluated and, and modulation of macrophages from M2 to M1 phenotypes are reported here. These studies are ongoing in our laboratories to fully assess the potential of TAM reprogramming agents and combination with chemotherapy (immunochemotherapies) in combination with pulmonary administration as well as with the use of nanotechnologies to enhance the performance of these therapies.

6.2 Materials and Methods

6.2.1 Materials

Penicillin/Streptomycin Solution was purchased from Gemini Bio-Products (West Sacramento, CA, USA). Puromycin Dihydrochloride, Powder (Corning®), Dulbecco's Modification of Eagle's Medium (DMEM), Corning®, 4.5 g/L glucose, L-glutamine [-] sodium pyruvate, N-methylmorpholine (NMM), isobutyl chloroformate (IBCF), anhydrous dimethyl sulfoxide (DMSO), dimethylformamide (DMF), and methanol (MeOH) were purchased from VWR International (Radnor, PA, USA). Fetal Bovine Serum (FBS), USA Origin, was purchased from Serum Source International (Charlotte, NC, USA). Generation four, succinamic acid, poly(amidoamine) (PAMAM) dendrimer (G4-SA) provided in water was purchased from Dendritech Inc. (Midland, MI). D-luciferin Potassium Salt was purchased from Syd Labs. (Natick, MA, USA). Doxorubicin hydrochloride salt (DOX•HCl) was purchased from LC Laboratories (Woburn, MA, USA).

Pexidartinib (PLX3397, PLX) was purchased from Chemgood (Glen Allen, VA, USA). Tert-Butyl carbamate (TBC), trifluoroacetic acid (TFA), triethylamine (TEA), 2,5-dihydroxybenzoic acid (DHB), and Tween #80 was purchased from Sigma Aldrich (St Louis, MO, USA). Dimethyl Sulfoxide-D6 (with TMS - 0.03 vol%) and magnesium sulfate anhydrous were purchased from EMD Millipore (Burlington, MA, USA). Spectra/Por® 7 RC membrane dialysis tubing (MWCO = 3 kDa) was purchased from Spectrum Laboratories, Inc. (Rancho Dominguez, CA, USA). Amicon Ultra-15 centrifugal filter (NMWL = 3,000) was purchased from MilliporeSigma (Burlington, MA, USA). Thin layer chromatography (TLC) silica gel 60 F254 purchased from Merck KGaA (Darmstadt, Germany).

6.2.2 Synthesis and Characterization of G4SA-hyd-DOX (DDOX)

The synthesis and characterization of doxorubicin conjugated to G4SA PAMAM dendrimer (1 mol eqv) to form was described in detail, previously.⁷⁷ Briefly, G4SA (3.80 μ mol) was mixed with NMM (1.07 mmol) and IBCF (1.02 mmol) in a mixture of DMSO/DMF (10/90, v/v) at 0°C for 5 min before the addition of TBC (0.243 mmol), in which the reaction was kept at 0°C for an additional 30 min followed by continuation of the reaction at room temperature for 48 h. The DMSO/DMF solvent mixture was removed under high pressure and product was redissolved in 0.1 M Phosphate buffer (pH = 10.00) followed by deionized (DI) water and purified using Amicon Ultra-15 centrifugal filter to form G4SA-TBC. The G4SA-TBC product was frozen and lyophilized. The removal of Boc groups from TBC occurred by addition of G4SA-TBC in TFA/DCM (80/20, v/v) stirred at 0°C for 30 min. The solvents were again removed, and product was purified by redissolving it in 0.1 M Phosphate buffer (pH = 10.00) followed by DI water and purified

using Amicon Ultra-15 centrifugal filter. The water was removed by freezing and lyophilizing the product – G4SA-hyd. The addition of DOX (34.48 μmol) was done by dissolving G4SA-hyd (1.05 μmol) in with DOX in methanol and using TFA (16 mol eqv) as acid catalyst. The reaction was allowed to occur for 24 hours followed by removal of methanol solvent, redissolved in water, and purified by Amicon Ultra-15 centrifugal filter. The final G4SA-hyd-DOX (DDOX) product was frozen and lyophilized to obtain sticky red product. The product was fully characterized by MALDI-TOF (Voyager-DE PRO, JBI Scientific) and ^1H NMR (Bruker NanoBay Avance III 400 MHz NMR spectrometer).

6.2.3 Cell Culture

Mouse stage IV breast cancer cell line (4T1) was kindly gifted by Dr. Arun Rishi from Oncology Department in School of Medicine at Wayne State University. 4T1 cells were grown on 75 cm^2 cell culture flasks (Corning[®]) in DMEM medium supplemented with 10% FBS and 1% antibiotics (AB) (100 U/mL Penicillin and 100 $\mu\text{g}/\text{mL}$ Streptomycin) and cultured at 37°C with 5% CO_2 . 4T1-luc-tdTomato cells were also grown on 75 cm^2 cell culture flasks (Corning[®]) in DMEM + 10% FBS + 4 $\mu\text{g}/\text{ml}$ puromycin and cultured at 37°C with 5% CO_2 .

6.2.4 Animals for *In Vivo* Experiments

Female BALB/C mice (8-10 weeks, 16-20 g) mice were purchased by Jackson Laboratory (Bar Harbor, ME, USA). Male and Female BALB/C mice (3-4 weeks) were also purchased from Jackson Laboratory and bred at Massey Cancer Center at Virginia Commonwealth University. Purchased or bred female BALB/C mice (8-10 weeks) were used for further study. The mice were housed in 12 h light/dark cycles with food and water provided *ad libitum* and acclimatized a minimum of one week prior to any experiment

performed. All animal experiments were performed in accordance with guidelines established by Institutional Animal Care and Use Committee at Virginia Commonwealth University.

6.2.5 Transformation of 4T1 Cells to Express tdTomato Fluorescence and Luciferase Bioluminescence.

To determine the minimum concentration required to kill all 4T1 cells, a Puromycin cell kill curve was performed following the protocol by Dharmacon™ and measured by MTT assay (Molecular Probes). Briefly, 10,000 cells/well of 4T1 cells were seeded into a 96-well plate (CoStar®, Corning Inc.) and left overnight. The following day, increasing puromycin concentrations (0-10 µg/ml) were in DMEM + 10% FBS were exposed to the cells for 48 h. After 48 h, medium was removed and 110 µl of 1 mM MTT solution was added to each well and incubated for 4 h at 37°C, 5% CO₂. 75 µl was removed and 60 µl of DMSO was added to each well and incubated at same conditions above for an additional 10 minutes. Subsequently, the absorbance was measured at 540 nm using Synergy H1 microplate reader (BioTek). Cell viability at each concentration was calculated as follows: % Cell viability = (absorbance of treated cells/absorbance of control cells) x 100%.

4T1 cells were genetically modified to express firefly luciferase and tdTomato (bright red fluorescent protein) according to modified protocols from GenTarget³⁰⁷ and protocol provided by Dr. Yemelyanov and Dr. Bhalla from Northwestern University. Briefly, 25,000 4T1 cells (P14-P15 passages) were seeded in each well a 24-well microplate cultured with 500 µL of DMEM+10%FBS+1% AB at 37°C and 5% CO₂. The following day, 0.833 µl lentivirus containing luciferase and tdTomato expression (10¹⁰

TU/ml) (pFULT Ubi>Luciferase-2TA-dtTomato, Skin Disease Research Center, Northwestern University) was mixed with polybrene (8 µg/ml final concentration) in DMEM and mixed at room temperature for 5 min to form viral transduction mixture. 500 µl of viral transduction mixture was added to each well after each well was washed one with 1xPBS. The plate was then incubated at 37°C and 5% CO₂ gently rocking overnight. The following day, the medium containing the virus was replaced with fresh DMEM +10% FBS+ 1%AB for 2.5 h. A new batch of transduction mixture was made and added for an additional 8 hours and allowed to incubate at 37°C and 5% CO₂ while gently rocking. The medium was then removed and replaced with fresh DMEM+10% FBS+ 1% AB allowed to incubate for an additional 72 hours. After the 72 hours, the cells were removed from the 24-well microplate and transferred to a T-25 flask with the addition of puromycin-selective medium (DMEM + 10% FBS + 4 µg/ml puromycin) to select for only cells that express the lentivirus. The cells grew under these conditions until they reached confluency. The modified cells were then sorted twice using tdTomato fluorescence expression by fluorescence-activating cell sorting (FACS, SC Aria- BD FACSAria™ II High-Speed Cell Sorter, Flow Cytometry Shared Resource Core, Virginia Commonwealth University). After sorting 4T1-luc-tdTomato cells were cultured in DMEM+10%FBS+1%AB+4 µg/ml puromycin. Cells were monitored with flow cytometry before *in vivo* experiments were performed (CytoFLEX Flow Cytometer, Beckman Coulter).

6.2.6 *In Vitro* Bioluminescence Kinetics Assay of 4T1-luc-tdTomato cells

To assess the bioluminescence of transfected 4T1-luc-tdTomato cells, kinetics of bioluminescent property was performed in IVIS imaging. 4T1-luc-tdTomato cells were seeded in a 96-well microplate at 12,500, 25,000, 50,000 and 100,000 cells per well or at

15,625, 31,250, 62,500, 125,000 and 250,000 cells per well in DMEM medium. A final concentration of 150 µg/ml of luciferin was added to each well and images were taken at 0.5, 3, 5, 10, and 20 min using the IVIS imaging system (Xenogen IVIS Spectrum Preclinical In Vivo Imaging System, Cancer Mouse Models Developing Shared Resource Core, Virginia Commonwealth University). The *in vitro* kinetics of the bioluminescent signal was determined by plotting total flux vs time for each cell concentration.

6.2.7 Evaluation of 4T1-luc-tdTom Metastatic Growth to the Lungs in Female BALB/C mice

The first study comprised of 100 µl of 1xPBS containing 100,000 4T1-luc-tdTomato cells were injected IV into the tail vein of female BALB/C mice (10 weeks of age). The tumor growth was monitored *in vivo* and *ex vivo* by measurement of bioluminescent signal produced by 4T1-luc-tdTomato cells using IVIS imaging system (Xenogen IVIS Spectrum Preclinical In Vivo Imaging System, Cancer Mouse Models Developing Shared Resource Core, Virginia Commonwealth University). Imaging was performed on days 5, 8, 11, 14, and 18 post IV tail vein injection. All animals were sacrificed on Day 18 where *ex vivo* imaging was conducted with the lung tissue. In the second study, 100 µl of 1xPBS containing 250,000 4T1-luc-tdTomato cells were injected IV into the tail vein of five female BALB/C mice (10 weeks old). The tumor growth was monitored *in vivo* and *ex vivo* by measurement of bioluminescent signal produced by 4T1-luc-tdTomato cells using IVIS imaging system. Imaging was performed on days 5, 7, 9, and 12 days post IV injection. One animal was sacrificed on each day where *ex vivo* imaging was conducted with the lung tissue. For the *in vivo* imaging, D-luciferin (150mg/kg) substrate was added to each animal via subcutaneous injection and exposed to isoflurane for 10 min prior to being

imaged in the IVIS imaging system. For *ex vivo* imaging, each lung was soaked in 5-10 mL 1XPBS containing 300µg/ml of luciferin prior to imaging. StudyLog Desktop was used to record and monitor animal health during the experiments. Living Image® 4.5.5 Software (Perkin Elmer) was used to analyze images. Only analysis of upper portion of mouse was analyzed for *in vivo* images, since establishment of lung tumors was the main interest of this study.

6.2.8 *In vivo* efficacy of PLX3397 for the treatment of Lung Metastases

Female BALB/C mice (8-10 weeks) were injected with 250,000 4T1-luc-tdTomato cells in 100 µl of 1x PBS to establish lung metastasis. IVIS imaging (Xenogen IVIS Spectrum Preclinical In Vivo Imaging System, Cancer Mouse Models Developing Shared Resource Core, Virginia Commonwealth University) was performed starting at 5 days post tumor inoculation and continued every other day till day of sacrifice to monitor tumor growth *in vivo*. Prior to treatment, mice were randomized into treatment groups. Treatments of (I) vehicle (1xPBS containing 5% Tween and 1% DMSO, v/v); (ii) 1 mg/kg of PLX3397 (PLX), (III) free doxorubicin (DOX), or (IV) PAMAM G4SA-hydDOX conjugate (DDOX) in vehicle or a combination of (V) 1 mg/kg of DOX and 1 mg/kg of PLX or (VI) 1 mg/kg of DDOX and 1 mg/kg of PLX was given either intravenously through retroorbital injection (90-140 µl) or through pulmonary administration (PA) by intratracheal intubation (20-30 µl). DDOX synthesis in characterization has been previously described.¹²⁷ Mice were anesthetized by isoflurane exposure for 5-10 min before either administration was conducted. Briefly, for intratracheal intubation, anesthetized mice were laid on their back and hung by their incisors with thread on a SurgiSuite Surgical Platform (Mouse Endotracheal Intubation Kit, Kent Scientific, Torrington, CT, USA). The angle of the

mouse throat to the board was placed at 45°. A soft 20 G catheter was inserted into the mouse trachea guided by Trans-Tracheal illuminator containing fiber optic cable lighted by LED light. Once catheter was inserted into the trachea, the drug solution in vehicle was added to catheter, and the mice inhaled the solution into the lungs. Mice were kept under anesthesia during the process. All mice were returned to the cage and monitored after treatment to ensure no adverse effects from treatment. Treatments was given once on days 7, 9, 11 post tumor inoculation for a total of three treatments. The drugs used in combination were formulated in one solution and administered together. Mice were monitored daily for behavior, food intake, grooming, and body weight. Mice were euthanized on day 15 post tumor inoculation. On day the mice were euthanized, *in vivo* IVIS imaging was performed followed by *ex vivo* IVIS imaging of lungs – in same procedure as discussed in section 7.2.6 – and lungs weighed to assess overall lung tumor burden.

6.2.9 Measurement of Macrophage Polarization by Flow Cytometry

Flow cytometry was utilized to assess the macrophage populations and TAM phenotypes (M1/M2) in the lungs. Mouse lungs taken on Day 15 post tumor inoculation were diluted in 0.5 ml of Liberase TL Roche (Sigma)/RPMI medium solution and cut into pieces in a 15 mL falcon tube. The lungs were then incubated at 37°C for 25 min shaking. 10 ml of Wash Buffer (RPMI medium + 10% FBS) was added to each tube and samples were then filtered using 100 µm filter followed by centrifugation at 350 x g for 5 minutes. Sample of extracted cells were then resuspended in 1-2 ml of Wash buffer where cell suspension was adjusted to concentration of 1-5 x 10⁶ cells/ml. The cells are then centrifuged at 350xg for 3 min and resuspended in 40 µl of FcBlock (2.4G2 sup) with 40

μl of 2x antibody dilution and stain is added and incubated on ice for 20 min. 200 μl of FACS buffer (1L PBS+ 5g BSA+1ml 0.5M EDTA) was added and centrifuged again at 350 x g for 3 min, then resuspend the cells in 80-200 μl of FACS buffer and run in samples through flow cytometer (The BD LSRFortessa-X20™). The antibody stains included CD11b (clone M1/70, eBioscience™), F4/80 (clone BM8, BioLegend®), MHC II (clone M5/114.15.2, TONBO Biosciences), and CD206 (clone MR5D3, AbD Serotec).

6.2.10 Statistical Analysis.

All data is presented as a mean \pm standard deviation. One-way or Two-way analysis of variance (ANOVA) followed by Tukey's Multiple Comparison Test was performed utilizing GraphPad Prism 7.00 software. Means were considered statistically significant if $p < 0.05$.

6.3 Results

6.3.1 Synthesis and Characterization of G4SA-hyd-DOX (DDOX)

The formation of DOX conjugated by carboxyl-terminated PAMAM dendrimer by linkage through a hydrazine linker to form G4SA-hyd-DOX (DDOX) was fully described in detail, previously.⁷⁷ The synthetic scheme, ¹H NMR, and MALDI-TOF characterization can be found in Appendix D – Scheme D1, Figure D1. Each NMR and MALDI-TOF for each step in the synthesis is summarized here.

G4SA-TBC: ¹H NMR (DMSO-*d*₆, 400MHz, ppm): δ 9.52 (s, 32.30H, -NHBoc in TBC), 8.67 (s, 29.58H, -NHCO- in TBC), 7.89-7.70 (m, 156.84H, -NHCO- in G4COOH), 3.06 (m, 372.38H, -CONHCH₂- (H_e) in G4COOH), 2.63-2.56 (m, 328.45H, -NCH₂- (H_d) and -COCH₂CH₂CO (H_{j3}) in G4COOH), 2.41 (m, 126.38H, -CH₂N- (H_{b,c}) in G4COOH), 2.29 (m, 150.53H, -CH₂CH₂CONHNH- (succinic methylene, H_{j2}) in G4COOH), 2.18 (m,

248.00H, $-\text{CH}_2\text{CO}-$ (H_a) in G4COOH), 1.36 (m, 305.54H, $-(\text{CH}_3)_3$ in TBC). **MALDI-TOF** m/z (Da): 20531.79.

G4SA-hyd: $^1\text{HNMR}$ (DMSO- d_6 , 400MHz, ppm): δ 9.02 (s, 19.06H, $\text{NH}_2\text{NHCO}-$ in hydrazide), 8.03 (m, 175.56H, $-\text{NHCO}-$ in G4COOH), 3.05 (m, 258.24H, $-\text{CONHCH}_2-$ (H_e) in G4COOH), 2.620 (m, 188.96H, $-\text{NCH}_2-$ (H_d) and $-\text{COCH}_2\text{CH}_2\text{CO}-$ (H_{jr3}) in G4COOH), 2.41 (m, 87.18H, $\text{CH}_2\text{N}-$ ($\text{H}_{b,c}$) in G4COOH), 2.23 (m, 151.22H, $-\text{CH}_2\text{CONHNNH}_2$ (succinic methylene (H_{jr2}) in G4COOH), 2.18 (m, 248.00H, $-\text{CH}_2\text{CO}-$ (H_a) in G4COOH). **MALDI-TOF** m/z (Da): 17780.33.

G4SA-hyd-DOX (DDOX): $^1\text{HNMR}$ (DMSO- d_6 , 400MHz, ppm): δ 9.02 (s, 20.41H, $\text{NH}_2\text{NHCO}-$ in hydrazide), 8.05 (m, 167.13H, $-\text{NHCO}-$ and Ar-H in G4COOH and DOX), 5.26 (s, 11.99H, $-\text{CH}-$ in DOX), 4.89 (d, 12.72H, $-\text{CH}-$ in DOX), 4.570 (m, 24.72H, $-\text{CH}_2\text{OH}$ in DOX), 4.17 (s, 11.02H, $-\text{CH}-$ in DOX), 3.94 (s, 35.23H, $-\text{OCH}_3$ in DOX), 3.05 (m, 255.54H, $-\text{CONHCH}_2-$ (H_e) in G4COOH), 2.620 (m, 217.26H, $-\text{NCH}_2-$ (H_d) and $-\text{COCH}_2\text{CH}_2\text{CO}-$ (H_{jr3}) in G4COOH), 2.41 (m, 109.82H, $\text{CH}_2\text{N}-$ ($\text{H}_{b,c}$) in G4COOH), 2.29 (m, 152.93H, $-\text{CH}_2\text{CONHNNH}_2$ (succinic methylene ($\text{H}_{jr1, jr2}$) in G4COOH), 2.18 (m, 248.00H, $-\text{CH}_2\text{CO}-$ (H_a) in G4COOH), 1.86 and 1.65 (d, 23.96H, $-\text{CH}_2-$ in DOX), 1.12 (s, 36.10H, $-\text{CH}_3$ in DOX). **MALDI-TOF** m/z (Da): 23860.59. The resulting DOX loading in the DDOX was as 22% w/w, conjugation of on average 11 DOX per dendrimer.

6.3.2 Transformation of 4T1 Cells to Express tdTomato Fluorescence and Luciferase Bioluminescence

4T1 murine mammary carcinoma cells (animal model for stage IV human breast cancer) were transformed to contain tdTomato fluorescence to track cells via flow cytometry and luciferase bioluminescence to track tumor cells *in vivo* using a lentivirus

that contained puromycin resistance. Firstly, a puromycin kill curve (Figure D2) was conducted to find the minimum concentration to kill all 4T1 cells that would not contain puromycin resistance (4T1-WT). It was found that a minimum of 4 µg/ml was required to kill all 4T1-WT cells (Figure D2). This allows for selection of cells only containing lentivirus to be cultured and maintained over various subcultures of transformed cell line. The 4T1-WT cell line was then transformed with lentivirus and sorted by cell sorting using tdTomato fluorescent expression as successful integration of lentivirus into cells. The cells were therefore, renamed as follows: 4T1-luc-tdTomato. Successful selection and high expression of lentivirus in cells was checked and maintained using tdTomato expression measured by flow cytometry (Figure 6.1). Figure 6.1 demonstrates the difference in fluorescent expression of 4T1-WT and 4T1-luc-tdTomato using A) dot plots and B) histogram plots to demonstrate a good expression and good separation of the two populations of cells. This allows for distinction of cell expressing fluorescence from those that are not expressing the tdTomato fluorescence, demonstrating the 4T1-luc-tdTomato cell having 99% expression of tdTomato fluorescence. The tdTomato expression was checked and maintained throughout experiment and checked using flow cytometry with 4T1-luc-tdTomato cells maintaining tdTomato expression at 97% or above.

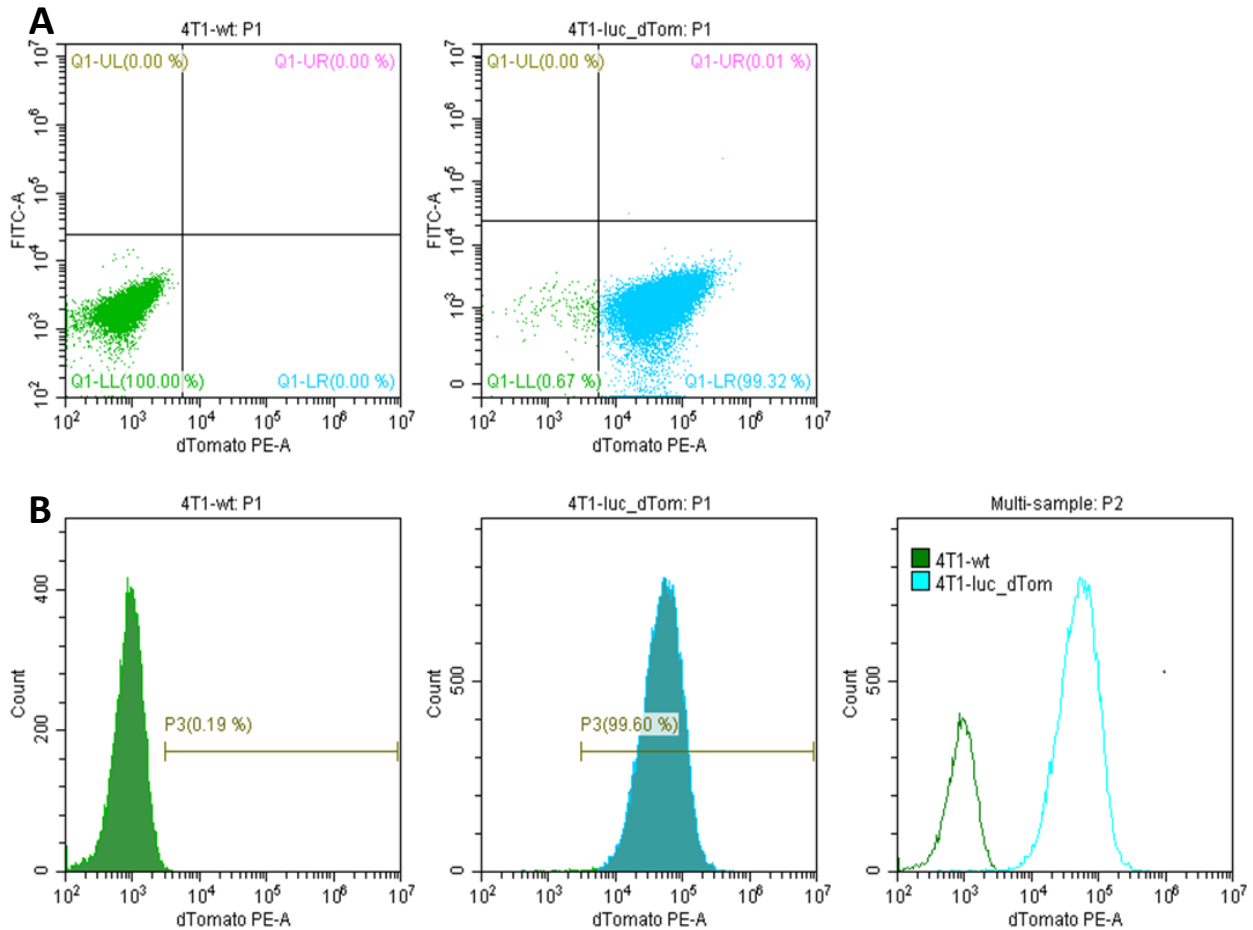
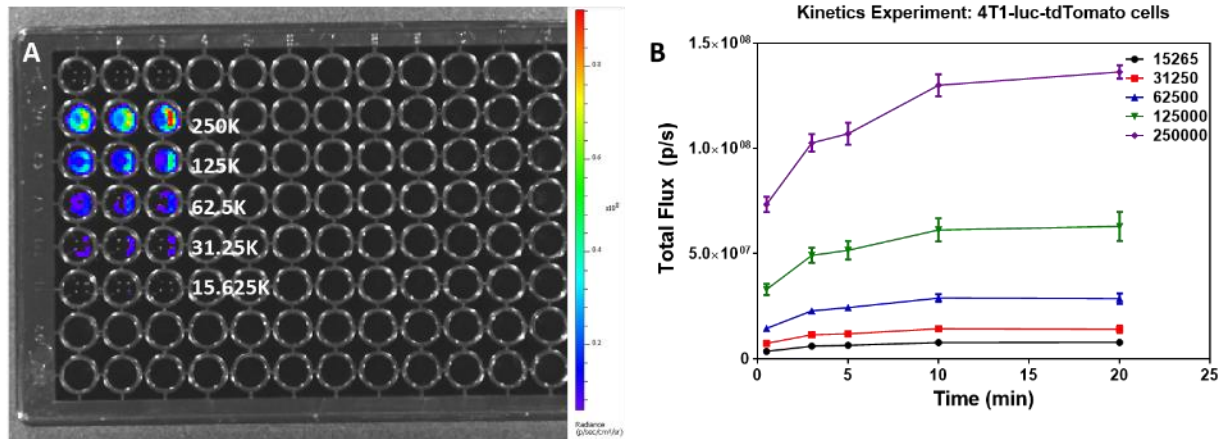


Figure 6.1. Flow cytometry results of 4T1-luc-tdTomato cells after puromycin selection and sorting twice from cell sorter. **A)** Dot plots and **B)** histogram plots of wild-type 4T1 (green) and 4T1-luc-tdTomato cells (blue) distinguish a distinct cell population based on tdTomato fluorescence.

6.3.3 *In Vitro* Bioluminescence Kinetics Assay of 4T1-luc-tdTomato cells

The bioluminescence from firefly luciferase was also demonstrated *in vitro* by running cells through *in vitro* bioluminescence kinetics assay. Results from 4T1-luc-tdTomato cells seeded at densities 250k, 125k, 62.5k, 31.25k and 15.265k were evaluated over time for bioluminescent expression after addition of d-luciferin to cells (Figure 6.2). Figure 6.2A is a representative IVIS image of total flux signal given from the

cells, and the kinetics (Figure 6.2B) at different cell densities was plotted.



The presence of signal indicated bioluminescent and presence of firefly luciferase was incorporated into the 4T1-luc-tdTomato cells. Also, the kinetics reveals that the bioluminescent signal at every cell density increases till around 10 min, in which it plateaus till 20 min. After 20 min, the bioluminescent signal begins to decline at every cell density tested. A 250k cell density was chosen to match the maximum number of cells used for tail vein (TV) injection into BALB/C mice. The results also provide for a time window in which *in vivo* bioluminescence needs to be performed to evaluate tumor burden at peak bioluminescence levels.

6.3.4 Evaluation of 4T1-luc-tdTom Metastatic Growth to the Lungs in Female BALB/C mice

An evaluation of tumor growth rate of lung metastases established by tail vein (TV) injection of 4T1-luc-tdTomato cells was performed. Initially, 100k cells were injected in TV of female BALB/C mice. *In vivo* IVIS images of the dorsal and ventral side of mice from

Day 5 to Day 18 after TV injection were imaged and the total (sum) flux was evaluated (Figure 6.3). The total flux between days was evaluated (comparison between total flux on Day 5 vs 8, Day 8 vs, Day 11, Day 11 vs Day 14, and Day 14 vs Day 18) to determine between which days the largest increase tumor growth was seen. The largest increase in total flux was seen between Day 8 and 11 for all mice, with an average increase in flux by 11 ± 6 times in the total flux seen on Day 11 as compared to Day 8 for the three mice evaluated. Other days saw a total increase in total flux signal by 5.0 ± 1.2 times from Day 5 to Day 8, 7 ± 3 times from Day 11 to Day 14, and 4 ± 2 times from Day 14 to Day 18.

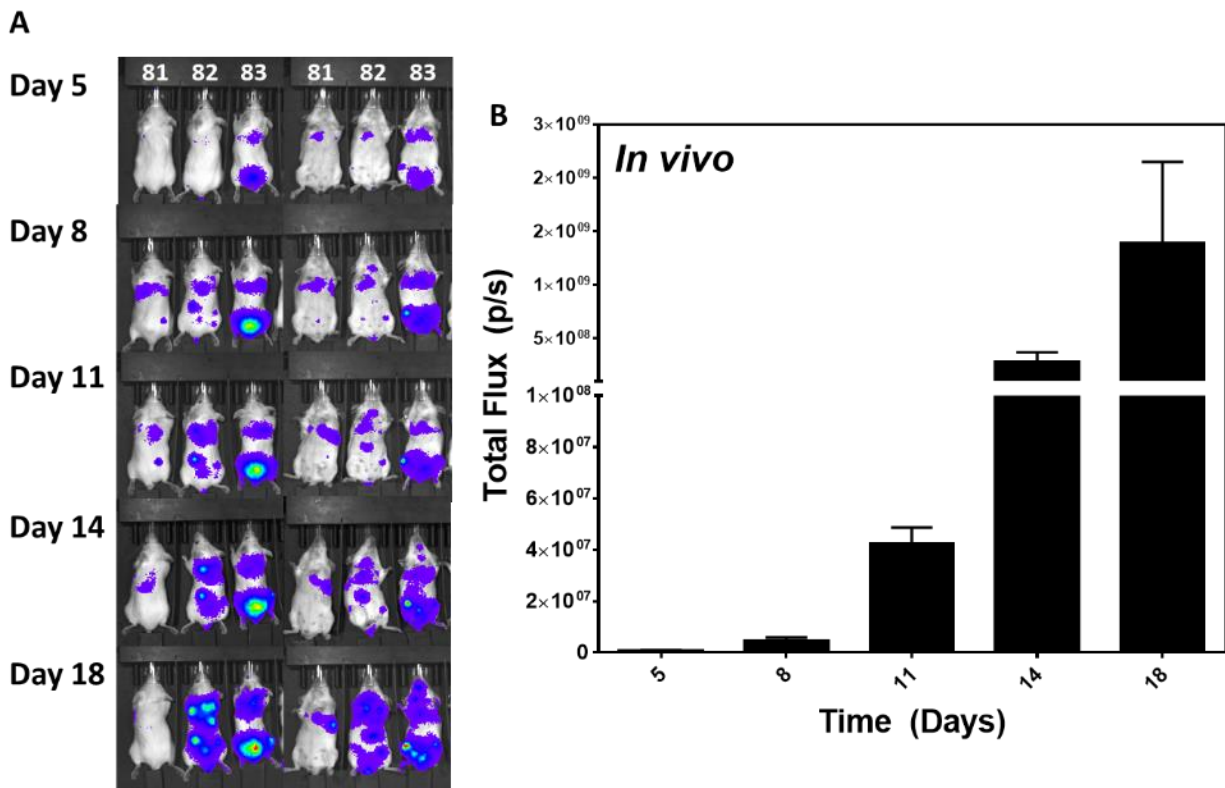


Figure 6.3. Preliminary tumor growth experiment. **A)** IVIS images of mice from day 5 go day 18 after TV injection of 100k 4T1-luc-tdTomato cells. **B)** Measurement of total flux from IVIS images by combined signal from the dorsal and ventral side of each mouse focused in the lung region area.

To evaluate the establishment of lung metastases more directly, a second group of female BALB/C mice were injected via TV with 250k 4T1-luc-tdTomato cells, in which a mouse was sacrificed on different days and lungs were imaged directly with IVIS. The results of *in vivo* IVIS imaging and IVIS imaging of the lungs was compared and evaluated over 12 days post TV injection (Figure 6.4). Based on these results, the total flux over various days demonstrated the same trend for *in vivo* IVIS images and *ex vivo* lung IVIS images. Both demonstrated the highest total flux increase between day 9 and day 12 post TV injection of cells (Figure 6.4) with an increase in 5.5 times the signal of total flux for *in vivo* images and 9.3 times for *ex vivo* lungs from total flux measured on Day 12 compared to that of Day 9.

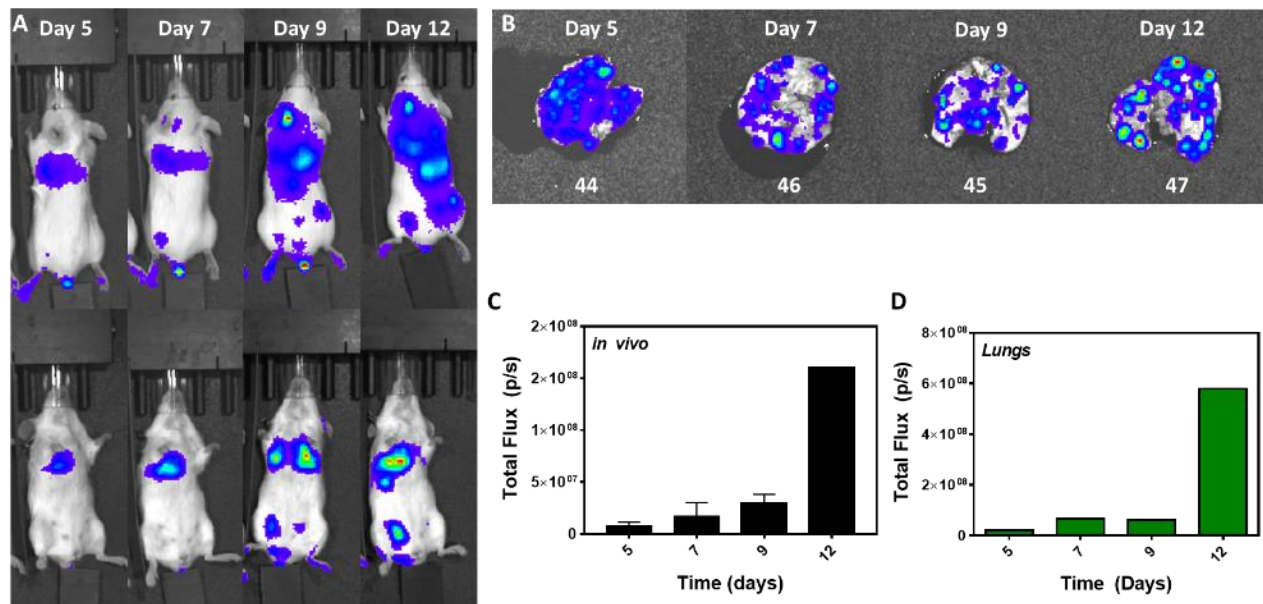


Figure 6.4. Preliminary tumor growth experiment from TV injection of 250k 4T1-luc-tdTomato cells. **A)** *in vivo* IVIS images of dorsal and ventral side of mouse over 12 days post TV injection of tumor cells. **B)** IVIS images of lungs taken on specific days after TV injection. The number below lung refers to mouse number. **C)** Total flux (flux of ventral and dorsal images combined focused on lung region) from *in vivo* IVIS images of mice over various days post TV injection. **D)** Total flux taken from lungs on each day.

6.3.5 *In vivo* efficacy of PLX3397 (PLX) for the treatment of Lung Metastases

The efficacy of treatment of breast cancer lung metastases established by 4T1-luc-dtTomato cells was evaluated for DOX, PLX, DDOX and combination treatments. The first experimental set was used to compare vehicle (as negative control) with pulmonary administration (PA) of DOX, PLX and the combination of DOX with PLX at a dose of 1 mg/kg with combination at a dose of 1 mg/kg for each drug. A second experimental set evaluated the PA of DDOX, DDOX+PLX, and IV administration of PLX alone. The overall treatment strategy can be seen on Figure 6.5.

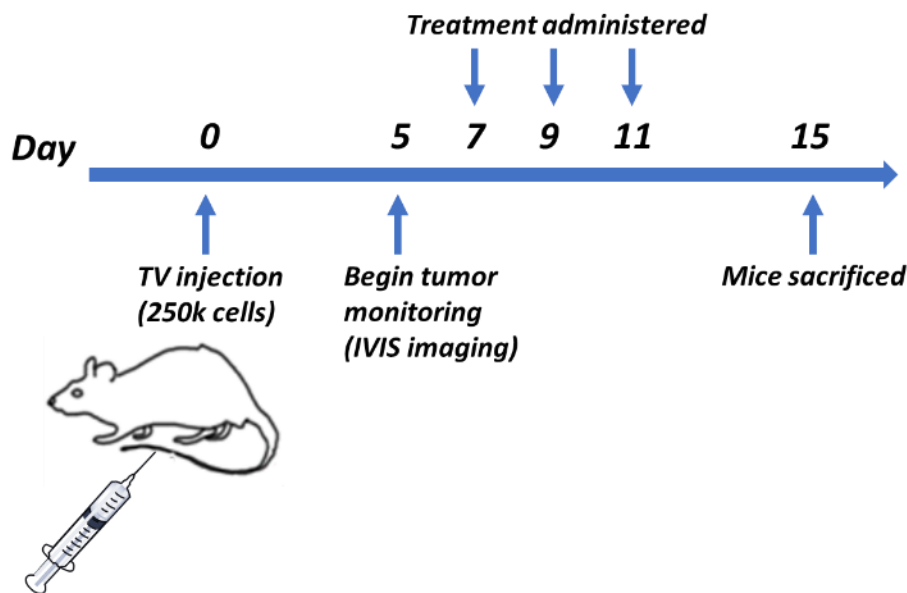


Figure 6.5. The *in vivo* treatment strategy plan in treatment of lung metastases induced by 4T1-luc-tdTomato cells. 250k cells were injected TV in female BALB/C mice. Monitoring of tumor growth began by *in vivo* IVIS imaging of mice on Day 5 post tumor inoculation and continued for every other day till Day 15. Treatment was given three times on days 7, 9, and 11 post-tumor implantation. Mice were sacrificed on Day 15.

After 3 treatments, all mice were sacrificed (day 15 post tumor inoculation), and the lung tissue was directly evaluated (Figure 6.6 and 6.7). The total flux of lungs for both groups as measured by IVIS of the lung tissues demonstrated no significant difference in overall

tumor burden between any of the groups as seen in p values calculated after One-way ANOVA analysis followed by Tukey's Multiple Comparison Test (Figure 6.6).

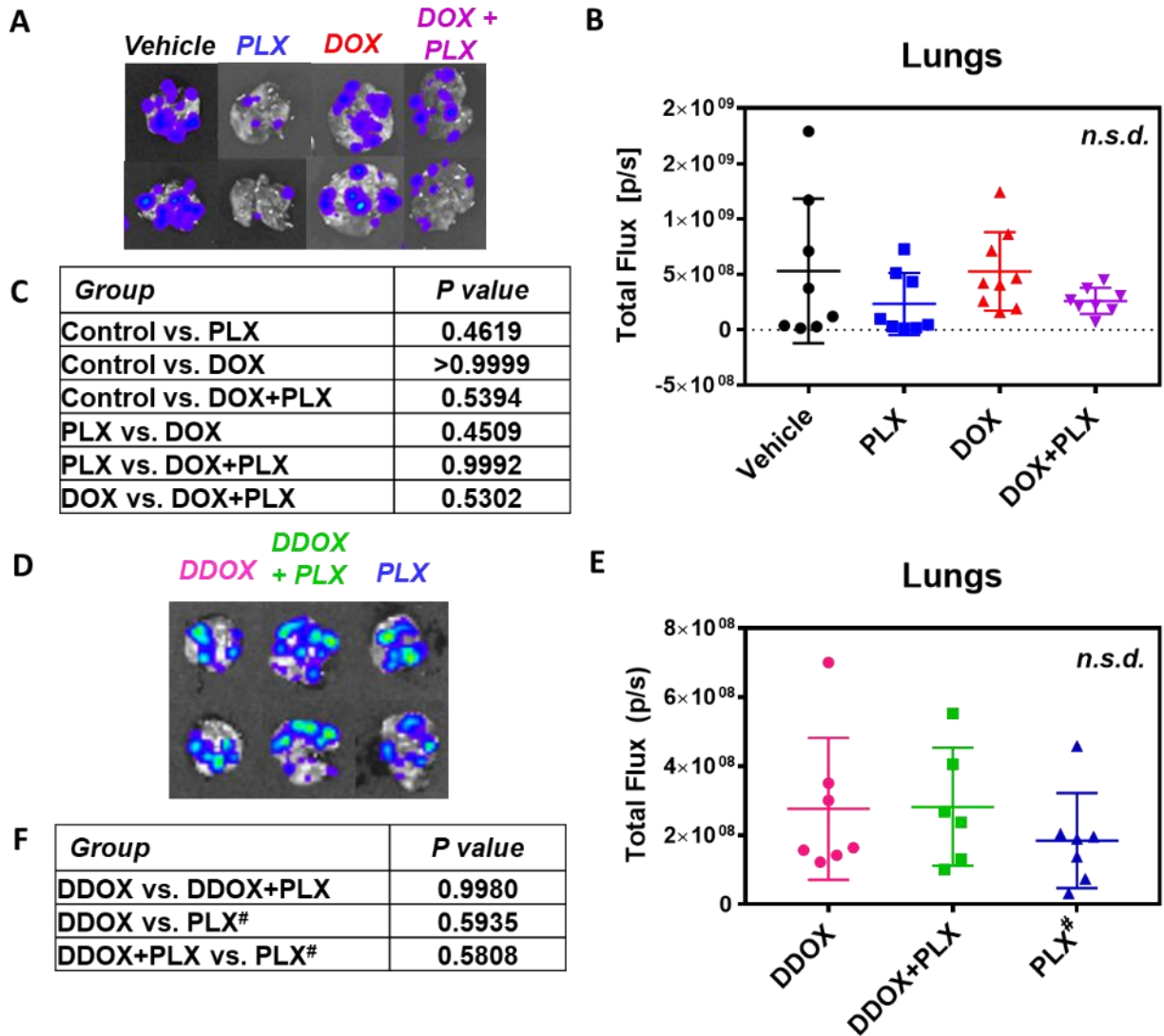


Figure 6.6. Evaluation of lung tumor burden by *ex vivo* imaging of lungs using IVIS. **A) & D)** *Ex vivo* lung images of treatment groups. **B & E)** corresponding total flux of lungs by combining flux of lungs imaged on two sides for each group as evaluated from IVIS images. **C & F:** Corresponding p-values comparing total flux of groups after running One-Way ANOVA analysis followed by Tukey's Multiple Comparison Test. All drugs were given via pulmonary route except PLX# group seen in D) in which PLX was delivered IV route.

A trend can be noted, however, in which the overall tumor burden measured by total flux of tumor cells was least in PLX groups when delivered PA as well as IV,

indicating potential of the macrophage immunotherapy treatment. Surprisingly, DOX alone did not help decrease tumor burden, with results similar to the control group (vehicle). The DOX+PLX group demonstrated a lower tumor burden on lungs, but not as effective as PLX alone, indicating that DOX is actually negating any positive effects of PLX. It is noted that DOX not only does not provide for an effective treatment, but it is also very toxic. Animals treated with DOX alone or in combination with PLX had a significant decrease in body weight (Figure D3) as well as increase in overall lung weight (Figure 6.7). DDOX and combination of DDOX+PLX delivered via the pulmonary route demonstrated overall tumor burden to be almost similar with PLX delivered IV, which showed slightly lower tumor burden (Figure 6.6). The change in body weight (Figure D3) and overall lung weights (Figure 6.7) for these groups showed no significant differences.

To provide a more representative version of the *in vivo* data when measuring total flux of each mouse, the % tumor growth rate was calculated by normalization of total flux signal from Day 7 post tumor inoculation (1st treatment day) to be comprised of 100% tumor growth (Figure D3). Since total flux for each mouse varied, a way to try to compare rate of tumor growth was to normalize total flux signal. The normalization at 100% tumor growth rate occurred on Day 7 post tumor inoculation since this corresponded to the first day of treatment. The % tumor growth rate calculated by *in vivo* total flux (combined dorsal and ventral images) revealed similar trends (Figure D4, Table D1) to the results discussed above. However, for combination DOX+PLX group, the overall % tumor growth rate was shown to be the highest of all groups, which is not demonstrated when imaging of lungs only, and was statistically different from PLX group on Day 15 (Figure D4). This may be due to total flux captured *in vivo* was also capturing metastasis to other sites besides

lungs, such as lymph nodes and bone, in upper portion of mouse. Therefore, if DOX+PLX demonstrated lower results in lungs, it may not correspond to effective treatment to other sites. However, no group proved to have any significant difference from vehicle, our negative control. Trends for DDOX, DDOX+PLX, and PLX (given IV) in % tumor growth rate (Figure D4, Table D1) proved to show similar trends as the tumor burden measured by the lungs (Figure 6.6). The DDOX+PLX group showed highest % tumor growth by Day 15 as compared to DOX alone, and which PLX demonstrated the lowest % tumor growth by day 15. Overall, for both experimental groups, PLX delivered by PA and by IV demonstrated lowest tumor burden by Day 15.

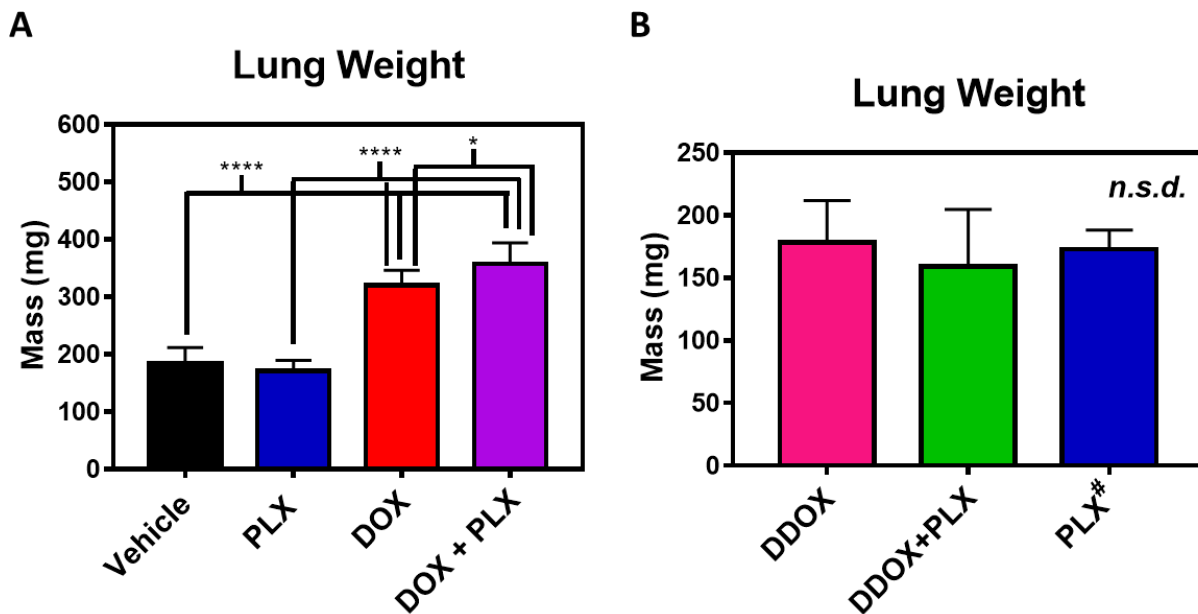


Figure 6.7. Average lung weight for corresponding group with **A)** representing first experimental group in which all drugs were given via pulmonary route and **B)** the second experimental group in which DDOX and DDOX+PLX were given pulmonary route and PLX# was given IV route, (* $p < 0.05$, **** $p < 0.0001$, n.s.d. = not statistically different).

6.3.6 Measurement of Macrophage Polarization by Flow Cytometry

The macrophage population and macrophage polarization within the lungs of mice from Day 15 (n=3) post-tumor implantation was assessed by flow cytometry (Figure 6.8).

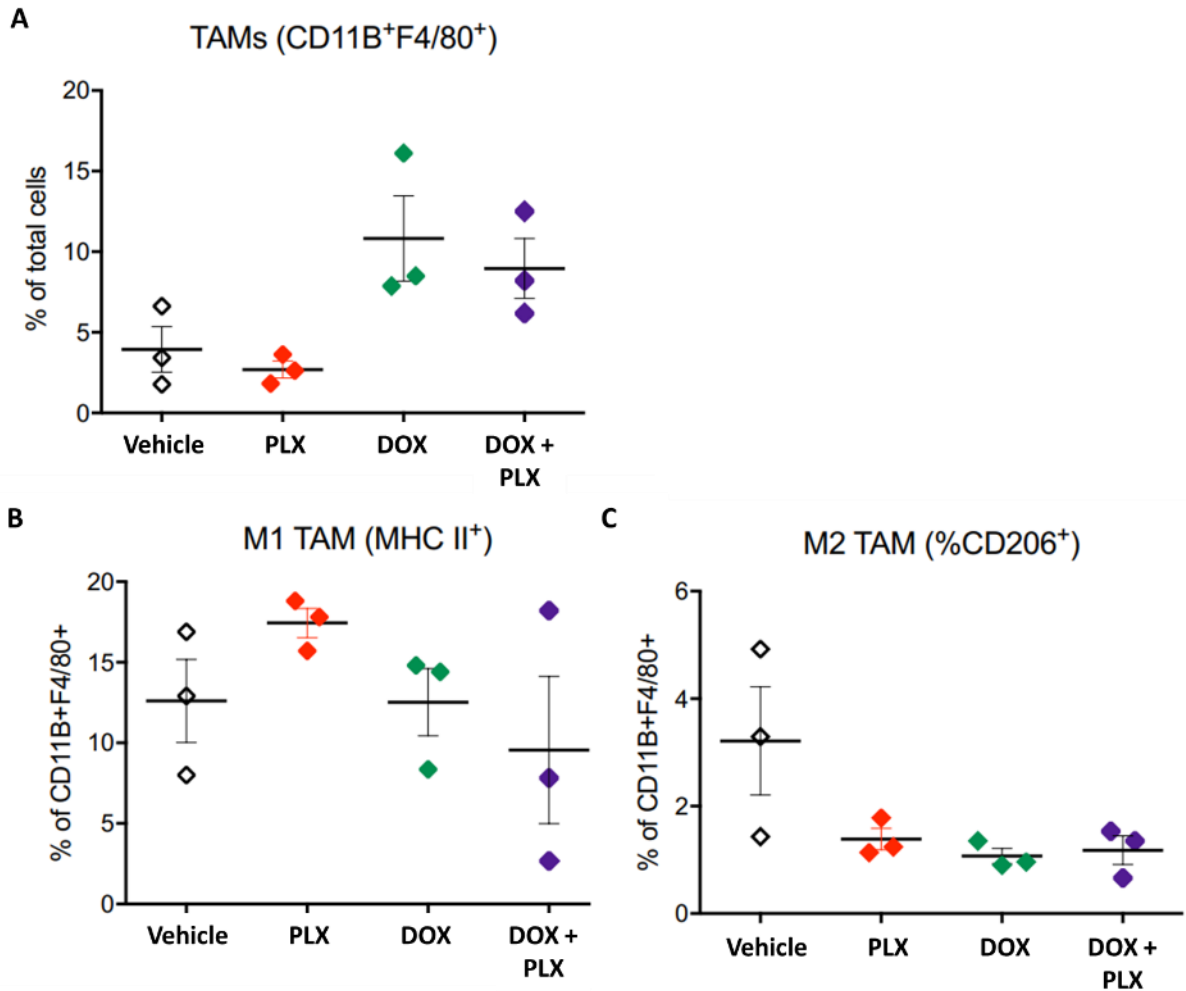


Figure 6.8. Macrophage tracking by flow cytometry. **A)** % total of macrophages compared to all cells in lung sample. **B)** % of Cells considered M1 TAM phenotype. **C)** % of cells considered that of M2 TAM phenotype.

In these exploratory experiments, total TAMs and M1 and M2 population was measured during the first set of experiments where all drugs were delivered via the pulmonary route. The overall number of macrophages found in the lung samples of PLX treated animals was lower than the vehicle (negative control). On the other hand, total macrophage

population in the lungs for DOX and DOX+PLX treatment groups resulted in an overall increase in number of macrophages (Figure 6.8A). The percentage of cells considered M1 TAM phenotype increased and M2 TAM phenotype decreased for PLX group when compared to the vehicle (Figure 6.8). The DOX group had similar % of cells to be of M1 phenotype and lower % of M2 cells as compared to control, while the combination group revealed a lowering of both M1 and M2 TAM percentages when compared to the vehicle.

6.4 Discussion

Metastatic relapse is typically accompanied by MDR, which is the main cause of cancer death for most cancer patients^{6, 7, 23}. Breast cancer remains the leading type of cancer in terms of new cases for women in the USA, and the metastatic form of breast cancer most commonly metastasizes to the lung, along with liver and bone, and lymph nodes.^{2, 7, 8} The metastatic form of breast cancer remains the leading cause of death in these patients and where current clinical intervention proves unbeneficial.^{9, 10} Not including only breast cancer, but secondary lung tumors (tumors that metastasize to the lung) can be found in 30-55% of all cancer patients.⁶ Therefore, a push for alternative treatments including immunotherapy have given a new therapeutic strategy to treat patients not only with primary lung cancers, but also secondary tumors that metastasize to the lungs. The small molecule immune modulator PLX is an attractive therapeutic agent as it has shown great efficacy as a monotherapy and combination therapy and is currently being studied in many current clinical trials.^{20, 82} In this investigation, we seek to evaluate the potential of locally delivered PLX to the lung tissue as a strategy to treat primarily and secondary lung cancers, and the impact of combination therapies with cytoreductive agents (in this case DOX). DOX itself is used as one of the main chemotherapies in the

late stages of advanced breast cancer,⁷¹ making it a relevant choice for this metastatic breast cancer model used in this study. A more direct delivery route for the treatment of primary and secondary lung tumors is an attractive strategy. Advantages of the pulmonary route include the fact that it is a non-invasive route of delivery to lungs, it has higher lung selectivity to direct more drug to target lung tumor sites, and lower systemic exposure to reduce off-target effects.^{72, 73} It can also serve as a non-invasive systemic delivery route by lungs having a large alveolar surface area and thin epithelial air-blood barrier allowing for rapid absorption of molecules from the alveolar space to the blood stream.⁷³ This is attractive for metastatic models which some circulating cancerous cells can also be targeted, as for example the lymph nodes, the first site of metastases from lung cancer. Reducing systemic toxicity is critical not only to cytoreductive agents, but also to immunotherapies, including CSF1Ris, that have also demonstrated associated toxicities and a direct route of administration to the targeted tissue may help overcome challenges that may prevent their use alone or in combination. The combination of pulmonary route, chemotherapy, and immunotherapy, and nanotechnology for controlled and targeted delivery of the cytoreductive agents (nanochemoimmunotherapy) was tested to assess its potential for the treatment of primary and secondary lung tumors.

In this case, a breast cancer metastatic *in vivo* needed to be established. The establishment of a transformed 4T1 cell line (murine mammary adenocarcinoma), a mouse cell model for stage IV human breast cancer, was the first step in this study. It was transformed to incorporate fluorescent and bioluminescent properties by incorporation of a lentiviral vector containing tdTomato and firefly luciferase. The tdTomato fluorescent expression allowed for the tracking of the tumor cells via fluorescent

property utilizing flow cytometry (Figure 6.1). The bioluminescence from the luciferase allowed for visualization and monitoring of tumor growth rate *in vivo* and directly of lung tissues *ex vivo* with the use of IVIS imaging. These 4T1 cells were referred to as 4T1-luc-tdTomato. The puromycin resistance was also added to the lentivirus to allow for selective selection of 4T1 cells that only contain vector, allowing for subculturing of the cells without loss of expression. The success of such an established cell line was monitored by both checking of fluorescent signal (Figure 6.1) and bioluminescent signal (Figure 6.2) and it is being continuously monitored to assure quality.

Once the 4T1-luc-tdTomato cell line was established, a tumor growth rate study was conducted to evaluate the effectiveness of tail vein (TV) injection of cells to establish tumors in the lungs. This was conducted in female BALB/C mice, as these tumor cells are syngeneic to this strain of mouse. TV injection of 4T1 cells into BALB/C mice was evaluated previously, and compared to 4T1-luc2 cells implanted subcutaneously, orthotopically, and via TV.³⁰⁸ It was concluded that lung metastasis from breast cancer when established by orthotopic injection or TV injection did not show any significant differences in gene profiles, and they were thus considered genetically similar.³⁰⁸ This conclusion confirms TV injection of 4T1 cells to form breast cancer lung metastasis is a relevant *in vivo* model of secondary lung cancer.

Based on *in vivo* IVIS images (Figure 6.3) and *ex vivo* images of lungs (Figure 6.4) as a function of days post tumor implantation, it was demonstrated that around one week is required for the tumor cells to establish in the lungs and to begin to expand exponentially. A good correlation between the *in vivo* and *ex vivo* images was also seen. These results, therefore, also established that the tumor growth could be monitored *in*

vivo as the study was being conducted. The establishment of which day to start treatment was also determined based on the tumor growth profile. Day 7 post tumor implantation was selected based on establishment of tumor by this day This is different from studies starting treatment at day 0. Therefore, our work more closely mimics what typically happens in the clinic for tumors when metastases had already ensued.

The pulmonary delivery of PLX, DOX, DOX+PLX, DDOX, and DOX+PLX was evaluated for treatment of lung metastasis established by 4T1-luc-tdTomato cells in female BALB/C mice as direct pulmonary delivery to the lungs provides a relevant route to treat such metastasis as discussed above. However, IV administration of PLX was also tested as control – PLX is typically dosed orally. The first set of comparisons were of pulmonary delivered DOX, PLX, DOX+PLX, as compared to the vehicle, the negative control (no treatment). The second set of comparisons was conducted on an experimental group in which DDOX, DDOX+PLX groups administered via the pulmonary route and a third group where PLX was administered the IV route.

The results seen from evaluating tumor burden on lungs via total flux from tumor cells *ex vivo* (Figure 6.6) reveals that there was no statistical significant difference within the various groups tested. Therefore, none of the treatments demonstrated efficacy by Day 15 post tumor inoculation. These exploratory experiments reveal few trends and allowed us to draw some important conclusions, however, that may guide the next set of experiments.

Another way to look at tumor burden is to measure the % growth relative to the last day the tumor was monitored before treatment. This strategy is also important as it takes into account natural variability among the animals within a group and between groups as

this particular model is susceptible to significantly different rates of growth compare to for example xerograph models implanted subcutaneously.

The % tumor growth evaluated from *in vivo* IVIS images is shown in Figure D3 and p values calculated on Day 15 in Table D1. Their results show somewhat similar trends as with the *ex vivo* imaging of the lungs. The DOX and DOX+PLX treatments upon PA revealed a higher tumor growth rate compared to vehicle., indicating not only lack of efficacy from the cytoreductive therapy, but an unwanted effect that promotes tumor growth. The DOX+PLX group showed the highest % tumor growth rate, which differs from the total flux seen in the lungs *ex vivo*. These results are statistically different (greater rate of growth) from the PLX group by Day 15 post tumor inoculation.

Interestingly DDOX+PLX also demonstrated the highest % tumor growth by Day 15 (although no statistical differences noted). Therefore, the combination of PLX and DOX or DDOX did not provide a synergistic action, and actually seemed to provide the opposite effect on tumor burden (% tumor growth). The combination of these two drugs given together proved to be a poor combination.

The main trend seen with all the groups is that the delivery of PLX alone either by pulmonary delivery or by IV delivery demonstrated the most effective decrease in tumor burden. This demonstrates that PLX alone could potentially act as a monotherapy for treatment of breast cancer metastasis or be used in combination with other therapies.

Another major aspect to be noticed is that DOX at 1 mg/kg dose, when delivered the pulmonary route, proved to be highly toxic to the mice with this tumor model, in both DOX treatment group and DOX+PLX treatment group. Toxicity was observed by the decrease in average body weight of the mice (Figure D3) starting after treatment, as well

as increase in lung weight in those groups (Figure 6.7) to a large extent due to inflammation and not overall tumor burden, which remained statistically insignificant (Figure 6.6). This was somewhat surprising, given that the same dose was used previously in B16F10 (melanoma in C57Bl/6) induced lung tumor model without any toxicity and with significant reduction in tumor burden.⁷⁷ However, changes in drug formulation and animal model may have contributed to this result.

Therefore, an alternative DOX treatment was decided to be tested to ascertain if tumor burden and toxicity of DOX could be reduced/avoided. DDOX was chosen, as our group had demonstrated DDOX to be more effective than free DOX in a previous study in a B16F10-induced lung tumors.⁷⁷ DDOX also had the lowest IC₅₀ value (0.96 μ M) *in vitro* (Table D2) when tested against other DOX formulations (Figure D5). The DDOX formulation did prove to decrease the toxicity of DOX at same free DOX equivalent concentration (1 mg/kg) – as seen with the lack of any significant drop in mouse weight (Figure D2) and no inflammation in lungs or increase in lung weight (Figure 6.7). However, despite these benefits, it still did not prove to be better than PLX alone.

Overall PLX alone when given through pulmonary route or through IV route has proven here to have the best chance of treatment for lung metastasis from breast cancer. It is worth noticing that the expected dose of PLX expected to reach the lungs is very small upon IV administration. Given its efficacy, we expect to be able to reduce the total dose of PLX necessary upon PA to achieve same level of efficacy at IV. Upon finding the right combination of PLX and cytoreductive therapy, lower doses of the combination may lead to efficacy and reduced overall toxicity.

Many reports reveal that no dose limiting toxicities were found in phase 1 and 2 clinical studies of CSF1R inhibitors,²⁰ which correlates with this investigation. However, some dose limiting toxicities may occur at maximum tolerated dose and should be noted. One Phase 3 clinical trial using PLX3397 had 2 of 121 patients experience non-fatal serious liver toxicity, which led to suspension of the trial (NCT02371369).²⁰ If this was due to inhibition of other receptor kinases in liver remains unclear.²⁰ Also, whether this toxicity would be seen if delivered via other routes (IV and PA) compared to oral delivery is also unknown. But if liver toxicity could be avoided by alternative route of delivery, this would be an incentive to deliver PLX via alternative routes.

In terms of mechanism of action of PLX, some preliminary results were performed with the help of the Bos group at VCU (tagging of lung tumor cell suspension provided and data analysis). PLX treatment was seen to induced macrophage polarization from M2 to M1 as seen in flow cytometry results (Figure 7.8). An overall decrease in macrophage population was seen compared to vehicle control, with an increase in M1 TAMs and decrease in M2 TAMs demonstrating a 3-fold overall increase in M1/M2 ratio (from ca. 4 to ca. 12). Therefore, a decrease in overall TAMs as well as repolarization did occur with PLX treatment, an indication that this CSF1Ri is affecting overall TAMs found within the lungs on this secondary model.

Overall efficacy was not determined from this study as no statistical differences were seen in treatment groups. However, based on these results, PLX alone has the best indication to expand on these preliminary results, as combination therapies and different treatment regimens are evaluated. For example, a longer study may prove overall efficacy of PLX alone in both delivery routes (PA and IV) and is currently being studied in

the group. Also, the dosing schedule for PLX and maximum tolerated dose could also be explored to enhance overall efficacy. An overall more in-depth study of macrophage population and interaction with other immune cell populations (T effector and T regulatory cells) is desired to provide more insight into the role of PLX in modulation of the immune system. PLX also downregulates CSF1R by inhibition of phosphorylation of kinase domain on the receptor. This could be further elucidated the mechanism of tumor inhibition when looking at amount of phosphorylation seen in CSF1R on TAMs to understand the molecular mechanism of PLX.

PLX in combination with other therapies could also enhance efficacy. The combination of PLX and other CSF1R inhibitors with immune checkpoint therapies has the highest number of clinical trials to date.²⁰ Immune-checkpoint therapies have revolutionized immune therapy for cancer treatment. A combination of CSF1Ri and T-cell-enhancing therapies (PD1/PDL1 inhibitors) have shown synergistic action and proven to be effective when PD1/PDL1 inhibitors were shown limited efficacy on its own.³⁰⁹ This combination has led to many clinical trials in Phase 1/2 stages to determine dosing, safety, and clinical efficacy, with results yet to be remaining.²⁰ Therefore, this combination of PLX with PD1/PDL1 inhibitor could prove to be a synergistic combination and should be tested in breast cancer metastasis model established here.

6.5 Conclusion

Treatment of primary and secondary lung tumors remain a significant clinical challenge in which current standard of care with cytoreductive therapies offer relatively small clinical benefit. This study focused on the treatment of secondary lung tumors metastasized from breast cancer in order to evaluate a new treatment strategy for lung

metastases that includes (i) immunotherapy with a macrophage reductive and repolarization agent (PLX); (ii) combination of cytoreductive therapy (DOX) and immunotherapy (immunochemotherapy); and (iii) use of dendrimer nanocarriers for improved efficacy and reduced toxicity of cytoreductive agent in combination with CSF1Ri (nanochemoimmunotherapy).

Here pulmonary delivery of DOX, PLX, PAMAM G4SA-hyd-DOX (DDOX) and combination of PLX with DOX or DDOX formulations was tested via pulmonary delivery on an *in vivo* model of 4T1-induced secondary lung tumors in female BALB/C mice. It was demonstrated that of all treatment groups, PLX alone proved to show the most promising strategy by showing the lowest tumor burden on lungs when PLX was delivered PA or IV, and no dose-limiting side effects. Surprisingly, free DOX alone or in combination with CSF1Ri showed significant toxicity and no ability to reduce tumor burden.

PLX seems to work by leading to an overall decrease in TAMs and TAM repolarization as demonstrated via flow cytometry. However, efficacy and most effective dosing schedule as well as total dose remains to be further investigated. Also, a combination with immune-checkpoint therapies has also a potential for a synergistic combination treatment strategy, which was not seen with DOX and PLX. Therefore, immunotherapy with PLX remains a promising therapy for treatment of metastatic breast cancer to the lungs.

6.6 Acknowledgements

This work was performed along with Sulaiman Alhudaithi and Hanming Zhang, two colleagues in the da Rocha group. The authors would like to give thanks for the financial support given NSF-DMR Grant: # 1508363. A special thanks to Dr. Jennifer Koblinski

from the Mouse Core at Massey Cancer Center (MCC) and Department of Pathology at Virginia Commonwealth University (VCU) for the gift of the lentivirus used for 4T1-transfection. The authors would also like to thank Ms. Julie Farnsworth for cell sorting of 4T1-luc-tdTomato cells in the Flow Cytometry Shared Resource Core. A special thanks to Dr. Bin Hu at MCC/VCU for all the help in establishing the 4T1-induced lung metastasis model and training on IVIS imager. Another special thanks for Dr. Paula Bos in Department of Pathology at VCU for all very fruitful discussions on the subject, and for running the tagging and analysis of flow cytometry results for the TAM population in the lungs. The authors would also like to give a special thanks to Dr. Wei Du in the Bos group for helping in TV injections for tumor model establishment as well as running of flow cytometry experiments for macrophage cell tagging. Another special thanks for IVIS imaging resources from VCU Massey Cancer Center Shared resources. Thanks also to Hanming Zhang for maintaining the breeding colonies. Services and products in support of the research project were generated by the VCU Massey Cancer Center Cancer Mouse Model Shared Resource and VCU Massey Cancer Center Flow Cytometry Shared Resource, supported, in part, with funding from NIH-NCI Cancer Center Support Grant P30 CA016059.

CHAPTER 7 – CONCLUSIONS AND FUTURE DIRECTIONS

Lung cancer remains the number one cause of cancer death in the United States.² Approximately 57% of cases are diagnosed at the metastatic stage, with a 4.7% five-year survival rate.³ Treatment success is radically different in other types of cancers such as prostate cancer where rate of incidence has fallen 10% annually from 2010-2014 and has a 5-year survival rate of 99%.^{2, 3} Not only lung cancer, but secondary lung tumors found in 30-55% of all cancer patients .⁶ Most metastatic tumors cannot be cured with existing therapies.¹² Chemoresistance (multi drug resistance – MDR) that develops intrinsically or acquired becomes the final leading cause of death in these patients.^{6, 9, 11, 22} MDR develops from a variety of changes that occur within tumor cells and the complex characteristics of the tumor microenvironment (TME). Several mechanisms of resistance are utilized by tumors concurrently or consecutively, thus making treatment effectiveness difficult.²⁴ Current therapies often have slowed tumor progression or alleviated symptoms, but rarely lead to a cure.¹² Immunotherapy, including the use of checkpoint inhibitors has shown promise in which alternative therapies have not proven beneficial. However, only a relatively small fraction of tumor types and of patients have been benefited so far.^{20, 21} Immunotherapies are unfortunately not devoid of toxicity, and this is an important issue that is becoming more obvious and relevant as the number of new immunotherapy-based regimens are rapidly growin.¹⁷ Establishing new treatments, alone or in combination, that can (i) increase the rate of survival of lung cancer patients at early stages or at later stages when metastatic relapse and MDR may have developed, and (ii) reduce intrinsic toxicity associated with the various treatments is, therefore, of great potential relevance in pulmonary oncology.

Here we described alternative treatment modalities with pre-clinical studies that suggest their potential to help address the onset of MDR and potentially prolong the rate of survival of patients with primary and secondary lung tumors. We use a combination of local lung targeting (high payload to relevant site with reduced systemic toxicity), nanocarriers (modulation of the interaction with the physiological environment), intracellular/organelles targeting (repurposing cytoreductive therapies), siRNA as therapeutic agent (selective target apoptotic pathways), and macrophage repolarization immunotherapy (use TME to support other therapies) are reported.

The main conclusions from these studies and suggested overall future directions are discussed here:

(i) *We were able to develop mitochondrial-targeted dendrimer nanocarriers (DNCs) as a platform for the repurposing of chemotherapeutics with potential applicability in the treatment of MDR in primary and secondary lung tumors.* Mitochondria have become attractive targets for cancer therapies since they play a crucial role in cellular homeostasis and intrinsic apoptosis and have altered functions in tumors.^{48, 50} TPP, a common mitochondrial targeting agent, has been utilized to target small molecules^{54-57, 92} as well as various nanocarriers⁸⁷⁻⁸⁹ for delivery of therapeutics and treatment tumors and MDR-associated tumors. We are the first group to directly address TPP density and effect of PEG linker between TPP (PEGTPP) on cellular internalization, toxicity, and mitochondrial targeting of dendrimers, including PAMAM. We demonstrated this as a potential delivery platform for therapeutics to address issues with MDR.

Here, we were able to determine that TPP attachment to G4NH₂ PAMAM dendrimers lead to an enhancement of mitochondrial targeting of these dendrimers. TPP

was either directly conjugated (G4NH₂-TPP) or through PEG linker (G4NH₂-PEGTPP). PEG was added as a flexible linker between G4NH₂ dendrimer as PEG has desirable characteristics including increasing solubility, biocompatibility, enhanced pharmacokinetics and modulation of interaction between the dendrimer and the physiological environment.^{116, 122, 241} Both strategies demonstrated significant mitochondrial targeting as compared with G4NH₂ without TPP. G4NH₂-TPP groups demonstrated an increase in targeting with increase in density, while G4NH₂-PEGTPP demonstrated significant mitochondrial targeting without being affected by degree of PEGylation present. Modulation in overall toxicity and internalization was seen as TPP density varied, with an increase in *in vitro* toxicity and cellular internalization in G4NH₂-TPP with increasing TPP-density, whereas G4NH₂-PEGTPP has decreasing *in vitro* toxicity when PEGTPP density is above 5 per dendrimer (>8% coverage). Therefore, modulation of the properties of G4NH₂ dendrimer can be achieved with the presence of PEG without affecting the overall mitochondrial targeting ability. It was concluded, therefore, that both direct and indirect conjugation, separately or in combination, are potential strategies for the delivery of therapeutics to the mitochondria, which can be utilized to address MDR and treatment of primary and secondary lung tumors.

More work is required to test overall efficacy of TPP-dendrimer targeted strategy. G4NH₂-TPP and G4NH₂-PEGTPP dendrimers can be further modified upon conjugation of a chemotherapeutic agent directly to the dendrimer. One chemotherapeutic that has shown efficacy when targeting mitochondria is DOX.^{54-57, 94, 177, 182} The Complex I in the electron transport chain in mitochondria can modify DOX into a more reactive semiquinone radical, resulting in increased ROS production and higher oxidative

stress.^{178, 179} DOX may also inhibit Complex I and II, increasing ROS production, which can ultimately lead to induction of apoptosis.^{178, 179} The conjugation of DOX to a mitochondrial-targeted dendrimer nanocarrier or conjugation of DOX with TPP (DOXTPP) and then to dendrimer should be considered and tested *in vitro* and *in vivo*.^{54-57, 177} This may prove to be an effective strategy to address drug resistance, particularly when combined with pulmonary delivery.

(ii) *We developed siRNA/TPP-DNC complexes as a platform for pulmonary delivery of siRNAs with potential applicability in the treatment of MDR in primary and secondary lung cancer.* siRNA delivery to the lungs can be utilized to address MDR by modulating genes overexpressed in tumors and assist in apoptosis induction when delivered alone or in combination with other treatments.⁵⁸ However, efficient siRNA delivery to lung tumors has many challenges including physiological barriers and cellular internalization barriers. Here, we were able to demonstrate the enhancement of *in vitro* transfection ability of siRNA in lung alveolar cells by the use of dendrimer-TPP conjugates to form nanometer scale TPP-DNCs complexes with siRNA, and the successful aerosol formulations of those complexes in both pMDIs and DPIs. This provides an overall platform for local siRNA targeting to the lungs that can be utilized to help address MDR and treat primary and secondary lung tumors.

The impact of TPP surface modification on G4NH₂ dendrimers was evaluated for their interaction with siRNA and their overall gene knockdown ability in an *in vitro* model of the pulmonary epithelium at various TPP densities and varied N/P ratios (amount of dendrimer vs siRNA in the complex). The eGFP knockdown ability in eGFP-A549 cells of dendrimers was enhanced with the presence of TPP on the dendrimer surface with

G4NH₂-12TPP, and at N/P 30 demonstrating the highest gene knockdown efficiency. Improvements with transfection ability was associated with looser complexation between the siRNA and G4NH₂-TPP dendrimer and could be associated with other factors including mitochondrial targeting, heightened cellular internalization, and more effective endolysosomal escape. Micron-sized particles were engineered by G4NH₂-12TPP-dendriplexes being spray dried with mannitol. We demonstrated that such micron particles are conducive to deep lung deposition when formulated in pMDIs and DPIs. We have also shown these to be viable formulations in that siRNA maintained its biological activity during the preparation of the micron particles, formulation and delivery (*in vitro* model of the lung). Therefore, this strategy provides for a platform for efficient siRNA delivery to the lungs.

Further work can help be performed to help elucidated the potential of this strategy in context of lung tumors and MDR by delivering siRNA that targets well-known genes that are overexpressed in lung tumors. In this context, the gene targets of most interest have been Bcl-2 and Survivin. Bcl-2 is a protein cell survival and cell death by prevention of intrinsic (mitochondrial-dependent) apoptosis in which it interacts with other Bcl-2 family proteins on the outer mitochondrial membrane.^{204, 205} It has been implicated in MDR and associated with poor prognosis.²² Survivin is a member of the Inhibitor of Apoptosis Protein (IAP) family^{68, 206} and promotes cell survival by inhibiting caspases, proteins known to implement programmed cell death.^{66, 95, 206, 207} Survivin expression is not normally found in adult tissues, but has been expressed in high levels in NSCLC, and also shown unfavorable prognosis, increase recurrence rates, and tumor resistance in these instances.^{66, 206, 209} Therefore, the delivery of siRNA containing gene sequences

that target Bcl-2 or Survivin have great potential in addressing MDR in lung tumors, and should be tested utilizing the strategy we presented here *in vitro* and *in vivo*. This strategy can also be tested as a combination therapy, where gene targets and other treatment modalities (chemo- or immuno-therapies, for example) are used to elicit synergistic effects.

(iii) *We were able to synthesize dendrons with various surface chemistries and a cyto-reductive molecule (DOX). Conjugation of these asymmetric dendrons has the potential to enhance therapeutic efficacy of the chemotherapeutic and in combination with local lung delivery be used in the treatment of MDR in primary and secondary lung cancers.* As the complexity and versatility in dendrimer chemistry increases, so does the opportunities to use such versatile carriers in biomedical applications.³⁹⁻⁴¹ Bis-MPA polyester dendrimers have been demonstrated to be highly biocompatibility and are also degraded under physiological conditions.³⁸ They are thus highly desirable as drug delivery carriers. The multifunctionality of Bis-MPA asymmetric dendrimers have thus tremendous potential, but their chemistry remains highly complex.^{45, 167}

In this work, we were able to synthesize and characterize various surface modifications to N₃-G5-OH polyester dendrons for the potential formation of asymmetric dendrimers containing DOX and varying surface chemistries unmodified neutral (-OH), -COOH (anionic), -NH₂ (cationic), hydrophilic (-PEG), and hydrophobic (-Lauryl) functionalities. All surface modifications were made via a liable ester bond. Overall, the various surface modifications represent different surface properties, which have implications in altering cellular internalization and trafficking pathways, and thus their

intracellular fate, as seen with other dendrimers,⁴⁷ but with a highly controlled and asymmetric chemistry.

While dendrons have been prepared, due to the complexity of the synthesis, the preparation of the asymmetric dendrimers was not accomplished during this work and will be part of future work in our group. A potential strategy of DOX conjugation to an acet-G5-GA dendron via a -GFLG- peptide linker has been proposed. The formation of GFLG-DOX remains the limiting factor, and the synthesis of such will remain to be executed in the future. The synthesis and purification of asymmetric dendrimers from dendrons containing GFLG-DOX on one side and varying surface chemistries has also been tested and proposed. These strategies can be utilized to form final asymmetric dendrimers via click chemistry.

Once asymmetric dendrimer chemistry is completed, the testing *in vitro* and *in vivo* is recommended to be conducted. Cellular internalization and intracellular trafficking, and drug efficacy *in vitro* will be conducted to elucidate how asymmetric surface chemistries can affect cellular internalization mechanisms, and thus influence overall DOX efficacy. The delivery of such systems via PA route should be conducted in order to address how asymmetry and varying surface chemistries could affect overall drug efficacy. This can be compared to results of DOX directly conjugated to a polyester dendrimer to elucidate the effect of high asymmetry. These nanocarriers should be also tested in MDR tumors to elucidate the impact of asymmetry.

(iv) *We were able to assess the impact locally delivered, TAM-targeting immunotherapy with potential applicability in the treatment of MDR in primary and secondary lung tumors.* Metastatic tumors are associated with poor prognosis and drug

resistance, and remains the main cause of cancer death and challenge in pulmonary oncology.^{6, 7, 23} Modulation of TAMs by CSF1Ri have shown great promise in many current clinical trials.^{20, 82} In this investigation, we sought to determine the ability of a CSF1Ri (PLX) alone or in combination with a cytoreductive agent in its free form (DOX) or conjugated to PAMAM dendrimers (DDOX) to reduce the tumor burden in an *in vivo* model of secondary lung cancer (breast cancer lung metastases) upon PA administration. This work represents the first to test the delivery of PLX via pulmonary route as potential treatment secondary lung tumors and potential to address MDR. This is relevant as such therapies have potential associated toxicities, and local administration may help mitigate undesirable effects, and thus potentially allow studies with combination therapies as well (where those therapies may also have their own associated toxicity).

PA of DOX, PLX, DDOX and combination of PLX with DOX or DDOX formulations was tested in an *in vivo* model of 4T1-induced secondary lung tumors in female BALB/C mice. No treatment groups were able to demonstrate statistical significant differences from the control. However, trends for PLX alone indicated an overall decrease in tumor burden when delivered via PA, and incurring in no adverse effects, thus suggesting potential of the proposed strategy. Preliminary results also suggest that groups that received PLX treatment lead to an overall decrease in TAMs number and TAM repolarization towards a higher M1/M2 ratio.

Future work in related to such strategy is to explore different regimens of PLX and combination therapies. First, the overall efficacy of PLX alone via IV and PA should be determined by lengthening the overall study to measure survival in this tumor model. A more effective dosing schedule as well as dose-escalation studies could reveal increased

efficacy and determine if any adverse reactions with PLX can be reached, as well as the potential to reduce dose upon PA administration. The combination of TAM reduction/repolarization with immune-checkpoint therapies has also a potential as a synergistic combination treatment strategy.²⁰ The solubility of PLX also remains a problem in which a complex formulation including DMSO and Tween are required to solubilize PLX. Therefore, new nanoformulations to increase overall solubility of PLX are greatly desired and should be studied in future work.

In conclusion, this work and future work has represented potential treatment strategies to address MDR and for the treatment primary and secondary lung tumors. We have demonstrated mitochondrial targeting, pulmonary siRNA delivery, use of novel polyester asymmetric dendrimers, and pulmonary delivery of CSF1Ri as potential platforms for treatment of primary and secondary lung tumors as well as address issues concerning MDR. These strategies present varied alternative pathways that when used alone or combined can greatly affect outcome in patients with poor prognosis, and could in other context, be used to treat other alternative disease states in the lungs.

APPENDIX A**SUPPORTING INFORMATION FOR CHAPTER 3**

Supporting Information. The characterization of G4NH₂-TPP and G4NH₂-PEGTPP conjugates as described by ¹H NMR (Figure A1). The structure with associated bonds as well as the spectra is given for each conjugate.

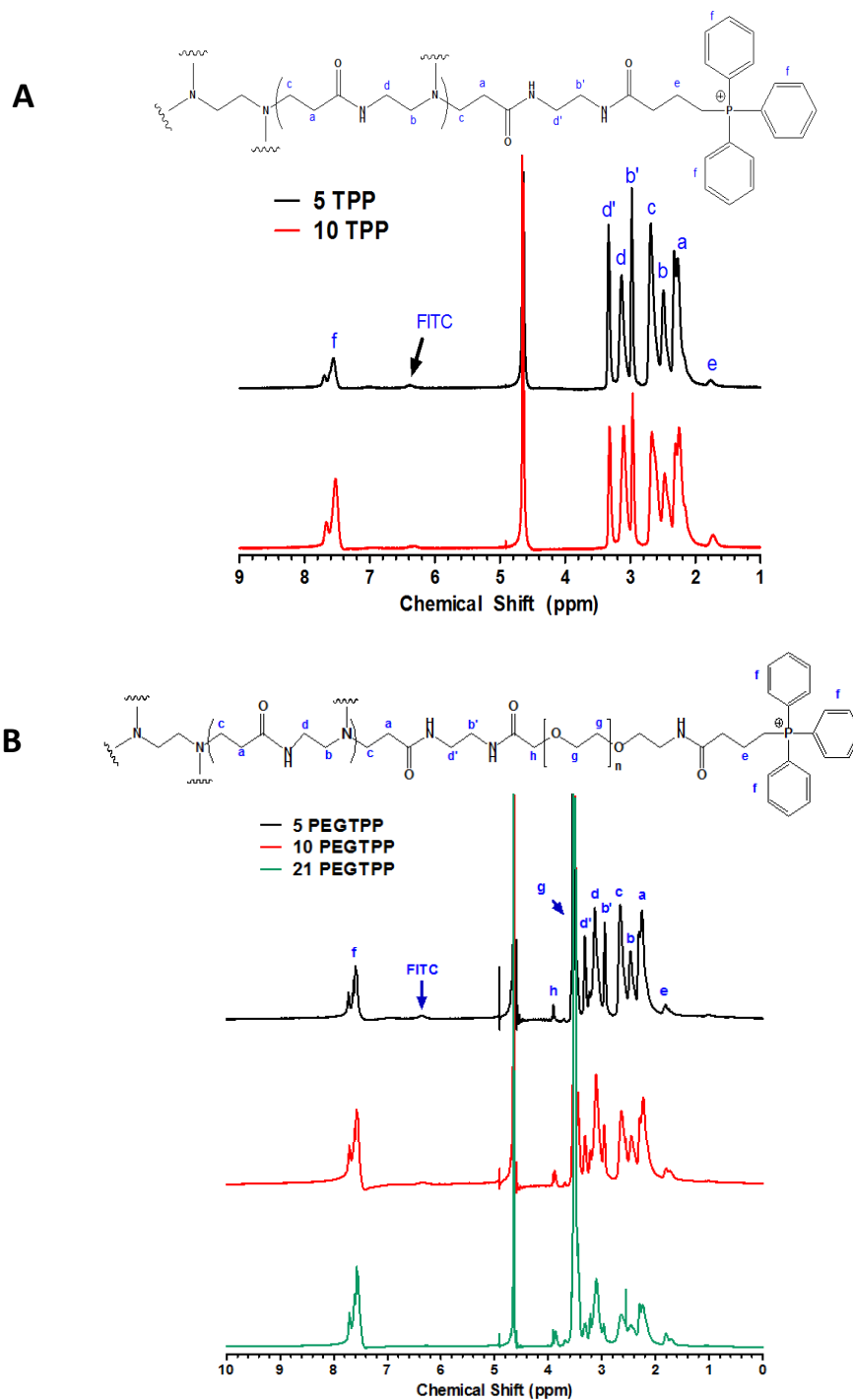


Figure A1. ^1H NMR spectra of the A) $\text{G4NH}_2\text{-FITC-TPP}$ and B) $\text{G4NH}_2\text{-FITC-PEGTPP}$ dendrimer conjugates in D_2O at 400 MHz on Agilent Mercury Spectrometer. The chemical structures are shown above with the corresponding peak shifts.

APPENDIX B

SUPPORTING INFORMATION FOR CHAPTER 4

Table B1. Deposition of dendriplex mannitol micron particles (weight) and siRNA (densitometry) on different stages of the Andersen Cascade Impactor (ACI) from a pMDI formulation at a flow rate of 28.3 L/min. pMDI formulations at 2 mg microparticles/1 mL HFA227 propellant at 25 °C and saturation pressure of propellant. The payload of siRNA in microparticle is 0.025% wt/wt. The results were based on 20 actuations and represented with mean \pm s.d. (n=3). AC: actuator, IP: induction port, 0-7: plate 0-7, and F: filter. RF, FPF, MMAD and GSD refer to respirable fraction, fine particle fraction, mass median aerodynamic diameter and geometric standard deviation, respectively.

Stage	Mass of microparticles (mg)	Mass of siRNA (ng)
AC	0.36 \pm 0.08	80 \pm 8
IP	0.69 \pm 0.06	121 \pm 6
0 (9.0-10.0 μ m)	0.08 \pm 0.03	34 \pm 19
1 (5.8-9.0 μ m)	0.14 \pm 0.04	38 \pm 11
2 (4.7-5.8 μ m)	0.17 \pm 0.05	62 \pm 11
3 (3.3-4.7 μ m)	0.55 \pm 0.16	105 \pm 15
4 (2.1-3.3 μ m)	0.32 \pm 0.05	76 \pm 11
5 (1.1-2.1 μ m)	0.12 \pm 0.05	46 \pm 9
6 (0.7-1.1 μ m)	0.04 \pm 0.02	24 \pm 14
7 (0.4-0.7 μ m)	0.03 \pm 0.01	33 \pm 7
F (<0.4 μ m)	0.03 \pm 0.01	12 \pm 8
RF (%)	59 \pm 6	66 \pm 3
FPF (%)	50 \pm 3	54 \pm 3
MMAD (μ m)	3.8 \pm 0.2	3.6 \pm 0.1
GSD	1.4 \pm 0.1	1.8 \pm 0.2

Table B2. siRNA Deposition on the different stages of Andersen Cascade Impactor (ACI), as determined by densitometry. The 10-20 mg micron particles loaded into capsule were released into ACI from Rotahaler® (DPI formulation) at 25°C, 75% relative humidity, and a flow rate of 28.3 L/min for 4 s inspiration. The results are represented with mean \pm s.d. (n=3). IH: inhaler, IP: induction port, 0-7: plate 0-7, and F: filter. ED, RF, FPF, MMAD and GSD refer to emitted dose, respirable fraction, fine particle fraction, mass median aerodynamic diameter and geometric standard deviation, respectively.

Stage	Mass of siRNA (ng)
IH	1860 \pm 90
IP	330 \pm 130
0 (9.0-10.0 μ m)	260 \pm 40
1 (5.8-9.0 μ m)	215 \pm 15
2 (4.7-5.8 μ m)	354 \pm 9
3 (3.3-4.7 μ m)	310 \pm 7
4 (2.1-3.3 μ m)	225 \pm 7
5 (1.1-2.1 μ m)	81 \pm 7
6 (0.7-1.1 μ m)	81 \pm 4
7 (0.4-0.7 μ m)	29 \pm 14
F (<0.4 μ m)	2 \pm 2
ED (%)	50 \pm 2
RF (%)	42 \pm 3
FPF (%)	39 \pm 3
MMAD (μ m)	4.8 \pm 0.3
GSD	1.4 \pm 0.2

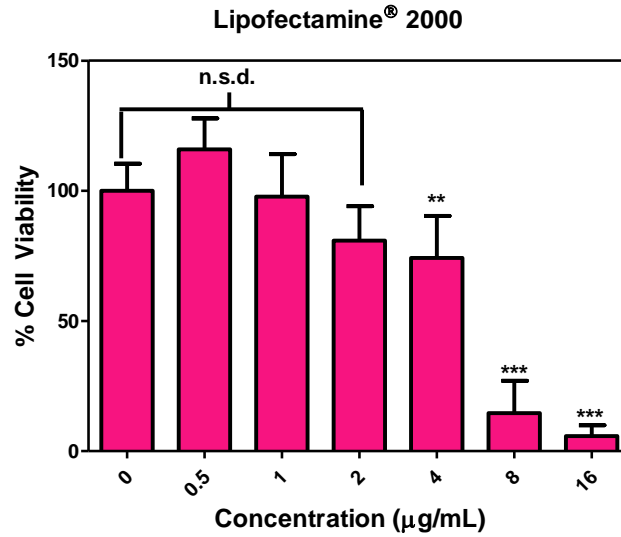
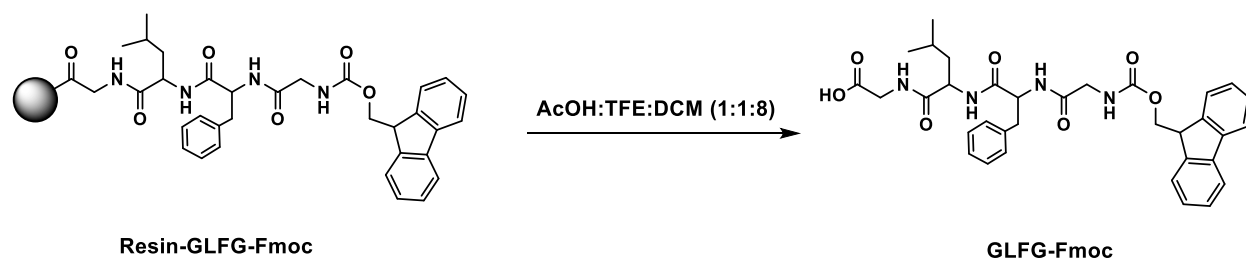


Figure B1. The cell viability of A549 cells contacted with Lipofectamine® 2000 reagent at increasing concentrations as measured by the MTS assay after 48 h incubation. Statistical analysis between the control group indicated at 0 µM representing 100 % cell viability and those of increasing concentrations was analyzed by One-Way ANOVA followed by Tukey's Multiple Comparison Test ($n < 7$). ** $p \leq 0.01$, *** $p < 0.001$, n.s.d. = not statistically different.

APPENDIX C**SUPPORTING INFORMATION FOR CHAPTER 5****C1. Materials**

Polyester-32-hydroxyl-1-acetylene bis-MPA dendron, generation 5, 97% (Acet-G5-OH), glutaric anhydride (GA), 2,5-dihydroxybenzoic acid (DHB), 4-Nitrophenol, and piperidine, were purchased from Sigma-Aldrich (St Louis, MO, USA). Doxorubicin hydrochloride salt (DOX•HCl) was purchased from LC Laboratories (Woburn, MA, USA). The H-Gly-2-Cl-Trt resin was purchased from AAPTEC (Louisville, KY, USA). Fmoc-glycine, Fmoc-L-leucine, Fmoc-L-Phenylalanine, N,N'-Diisopropylcarbodiimide (DIC), and 1-Hydroxybenzotriazole hydrate (HoBt) were purchased from Chem-Impex International (Wood Dale, IL, USA). 2,2,2-Trifluoroethanol (TFE) and N,N-Diisopropylethylamine (DIPEA) was purchased from TCI Co., Ltd. (Tokyo, Japan). Acetic Acid (AcOH), dichloromethane (DCM), dimethylformamide (DMF), dimethyl sulfoxide (DMSO), ethyl ether (Et₂O), methanol (MeOH) were purchased from VWR International (Radnor, PA, USA). 1-(3-Dimethylaminopropyl)-3-ethylcarbodiimide hydrochloride (EDC), N,N-Dimethylformamide (DMF), anhydrous, 99/8+%, N-Hydroxysuccinimide, 98+% (NHS), copper (I) iodide, and 4M Hydrogen chloride in 1,4-dioxane was purchased from Alfa Aesar (Haverhill, MA, USA). Acetonitrile was purchased from Avantar Performance Materials (Center Valley, PA, USA). Dimethyl Sulfoxide-D₆ (with TMS - 0.03 vol%) and magnesium sulfate anhydrous were purchased from EMD Millipore (Burlington, MA, USA). Deuterium Oxide (D, 99.9%) was purchased from Cambridge Isotope Laboratories, Inc. (Tewksbury, MA, USA). Sephadex LH-20 were purchased from GE Healthcare Bio-Science (Uppsala, Sweden).

C2. Synthesis of GLFG-Fmoc peptide

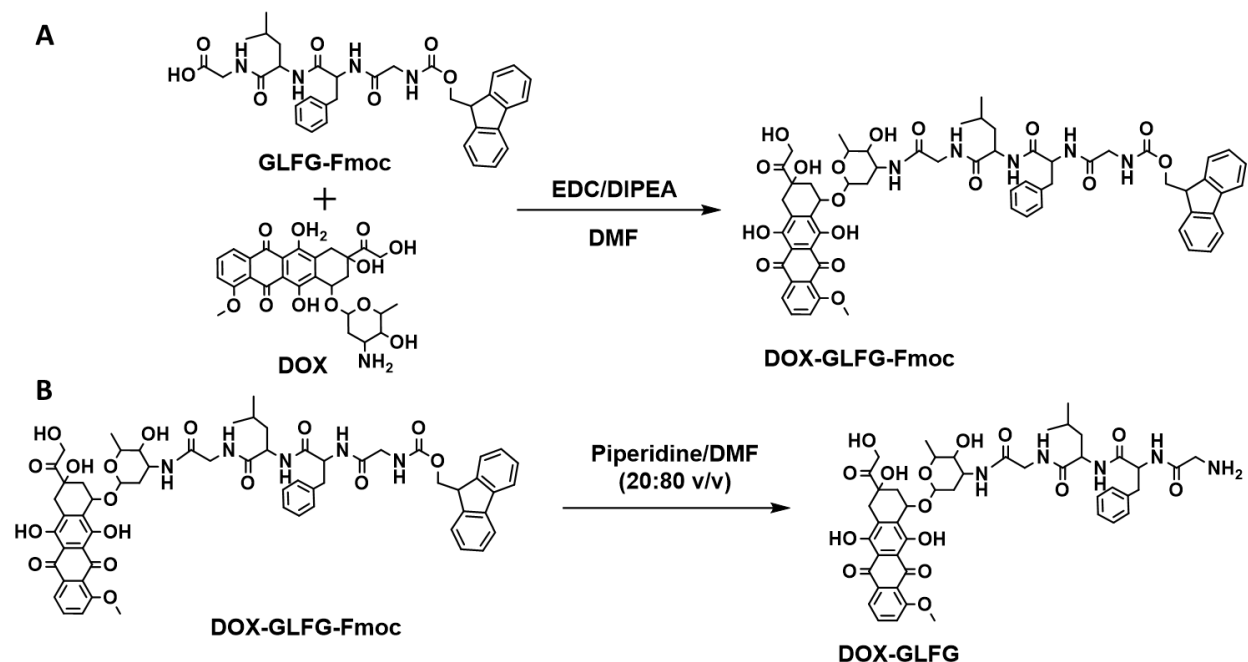


Scheme C1. Deprotection of GLFG-Fmoc from the resin. AcOH: acetic acid, TFE: Trifluoroethanol, DCM: dichloromethane. G-L-F-G: Peptide of glycine-leucine-phenylalanine – glycine.

Resin-GLFG-Fmoc peptide (0.5 mmol) was synthesized on a Liberty Blue Automated Microwave Peptide Synthesizer (CEM, Matthews, NC, USA) using a standard protocol for solid-phase peptide synthesis (Scheme B1). GLFG-Fmoc was cleaved from the resin by diluting product in a mixture of AcOH/TFE/DCM (1:1:8) stirring at room temperature for 0.5 h. The resin was filtered off and solution collected and diluted in hexane (15 x volume). The solvents were removed utilizing rotary evaporation and product collected giving a white solid. The GLFG-Fmoc was characterized by ^1H NMR and MALDI-TOF.

Fmoc-GFLG: ^1H NMR (DMSO- d_6 400 MHz, ppm) δ : 0.84 (d, $-\text{CH}_3$, 3H, Leu), 0.88 (d, $-\text{CH}_3$, 3H, Leu), 1.49 (t, $-\text{CH}_2$, 2H, Leu), 1.61 (sept, $-\text{CH}$, 1H, Leu), 2.78 (dd, $-\text{CH}$, 1H, Phe), 3.04 (dd, $-\text{CH}$, 1H, Phe), 3.49-3.73 (m, 4H, Gly), 4.22-4.56 (m, 4H), 7.22 (d, $-\text{CH}$, 4H, Phe), 7.31-8.18 (m, 9H) **MALDI-TOF:** Obtained: $[\text{M}+\text{Na}]^+$ 637.52; $[\text{M}+\text{K}]^+$ 653.47
Calculated: 614.70 Da

C3. Synthesis of GFLG-DOX by Conjugation of DOX to GLFG-Fmoc followed by deprotection of Fmoc



Scheme C2. A) Conjugation of DOX to GLFG-Fmoc to form DOX-GLFG-Fmoc, **B)** Deprotection of Fmoc from DOX-GLFG-Fmoc to form DOX-GLFG. EDC: (1-(3-Dimethylaminopropyl)-3-ethylcarbodiimide hydrochloride DIPEA: N,N-Diisopropylethylamine, DMF: dimethylformamide.

Conjugation of GFLG-DOX can be seen in Scheme B2. To conjugate DOX to the GLFG-Fmoc peptide, 30 mg (0.05 mmol) of GLFG-Fmoc, 10.4 mg (0.075 mmol) of 4-Nitrophenol were dissolved in 2 ml of DMF and cooled down to $\sim 0^{\circ}\text{C}$ using ice/water bath. 14.37 mg (0.075 mmol) EDC in 200 μL of DMF was added dropwise to the reaction and left to react stirring at $\sim 0^{\circ}\text{C}$ for 30 min. The reaction was then allowed to reach room temperature and allowed to react for an additional 12 h. After 12 h, the reaction was again cooled down to $\sim 0^{\circ}\text{C}$ using an ice/water bath in which 34.8 mg (0.06 mmol) of DOX dissolved in 500 μl of DMF and added to the reaction followed by the addition of 10 μl (0.06 mmol) of DIPEA. The reaction was allowed to stir for an additional 48 h. After the

20.19 mg (5.5 μmol) Acet-G5-OH was reacted with 62.76 mg (550.0 μmol) of GA with 104.8 μl (616.2 μmol) of DIPEA in 1.5 ml of DMF and allowed to stir at room temperature for 24 h to form Acet-G5-GA dendron. Following the reaction, the Acet-G5-GA product was purified by the removal of DMF solvent by vacuum followed by dialysis against DMSO using Spectra/Por[®] 7 RC membrane dialysis tubing (MWCO = 1 kDa, Spectrum Laboratories, Inc., Rancho Dominguez, CA, USA) for two days. The product was removed from dialysis and DMSO solvent removed by vacuum, redissolved in 1xPBS (pH = 7.4) and filtered using Amicon Ultra-15 centrifugal filter (NMWL = 3,000, MilliporeSigma, Burlington, MA, USA) against 1xPBS followed by DI water. The product was then collected from the Amicon filter, frozen, and lyophilized in freeze dryer (Labconco, Kansas City, MO, USA) to obtain white powder. The Acet-G5-GA product was characterized by MALD-TOF and ¹H NMR (Figure C1). **Acet-G5-GA:** ¹H-NMR (D₂O, 400MHz, ppm): δ 4.29-4.23 (m, 124H), 2.37 (t, 64H, J=7x(2)), 2.17 (t, 64H J=7.2x(2)), 1.78 (t, 64H J=7.2x(2)) 1.30-1.24 (m, 93H). MALDI-TOF MS: 7329.0.

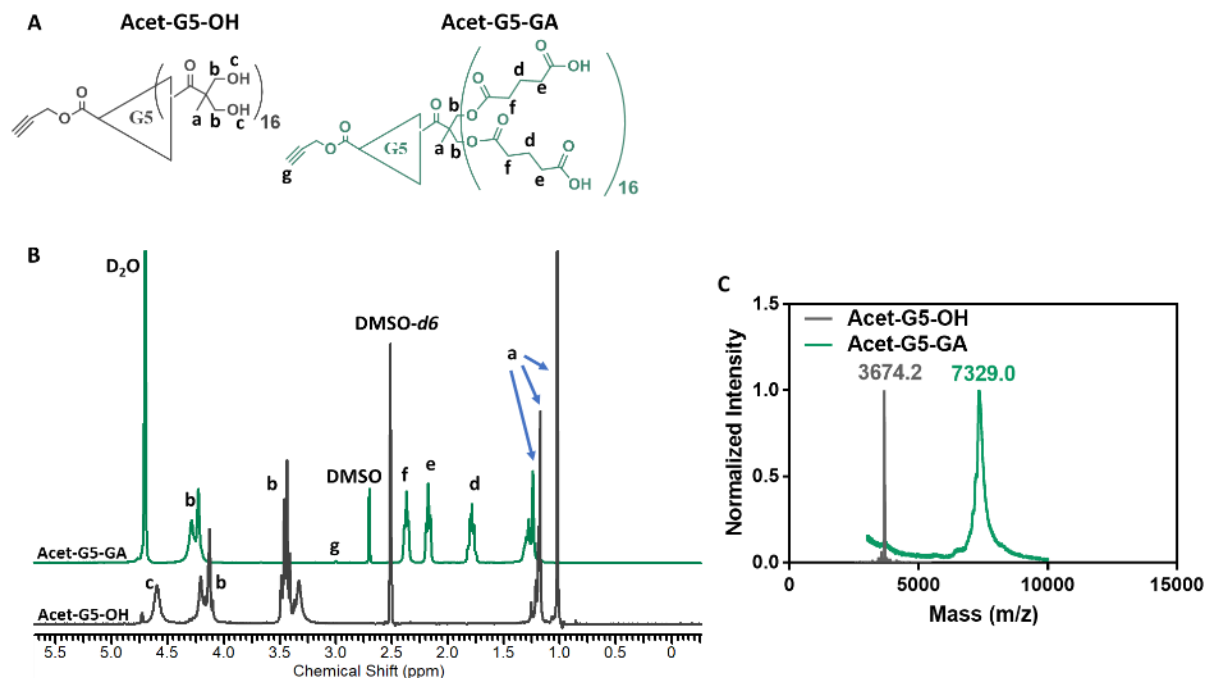
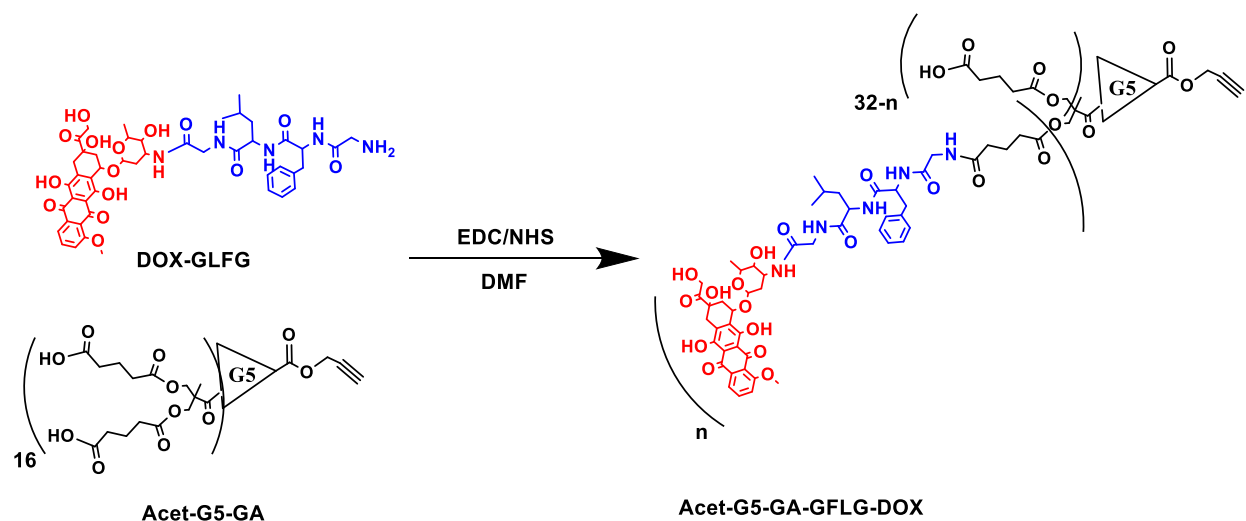


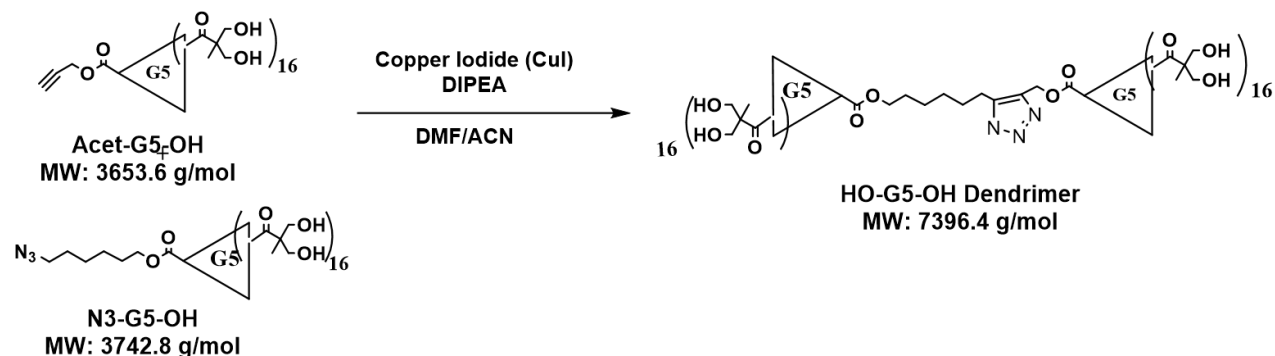
Figure C1. A) Chemical structure of Acet-G5-OH and Acet-G5-GA and the corresponding B) ^1H NMR and C) MALDI-TOF spectra.



Scheme C4. Conjugation of DOX-GLFG to Acet-G5-GA dendron to form Acet-G5-GA-GFLG-DOX dendron. EDC: (1-(3-Dimethylaminopropyl)-3-ethylcarbodiimide hydrochloride) NHS: N-Hydroxysuccinimide, DMF: dimethylformamide.

C5. Azide/Alkyne Click Chemistry of Acet-G5-OH and N₃-G5-OH dendrons to form (OH)₃₂-[G5]-[G5]-(OH)₃₂ dendrimer.

Formation of Polyester dendrimer from dendrons using click chemistry is described in Scheme B5.



Scheme C5. Conjugation of HO-G₅-OH dendrimer from to Acet-G₅-OH and N₃-G₅-OH dendrons utilizing copper click chemistry. DIPEA: N,N-Diisopropylethylamine, DMF: dimethylformamide, ACN: Acetonitrile.

5.33 mg (1.42 μmol) of Azide (Polyester bis-MPA dendron, 32 hydroxyl, 1 azide, generation 5, 95%) (N₃-G₅-OH) and 5.01 mg (1.37 μmol) of Acetylene (Polyester-32-hydroxyl-1-acetylene bis-MPA dendron, generation 5, 97%) (Acet-G₅-OH) were added with 8.53 mg (44.79 μmol) of copper (I) iodide and 1.16 μl (6.82 μmol) of N,N-Diisopropylethylamine (DIPEA) with 40 μl of degassed, anhydrous DMF and 400 μl of acetonitrile and put on thermal mixer (ThermoFisher Scientific) shaking at 1400 rpm, 80°C, overnight followed by 50°C for an additional 24 h. After the additional 24 h, the acetonitrile was removed by airflow followed by the removal of DMF by high vacuum. The product was then dissolved in 250 μl of 1xPBS (pH 7.4) and centrifuged to pellet excess copper iodide (1400 rpm, 2 min at 20°C), then loaded into 0.7 x 50 cm Econo-Column Chromatography Column (Bio-Rad) containing Bio-Gel P-10 Gel (2 g) in which fractions were collected and analyzed by MALDI-TOF. Fractions were combined, and the final

product characterized by MALDI-TOF (Figure C2). **(OH)₃₂-[G5]-[G5]-(OH)₃₂ dendrimer:**

MALDI-TOF MS, mass (m/z): 7393.9 LS ζ -potential: -31 ± 7 mV

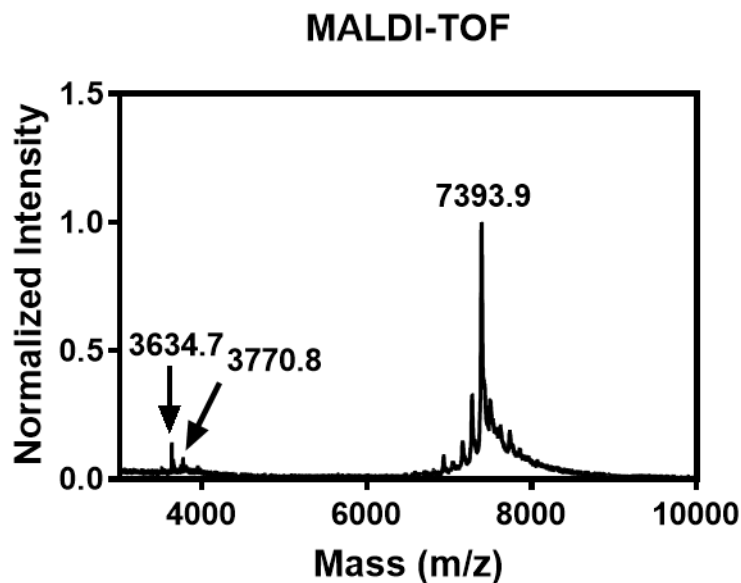
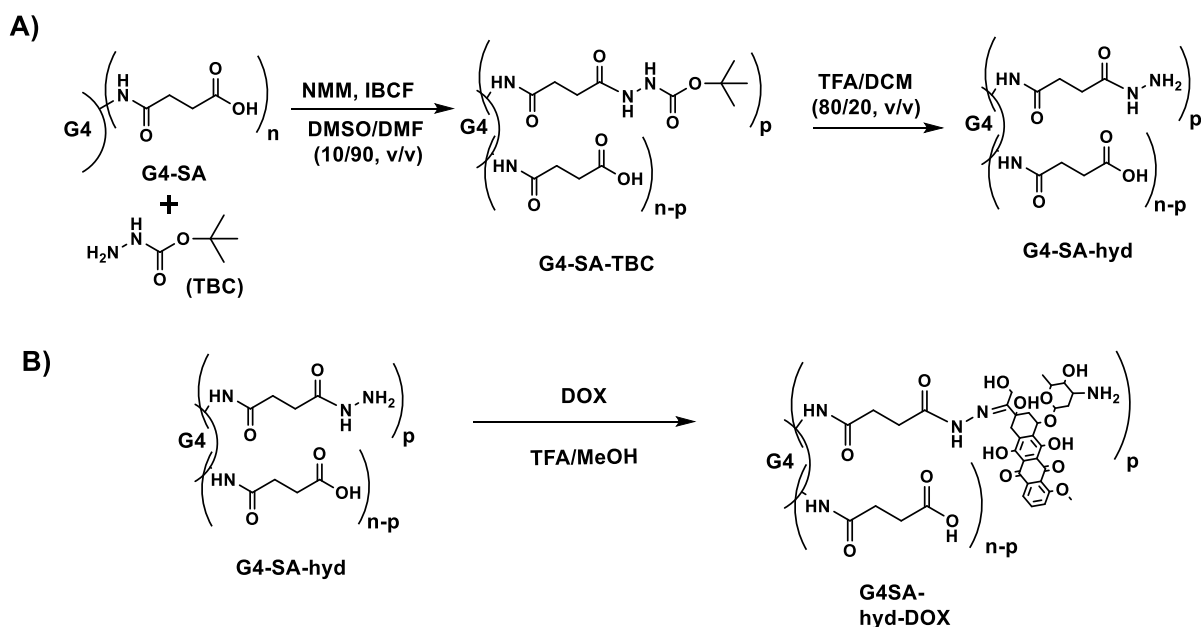


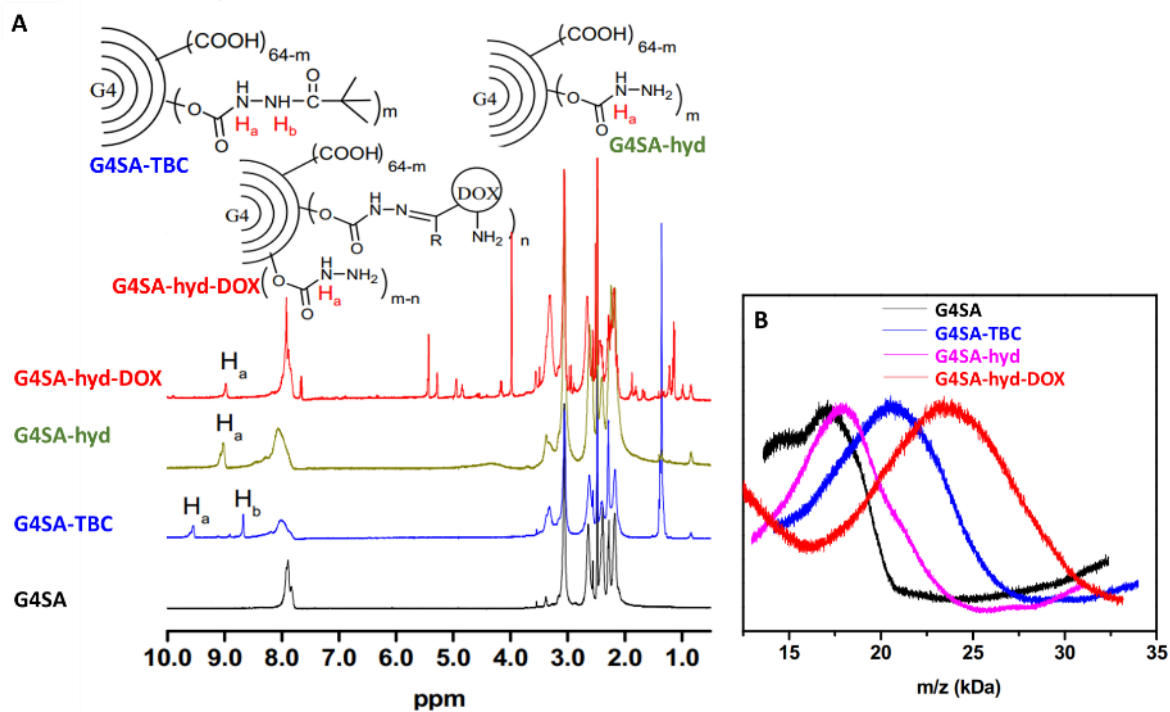
Figure C2. MALDI-TOF of purified HO-G5-OH dendrimer after size exclusion chromatography. The expected MW (7393.9) as determined found for dendrimer while only very insignificant amount of dendrons remained in the product (Acet-G5-OH – 3634.7, N₃-G5-OH – 3770.8).

APPENDIX D

SUPPORTING INFORMATION FOR CHAPTER 6



Scheme D1. A) Synthesis of hydrazine bond to the G4SA PAMAM dendrimer. TBC is added to G4SA by addition of NMM and IBCF in DMSO/DMF (10/90, v/v) followed by Boc deprotection by exposure to TFA/DCM (80/20, v/v). **B)** DOX addition by hydrazone bond was completed with TFA as acid catalyst and MeOH as solvent. G4SA: Generation 4 PAMAM succinamic acid surface dendrimer DMSO: dimethylsulfoxide DMF: dimethylformamide TBC: tert-butyl carbazate NMM: N-Methylmorpholine IBCF: isobutyl chloroformate TFA: trifluoroacetic acid DCM: dichloromethane MeOH: methanol DOX: doxorubicin.



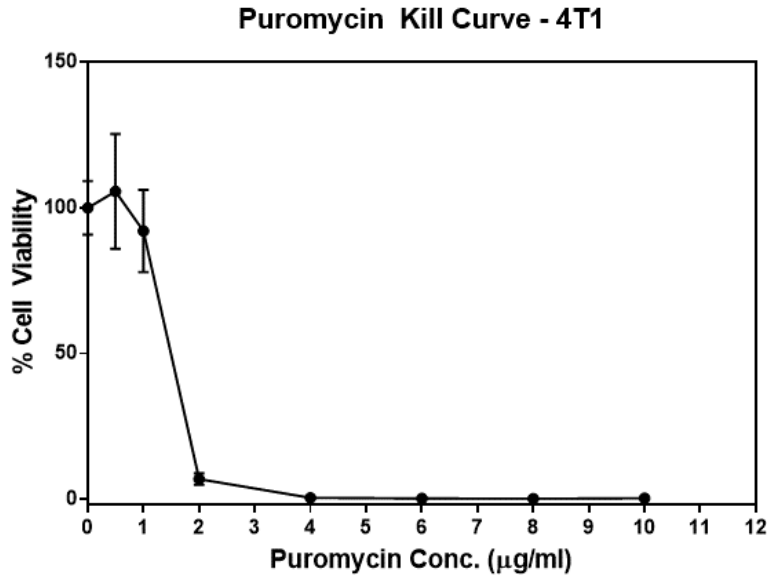


Figure D2. Puromycin kill curve. 4T1 cells were exposed to various concentrations of puromycin (0-10 µg/ml) for 48 hours to determine the minimum amount of puromycin to kill all 4T1 cells.

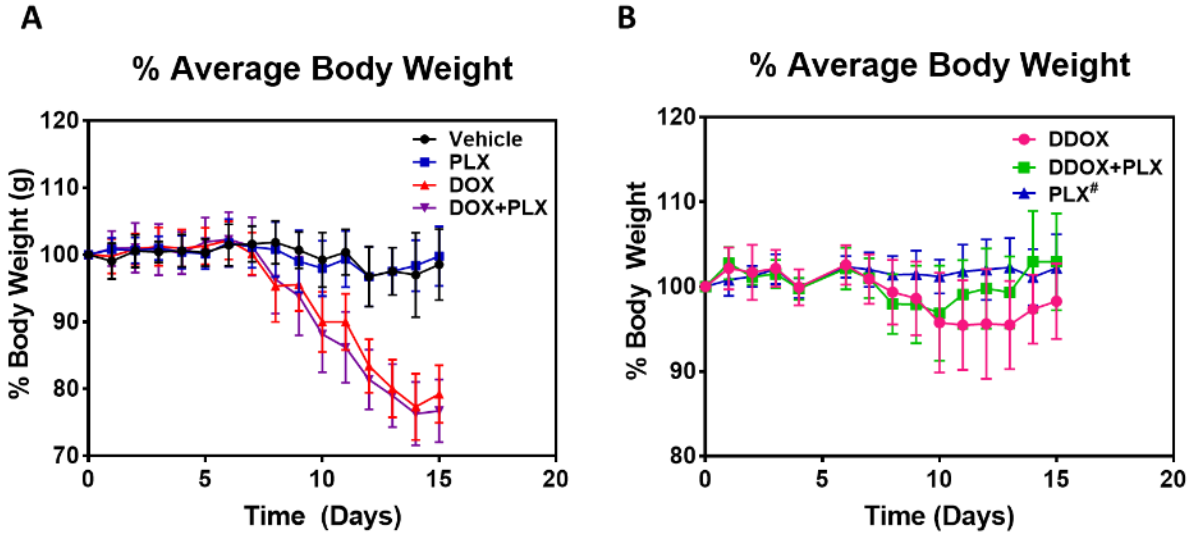


Figure D3. % Average body weight of mice for **A)** first experimental group in which all drugs administered were given pulmonary route and **B)** second experimental group in which DDOX and DDOX+PLX groups were given pulmonary route and PLX# was given IV route.

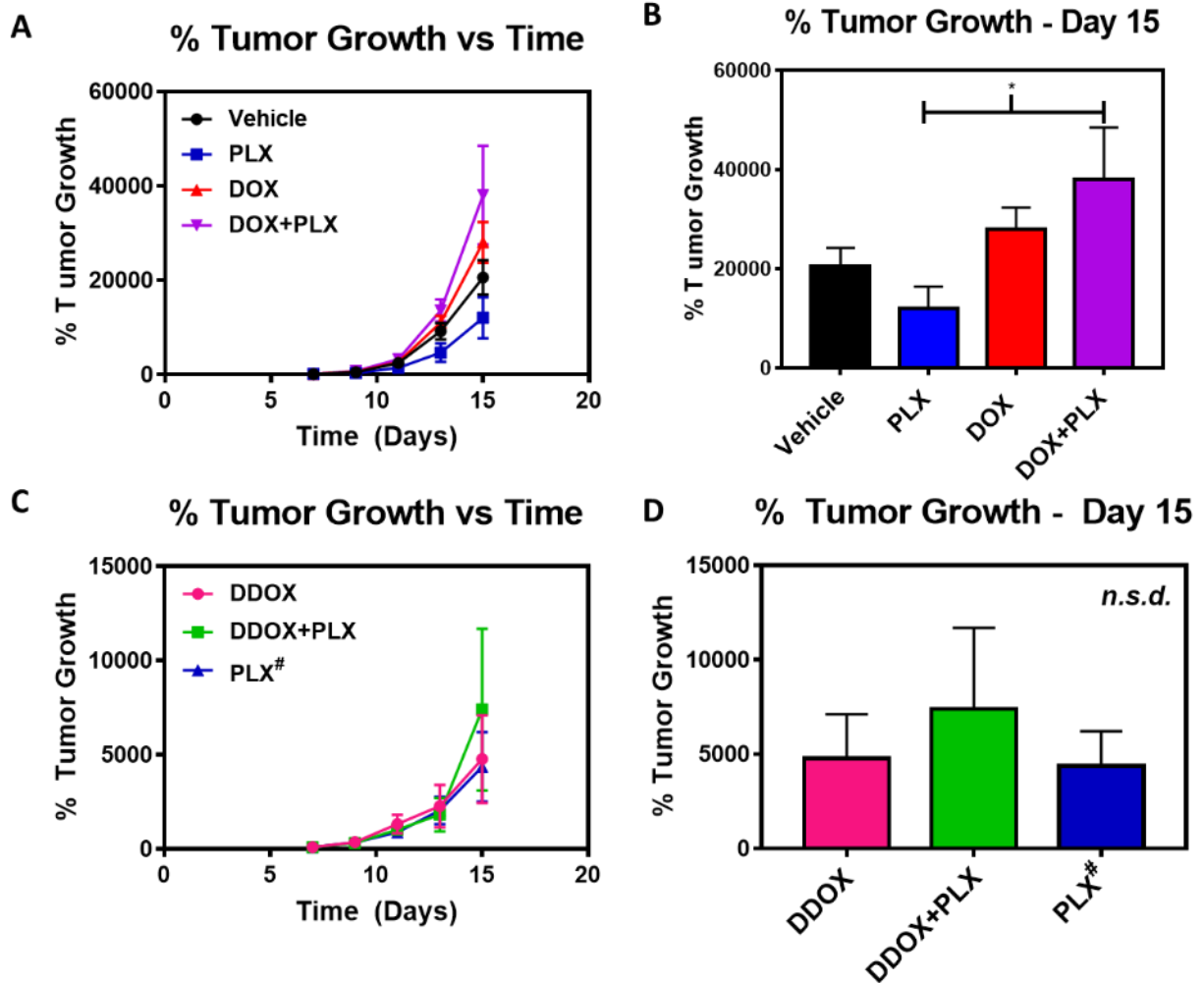


Figure D4. Evaluation of lung tumor burden by *in vivo* imaging of mice near lung region using IVIS. **A) & C)** % Tumor growth rate over time. Day 7 total flux from *in vivo* IVIS images was normalized to 100% for each mouse. **B & D)** The corresponding % Tumor growth *in vivo* on Day 15 – final day of experiment imaged on two sides for each group as evaluated from IVIS images, * $p < 0.05$. All drugs were given via pulmonary route except PLX# group seen in D) in which PLX was delivered IV route.

Table D1. p-values calculated after One-Way ANOVA by Tukey's Multiple Comparison ($n \geq 6$) for % tumor growth seen on Day 15 post tumor inoculation.

Group	p-value
Vehicle vs. PLX	0.7766
Vehicle vs. DOX	0.8260
Vehicle vs. DOX+PLX	0.2276
PLX vs. DOX	0.2762
PLX vs. DOX+PLX	0.0329
DOX vs. DOX+ PLX	0.6592
DDOX vs. DDOX+PLX	0.2681
DDOX vs. PLX [#]	0.9629
DDOX+PLX vs. PLX [#]	0.1798

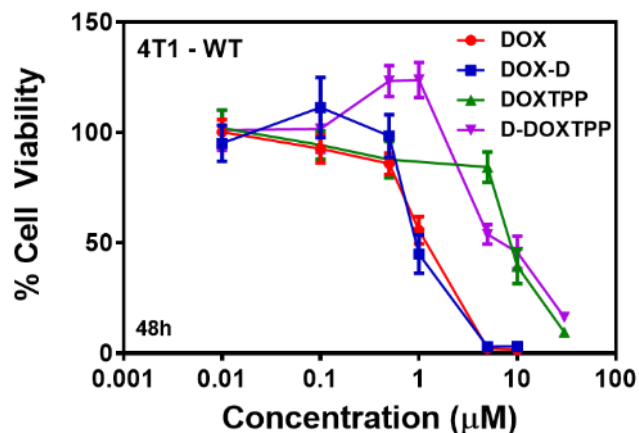


Figure D5. % Cell viability (measured by MTT) of doxorubicin and modified doxorubicin formulations against 4T1-WT cells after 48-hour incubation. DOX= doxorubicin, DDOX= PAMAM G4COOH-DOX conjugate, DOXTPP = Triphenylphosphonium-modified doxorubicin, DDOXTPP = PAMAM G4COOH-DOXTPP conjugate.

Table D2. IC₅₀ values of drugs when tested against 4T1-WT cells line. This was conducted after 48 h incubation and measured by MTT. DOX= doxorubicin, DDOX= PAMAM G4COOH-DOX conjugate, DOXTPP = Triphenylphosphonium-modified doxorubicin, DDOXTPP = PAMAM G4COOH-DOXTPP conjugate.

Drug	IC ₅₀ Value (μM)
DOX	1.12
DDOX	0.96
DOXTPP	8.53
DDOXTPP	4.40

APPENDIX E

PUBLICATION 1

Effect of the Conjugation Density of Triphenylphosphonium Cation on the Mitochondrial Targeting of Poly(amidoamine) Dendrimers

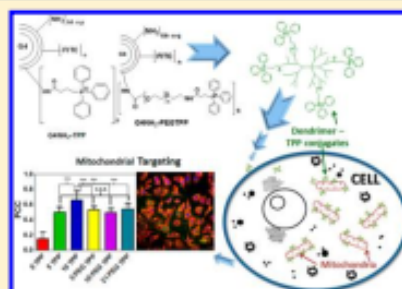
Elizabeth R. Bielski, Qian Zhong, Matthew Brown, and Sandro R. P. da Rocha*

Department of Chemical Engineering and Materials Science, Wayne State University, Detroit, Michigan 48202, United States

Supporting Information

ABSTRACT: Many clinically relevant diseases with known poor therapeutic outcomes, including cancer and neurodegenerative disorders, have been directly linked to mitochondrial dysfunction. The ability to efficiently target therapeutics to intracellular organelles such as mitochondria may represent new opportunities for the effective treatment of such ailments. The present study reports the synthesis, cellular uptake, cytotoxicity, and mitochondrial colocalization of conjugates of triphenylphosphonium cation (TPP) to amine-terminated, generation 4, poly(amidoamine) (PAMAM) dendrimer (G4NH₂) nanocarriers. The mitochondrial-targeting moiety TPP was either directly conjugated to G4NH₂ (G4NH₂-TPP) or to the dendrimer through a flexible polyethylene glycol (PEG) linker (G4NH₂-PEGTPP). Conjugation was done at various TPP densities to assess their biological activity and potential for mitochondrial-targeted drug delivery. Tests in an *in vitro* model of the human alveolar carcinoma (A549 cells) showed that even at a low TPP density (~5 TPP) both the cellular internalization and mitochondrial targeting increase significantly, as determined by fluorescence activated cell sorting (FACS) and confocal microscopy (CM), respectively. At a density of ~10 TPP per G4NH₂, further increase in cellular internalization and mitochondrial targeting was achieved. However, at this higher density, the nanocarriers also showed pronounced cytotoxicity. It was observed that the toxicity of the conjugates is decreased upon the addition of a PEG linker between the dendrimer and TPP (G4NH₂-PEGTPP), while the mitochondrial targeting ability of the nanocarriers is not affected as the PEG density increases. The proposed strategies indicate that TPP-conjugated G4NH₂ dendrimers represent a potentially viable strategy for the targeting of therapeutic molecules to mitochondria, which may help improve therapeutic outcomes of diseases related to mitochondrial dysfunction.

KEYWORDS: mitochondrial targeting, PAMAM dendrimers, polyethylene glycol, PEG, triphenylphosphonium cation, TPP, drug delivery



1. INTRODUCTION

Mitochondria are responsible for maintaining cellular homeostasis and producing cellular energy (adenosine triphosphate, ATP) via oxidative phosphorylation.^{1,2} They are also key players in the production of reactive oxygen species as well as regulating calcium homeostasis and the intrinsic apoptotic pathway.^{3,4} Mitochondria are organelles of great relevance in a variety of important highly energy-dependent tissues, including brain, heart, and muscle.^{1,5} As a consequence, mitochondrial dysfunction has been linked to a range of diseases in these tissues (and others) including neurodegenerative and neuromuscular disorders, cancer, ischemia-reperfusion injury, metabolic diseases such as diabetes and obesity, chronic autoimmune inflammatory diseases, kidney and liver diseases, and aging.^{1,3,6–10} In spite of the clinical relevance of these mitochondrial-related diseases many still lack effective therapeutic options.^{1,11} The ability to design mitochondrial-targeting systems may therefore provide valuable alternative strategies to enhance therapeutic outcomes of mitochondrial-

related diseases while at the same time minimizing side effects associated with the therapeutic molecules.¹²

One major class of mitochondrial-targeting molecules is delocalized lipophilic cations (DLCs). Triphenylphosphonium cation (TPP),^{1,3} one of the most common DLCs, has been shown to accumulate preferentially at the inner mitochondrial membrane,³ at concentrations approximately 5–10-fold greater in the cytoplasm compared to the extracellular environment, with a further accumulation of hundreds of times within the mitochondria when compared to the cytoplasm.⁵ The colocalization efficiency of TPP with the mitochondria is related to its lipophilic nature and delocalized positive charge, which allows TPP to permeate through membrane bilayers (hydrophobic) that have large negative potentials such as that of the mitochondria: 150–180 mV.^{13,14} The unique properties

Received: April 23, 2015

Revised: June 19, 2015

Accepted: July 9, 2015

Published: July 9, 2015

APPENDIX F

PUBLICATION 2

Conjugation to Poly(amidoamine) Dendrimers and Pulmonary Delivery Reduce Cardiac Accumulation and Enhance Antitumor Activity of Doxorubicin in Lung Metastasis

Qian Zhong,[†] Elizabeth R. Bielski,[†] Leonan S. Rodrigues,[†] Matthew R. Brown,[†] Joshua J. Reineke,[‡] and Sandro R. P. da Rocha^{*,†,§}

[†]Department of Chemical Engineering and Materials Science, College of Engineering, Wayne State University, 5050 Anthony Wayne Drive, Detroit, Michigan 48202, United States

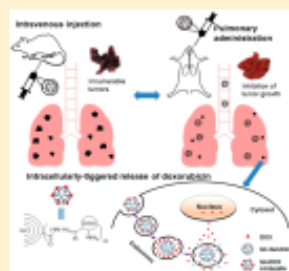
[‡]Department of Pharmaceutical Sciences, College of Pharmacy, South Dakota State University, Brookings, South Dakota 57007, United States

[§]Department of Pharmaceutics, College of Pharmacy, and Department of Chemical and Life Science Engineering, Virginia Commonwealth University, Richmond, Virginia 23298, United States

S Supporting Information

ABSTRACT: Lung is one of the most common sites to which almost all other primary tumors metastasize. The major challenges in the chemotherapy of lung metastases include the low drug concentration found in the tumors and high systemic toxicity upon systemic administration. In this study, we combine local lung delivery and the use of nanocarrier-based systems for improving pharmacokinetics and biodistribution of the therapeutics to fight lung metastases. We investigate the impact of the conjugation of doxorubicin (DOX) to carboxyl-terminated poly(amidoamine) dendrimers (PAMAM) through a bond that allows for intracellular-triggered release, and the effect of pulmonary delivery of the dendrimer–DOX conjugate in decreasing tumor burden in a lung metastasis model. The results show a dramatic increase in efficacy of DOX treatment of the melanoma (B16-F10) lung metastasis mouse model upon pulmonary administration of the drug, as indicated by decreased tumor burden (lung weight) and increased survival rates of the animals (male C57BL/6) when compared to iv delivery. Conjugation of DOX further increased the therapeutic efficacy upon lung delivery as indicated by the smaller number of nodules observed in the lungs when compared to free DOX. These results are in agreement with the biodistribution characteristics of the DOX upon pulmonary delivery, which showed a longer lung accumulation/retention compared to iv administration. The distribution of DOX to the heart tissue is also significantly decreased upon pulmonary administration, and further decreased upon conjugation. The results show, therefore, that pulmonary administration of DOX combined to conjugation to PAMAM dendrimer through an intracellular labile bond is a potential strategy to enhance the therapeutic efficacy and decrease systemic toxicity of DOX.

KEYWORDS: Polyamidoamine dendrimer, doxorubicin, pulmonary delivery, lung cancer, controlled intracellular release, cardiac toxicity



1. INTRODUCTION

Cancer is the second most common cause of death for both men and women in the United States, second only to heart diseases.¹ Among the many malignant tumors, lung cancers are the leading cause of death. More patients die from lung cancers than breast, pancreatic, and prostate cancers combined.² Although curative surgery is the first choice in the clinic for treating primary lung tumors, chemotherapy plays a vital role in inhibiting tumor growth after surgery, partly due to the high rates of recurrence.^{3,4} Additionally, the lungs are the most common site for metastasis for almost all other primary tumors.⁵ Metastatic tumors are also associated with more than 90% of cancer-related deaths.⁶ The development of new strategies that can help improve chemotherapeutic outcomes

during the treatment of lung metastasis may have, therefore, a significant societal impact.

One of the major challenges limiting the success of systemically administered chemotherapeutics in the treatment of lung metastases is the low concentration of anticancer agents in the lung tissue and lung tumor.^{7–9} Upon systemic administration, such as intravenous injection (iv), only a few percent of the total dose (TD) (<ca. 4%) actually reaches the tumor site.⁹ Because of typical systemic toxicity of anticancer

Received: February 14, 2016

Revised: May 25, 2016

Accepted: June 2, 2016

Published: June 2, 2016

APPENDIX G

PUBLICATION 3

International Journal of Pharmaceutics 527 (2017) 171–183



Contents lists available at ScienceDirect

International Journal of Pharmaceutics

journal homepage: www.elsevier.com/locate/ijpharm

TPP-dendrimer nanocarriers for siRNA delivery to the pulmonary epithelium and their dry powder and metered-dose inhaler formulations



Elizabeth Bielski^{a,c}, Qian Zhong^{a,c}, Hamad Mirza^a, Matthew Brown^a, Ashura Molla^a,
Teresa Carvajal^b, Sandro R.P. da Rocha^{a,c,*}

^a Department of Chemical Engineering and Materials Science, Wayne State University, Detroit, MI, 48202, USA

^b Department of Agricultural & Biological Engineering, Purdue University, West Lafayette, IN, 47907, USA

^c Department of Pharmaceutics, School of Pharmacy & Department of Chemical and Life Science Engineering, School of Engineering, Virginia Commonwealth University, Richmond, VA, 23284, USA

ARTICLE INFO

Article history:

Received 11 January 2017

Received in revised form 5 May 2017

Accepted 21 May 2017

Available online 23 May 2017

Keywords:

PAMAM dendrimers

Dendriplexes

Triphenylphosphonium (TPP) ion

Short interfering RNA (siRNA)

Inhalation therapy

Pressurized metered dose inhalers (pMDIs)

Dry powder inhalers (DPIs)

ABSTRACT

The regulation of genes utilizing the RNA interference (RNAi) mechanism via the delivery of synthetic siRNA has great potential in the treatment of a variety of lung diseases. However, the delivery of siRNA to the lungs is challenging due to the poor bioavailability of siRNA when delivered intravenously, and difficulty in formulating and maintaining the activity of free siRNA when delivered directly to the lungs using inhalation devices. The use of non-viral vectors such as cationic dendrimers can help enhance the stability of siRNA and its delivery to the cell cytosol. Therefore, in this work, we investigate the ability of a triphenylphosphonium (TPP) modified generation 4 poly(amidoamine) (PAMAM) dendrimer (G4NH₂-TPP) to enhance the *in vitro* transfection efficiency of siRNA in a model of the pulmonary epithelium and their aerosol formulations in pressurized metered dose inhalers (pMDIs) and dry powder inhalers (DPIs). Complexes of siRNA and G4NH₂-TPP were prepared with varying TPP densities and increasing N/P ratios. The complexation efficiency was modulated by the presence of the TPP on the dendrimer surface, allowing for a looser complexation compared to unmodified dendrimer as determined by gel electrophoresis and polyanion competition assay. An increase in TPP density and N/P ratio led to an increase in the *in vitro* gene knockdown of stably green fluorescent protein (eGFP) expressing lung alveolar epithelial (A549) cells. G4NH₂-12TPP dendriplexes (G4NH₂ PAMAM dendrimers containing 12 TPP molecules on the surface complexed with siRNA) at N/P ratio 30 showed the highest *in vitro* gene knockdown efficiency. To assess the potential of TPP-dendriplexes for pulmonary use, we also developed micron particle technologies for both pMDIs and DPIs and determined their aerosol characteristics utilizing an Andersen Cascade Impactor (ACI). Mannitol microparticles encapsulating 12TPP-dendriplexes were shown to be effective in producing aerosols suitable for deep lung deposition for both pMDI formulations (fine particle fraction of 50–53%) and DPI formulations (fine particle fraction of 39%) with no impact on the *in vitro* gene knockdown efficiency of the siRNA. This work demonstrates the potential benefits of utilizing TPP-conjugated dendrimers in the formation of dendriplexes for siRNA delivery to the pulmonary epithelium and their aerosol formulation for local delivery to the lungs using portable inhalers.

© 2017 Elsevier B.V. All rights reserved.

Abbreviations: RNAi, RNA interference; siRNA, short interfering RNA; PAMAM, poly(amidoamine); G4NH₂, generation 4 amine-terminated PAMAM dendrimer; TPP, triphenylphosphonium(3-carboxypropyl)triphenylphosphonium bromide; pMDIs, pressurized metered dose inhalers; HFAs, hydrofluoroalkanes; DPI, dry powder inhaler; ACI, Anderson cascade impactor; GFP, green fluorescent protein; LS, light scattering; RF, respirable fraction; FPF, fine particle fraction; MMAD, mean mass aerodynamic diameter; GSD, geometric standard deviation; ED, emitted dose; SEM, scanning electron microscopy.

* Corresponding author at: Department of Pharmaceutics, School of Pharmacy & Department of Chemical and Life Science Engineering, School of Engineering, Virginia Commonwealth University, Smith Building, 4th Floor, Room 450A, 410 North 12th Street, P.O. Box 980533, Richmond, VA 23298-0533, USA.

E-mail addresses: srdarocha@vcu.edu, darochasdr@gmail.com (S.R.P. da Rocha).

<http://dx.doi.org/10.1016/j.ijpharm.2017.05.046>
0378-5173/© 2017 Elsevier B.V. All rights reserved.

REFERENCES

1. GLOBOCAN Lung Cancer: Estimated Incidence, Mortality and Prevalence Worldwide in 2012. http://globocan.iarc.fr/Pages/fact_sheets_cancer.aspx?cancer=lung
2. Siegel, R. L.; Miller, K. D.; Jemal, A. Cancer statistics, 2018. *CA: a cancer journal for clinicians* **2018**, 68, (1), 7-30.
3. Howlader N, N. A., Krapcho M, Miller D, Bishop K, Kosary CL, Yu M, Ruhl J, Tatalovich Z, Mariotto A, Lewis DR, Chen HS, Feuer EJ, Cronin KA (eds). SEER Cancer Statistics Factsheets: Lung and Bronchus Cancer. . <https://seer.cancer.gov/statfacts/html/lungb.html> (April 18, 2018),
4. Pore, M. M.; Hiltermann, T. J. N.; Kruyt, F. A. E. Targeting apoptosis pathways in lung cancer.(Report). *Cancer Letters* **2013**, (2), 359-368.
5. Howlader N, N. A., Krapcho M, Garshell J, Neyman N, Altekruse SF, Kosary CL, Yu M, Ruhl J, Tatalovich Z, Cho H, Mariotto A, Lewis DR, Chen HS, Feuer EJ, Cronin KA (eds). SEER Cancer Statistics Review, 1975-2010. http://seer.cancer.gov/csr/1975_2010/ (March 15),
6. Schwartz, D. S. Secondary Lung Tumors. <https://emedicine.medscape.com/article/426820-overview> (April 18, 2018),
7. Minn, A. J.; Gupta, G. P.; Siegel, P. M.; Bos, P. D.; Shu, W.; Giri, D. D.; Viale, A.; Olshen, A. B.; Gerald, W. L.; Massague, J. Genes that mediate breast cancer metastasis to lung. *Nature* **2005**, 436, (7050), 518-524.
8. Schroeder, A.; Heller, D. A.; Winslow, M. M.; Dahlman, J. E.; Pratt, G. W.; Langer, R.; Jacks, T.; Anderson, D. G. Treating metastatic cancer with nanotechnology. *Nature Reviews Cancer* **2012**, (1), 39.

9. Bao, L.; Haque, A.; Jackson, K.; Hazari, S.; Moroz, K.; Jetly, R.; Dash, S. Increased Expression of P-Glycoprotein Is Associated with Doxorubicin Chemoresistance in the Metastatic 4T1 Breast Cancer Model. *The American Journal of Pathology* **2011**, *178*, (2), 838-852.
10. Weigelt, B.; Peterse, J. L.; Van't Veer, L. J. Breast cancer metastasis: markers and models. *Nature reviews cancer* **2005**, *5*, (8), 591.
11. Babu, A. Nanoparticle-Based Drug Delivery for Therapy of Lung Cancer: Progress and Challenges. *Journal of nanomaterials* **2013**, *53*, (2), 1-11.
12. Metastatic Cancer. <https://www.cancer.gov/types/metastatic-cancer> (May 18, 2018),
13. Ettinger, D. S.; Akerley, W.; Bepler, G.; Blum, M. G.; Chang, A.; Cheney, R. T.; Chirieac, L. R.; D'Amico, T. A.; Demmy, T. L.; Ganti, A. K. P. Non-small cell lung cancer. *Journal of the national comprehensive cancer network* **2010**, *8*, (7), 740-801.
14. Alteri, R., Mamta Kalidas, Lynn Gadd, Tracy Wyant Chemotherapy for Non-Small Cell Lung Cancer. <https://www.cancer.org/cancer/non-small-cell-lung-cancer/treating/chemotherapy.html> (May 15),
15. Alteri, R., Mamta Kalidas, Lynn Gadd, Tracy Wyant Treatment of Breast Cancer by Stage. <https://www.cancer.org/cancer/breast-cancer/treatment/treatment-of-breast-cancer-by-stage.html> (May 18),
16. Martin, L. J. Types of Breast Cancer. <https://www.webmd.com/breast-cancer/guide/breast-cancer-types-er-positive-her2-positive#2> (May 18),

17. Postow, M. A.; Sidlow, R.; Hellmann, M. D. Immune-related adverse events associated with immune checkpoint blockade. *New England Journal of Medicine* **2018**, *378*, (2), 158-168.
18. Drake, C. G.; Lipson, E. J.; Brahmer, J. R. Breathing new life into immunotherapy: review of melanoma, lung and kidney cancer. *Nature reviews Clinical oncology* **2014**, *11*, (1), 24.
19. Anichini, A.; Tassi, E.; Grazia, G.; Mortarini, R. The non-small cell lung cancer immune landscape: emerging complexity, prognostic relevance and prospective significance in the context of immunotherapy. *Cancer Immunol Immunother* **2018**, *67*, (6), 1011-1022.
20. Cannarile, M. A.; Weisser, M.; Jacob, W.; Jegg, A.-M.; Ries, C. H.; Rüttinger, D. Colony-stimulating factor 1 receptor (CSF1R) inhibitors in cancer therapy. *Journal for immunotherapy of cancer* **2017**, *5*, (1), 53.
21. Ventola, C. L. Cancer Immunotherapy, Part 3: Challenges and Future Trends. *Pharmacy and Therapeutics* **2017**, *42*, (8), 514-521.
22. Holohan, C.; Van Schaeybroeck, S.; Longley, D. B.; Johnston, P. G. Cancer drug resistance: an evolving paradigm. *Nature Reviews Cancer* **2013**, *13*, (10), 714.
23. Bar-Zeev, M.; Livney, Y. D.; Assaraf, Y. G. Targeted nanomedicine for cancer therapeutics: Towards precision medicine overcoming drug resistance. *Drug Resistance Updates* **2017**, *31*, 15-30.
24. Cree, I. A.; Charlton, P. Molecular chess? Hallmarks of anti-cancer drug resistance. *BMC Cancer* **2017**, *17*, (1), 10.

25. Nie, S. Nanotechnology Applications in Cancer. *Annual review of biomedical engineering* **2007**, 9, (1), 257-288.
26. Caster, J. M.; Patel, A. N.; Zhang, T.; Wang, A. Investigational nanomedicines in 2016: a review of nanotherapeutics currently undergoing clinical trials. *Wiley Interdisciplinary Reviews: Nanomedicine and Nanobiotechnology* **2017**, 9, (1).
27. De Rosa, G. Nanotechnologies in Cancer. *Journal of drug delivery* **2013**, 2013, 1-3.
28. Patra, H. K. The potential legacy of cancer nanotechnology: cellular selection. *Trends in biotechnology (Regular ed.)* **2014**, 32, (1), 21-31.
29. Gao, Z.; Zhang, L.; Sun, Y. Nanotechnology applied to overcome tumor drug resistance. *J. Control. Release* **2012**, 162, (1), 45-55.
30. Breunig, M.; Bauer, S.; Goefferich, A. Polymers and nanoparticles: Intelligent tools for intracellular targeting? *Eur. J. Pharm. Biopharm.* **2008**, 68, (1), 112-128.
31. Ferrari, M. Cancer nanotechnology: opportunities and challenges. *Nature reviews. Cancer* **2005**, 5, (3), 161.
32. Cheng, Y.; Wang, J.; Rao, T.; He, X.; Xu, T. Pharmaceutical applications of dendrimers: promising nanocarriers for drug delivery. *Frontiers in bioscience : a journal and virtual library* **2008**, 13, 1447-1471.
33. Biswas, S. Surface conjugation of triphenylphosphonium to target poly(amidoamine) dendrimers to mitochondria. *Biomaterials* **2012**, 33, (18), 4773-4782.
34. Kurtoglu, Y. E. Drug release characteristics of PAMAM dendrimer–drug conjugates with different linkers. *Int. J. Pharm.* **2010**, 384, (1-2), 189-194.

35. Bharali, D. J.; Khalil, M.; Gurbuz, M.; Simone, T. M.; Mousa, S. A. Nanoparticles and cancer therapy: A concise review with emphasis on dendrimers. *International Journal of Nanomedicine* **2009**, *4*, (1), 1-7.
36. Cheng, Y. The effect of dendrimers on the pharmacodynamic and pharmacokinetic behaviors of non-covalently or covalently attached drugs. *European journal of medicinal chemistry* **2008**, *43*, (11), 2291-2297.
37. Kesharwani, P.; Iyer, A. K. Recent advances in dendrimer-based nanovectors for tumor-targeted drug and gene delivery. *Drug discovery today* **2015**, *20*, (5), 536-547.
38. Feliu, N.; Walter, M. V.; Montañez, M. I.; Kunzmann, A.; Hult, A.; Nyström, A.; Malkoch, M.; Fadeel, B. Stability and biocompatibility of a library of polyester dendrimers in comparison to polyamidoamine dendrimers. *Biomaterials* **2012**, *33*, (7), 1970-1981.
39. Gillies, E. R.; Dy, E.; Fréchet, J. M.; Szoka, F. C. Biological evaluation of polyester dendrimer: poly (ethylene oxide)“bow-tie” hybrids with tunable molecular weight and architecture. *Mol. Pharm.* **2005**, *2*, (2), 129-138.
40. Lee, C. C.; Gillies, E. R.; Fox, M. E.; Guillaudeu, S. J.; Fréchet, J. M. J.; Dy, E. E.; Szoka, F. C. A single dose of doxorubicin-functionalized bow-tie dendrimer cures mice bearing C-26 colon carcinomas. *Proceedings of the National Academy of Sciences* **2006**, *103*, (45), 16649-16654.
41. Guillot, M.; Eisler, S.; Weller, K.; Merkle, H. P.; Gallani, J.-L.; Diederich, F. Effects of structural modification on gene transfection and self-assembling properties of amphiphilic dendrimers. *Organic & Biomolecular Chemistry* **2006**, *4*, (5), 766-769.
42. Kesharwani, P.; Jain, K.; Jain, N. K. Dendrimer as nanocarrier for drug delivery. *Progress in Polymer Science* **2014**, *39*, (2), 268-307.

43. Grayson, S. M.; Frechet, J. M. Convergent dendrons and dendrimers: from synthesis to applications. *Chemical Reviews* **2001**, *101*, (12), 3819-3868.
44. Malkoch, M.; Claesson, H.; Löwenhielm, P.; Malmström, E.; Hult, A. Synthesis and characterization of 2, 2-bis (methylol) propionic acid dendrimers with different cores and terminal groups. *Journal of Polymer Science Part A: Polymer Chemistry* **2004**, *42*, (7), 1758-1767.
45. García-Gallego, S.; Nyström, A. M.; Malkoch, M. Chemistry of multifunctional polymers based on bis-MPA and their cutting-edge applications. *Progress in Polymer Science* **2015**, *48*, 85-110.
46. Kou, L.; Sun, J.; Zhai, Y.; He, Z. The endocytosis and intracellular fate of nanomedicines: Implication for rational design. *Asian Journal of Pharmaceutical Sciences* **2013**, *8*, (1), 1-10.
47. Menjoge, A. R.; Kannan, R. M.; Tomalia, D. A. Dendrimer-based drug and imaging conjugates: design considerations for nanomedical applications. *Drug discovery today* **2010**, *15*, (5-6), 171-185.
48. Fulda, S.; Galluzzi, L.; Kroemer, G. Targeting mitochondria for cancer therapy.(Report). *Nature Reviews Drug Discovery* **2010**, (6), 447.
49. Fulda, S. Exploiting mitochondrial apoptosis for the treatment of cancer. *Mitochondrion* **2010**, *10*, (6), 598-603.
50. Armstrong, J. S. Mitochondrial medicine: Pharmacological targeting of mitochondria in disease. *Br. J. Pharmacol.* **2007**, *151*, (8), 1154-1165.

51. Barbosa, I. A.; Machado, N. G.; Skildum, A. J.; Scott, P. M.; Oliveira, P. J. Mitochondrial remodeling in cancer metabolism and survival: Potential for new therapies. *Biochim. Biophys. Acta-Rev. Cancer* **2012**, *1826*, (1), 238-254.
52. Dong, L.-F.; Jameson, V. J. A.; Tilly, D.; Prochazka, L.; Rohlena, J.; Valis, K.; Truksa, J.; Zobalova, R.; Mahdavian, E.; Kluckova, K.; Stantic, M.; Stursa, J.; Freeman, R.; Witting, P. K.; Norberg, E.; Goodwin, J.; Salvatore, B. A.; Novotna, J.; Turanek, J.; Ledvina, M.; Hozak, P.; Zhivotovsky, B.; Coster, M. J.; Ralph, S. J.; Smith, R. A. J.; Neuzil, J. Mitochondrial targeting of α -tocopheryl succinate enhances its pro-apoptotic efficacy: A new paradigm for effective cancer therapy. *Free Radic. Biol. Med.* **2011**, *50*, (11), 1546-1555.
53. Biasutto, L.; Dong, L. F.; Zoratti, M.; Neuzil, J. Mitochondrially targeted anti-cancer agents. *Mitochondrion* **2010**, *10*, (6), 670-681.
54. Han, M. Mitochondrial Delivery of Doxorubicin via Triphenylphosphine Modification for Overcoming Drug Resistance in MDA-MB-435/DOX Cells. *Mol. Pharm.* **2014**, 140519153522008.
55. Liu, H.-N.; Guo, N.-N.; Wang, T.-T.; Guo, W.-W.; Lin, M.-T.; Huang-Fu, M.-Y.; Vakili, M. R.; Xu, W.-H.; Chen, J.-J.; Wei, Q.-C.; Han, M.; Lavasanifar, A.; Gao, J.-Q. Mitochondrial Targeted Doxorubicin-Triphenylphosphonium Delivered by Hyaluronic Acid Modified and pH Responsive Nanocarriers to Breast Tumor: in Vitro and in Vivo Studies. *Mol. Pharm.* **2018**, *15*, (3), 882-891.
56. Cui, H.; Huan, M.-l.; Ye, W.-l.; Liu, D.-z.; Teng, Z.-h.; Mei, Q.-B.; Zhou, S.-y. Mitochondria and Nucleus Dual Delivery System To Overcome DOX Resistance. *Mol. Pharm.* **2017**, *14*, (3), 746-756.

57. Shi, X.; Lv, G.; Sun, X.; Cao, D.; Wang, G.; Chang, Y. Amphiphilic copolymer and TPGS mixed magnetic hybrid micelles for stepwise targeted co-delivery of DOX/TPP–DOX and image-guided chemotherapy with enhanced antitumor activity in liver cancer. *RSC Adv.* **2017**, 7, (41), 25694-25701.
58. Abbasi, M.; Lavasanifar, A.; Uludag, H. Recent attempts at RNAi-mediated P-glycoprotein downregulation for reversal of multidrug resistance in cancer. *Med. Res. Rev.* **2013**, 33, (1), 33-53.
59. Günther, M.; Lipka, J.; Malek, A.; Gutsch, D.; Kreyling, W.; Aigner, A. Polyethylenimines for RNAi-mediated gene targeting in vivo and siRNA delivery to the lung. *Eur. J. Pharm. Biopharm.* **2011**, 77, (3), 438-449.
60. Aliabadi, H. M.; Mahdipoor, P.; Uludag, H. Polymeric delivery of siRNA for dual silencing of Mel-1 and P-glycoprotein and apoptosis induction in drug-resistant breast cancer cells. *Cancer Gene Ther.* **2013**, 20, (3), 169-177.
61. Alshamsan, A.; Hamdy, S.; Samuel, J.; El-Kadi, A. O. S.; Lavasanifar, A.; Uludag, H. The induction of tumor apoptosis in B16 melanoma following STAT3 siRNA delivery with a lipid-substituted polyethylenimine. *Biomaterials* **2010**, 31, (6), 1420-1428.
62. Beloor, J. Arginine-grafted biodegradable polymer for the systemic delivery of therapeutic siRNA. *Biomaterials* **2012**, 33, (5), 1640-1650.
63. Biswas, S.; Deshpande, P. P.; Navarro, G.; Dodwadkar, N. S.; Torchilin, V. P. Lipid modified triblock PAMAM-based nanocarriers for siRNA drug co-delivery. *Biomaterials* **2013**, 34, (4), 1289-1301.
64. Hu, J.; Hu, K.; Cheng, Y. Tailoring the dendrimer core for efficient gene delivery. *Acta biomaterialia* **2016**, 35, 1-11.

65. Zuckerman, J. E.; Davis, M. E. Clinical experiences with systemically administered siRNA-based therapeutics in cancer. *Nature reviews Drug discovery* **2015**, *14*, (12), 843.
66. Li, S. D.; Huang, L. Targeted delivery of antisense oligodeoxynucleotide and small interference RNA into lung cancer cells. *Mol. Pharm.* **2006**, *3*, (5), 579-588.
67. Indran, I. R.; Tufo, G.; Pervaiz, S.; Brenner, C. Recent advances in apoptosis, mitochondria and drug resistance in cancer cells. *Biochim. Biophys. Acta-Bioenerg.* **2011**, *1807*, (6), 735-745.
68. Kedingler, V.; Meulle, A.; Zounib, O.; Bonnet, M. E.; Gossart, J. B.; Benoit, E.; Messmer, M.; Shankaranarayanan, P.; Behr, J. P.; Erbacher, P.; Bolcato-Bellemin, A. L. Sticky siRNAs targeting survivin and cyclin B1 exert an antitumoral effect on melanoma subcutaneous xenografts and lung metastases. *BMC Cancer* **2013**, *13*, 11.
69. Liu, F.; Liu, S.; He, S.; Xie, Z.; Zu, X.; Jiang, Y. Survivin transcription is associated with P-glycoprotein/MDR1 overexpression in the multidrug resistance of MCF-7 breast cancer cells. *Oncology reports* **2010**, *23*, (5), 1469-1475.
70. Wang, S.; Huang, X.; Lee, C.; Liu, B. Elevated expression of erbB3 confers paclitaxel resistance in erbB2-overexpressing breast cancer cells via upregulation of Survivin. *Oncogene* **2010**, *29*, (29), 4225.
71. Alteri, R., Mamta Kalidas, Lynn Gadd, Tracy Wyant Chemotherapy for Breast Cancer. <https://www.cancer.org/cancer/breast-cancer/treatment/chemotherapy-for-breast-cancer.html> (May 18),
72. Laube, B. L. The Expanding Role of Aerosols in Systemic Drug Delivery, Gene Therapy, and Vaccination. *RESPIRATORY CARE* **2005**, *50*, (9), 1161-1176.

73. Beck-Broichsitter, M.; Merkel, O. M.; Kissel, T. Controlled pulmonary drug and gene delivery using polymeric nano-carriers. *J. Control. Release* **2012**, *161*, (2), 214-224.
74. Zhang, J.; Wu, L.; Chan, H.-K.; Watanabe, W. Formation, characterization, and fate of inhaled drug nanoparticles. *Advanced Drug Delivery Reviews* **2011**, *63*, (6), 441-455.
75. Marianecchi, C. Pulmonary Delivery: Innovative Approaches and Perspectives. *Journal of biomaterials and nanobiotechnology* **2011**, *2*, 567-575.
76. LUNGeivity Find it. Treat it. Live. http://events.lungevity.org/site/PageServer?pagename=v2_AboutLungCancer (March 15),
77. Zhong, Q.; Bielski, E. R.; Rodrigues, L. S.; Brown, M. R.; Reineke, J. J.; da Rocha, S. R. Conjugation to Poly (amidoamine) Dendrimers and Pulmonary Delivery Reduce Cardiac Accumulation and Enhance Antitumor Activity of Doxorubicin in Lung Metastasis. *Mol. Pharm.* **2016**.
78. Zhong, Q.; Merkel, O. M.; Reineke, J. J.; da Rocha, S. R. The Effect of the Route of Administration and PEGylation of Poly (amidoamine) Dendrimers on their Systemic and Lung Cellular Biodistribution. *Mol. Pharm.* **2016**.
79. von Roemeling, C.; Jiang, W.; Chan, C. K.; Weissman, I. L.; Kim, B. Y. Breaking down the barriers to precision cancer nanomedicine. *Trends in biotechnology* **2017**, *35*, (2), 159-171.
80. Yang, L.; Zhang, Y. Tumor-associated macrophages: from basic research to clinical application. *Journal of hematology & oncology* **2017**, *10*, (1), 58.

81. Brown, J. M.; Recht, L.; Strober, S. The promise of targeting macrophages in cancer therapy. *Clin. Cancer Res.* **2017**, *23*, (13), 3241-3250.
82. Mok, S.; Koya, R. C.; Tsui, C.; Xu, J.; Robert, L.; Wu, L.; Graeber, T. G.; West, B. L.; Bollag, G.; Ribas, A. Inhibition of CSF-1 receptor improves the antitumor efficacy of adoptive cell transfer immunotherapy. *Cancer Res.* **2014**, *74*, (1), 153-161.
83. Holmgaard, R. B.; Zamarin, D.; Lesokhin, A.; Merghoub, T.; Wolchok, J. D. Targeting myeloid-derived suppressor cells with colony stimulating factor-1 receptor blockade can reverse immune resistance to immunotherapy in indoleamine 2, 3-dioxygenase-expressing tumors. *EBioMedicine* **2016**, *6*, 50-58.
84. Heller, A.; Brockhoff, G.; Goepferich, A. Targeting drugs to mitochondria. *Eur. J. Pharm. Biopharm.* **2012**, *82*, (1), 1-18.
85. Abu-Gosh, S. E.; Kolvazon, N.; Tirosh, B.; Ringel, I.; Yavin, E. Multiple Triphenylphosphonium Cations Shuttle a Hydrophilic Peptide into Mitochondria. *Mol. Pharm.* **2009**, *6*, (4), 1138-1144.
86. Wang, F.; Ogasawara, M. A.; Huang, P. Small mitochondria-targeting molecules as anti-cancer agents. *Mol. Asp. Med.* **2010**, *31*, (1), 75-92.
87. Biswas, S.; Dodwadkar, N. S.; Deshpande, P. P.; Torchilin, V. P. Liposomes loaded with paclitaxel and modified with novel triphenylphosphonium-PEG-PE conjugate possess low toxicity, target mitochondria and demonstrate enhanced antitumor effects in vitro and in vivo. *J. Control. Release* **2012**, *159*, (3), 393-402.
88. Zhou, J.; Zhao, W. Y.; Ma, X.; Ju, R. J.; Li, X. Y.; Li, N.; Sun, M. G.; Shi, J. F.; Zhang, C. X.; Lu, W. L. The anticancer efficacy of paclitaxel liposomes modified with

mitochondrial targeting conjugate in resistant lung cancer. *Biomaterials* **2013**, *34*, (14), 3626-3638.

89. Malhi, S. S.; Budhiraja, A.; Arora, S.; Chaudhari, K. R.; Nepali, K.; Kumar, R.; Sohi, H.; Murthy, R. S. R. Intracellular delivery of redox cycler-doxorubicin to the mitochondria of cancer cell by folate receptor targeted mitocancerotropic liposomes. *Int. J. Pharm.* **2012**, *432*, (1-2), 63-74.

90. Theodossiou, T. A.; Sideratou, Z.; Katsarou, M. E.; Tsiourvas, D. Mitochondrial Delivery of Doxorubicin by Triphenylphosphonium-Functionalized Hyperbranched Nanocarriers Results in Rapid and Severe Cytotoxicity. *Pharm. Res.* **2013**, *30*, (11), 2832-2842.

91. Panagiotaki, K. N.; Sideratou, Z.; Vlahopoulos, S. A.; Paravatou-Petsotas, M.; Zachariadis, M.; Khoury, N.; Zoumpourlis, V.; Tsiourvas, D. A Triphenylphosphonium-Functionalized Mitochondriotropic Nanocarrier for Efficient Co-Delivery of Doxorubicin and Chloroquine and Enhanced Antineoplastic Activity. *Pharmaceuticals* **2017**, *10*, (4), 91.

92. Chen, W.-H.; Xu, X.-D.; Luo, G.-F.; Jia, H.-Z.; Lei, Q. Dual-Targeting Pro-apoptotic Peptide for Programmed Cancer Cell Death via Specific Mitochondria Damage. *Scientific reports* **2013**, *3*.

93. Kim, K. Y.; Jin, H.; Park, J.; Jung, S. H.; Lee, J. H.; Park, H.; Kim, S. K.; Bae, J.; Jung, J. H. Mitochondria-targeting self-assembled nanoparticles derived from triphenylphosphonium-conjugated cyanostilbene enable site-specific imaging and anticancer drug delivery. *Nano Research* **2018**, *11*, (2), 1082-1098.

94. Xiong, X. B.; Ma, Z. S.; Lai, R.; Lavasanifar, A. The therapeutic response to multifunctional polymeric nano-conjugates in the targeted cellular and subcellular delivery of doxorubicin. *Biomaterials* **2010**, *31*, (4), 757-768.
95. Belyanskaya, L. L.; Hopkins-Donaldson, S.; Kurtz, S.; Simões-Wüst, A. P.; Yousefi, S.; Simon, H.-U.; Stahel, R.; Zangemeister-Wittke, U. Cisplatin activates Akt in small cell lung cancer cells and attenuates apoptosis by survivin upregulation. *International Journal of Cancer* **2005**, *117*, (5), 755-763.
96. Conti, D. S.; Brewer, D.; Grashik, J.; Avasarala, S.; da Rocha, S. R. P. Poly(amidoamine) Dendrimer Nanocarriers and Their Aerosol Formulations for siRNA Delivery to the Lung Epithelium. *Mol. Pharm.* **2014**, *11*, (6), 1808-1822.
97. Y.T. Chow, M.; K.W. Lam, J. Dry Powder Formulation of Plasmid DNA and siRNA for Inhalation. *Curr. Pharm. Design* **2015**, *21*, (27), 3854-3866.
98. De Backer, L.; Cerrada, A.; Pérez-Gil, J.; De Smedt, S. C.; Raemdonck, K. Bio-inspired materials in drug delivery: Exploring the role of pulmonary surfactant in siRNA inhalation therapy. *J. Control. Release* **2015**, *220*, Part B, 642-650.
99. Lam, J. K.-W.; Liang, W.; Chan, H.-K. Pulmonary delivery of therapeutic siRNA. *Advanced Drug Delivery Reviews* **2012**, *64*, (1), 1-15.
100. Jevprasesphant, R.; Penny, J.; Jalal, R.; Attwood, D.; McKeown, N.; D'emanuele, A. The influence of surface modification on the cytotoxicity of PAMAM dendrimers. *Int. J. Pharm.* **2003**, *252*, (1-2), 263-266.
101. Mukherjee, S. P.; Davoren, M.; Byrne, H. J. In vitro mammalian cytotoxicological study of PAMAM dendrimers—towards quantitative structure activity relationships. *Toxicology in Vitro* **2010**, *24*, (1), 169-177.

102. Mukherjee, S. P.; Lyng, F. M.; Garcia, A.; Davoren, M.; Byrne, H. J. Mechanistic studies of in vitro cytotoxicity of poly (amidoamine) dendrimers in mammalian cells. *Toxicology and applied pharmacology* **2010**, *248*, (3), 259-268.
103. Malik, N.; Wiwattanapatapee, R.; Klopsch, R.; Lorenz, K.; Frey, H.; Weener, J. W.; Meijer, E. W.; Paulus, W.; Duncan, R. Dendrimers:: Relationship between structure and biocompatibility in vitro, and preliminary studies on the biodistribution of 125I-labelled polyamidoamine dendrimers in vivo. *J. Control. Release* **2000**, *65*, (1–2), 133-148.
104. Duncan, R.; Izzo, L. Dendrimer biocompatibility and toxicity. *Advanced Drug Delivery Reviews* **2005**, *57*, (15), 2215-2237.
105. Modok, S.; Mellor, H. R.; Callaghan, R. Modulation of multidrug resistance efflux pump activity to overcome chemoresistance in cancer. *Current Opinion in Pharmacology* **2006**, *6*, (4), 350-354.
106. Roa, W. H.; Azarmi, S.; Al-Hallak, M. H. D. K.; Finlay, W. H.; Magliocco, A. M.; Löbenberg, R. Inhalable nanoparticles, a non-invasive approach to treat lung cancer in a mouse model. *Journal Of Controlled Release: Official Journal Of The Controlled Release Society* **2011**, *150*, (1), 49-55.
107. Bielski, E.; Zhong, Q.; Mirza, H.; Brown, M.; Molla, A.; Carvajal, T.; da Rocha, S. R. TPP-Dendrimer Nanocarriers for siRNA Delivery to the Pulmonary Epithelium and their Dry Powder and Metered-dose Inhaler Formulations. *Int. J. Pharm.* **2017**.
108. Perumal, O. P. The effect of surface functionality on cellular trafficking of dendrimers. *Biomaterials* **2008**, *29*, (24-25), 3469-3476.

109. Saovapakhiran, A.; D'Emanuele, A.; Attwood, D.; Penny, J. Surface modification of PAMAM dendrimers modulates the mechanism of cellular internalization. *Bioconjugate chemistry* **2009**, *20*, (4), 693-701.
110. Jevprasesphant, R.; Penny, J.; Attwood, D.; McKeown, N. B.; D'emanuele, A. Engineering of dendrimer surfaces to enhance transepithelial transport and reduce cytotoxicity. *Pharm. Res.* **2003**, *20*, (10), 1543-1550.
111. Lung Cancer Statistics. <https://lungevity.org/for-supporters-advocates/lung-cancer-statistics> (April 18, 2018),
112. NCI Dictionary of Cancer Terms. <https://www.cancer.gov/publications/dictionaries/cancer-terms/def/metastasis> (May 17, 2018),
113. Liu, F.-S. Mechanisms of chemotherapeutic drug resistance in cancer therapy—a quick review. *Taiwanese Journal of Obstetrics and Gynecology* **2009**, *48*, (3), 239-244.
114. Trédan, O.; Galmarini, C. M.; Patel, K.; Tannock, I. F. Drug resistance and the solid tumor microenvironment. *Journal of the National Cancer Institute* **2007**, *99*, (19), 1441-1454.
115. Baguley, B. C. Multiple drug resistance mechanisms in cancer. *Molecular biotechnology* **2010**, *46*, (3), 308-316.
116. Bai, S. Synthesis and evaluation of pegylated dendrimeric nanocarrier for pulmonary delivery of low molecular weight heparin. *Pharm. Res.* **2009**, *26*, (3), 539-48.
117. He, H. PEGylated Poly(amidoamine) dendrimer-based dual-targeting carrier for treating brain tumors. *Biomaterials* **2011**, *32*, (2), 478-487.

118. Inapagolla, R.; Guru, B. R.; Kurtoglu, Y. E.; Gao, X.; Lieh-Lai, M.; Bassett, D. J. P.; Kannan, R. M. In vivo efficacy of dendrimer–methylprednisolone conjugate formulation for the treatment of lung inflammation. *Int. J. Pharm.* **2010**, *399*, (1–2), 140-147.
119. Khandare, J. Synthesis, Cellular Transport, and Activity of Polyamidoamine Dendrimer–Methylprednisolone Conjugates. *Bioconjugate chemistry* **2005**, *16*, (2), 330-337.
120. Kolhe, P. Drug complexation, in vitro release and cellular entry of dendrimers and hyperbranched polymers. *Int. J. Pharm.* **2003**, *259*, (1-2), 143-160.
121. Wijagkanalan, W. Designing Dendrimers for Drug Delivery and Imaging: Pharmacokinetic Considerations. *Pharm. Res.* **2011**, *28*, (7), 1500-1519.
122. Zhu, S. Partly PEGylated polyamidoamine dendrimer for tumor-selective targeting of doxorubicin: The effects of PEGylation degree and drug conjugation style. *Biomaterials* **2010**, *31*, (6), 1360-1371.
123. Liu, R. Interplay of stimuli-responsiveness, drug loading and release for a surface-engineered dendrimer delivery system. *Int. J. Pharm.* **2014**, *462*, (1/2), 103-107.
124. Kolhe, P. Preparation, cellular transport, and activity of polyamidoamine-based dendritic nanodevices with a high drug payload. *Biomaterials* **2006**, *27*, (4), 660-669.
125. Papagiannaros, A. Doxorubicin–PAMAM dendrimer complex attached to liposomes: cytotoxic studies against human cancer cell lines. *Int. J. Pharm.* **2005**, *302*, (1), 29.
126. Sadekar, S. Transepithelial transport and toxicity of PAMAM dendrimers: Implications for oral drug delivery. *Advanced drug delivery reviews* **2012**, *64*, (6), 571-588.

127. Zhong, Q.; da Rocha, S. R. P. Poly(amidoamine) Dendrimer–Doxorubicin Conjugates: In Vitro Characteristics and Pseudosolution Formulation in Pressurized Metered-Dose Inhalers. *Mol. Pharm.* **2016**, *13*, (3), 1058-1072.
128. Lai, P.-S.; Lou, P.-J.; Peng, C.-L.; Pai, C.-L.; Yen, W.-N.; Huang, M.-Y.; Young, T.-H.; Shieh, M.-J. Doxorubicin delivery by polyamidoamine dendrimer conjugation and photochemical internalization for cancer therapy. *J. Control. Release* **2007**, *122*, (1), 39-46.
129. Jia, L.; Xu, J.-P.; Wang, H.; Ji, J. Polyamidoamine dendrimers surface-engineered with biomimetic phosphorylcholine as potential drug delivery carriers. *Colloids and Surfaces B: Biointerfaces* **2011**, *84*, (1), 49-54.
130. Fu, F.; Wu, Y.; Zhu, J.; Wen, S.; Shen, M.; Shi, X. Multifunctional lactobionic acid-modified dendrimers for targeted drug delivery to liver cancer cells: investigating the role played by PEG spacer. *ACS applied materials & interfaces* **2014**, *6*, (18), 16416-16425.
131. Gu, Z.; Wang, M.; Fang, Q.; Zheng, H.; Wu, F.; Lin, D.; Xu, Y.; Jin, Y. Preparation and in vitro characterization of pluronic-attached polyamidoamine dendrimers for drug delivery. *Drug development and industrial pharmacy* **2015**, *41*, (5), 812-818.
132. Wang, K.; Zhang, X.; Zhang, L.; Qian, L.; Liu, C.; Zheng, J.; Jiang, Y. Development of biodegradable polymeric implants of RGD-modified PEG-PAMAM-DOX conjugates for long-term intratumoral release. *Drug delivery* **2015**, *22*, (3), 389-399.
133. Li, X.; Takashima, M.; Yuba, E.; Harada, A.; Kono, K. PEGylated PAMAM dendrimer–doxorubicin conjugate-hybridized gold nanorod for combined photothermal-chemotherapy. *Biomaterials* **2014**, *35*, (24), 6576-6584.

134. Zhong, Q.; Humia, B. V.; Punjabi, A. R.; Padilha, F. F.; da Rocha, S. R. The interaction of dendrimer-doxorubicin conjugates with a model pulmonary epithelium and their cosolvent-free, pseudo-solution formulations in pressurized metered-dose inhalers. *European Journal of Pharmaceutical Sciences* **2017**, *109*, 86-95.
135. Kaminskas, L. M.; McLeod, V. M.; Ryan, G. M.; Kelly, B. D.; Haynes, J. M.; Williamson, M.; Thienthong, N.; Owen, D. J.; Porter, C. J. Pulmonary administration of a doxorubicin-conjugated dendrimer enhances drug exposure to lung metastases and improves cancer therapy. *J. Control. Release* **2014**, *183*, 18-26.
136. Pooja, D.; Kulhari, H.; Singh, M. K.; Mukherjee, S.; Rachamalla, S. S.; Sistla, R. Dendrimer-TPGS mixed micelles for enhanced solubility and cellular toxicity of taxanes. *Colloids and Surfaces B: Biointerfaces* **2014**, *121*, 461-468.
137. Bhadra, D.; Bhadra, S.; Jain, S.; Jain, N. A PEGylated dendritic nanoparticulate carrier of fluorouracil. *Int. J. Pharm.* **2003**, *257*, (1-2), 111-124.
138. Matai, I.; Sachdev, A.; Gopinath, P. Multicomponent 5-fluorouracil loaded PAMAM stabilized-silver nanocomposites synergistically induce apoptosis in human cancer cells. *Biomaterials science* **2015**, *3*, (3), 457-468.
139. Rengaraj, A.; Subbiah, B.; Haldorai, Y.; Yesudhas, D.; Yun, H. J.; Kwon, S.; Choi, S.; Han, Y.-K.; Kim, E.-S.; Huh, Y. S. PAMAM/5-fluorouracil drug conjugate for targeting E6 and E7 oncoproteins in cervical cancer: a combined experimental/in silico approach. *RSC Adv.* **2017**, *7*, (9), 5046-5054.
140. Zheng, W.; Cao, C.; Liu, Y.; Yu, Q.; Zheng, C.; Sun, D.; Ren, X.; Liu, J. Multifunctional polyamidoamine-modified selenium nanoparticles dual-delivering siRNA

and cisplatin to A549/DDP cells for reversal multidrug resistance. *Acta biomaterialia* **2015**, *11*, 368-380.

141. Yellepeddi, V. K.; Kumar, A.; Maher, D. M.; Chauhan, S. C.; Vangara, K. K.; Palakurthi, S. Biotinylated PAMAM dendrimers for intracellular delivery of cisplatin to ovarian cancer: role of SMVT. *Anticancer research* **2011**, *31*, (3), 897-906.

142. Nguyen, H.; Nguyen, N. H.; Tran, N. Q.; Nguyen, C. K. Improved method for preparing cisplatin-dendrimer nanocomplex and its behavior against NCI-H460 lung cancer cell. *Journal of nanoscience and nanotechnology* **2015**, *15*, (6), 4106-4110.

143. Zhang, Y.; Thomas, T. P.; Lee, K.-H.; Li, M.; Zong, H.; Desai, A. M.; Kotlyar, A.; Huang, B.; Holl, M. M. B.; Baker Jr, J. R. Polyvalent saccharide-functionalized generation 3 poly (amidoamine) dendrimer–methotrexate conjugate as a potential anticancer agent. *Bioorg. Med. Chem.* **2011**, *19*, (8), 2557-2564.

144. Quintana, A.; Raczka, E.; Piehler, L.; Lee, I.; Myc, A.; Majoros, I.; Patri, A. K.; Thomas, T.; Mulé, J.; Baker, J. R. Design and Function of a Dendrimer-Based Therapeutic Nanodevice Targeted to Tumor Cells Through the Folate Receptor. *Pharm. Res.* **2002**, *19*, (9), 1310-1316.

145. Tekade, R. K.; Dutta, T.; Gajbhiye, V.; Jain, N. K. Exploring dendrimer towards dual drug delivery: pH responsive simultaneous drug-release kinetics. *Journal of microencapsulation* **2009**, *26*, (4), 287-296.

146. Yamashita, S.; Katsumi, H.; Sakane, T.; Yamamoto, A. Bone-targeting dendrimer for the delivery of methotrexate and treatment of bone metastasis. *J. Drug Target.* **2018**, 1-11.

147. Zong, H.; Thomas, T. P.; Lee, K.-H.; Desai, A. M.; Li, M.-h.; Kotlyar, A.; Zhang, Y.; Leroueil, P. R.; Gam, J. J.; Banaszak Holl, M. M.; Baker, J. R. Bifunctional PAMAM Dendrimer Conjugates of Folic Acid and Methotrexate with Defined Ratio. *Biomacromolecules* **2012**, *13*, (4), 982-991.
148. Khandare, J. J.; Jayant, S.; Singh, A.; Chandna, P.; Wang, Y.; Vorsa, N.; Minko, T. Dendrimer versus linear conjugate: Influence of polymeric architecture on the delivery and anticancer effect of paclitaxel. *Bioconjugate Chemistry* **2006**, *17*, (6), 1464-1472.
149. Teow, H. M.; Zhou, Z.; Najlah, M.; Yusof, S. R.; Abbott, N. J.; D'Emanuele, A. Delivery of paclitaxel across cellular barriers using a dendrimer-based nanocarrier. *Int. J. Pharm.* **2013**, *441*, (1-2), 701-711.
150. Liu, Y.; Ng, Y.; Toh, M. R.; Chiu, G. N. C. Lipid-dendrimer hybrid nanosystem as a novel delivery system for paclitaxel to treat ovarian cancer. *J. Control. Release* **2015**, *220*, 438-446.
151. Hui, H.; Xiao-dong, F.; Zhong-lin, C. Thermo- and pH-sensitive dendrimer derivatives with a shell of poly(N,N-dimethylaminoethyl methacrylate) and study of their controlled drug release behavior. *Polymer* **2005**, *46*, (22), 9514-9522.
152. Bielawski, K.; Bielawska, A.; Muszyńska, A.; Popławska, B.; Czarnomysy, R. Cytotoxic activity of G3 PAMAM-NH₂ dendrimer-chlorambucil conjugate in human breast cancer cells. *environmental toxicology and pharmacology* **2011**, *32*, (3), 364-372.
153. Yalçın, S.; Erkan, M.; Ünsoy, G.; Parsian, M.; Kleeff, J.; Gündüz, U. Effect of gemcitabine and retinoic acid loaded PAMAM dendrimer-coated magnetic nanoparticles on pancreatic cancer and stellate cell lines. *Biomedicine & Pharmacotherapy* **2014**, *68*, (6), 737-743.

154. Parsian, M.; Mutlu, P.; Yalcin, S.; Tezcaner, A.; Gunduz, U. Half generations magnetic PAMAM dendrimers as an effective system for targeted gemcitabine delivery. *Int. J. Pharm.* **2016**, *515*, (1-2), 104-113.
155. Yoyen-Ermis, D.; Ozturk-Atar, K.; Kursunel, M. A.; Aydin, C.; Ozkazanc, D.; Gurbuz, M. U.; Uner, A.; Tulu, M.; Calis, S.; Esendagli, G. Tumor-Induced Myeloid Cells Are Reduced by Gemcitabine-Loaded PAMAM Dendrimers Decorated with Anti-Flt1 Antibody. *Mol. Pharm.* **2018**, *15*, (4), 1526-1533.
156. Kulhari, H.; Pooja, D.; Shrivastava, S.; Kuncha, M.; Naidu, V.; Bansal, V.; Sistla, R.; Adams, D. J. Trastuzumab-grafted PAMAM dendrimers for the selective delivery of anticancer drugs to HER2-positive breast cancer. *Scientific reports* **2016**, *6*, 23179.
157. Marcinkowska, M.; Sobierajska, E.; Stanczyk, M.; Janaszewska, A.; Chworos, A.; Klajnert-Maculewicz, B. Conjugate of PAMAM Dendrimer, Doxorubicin and Monoclonal Antibody—Trastuzumab: The New Approach of a Well-Known Strategy. *Polymers* **2018**, *10*, (2), 187.
158. Heiden, T. C. K.; Dengler, E.; Kao, W. J.; Heideman, W.; Peterson, R. E. Developmental toxicity of low generation PAMAM dendrimers in zebrafish. *Toxicology and applied pharmacology* **2007**, *225*, (1), 70-79.
159. Nyitrai, G.; Kékesi, O.; Pál, I.; Keglevich, P.; Csíki, Z.; Fügedi, P.; Simon, Á.; Fitos, I.; Németh, K.; Visy, J.; Tárkányi, G.; Kardos, J. Assessing toxicity of polyamidoamine dendrimers by neuronal signaling functions. *Nanotoxicology* **2012**, *6*, (6), 576-586.
160. Kolhatkar, R. B.; Kitchens, K. M.; Swaan, P. W.; Ghandehari, H. Surface Acetylation of Polyamidoamine (PAMAM) Dendrimers Decreases Cytotoxicity while Maintaining Membrane Permeability. *Bioconjugate Chemistry* **2007**, *18*, (6), 2054-2060.

161. Ihre, H.; Hult, A.; Söderlind, E. Synthesis, characterization, and ^1H NMR self-diffusion studies of dendritic aliphatic polyesters based on 2, 2-bis (hydroxymethyl) propionic acid and 1, 1, 1-tris (hydroxyphenyl) ethane. *Journal of the American Chemical Society* **1996**, *118*, (27), 6388-6395.
162. Almutairi, A.; Akers, W. J.; Berezin, M. Y.; Achilefu, S.; Fréchet, J. M. J. Monitoring the biodegradation of dendritic near infrared nanoprobes by in vivo fluorescence imaging. *Mol. Pharm.* **2008**, *5*, (6), 1103-1110.
163. Almutairi, A.; Rossin, R.; Shokeen, M.; Hagooly, A.; Ananth, A.; Capoccia, B.; Guillaudeu, S.; Abendschein, D.; Anderson, C. J.; Welch, M. J. Biodegradable dendritic positron-emitting nanoprobes for the noninvasive imaging of angiogenesis. *Proceedings of the National Academy of Sciences* **2009**, *106*, (3), 685-690.
164. Heyder, R. S.; Zhong, Q.; Bazito, R. C.; da Rocha, S. R. P. Cellular internalization and transport of biodegradable polyester dendrimers on a model of the pulmonary epithelium and their formulation in pressurized metered-dose inhalers. *Int. J. Pharm.* **2017**, *520*, (1), 181-194.
165. Cao, W.; Zhou, J.; Mann, A.; Wang, Y.; Zhu, L. Folate-functionalized unimolecular micelles based on a degradable amphiphilic dendrimer-like star polymer for cancer cell-targeted drug delivery. *Biomacromolecules* **2011**, *12*, (7), 2697-2707.
166. Padilla De Jesús, O. L.; Ihre, H. R.; Gagne, L.; Fréchet, J. M. J.; Szoka, F. C. Polyester Dendritic Systems for Drug Delivery Applications: In Vitro and In Vivo Evaluation. *Bioconjugate Chemistry* **2002**, *13*, (3), 453-461.
167. Gillies, E. R.; Fréchet, J. M. J. Designing Macromolecules for Therapeutic Applications: Polyester Dendrimers Poly(ethylene oxide) "Bow-Tie" Hybrids with Tunable

Molecular Weight and Architecture. *Journal of American Chemical Society* **2002**, *124*, 14137-14146.

168. Wu, P.; Malkoch, M.; Hunt, J. N.; Vestberg, R.; Kaltgrad, E.; Finn, M. G.; Fokin, V. V.; Sharpless, K. B.; Hawker, C. J. Multivalent, bifunctional dendrimers prepared by click chemistry. *Chemical Communications (Cambridge, United Kingdom)* **2005**, (46), 5775-5777.

169. Walter, M. V.; Lundberg, P.; Hult, A.; Malkoch, M. Novel macrothiols for the synthesis of a structurally comprehensive dendritic library using thiol-ene click chemistry. *Journal of Polymer Science Part A: Polymer Chemistry* **2011**, *49*, (13), 2990-2995.

170. Ledin, P. A.; Friscourt, F.; Guo, J.; Boons, G. J. Convergent assembly and surface modification of multifunctional dendrimers by three consecutive click reactions. *Chemistry-A European Journal* **2011**, *17*, (3), 839-846.

171. Goodwin, A. P.; Lam, S. S.; Fréchet, J. M. J. Rapid, Efficient Synthesis of Heterobifunctional Biodegradable Dendrimers. *Journal of the American Chemical Society* **2007**, *129*, (22), 6994-6995.

172. Smith, R. A. Delivery of bioactive molecules to mitochondria in vivo. *Proceedings of the National Academy of Sciences - PNAS* **2003**, *100*, (9), 5407-12.

173. Biswas, S.; Dodwadkar, N. S.; Sawant, R. R.; Koshkaryev, A.; Torchilin, V. P. Surface modification of liposomes with rhodamine-123-conjugated polymer results in enhanced mitochondrial targeting. *J. Drug Target.* **2011**, *19*, (7), 552-561.

174. Wang, X. X.; Li, Y. B.; Yao, H. J.; Ju, R. J.; Zhang, Y.; Li, R. J.; Yu, Y.; Zhang, L.; Lu, W. L. The use of mitochondrial targeting resveratrol liposomes modified with a

dequalinium polyethylene glycol-distearoylphosphatidyl ethanolamine conjugate to induce apoptosis in resistant lung cancer cells. *Biomaterials* **2011**, *32*, (24), 5673-5687.

175. Yoong, S. L.; Wong, B. S.; Zhou, Q. L.; Chin, C. F.; Li, J.; Venkatesan, T.; Ho, H. K.; Yu, V.; Ang, W. H.; Pastorin, G. Enhanced cytotoxicity to cancer cells by mitochondria-targeting MWCNTs containing platinum(IV) prodrug of cisplatin. *Biomaterials* **2014**, *35*, (2), 748-759.

176. Marrache, S.; Dhar, S. Engineering of blended nanoparticle platform for delivery of mitochondria-acting therapeutics. *Proc. Natl. Acad. Sci. U. S. A.* **2012**, *109*, (40), 16288-16293.

177. Zeng, X. H.; Morgenstern, R.; Nystrom, A. M. Nanoparticle-directed sub-cellular localization of doxorubicin and the sensitization breast cancer cells by circumventing GST-Mediated drug resistance. *Biomaterials* **2014**, *35*, (4), 1227-1239.

178. Carvalho, F. S.; Burgeiro, A.; Garcia, R.; Moreno, A. J.; Carvalho, R. A.; Oliveira, P. J. Doxorubicin-Induced Cardiotoxicity: From Bioenergetic Failure and Cell Death to Cardiomyopathy. *Med. Res. Rev.* **2014**, *34*, (1), 106-135.

179. Gilliam, L. A. A.; Fisher-Wellman, K. H.; Lin, C. T.; Maples, J. M.; Cathey, B. L.; Neuffer, P. D. The anticancer agent doxorubicin disrupts mitochondrial energy metabolism and redox balance in skeletal muscle. *Free Radic. Biol. Med.* **2013**, *65*, 988-996.

180. Cheng, Z.; DiMichele, L. A.; Rojas, M.; Vaziri, C.; Mack, C. P.; Taylor, J. M. Focal adhesion kinase antagonizes doxorubicin cardiotoxicity via p21(CiP1). *J. Mol. Cell. Cardiol.* **2014**, *67*, 1-11.

181. Kulkarni, P. S.; Haldar, M. K.; Confeld, M. I.; Langaas, C. J.; Yang, X.; Qian, S. Y.; Mallik, S. Mitochondria-targeted fluorescent polymersomes for drug delivery to cancer cells. *Polymer chemistry* **2016**, *7*, (25), 4151-4154.
182. Song, Y.-f.; Liu, D.-z.; Cheng, Y.; Liu, M.; Ye, W.-l.; Liu, X.-y.; Zhou, S.-y. Dual subcellular compartment delivery of doxorubicin to overcome drug resistant and enhance antitumor activity. *Scientific reports* **2015**, *5*, 16125.
183. Kuznetsov, A. V.; Margreiter, R.; Amberger, A.; Saks, V.; Grimm, M. Changes in mitochondrial redox state, membrane potential and calcium precede mitochondrial dysfunction in doxorubicin-induced cell death. *Biochim. Biophys. Acta-Mol. Cell Res.* **2011**, *1813*, (6), 1144-1152.
184. Riganti, C.; Rolando, B.; Kopecka, J.; Campia, I.; Chegaev, K.; Lazzarato, L.; Federico, A.; Fruttero, R.; Ghigo, D. Mitochondrial-Targeting Nitrooxy-doxorubicin: A New Approach To Overcome Drug Resistance. *Mol. Pharm.* **2013**, *10*, (1), 161-174.
185. Chen, Y. C.; Bathula, S. R.; Li, J.; Huang, L. Multifunctional Nanoparticles Delivering Small Interfering RNA and Doxorubicin Overcome Drug Resistance in Cancer. *J. Biol. Chem.* **2010**, *285*, (29), 22639-22650.
186. Duncan, R. Polymer conjugates as anticancer nanomedicines. *Nature reviews. Cancer* **2006**, *6*, (9), 688.
187. Wei, W.; Lv, P. P.; Chen, X. M.; Yue, Z. G.; Fu, Q.; Liu, S. Y.; Yue, H.; Ma, G. H. Codelivery of mTERT siRNA and paclitaxel by chitosan-based nanoparticles promoted synergistic tumor suppression. *Biomaterials* **2013**, *34*, (15), 3912-3923.
188. Dykxhoorn, D. M.; Novina, C. D.; Sharp, P. A. Killing the messenger: Short RNAs that silence gene expression. *Nat. Rev. Mol. Cell Biol.* **2003**, *4*, (6), 457-467.

189. Chen, Y. C.; Sen, J.; Bathula, S. R.; Yang, Q.; Fittipaldi, R.; Huang, L. Novel Cationic Lipid That Delivers siRNA and Enhances Therapeutic Effect in Lung Cancer Cells. *Mol. Pharm.* **2009**, *6*, (3), 696-705.
190. Conde, J.; Tian, F.; Hernández, Y.; Bao, C.; Cui, D.; Janssen, K.-P.; Ibarra, M. R.; Baptista, P. V.; Stoeger, T.; de la Fuente, J. M. In vivo tumor targeting via nanoparticle-mediated therapeutic siRNA coupled to inflammatory response in lung cancer mouse models. *Biomaterials* **2013**, *34*, (31), 7744-7753.
191. Patil, M. L.; Zhang, M.; Taratula, O.; Garbuzenko, O. B.; He, H. X.; Minko, T. Internally Cationic Polyamidoamine PAMAM-OH Dendrimers for siRNA Delivery: Effect of the Degree of Quaternization and Cancer Targeting. *Biomacromolecules* **2009**, *10*, (2), 258-266.
192. Li, J.; Wang, Y.; Zhu, Y.; Oupický, D. Recent advances in delivery of drug-nucleic acid combinations for cancer treatment. *J. Control. Release* **2013**, *172*, (2), 589-600.
193. Dong, D. W.; Xiang, B.; Gao, W.; Yang, Z. Z.; Li, J. Q.; Qi, X. R. pH-responsive complexes using prefunctionalized polymers for synchronous delivery of doxorubicin and siRNA to cancer cells. *Biomaterials* **2013**, *34*, (20), 4849-4859.
194. Li, J.; Wang, Y.; Zhu, Y.; Oupický, D. Recent advances in delivery of drug–nucleic acid combinations for cancer treatment. *J. Control. Release* **2013**, *172*, (2), 589-600.
195. Mainelis, G.; Seshadri, S.; Garbuzenko, O. B.; Han, T.; Wang, Z.; Minko, T. Characterization and Application of a Nose-Only Exposure Chamber for Inhalation Delivery of Liposomal Drugs and Nucleic Acids to Mice. *Journal of Aerosol Medicine and Pulmonary Drug Delivery* **2013**, *26*, (6), 345-354.

196. Meng, H.; Mai, W. X.; Zhang, H. Y.; Xue, M.; Xia, T.; Lin, S. J.; Wang, X.; Zhao, Y.; Ji, Z. X.; Zink, J. I.; Nel, A. E. Codelivery of an Optimal Drug/siRNA Combination Using Mesoporous Silica Nanoparticles To Overcome Drug Resistance in Breast Cancer in Vitro and in Vivo. *ACS Nano* **2013**, 7, (2), 994-1005.
197. Patil, Y. B.; Swaminathan, S. K.; Sadhukha, T.; Ma, L. A.; Panyam, J. The use of nanoparticle-mediated targeted gene silencing and drug delivery to overcome tumor drug resistance. *Biomaterials* **2010**, 31, (2), 358-365.
198. Taratula, O. Nanostructured lipid carriers as multifunctional nanomedicine platform for pulmonary co-delivery of anticancer drugs and siRNA. *J. Control. Release* **2013**, 171, (3), 349-357.
199. Taratula, O.; Garbuzenko, O. B.; Chen, A. M.; Minko, T. Innovative strategy for treatment of lung cancer: targeted nanotechnology-based inhalation co-delivery of anticancer drugs and siRNA. *J. Drug Target.* **2011**, 19, (10), 900-914.
200. Yadav, S.; van Vlerken, L. E.; Little, S. R.; Amiji, M. M. Evaluations of combination MDR-1 gene silencing and paclitaxel administration in biodegradable polymeric nanoparticle formulations to overcome multidrug resistance in cancer cells. *Cancer Chemother. Pharmacol.* **2009**, 63, (4), 711-722.
201. Yu, H.; Xu, Z.; Chen, X.; Xu, L.; Yin, Q. Reversal of Lung Cancer Multidrug Resistance by pH-Responsive Micelleplexes Mediating Co-Delivery of siRNA and Paclitaxel Reversal of Lung Cancer Multidrug Resistance *Macromolecular bioscience* **2014**, 14, (1), 100-109.

202. Zhang, L. M.; Lu, Z. X.; Zhao, Q. H.; Huang, J.; Shen, H.; Zhang, Z. J. Enhanced Chemotherapy Efficacy by Sequential Delivery of siRNA and Anticancer Drugs Using PEI-Grafted Graphene Oxide. *Small* **2011**, *7*, (4), 460-464.
203. Zhu, C. H.; Jung, S.; Luo, S. B.; Meng, F. H.; Zhu, X. L.; Park, T. G.; Zhong, Z. Y. Co-delivery of siRNA and paclitaxel into cancer cells by biodegradable cationic micelles based on PDMAEMA-PCL-PDMAEMA triblock copolymers. *Biomaterials* **2010**, *31*, (8), 2408-2416.
204. Cory, S. The Bcl2 family: regulators of the cellular life-or-death switch. *Nature reviews. Cancer* **2002**, *2*, (9), 647-656.
205. Rautureau, G. J. P. Intrinsically disordered proteins in bcl-2 regulated apoptosis. *International journal of molecular sciences* **2010**, *11*, (4), 1808.
206. Altieri, D. C. The molecular basis and potential role of survivin in cancer diagnosis and therapy. *Trends in Molecular Medicine* **2001**, *7*, (12), 542-547.
207. Cao, C.; Mu, Y.; Hallahan, D. E.; Lu, B. XIAP and survivin as therapeutic targets for radiation sensitization in preclinical models of lung cancer. *Oncogene* **2004**, *23*, (42), 7047-7052.
208. Li, F. Role of survivin and its splice variants in tumorigenesis. *Br J Cancer* **2004**, *92*, (2), 212-216.
209. Chen, Y.; Li, D.; Liu, H.; Xu, H.; Zheng, H.; Qian, F.; Li, W.; Zhao, C.; Wang, Z.; Wang, X. Notch-1 signaling facilitates survivin expression in human non-small cell lung cancer cells. *Cancer Biology & Therapy* **2011**, *11*, (1), 14-21.
210. Monzó, M.; Rosell, R.; Felip, E.; Astudillo, J.; Sánchez, J. J.; Maestre, J.; Martín, C.; Font, A.; Barnadas, A.; Abad, A. A Novel Anti-Apoptosis Gene: Re-expression of

Survivin Messenger RNA as a Prognosis Marker in Non–Small-Cell Lung Cancers. *Journal of Clinical Oncology* **1999**, 17, (7), 2100.

211. Zaffaroni, N.; Daidone, M. G. Survivin expression and resistance to anticancer treatments: perspectives for new therapeutic interventions. *Drug Resistance Updates* **2002**, 5, (2), 65-72.

212. Lee, W.-H.; Loo, C.-Y.; Traini, D.; Young, P. M. Inhalation of nanoparticle-based drug for lung cancer treatment: Advantages and challenges. *asian journal of pharmaceutical sciences* **2015**, 10, (6), 481-489.

213. Bailey, M. M. Nanoparticle formulations in pulmonary drug delivery. *Med. Res. Rev.* **2009**, 29, (1), 196-212.

214. Loira-Pastoriza, C.; Todoroff, J.; Vanbever, R. Delivery strategies for sustained drug release in the lungs. *Advanced drug delivery reviews* **2014**, 75, 81-91.

215. Choi, H. S. Rapid translocation of nanoparticles from the lung airspaces to the body. *Nature biotechnology* **2010**, 28, (12), 1300-1303.

216. Patton, J. S. Inhaling medicines: delivering drugs to the body through the lungs. *Nature reviews. Drug discovery* **2007**, 6, (1), 67-74.

217. Kunda, N. Nanocarriers Targeting Dendritic Cells for Pulmonary Vaccine Delivery. *Pharm. Res.* **2013**, 30, (2), 325-341.

218. Sanders, N.; Rudolph, C.; Braeckmans, K.; De Smedt, S. C.; Demeester, J. Extracellular barriers in respiratory gene therapy. *Advanced Drug Delivery Reviews* **2009**, 61, (2), 115-127.

219. Chiang, P.-C.; Alsup, J. W.; Lai, Y.; Hu, Y.; Heyde, B. R.; Tung, D. Evaluation of aerosol delivery of nanosuspension for pre-clinical pulmonary drug delivery. *Nanoscale research letters* **2009**, *4*, (3), 254.
220. El-Gendy, N.; Berkland, C. Combination chemotherapeutic dry powder aerosols via controlled nanoparticle agglomeration. *Pharm. Res.* **2009**, *26*, (7), 1752-1763.
221. Bielski, E.; Zhong, Q.; Mirza, H.; Brown, M.; Molla, A.; Carvajal, T.; da Rocha, S. R. P. TPP-dendrimer nanocarriers for siRNA delivery to the pulmonary epithelium and their dry powder and metered-dose inhaler formulations. *Int. J. Pharm.* **2017**, *527*, (1), 171-183.
222. Laoui, D.; Van Overmeire, E.; De Baetselier, P.; Van Ginderachter, J. A.; Raes, G. Functional relationship between tumor-associated macrophages and macrophage colony-stimulating factor as contributors to cancer progression. *Frontiers in immunology* **2014**, *5*, 489.
223. Yeh, Y.-M.; Hsu, S.-J.; Lin, P.-C.; Hsu, K.-F.; Wu, P.-Y.; Su, W.-C.; Chang, J.-Y.; Shen, M.-R. The c. 1085A> G genetic variant of CSF1R gene regulates tumor immunity by altering the proliferation, polarization, and function of macrophages. *Clin. Cancer Res.* **2017**, *23*, (20), 6021-6030.
224. Stanley, E. R.; Chitu, V. CSF-1 receptor signaling in myeloid cells. *Cold Spring Harbor perspectives in biology* **2014**, *6*, (6), a021857.
225. Yan, D.; Kowal, J.; Akkari, L.; Schuhmacher, A.; Huse, J.; West, B.; Joyce, J. Inhibition of colony stimulating factor-1 receptor abrogates microenvironment-mediated therapeutic resistance in gliomas. *Oncogene* **2017**, *36*, (43), 6049.

226. Murphy, M. P. Targeting Antioxidants to Mitochondria by Conjugation to Lipophilic Cations. *Annual review of pharmacology and toxicology* **2007**, 47, (1), 629-656.
227. Durazo, S. A.; Kompella, U. B. Functionalized nanosystems for targeted mitochondrial delivery. *Mitochondrion* **2012**, 12, (2), 190-201.
228. Edeas, M.; Weissig, V. Targeting mitochondria: Strategies, innovations and challenges: The future of medicine will come through mitochondria. *Mitochondrion* **2013**, 13, (5), 389-390.
229. Frantz, M.-C.; Wipf, P. Mitochondria as a target in treatment. *Environ. Mol. Mutagen.* **2010**, 51, (5), 462-475.
230. Yamada, Y.; Harashima, H. Mitochondrial drug delivery systems for macromolecule and their therapeutic application to mitochondrial diseases. *Advanced Drug Delivery Reviews* **2008**, 60, (13–14), 1439-1462.
231. Biswas, S.; Dodwadkar, N. S.; Piroyan, A.; Torchilin, V. P. Surface conjugation of triphenylphosphonium to target poly(amidoamine) dendrimers to mitochondria. *Biomaterials* **2012**, 33, (18), 4773-4782.
232. Torchilin, V. P., Recent approaches to intracellular delivery of drugs and DNA and organelle targeting. In *Annual Review of Biomedical Engineering*, 2006; Vol. 8, pp 343-375.
233. Murphy, M. P. Targeting lipophilic cations to mitochondria. *Biochimica et Biophysica Acta (BBA) - Bioenergetics* **2008**, 1777, (7–8), 1028-1031.
234. Sharma, A.; Soliman, G. M.; Al-Hajaj, N.; Sharma, R.; Maysinger, D.; Kakkar, A. Design and Evaluation of Multifunctional Nanocarriers for Selective Delivery of Coenzyme Q10 to Mitochondria. *Biomacromolecules* **2012**, 13, (1), 239-252.

235. Zhou, J.; Zhao, W.-Y.; Ma, X.; Ju, R.-J.; Li, X.-Y.; Li, N.; Sun, M.-G.; Shi, J.-F.; Zhang, C.-X.; Lu, W.-L. The anticancer efficacy of paclitaxel liposomes modified with mitochondrial targeting conjugate in resistant lung cancer. *Biomaterials* **2013**, *34*, (14), 3626-3638.
236. Chen, Z.; Zhang, L.; Song, Y.; He, J.; Wu, L.; Zhao, C.; Xiao, Y.; Li, W.; Cai, B.; Cheng, H.; Li, W. Hierarchical targeted hepatocyte mitochondrial multifunctional chitosan nanoparticles for anticancer drug delivery. *Biomaterials* **2015**, *52*, (0), 240-250.
237. Wang, X. Mitochondrial targeting dendrimer allows efficient and safe gene delivery. *Journal of materials chemistry. B, Materials for biology and medicine* **2014**, *2*, (17), 2546.
238. Marrache, S.; Tundup, S.; Harn, D. A.; Dhar, S. Ex Vivo Programming of Dendritic Cells by Mitochondria-Targeted Nanoparticles to Produce Interferon-Gamma for Cancer Immunotherapy. *ACS Nano* **2013**, *7*, (8), 7392-7402.
239. Cuchelkar, V.; Kopečková, P.; Kopeček, J. Novel HPMA Copolymer-Bound Constructs for Combined Tumor and Mitochondrial Targeting. *Mol. Pharm.* **2008**, *5*, (5), 776-786.
240. Zhang, C.-J.; Hu, Q.; Feng, G.; Zhang, R.; Yuan, Y.; Lu, X.; Liu, B. Image-guided combination chemotherapy and photodynamic therapy using a mitochondria-targeted molecular probe with aggregation-induced emission characteristics. *Chemical Science* **2015**.
241. Liao, H. Antitumor efficacy of doxorubicin encapsulated within PEGylated poly(amidoamine) dendrimers. *Journal of applied polymer science* **2014**, *131*, (11), n-a-n/a.

242. Li, Y.; He, H.; Jia, X.; Lu, W.-L.; Lou, J.; Wei, Y. A dual-targeting nanocarrier based on poly(amidoamine) dendrimers conjugated with transferrin and tamoxifen for treating brain gliomas. *Biomaterials* **2012**, *33*, (15), 3899-3908.
243. Thakur, S.; Tekade, R.; Kesharwani, P.; Jain, N. The effect of polyethylene glycol spacer chain length on the tumor-targeting potential of folate-modified PPI dendrimers. *J Nanopart Res* **2013**, *15*, (5), 1-16.
244. Niu, Y.; Sun, L.; Crooks, R. M. Determination of the Intrinsic Proton Binding Constants for Poly(amidoamine) Dendrimers via Potentiometric pH Titration. *Macromolecules* **2003**, *36*, (15), 5725-5731.
245. Diallo, M. S.; Christie, S.; Swaminathan, P.; Balogh, L.; Shi, X.; Um, W.; Papelis, C.; Goddard, W. A.; Johnson, J. H. Dendritic Chelating Agents. 1. Cu(II) Binding to Ethylene Diamine Core Poly(amidoamine) Dendrimers in Aqueous Solutions. *Langmuir* **2004**, *20*, (7), 2640-2651.
246. Cakara, D.; Kleimann, J.; Borkovec, M. Microscopic Protonation Equilibria of Poly(amidoamine) Dendrimers from Macroscopic Titrations. *Macromolecules* **2003**, *36*, (11), 4201-4207.
247. Yang, L.; da Rocha, S. R. P. PEGylated, NH₂-Terminated PAMAM Dendrimers: A Microscopic View from Atomistic Computer Simulations. *Mol. Pharm.* **2014**, *11*, (5), 1459-1470.
248. Weinberg, S. E.; Chandel, N. S. Targeting mitochondria metabolism for cancer therapy. *Nat Chem Biol* **2015**, *11*, (1), 9-15.
249. Xie, Y.; Kim, N. H.; Nadithe, V.; Schalk, D.; Thakur, A.; Kılıç, A.; Lum, L. G.; Bassett, D. J. P.; Merkel, O. M. Targeted delivery of siRNA to activated T cells via

transferrin-polyethylenimine (Tf-PEI) as a potential therapy of asthma. *J. Control. Release* **2016**, *229*, 120-129.

250. De Backer, L.; Naessens, T.; De Koker, S.; Zagato, E.; Demeester, J.; Grooten, J.; De Smedt, S. C.; Raemdonck, K. Hybrid pulmonary surfactant-coated nanogels mediate efficient in vivo delivery of siRNA to murine alveolar macrophages. *J. Control. Release* **2015**, *217*, 53-63.

251. Bangel-Ruland, N.; Tomczak, K.; Weber, W.-M. Targeting ENaC as a Molecular Suspect in Cystic Fibrosis. *Current drug targets* **2015**, *16*, (9), 951-957.

252. Zhang, W.; Yang, H.; Kong, X.; Mohapatra, S.; San Juan-Vergara, H.; Hellermann, G.; Behera, S.; Singam, R.; Lockey, R. F.; Mohapatra, S. S. Inhibition of respiratory syncytial virus infection with intranasal siRNA nanoparticles targeting the viral NS1 gene. *Nature medicine* **2005**, *11*, (1), 56-62.

253. Li, B.-j.; Tang, Q.; Cheng, D.; Qin, C.; Xie, F. Y.; Wei, Q.; Xu, J.; Liu, Y.; Zheng, B.-j.; Woodle, M. C. Using siRNA in prophylactic and therapeutic regimens against SARS coronavirus in Rhesus macaque. *Nature medicine* **2005**, *11*, (9), 944-951.

254. Liang, W.; Chow, M. Y. T.; Lau, P. N.; Zhou, Q. T.; Kwok, P. C. L.; Leung, G. P. H.; Mason, A. J.; Chan, H.-K.; Poon, L. L. M.; Lam, J. K. W. Inhalable Dry Powder Formulations of siRNA and pH-Responsive Peptides with Antiviral Activity Against H1N1 Influenza Virus. *Mol. Pharm.* **2015**, *12*, (3), 910-921.

255. Man, D. K. W.; Chow, M. Y. T.; Casettari, L.; Gonzalez-Juarrero, M.; Lam, J. K. W. Potential and development of inhaled RNAi therapeutics for the treatment of pulmonary tuberculosis. *Advanced Drug Delivery Reviews* **2016**, *102*, 21-32.

256. Guo, C.; Al-Jamal, W. T.; Toma, F. M.; Bianco, A.; Prato, M.; Al-Jamal, K. T.; Kostarelos, K. Design of Cationic Multiwalled Carbon Nanotubes as Efficient siRNA Vectors for Lung Cancer Xenograft Eradication. *Bioconjugate Chemistry* **2015**, *26*, (7), 1370-1379.
257. Soutschek, J.; Akinc, A.; Bramlage, B.; Charisse, K.; Constien, R.; Donoghue, M.; Elbashir, S.; Geick, A.; Hadwiger, P.; Harborth, J.; John, M.; Kesavan, V.; Lavine, G.; Pandey, R. K.; Racie, T.; Rajeev, K. G.; Rohl, I.; Toudjarska, I.; Wang, G.; Wuschko, S.; Bumcrot, D.; Koteliansky, V.; Limmer, S.; Manoharan, M.; Vornlocher, H.-P. Therapeutic silencing of an endogenous gene by systemic administration of modified siRNAs. *Nature* **2004**, *432*, (7014), 173-178.
258. Nasr, M.; Najlah, M.; D'Emanuele, A.; Elhissi, A. PAMAM dendrimers as aerosol drug nanocarriers for pulmonary delivery via nebulization. *Int. J. Pharm.* **2014**, *461*, (1–2), 242-250.
259. Jensen, L. B.; Pavan, G. M.; Kasimova, M. R.; Rutherford, S.; Danani, A.; Nielsen, H. M.; Foged, C. Elucidating the molecular mechanism of PAMAM–siRNA dendriplex self-assembly: Effect of dendrimer charge density. *Int. J. Pharm.* **2011**, *416*, (2), 410-418.
260. Yang, J.; Zhang, Q.; Chang, H.; Cheng, Y. Surface-Engineered Dendrimers in Gene Delivery. *Chemical Reviews* **2015**, *115*, (11), 5274-5300.
261. Bielski, E. R.; Zhong, Q.; Brown, M.; da Rocha, S. R. P. Effect of the Conjugation Density of Triphenylphosphonium Cation on the Mitochondrial Targeting of Poly(amidoamine) Dendrimers. *Mol. Pharm.* **2015**, *12*, (8), 3043-3053.
262. Merkel, O. M.; Rubinstein, I.; Kissel, T. siRNA Delivery to the lung: What's new? *Advanced Drug Delivery Reviews* **2014**, *75*, 112-128.

263. Durcan, N.; Murphy, C.; Cryan, S. A. Inhalable siRNA: Potential as a therapeutic agent in the lungs. *Mol. Pharm.* **2008**, *5*, (4), 559-566.
264. Labiris, N. R.; Dolovich, M. B. Pulmonary drug delivery. Part II: The role of inhalant delivery devices and drug formulations in therapeutic effectiveness of aerosolized medications. *British Journal of Clinical Pharmacology* **2003**, *56*, (6), 600-612.
265. Jensen, D. K.; Jensen, L. B.; Koocheki, S.; Bengtson, L.; Cun, D.; Nielsen, H. M.; Foged, C. Design of an inhalable dry powder formulation of DOTAP-modified PLGA nanoparticles loaded with siRNA. *J. Control. Release* **2012**, *157*, (1), 141-148.
266. Monteagudo, S.; Pérez-Martínez, F. C.; Pérez-Carrión, M. D.; Guerra, J.; Merino, S.; Sánchez-Verdú, M. P.; Ceña, V. Inhibition of p42 MAPK using a nonviral vector-delivered siRNA potentiates the anti-tumor effect of metformin in prostate cancer cells. *Nanomedicine* **2012**, *7*, (4), 493-506.
267. Wu, L.; Al-Haydari, M.; da Rocha, S. R. Novel propellant-driven inhalation formulations: engineering polar drug particles with surface-trapped hydrofluoroalkane-philic. *European journal of pharmaceutical sciences* **2008**, *33*, (2), 146-158.
268. Healy, A. M.; Amaro, M. I.; Paluch, K. J.; Tajber, L. Dry powders for oral inhalation free of lactose carrier particles. *Advanced drug delivery reviews* **2014**, *75*, 32-52.
269. Li, X.; Vogt, F. G.; Hayes Jr, D.; Mansour, H. M. Design, characterization, and aerosol dispersion performance modeling of advanced spray-dried microparticulate/nanoparticulate mannitol powders for targeted pulmonary delivery as dry powder inhalers. *Journal of aerosol medicine and pulmonary drug delivery* **2014**, *27*, (2), 81-93.

270. Lipka, J.; Semmler-Behnke, M.; Wenk, A.; Burkhardt, J.; Aigner, A.; Kreyling, W. Biokinetic studies of non-complexed siRNA versus nano-sized PEI F25-LMW/siRNA polyplexes following intratracheal instillation into mice. *Int. J. Pharm.* **2016**, *500*, (1), 227-235.
271. Luo, Y.; Zhai, X.; Ma, C.; Sun, P.; Fu, Z.; Liu, W.; Xu, J. An inhalable β 2-adrenoceptor ligand-directed guanidinylated chitosan carrier for targeted delivery of siRNA to lung. *J. Control. Release* **2012**, *162*, (1), 28-36.
272. Gary, D. J.; Puri, N.; Won, Y.-Y. Polymer-based siRNA delivery: Perspectives on the fundamental and phenomenological distinctions from polymer-based DNA delivery. *J. Control. Release* **2007**, *121*, (1–2), 64-73.
273. Dahlman, J. E.; Barnes, C.; Khan, O. F.; Thiriot, A.; Jhunjunwala, S.; Shaw, T. E.; Xing, Y.; Sager, H. B.; Sahay, G.; Speciner, L. In vivo endothelial siRNA delivery using polymeric nanoparticles with low molecular weight. *Nature nanotechnology* **2014**, *9*, (8), 648-655.
274. Tang, Y.; Li, Y.-B.; Wang, B.; Lin, R.-Y.; van Dongen, M.; Zurcher, D. M.; Gu, X.-Y.; Banaszak Holl, M. M.; Liu, G.; Qi, R. Efficient in vitro siRNA delivery and Intramuscular Gene Silencing using PEG-modified PAMAM Dendrimers. *Mol. Pharm.* **2012**, *9*, (6), 1812-1821.
275. Perez, A. P.; Romero, E. L.; Morilla, M. J. Ethylenediamine core PAMAM dendrimers/siRNA complexes as in vitro silencing agents. *Int. J. Pharm.* **2009**, *380*, (1–2), 189-200.

276. Ornelas-Megiatto, C. t.; Wich, P. R.; Fréchet, J. M. Polyphosphonium polymers for siRNA delivery: an efficient and nontoxic alternative to polyammonium carriers. *Journal of the American Chemical Society* **2012**, *134*, (4), 1902-1905.
277. Gujrati, M.; Malamas, A.; Shin, T.; Jin, E.; Sun, Y.; Lu, Z.-R. Multifunctional cationic lipid-based nanoparticles facilitate endosomal escape and reduction-triggered cytosolic siRNA release. *Mol. Pharm.* **2014**, *11*, (8), 2734-2744.
278. Pack, D. W.; Hoffman, A. S.; Pun, S.; Stayton, P. S. Design and development of polymers for gene delivery. *Nature Reviews Drug Discovery* **2005**, *4*, 581+.
279. Zhang, Q.; Chen, S.; Zhuo, R.-X.; Zhang, X.-Z.; Cheng, S.-X. Self-Assembled Terplexes for Targeted Gene Delivery with Improved Transfection. *Bioconjugate Chemistry* **2010**, *21*, (11), 2086-2092.
280. Maksimenko, A. V.; Mandrouguine, V.; Gottikh, M. B.; Bertrand, J.-R.; Majoral, J.-P.; Malvy, C. Optimisation of dendrimer-mediated gene transfer by anionic oligomers. *The Journal of Gene Medicine* **2003**, *5*, (1), 61-71.
281. Merkel, O. M.; Mintzer, M. A.; Librizzi, D.; Samsonova, O.; Dicke, T.; Sproat, B.; Garn, H.; Barth, P. J.; Simanek, E. E.; Kissel, T. Triazine dendrimers as non-viral vectors for in vitro and in vivo RNAi: The effects of peripheral groups and core structure on biological activity. *Mol. Pharm.* **2010**, *7*, (4), 969-983.
282. Hollins, A. J.; Omid, Y.; Benter, I. F.; Akhtar, S. Toxicogenomics of drug delivery systems: Exploiting delivery system-induced changes in target gene expression to enhance siRNA activity. *J. Drug Target.* **2007**, *15*, (1), 83-88.

283. Naito, Y.; Yamada, T.; Matsumiya, T.; Ui-Tei, K.; Saigo, K.; Morishita, S. dsCheck: highly sensitive off-target search software for double-stranded RNA-mediated RNA interference. *Nucleic Acids Research* **2005**, *33*, (suppl 2), W589-W591.
284. Tschuch, C.; Schulz, A.; Pscherer, A.; Werft, W.; Benner, A.; Hotz-Wagenblatt, A.; Barrionuevo, L. S.; Lichter, P.; Mertens, D. Off-target effects of siRNA specific for GFP. *BMC Molecular Biology* **2008**, *9*, (1), 1-14.
285. Merkel, O. M.; Beyerle, A.; Beckmann, B. M.; Zheng, M.; Hartmann, R. K.; Stöger, T.; Kissel, T. H. Polymer-related off-target effects in non-viral siRNA delivery. *Biomaterials* **2011**, *32*, (9), 2388-2398.
286. Grant, A. C.; Walker, R.; Hamilton, M.; Garrill, K. The ELLIPTA® dry powder inhaler: design, functionality, in vitro dosing performance and critical task compliance by patients and caregivers. *Journal of Aerosol Medicine and Pulmonary Drug Delivery* **2015**, *28*, (6), 474-485.
287. Bharatwaj, B.; Mohammad, A. K.; Dimovski, R.; Cassio, F. L.; Bazito, R. C.; Conti, D.; Fu, Q.; Reineke, J.; da Rocha, S. R. P. Dendrimer Nanocarriers for Transport Modulation Across Models of the Pulmonary Epithelium. *Mol. Pharm.* **2015**, *12*, (3), 826-838.
288. Rajabnezhad, S.; Casettari, L.; Lam, J. K. W.; Nomani, A.; Torkamani, M. R.; Palmieri, G. F.; Rajabnejad, M. R.; Darbandi, M. A. Pulmonary delivery of rifampicin microspheres using lower generation polyamidoamine dendrimers as a carrier. *Powder Technology* **2016**, *291*, 366-374.

289. Peltonen, L.; Valo, H.; Kolakovic, R.; Laaksonen, T.; Hirvonen, J. Electrospraying, spray drying and related techniques for production and formulation of drug nanoparticles. *Expert Opinion on Drug Delivery* **2010**, *7*, (6), 705-719.
290. Pilcer, G.; Amighi, K. Formulation strategy and use of excipients in pulmonary drug delivery. *International journal of pharmaceutics* **2010**, *392*, (1), 1-19.
291. Youngren-Ortiz, S. R.; Gandhi, N. S.; España-Serrano, L.; Chougule, M. B. Aerosol Delivery of siRNA to the Lungs. Part 1: Rationale for Gene Delivery Systems. *Kona : powder science and technology in Japan* **2016**, *33*, 63-85.
292. Sheth, P.; Stein, S. W.; Myrdal, P. B. Factors Influencing Aerodynamic Particle Size Distribution of Suspension Pressurized Metered Dose Inhalers. *AAPS PharmSciTech* **2015**, *16*, (1), 192-201.
293. Rogueda, P. G.; Traini, D. The nanoscale in pulmonary delivery. Part 1: deposition, fate, toxicology and effects. *Expert opinion on drug delivery* **2007**, *4*, (6), 595-606.
294. Paćławski, A.; Szłęk, J.; Lau, R.; Jachowicz, R.; Mendyk, A. Empirical modeling of the fine particle fraction for carrier-based pulmonary delivery formulations. *International Journal of Nanomedicine* **2015**, *10*, 801-810.
295. McCabe, J. C.; Koppenhagen, F.; Blair, J.; Zeng, X.-M. ProAir® HFA delivers warmer, lower-impact, longer-duration plumes containing higher fine particle dose than Ventolin® HFA. *Journal of aerosol medicine and pulmonary drug delivery* **2012**, *25*, (2), 104-109.
296. Lu, D.; Hickey, A. J. Pulmonary vaccine delivery. *Expert Review of Vaccines* **2007**, *6*, (2), 213-226.

297. Tomalia, D. A.; Reyna, L.; Svenson, S., Dendrimers as multi-purpose nanodevices for oncology drug delivery and diagnostic imaging. Portland Press Limited: 2007.
298. Kitchens, K. M.; Kolhatkar, R. B.; Swaan, P. W.; Eddington, N. D.; Ghandehari, H. Transport of poly (amidoamine) dendrimers across Caco-2 cell monolayers: influence of size, charge and fluorescent labeling. *Pharm. Res.* **2006**, *23*, (12), 2818-2826.
299. Lammers, T.; Kühnlein, R.; Kissel, M.; Subr, V.; Etrych, T.; Pola, R.; Pechar, M.; Ulbrich, K.; Storm, G.; Huber, P. Effect of physicochemical modification on the biodistribution and tumor accumulation of HPMA copolymers. *J. Control. Release* **2005**, *110*, (1), 103-118.
300. Chen, Z.; Zhang, P.; Cheetham, A. G.; Moon, J. H.; Moxley, J. W.; Lin, Y.-a.; Cui, H. Controlled release of free doxorubicin from peptide–drug conjugates by drug loading. *J. Control. Release* **2014**, *191*, 123-130.
301. Mohamed, M. M.; Sloane, B. F. Cysteine cathepsins: multifunctional enzymes in cancer. *Nature Reviews Cancer* **2006**, *6*, (10), 764.
302. Ackermann, L.; Potukuchi, H. K.; Landsberg, D.; Vicente, R. Copper-catalyzed “click” reaction/direct arylation sequence: modular syntheses of 1, 2, 3-triazoles. *Organic letters* **2008**, *10*, (14), 3081-3084.
303. Beck, A.; Wurch, T.; Bailly, C.; Corvaia, N. Strategies and challenges for the next generation of therapeutic antibodies. *Nature Reviews Immunology* **2010**, *10*, (5), 345.
304. Coates, A.; Abraham, S.; Kaye, S. B.; Sowerbutts, T.; Frewin, C.; Fox, R.; Tattersall, M. On the receiving end—patient perception of the side-effects of cancer chemotherapy. *European Journal of Cancer and Clinical Oncology* **1983**, *19*, (2), 203-208.

305. Hagane, K.; Akera, T.; Berlin, J. Doxorubicin: mechanism of cardiodepressant actions in guinea pigs. *J. Pharmacol. Exp. Ther.* **1988**, *246*, (2), 655-661.
306. Chatterjee, K.; Zhang, J.; Honbo, N.; Karliner, J. S. Doxorubicin cardiomyopathy. *Cardiology* **2010**, *115*, (2), 155-162.
307. Ready-to-use lentiviral Particles for GFP/ CFP/ YFP/ RFP/ BFP Product Manual. In *Pre-made Lentiviral Particles for Fluorescent Proteins*, GenTarget Inc: www.gentarget.com, 2017.
308. Rashid, O. M.; Nagahashi, M.; Ramachandran, S.; Dumur, C. I.; Schaum, J. C.; Yamada, A.; Aoyagi, T.; Milstien, S.; Spiegel, S.; Takabe, K. Is tail vein injection a relevant breast cancer lung metastasis model? *Journal of thoracic disease* **2013**, *5*, (4), 385.
309. Zhu, Y.; Knolhoff, B. L.; Meyer, M. A.; Nywening, T. M.; West, B. L.; Luo, J.; Wang-Gillam, A.; Goedegebuure, S. P.; Linehan, D. C.; DeNardo, D. G. CSF1/CSF1R blockade reprograms tumor-infiltrating macrophages and improves response to T-cell checkpoint immunotherapy in pancreatic cancer models. *Cancer Res.* **2014**, *74*, (18), 5057-5069.

ABSTRACT**DRUG DELIVERY STRATEGIES FOR THE TREATMENT OF ADVANCED LUNG
CANCER AND VARIOUS LUNG METASTASES**

by

ELIZABETH BIELSKI**August 2018****Advisor:** Dr. Sandro R. P. da Rocha**Major:** Chemical Engineering**Degree:** Doctor of Philosophy

Lung cancer remains the leading cause of cancer-related deaths in the United States. Secondary lung tumors metastasized from other cancer sites also remains highly prevalent, in which most metastatic tumors cannot be cured with existing therapies. Chemoresistance (multi drug resistance – MDR) that develops intrinsically or acquired is one of the key factors leading to fatality in these patients. MDR develops from a variety of resistance mechanisms that can occur consecutively or concurrently, therefore, making most current treatments unsuccessful. Current therapies have known to slow tumor growth, but rarely provide a cure. Immunotherapy has seen some promise, including the use of checkpoint inhibitors, when other therapies have not proven beneficial. However, only a small fraction of tumor types and patients have benefited from this type of treatment, and some toxicity has been stated. Therefore, establishing new types of treatments, as a single therapy or combination therapy, that can i) increase the rate of survival in patients suffering at early or late stages (when MDR and metastasis have developed) of lung cancer, and ii) reduce toxicity and adverse side effects of treatments is of great importance in pulmonary oncology.

In this work we describe alternative treatment modalities that suggest their potential to address MDR and prolong the rate of survival in patients suffering from primary and secondary lung tumors. A combination of local lung targeting (high payload to target site and reduced systemic toxicity), nanocarriers (to modulate interactions with physiological environment) intracellular organelle targeting (to repurpose cytoreductive therapies), siRNA as therapeutic agent (to target apoptotic pathways), and macrophage repolarization immunotherapy (to modulate the tumor microenvironment) are reported. We describe the development mitochondrial-targeted dendrimer nanocarriers (DNCs) as a platform for the repurposing of chemotherapeutics, the development of siRNA/TPP-DNC complexes (TPP-dendriplexes) as a platform for pulmonary delivery of siRNAs, the development of asymmetric dendrimers with a chemotherapeutic and varying surface functionalities to enhance tumor targeting and penetration, and address the impact of local pulmonary administration of tumor associated macrophage (TAM)-targeting immunotherapy. Overall, we conclude that all these strategies described above have the potential capability to address issues resulting from MDR and for the treatment of primary and secondary lung tumors.

AUTOBIOGRAPHICAL STATEMENT

ELIZABETH BIELSKI

Elizabeth Bielski received her Bachelor of Science in Biomedical Physics Honors with University Honors and Summa Cum Laude from Wayne State University (Detroit, MI, USA) in 2011, and her Master of Science in Biomedical Engineering from Wayne State University (WSU) in 2012. In the Fall of 2012 she joined the Chemical Engineering and Materials Science Department at WSU to pursue her PhD in Chemical Engineering under the guidance of Dr. Sandro da Rocha working on developing novel therapies for the treatment of primary and secondary lung tumors. From October 2014-July 2015, she traveled to Brazil to work with Dr. Reinaldo Bazito in the Chemistry Department at University of São Paulo (São Paulo, Brazil) learning chemical synthesis of polyester-based dendrons and dendrimers. She finished up her research work at the Department of Pharmaceutics at Virginia Commonwealth University (Richmond, VA, USA) starting in January 2016. During this time, she has authored or co-authored 6 publications in peer-reviewed journals (2 first-author) and has 4 more papers in preparation. She has also received numerous scholarships, awards, and recognitions including: *Graduate Professional Scholarship* from 2013-2014, *Outstanding Graduate Student Award* in 2014, *Graduate Student Professional Travel Award* (2013, 2015) from College of Engineering at WSU, and the *Student Research Award* in 2016 at the NanoDDS'16: Annual Nanomedicine and Drug Delivery Symposium by the Society for Biomaterials Drug Delivery Special Interest Group. She has accepted a ORISE Fellowship position at the Food and Drug Administration (FDA) to join the Division of Therapeutic Performance starting in August 2018.